

MEMBRANE TECHNOLOGIES FOR THE REMOVAL OF MICROPLASTICS

AN INVESTIGATION INTO MEMBRANE TECHNOLOGIES FOR THE REMOVAL OF
MICROPLASTICS FROM MUNICIPAL WASTEWATER TREATMENT PLANT EFFLUENTS

By RYAN J. LARUE, B.Eng.Mgmt

A Thesis Submitted to the School of Graduate Studies in Partial Fulfillment of the Requirements
for the Degree *Doctor of Philosophy*

McMaster University © Copyright Ryan J. LaRue, April 2023

McMaster University DOCTOR OF PHILOSOPHY (2023)

Hamilton, Ontario (Chemical Engineering)

TITLE: An Investigation into Membrane Technologies for the Removal of Microplastics from
Municipal Wastewater Treatment Plant Effluents

AUTHOR: Ryan J. LaRue, B.Eng.Mgmt (McMaster University)

SUPERVISOR: Dr. David R. Latulippe

PAGES: [xxiii](#), 299

Lay Abstract

The term “microplastics” (MPs) is used to describe microscopic plastic particles. Recent investigations have reported these MPs in lakes, rivers, and oceans across the globe. These reports are concerning as other studies demonstrate that MP pollution can be hazardous to aquatic life, yet the potential effects of MPs on human health remain largely unknown. Many MPs originate from municipal wastewater treatment plants (WWTPs) which discharge large numbers of these particles into the aquatic environment. Researchers often recommend the use of membranes as a barrier to prevent MPs from leaving in the final treated wastewater. This work seeks to assess that recommendation. Assessments of the effectiveness of membranes at withholding MP particles in wastewater are performed over various conditions. The propensity of MPs to interfere with the desired output of treated wastewater is also measured. Overall, findings indicate that carefully designed and operated membranes processes can be well-suited to this application.

Abstract

Microplastic (MP) pollution is ubiquitous in the aquatic environment. Though their properties are known to vary considerably, these particles are typically 1–5,000 μm in size and irregular in shape. Research suggests that MPs pose a significant hazard to aquatic ecosystems, lead to negative economic consequences, and may cause adverse human health effects. The effluents of municipal wastewater treatment plants (WWTPs) comprise a significant source of MPs, containing < 1 MP/L to > 440 MPs/L. Pursuant to the large volumes of wastewater processed, estimated daily effluxes can exceed one billion MPs/day in some WWTPs. Membrane technologies, like those used in some tertiary wastewater treatment applications, appear well-positioned to mitigate releases of MPs. However, research directly characterizing the performance of membranes in these applications is lacking. The studies in this work address this knowledge gap.

To this end, irregularly-shaped MPs were produced in a novel milling/sieving process. Ultrafiltration and microfiltration membranes were challenged to these MPs suspended in secondary effluent wastewater to elucidate their fouling behaviour under realistic solution conditions. Subsequently, MPs milled/sieved from a fluorescently-labelled plastic feedstock were utilized in microfiltration experiments. Bulk MP concentrations in samples were easily measured using a plate reader to quantify MP rejection. Improving upon this technique, a new protocol involving a flow cytometer was developed, enabling the identification of individual fluorescent MPs in filtration samples, even when complex solutions chemistries were used. A culminating investigation was performed to bridge a gap in the literature between studies considering small-scale laboratory filtration phenomena and observations of large-scale WWTPs. Thus, the performance of a hollow fiber crossflow microfiltration module was evaluated in the filtration of wastewater containing MPs.

Overall findings suggest that incidences of fouling by MPs can be managed via periodic cleaning processes, and the well-informed selection/operation of membrane technologies can contribute to high MP removal efficiencies ($> 99\%$) in tertiary wastewater applications.

Acknowledgements

The road to completing a PhD is long and winding, but as I have learned, also exceedingly rewarding. I would be remiss not to acknowledge those who have joined me along the way.

To Dr. David Latulippe: thank you for taking a chance on a second-year undergraduate student who did not understand how the NSERC USRA system worked. I am grateful that you chose to rehire me year-after-year as a summer researcher, and then as a PhD student years later. Over the past nine years, I have greatly appreciated your mentorship and guidance, your wisdom, your stalwart support of all my research endeavours, and your tacit approval of my little side-projects. I am grateful for all of the enthusiastic letters of support that you have written and for your words of recommendation that have afforded me extensive opportunities (*e.g.* Notre Dame, teaching, etc.). I leave your research group knowing that I have grown both as a chemical engineer and as a person.

To my supervisory committee members, Dr. Charles de Lannoy, Dr. Todd Hoare, & Dr. Jose Moran-Mirabal: thank you for your counsel over these last several years. Your helpful insights have greatly improved me as a researcher and have elevated my work to the next level. In addition, thank you for your patience while reading this thesis.

To my undergraduate student researchers during my PhD, Brianna Chester, Samuel Koo, Yves G. Mckay, Isabella Monaco, Susan O'Brien, Graham Van Every, and Ashleigh Warren: thank you for your enthusiasm, your willingness to learn, your diligence, and your patience during all the experiments which you performed. I have enjoyed watching you grow as researchers, chemical engineers, and as people. I wish you all the best in whatever the future has in store for you!

To the chemical engineering technical support staff, Justin Bernar, Mike Clarke, Paul Gatt, Doug Keller, Heera Marway, and Tim Stephens: thank you for providing me with the equipment, instrumentation, facilities, information, and training that I needed to perform my research effectively and safely. A special thank-you goes out to Paul and Justin who kindly supported my periodic “shopping trips” for parts and lent me a plethora of tools without question.

To the chemical engineering administrative staff, Linda Ellis, Laura Nease, Kristina Trollip, and Michelle Whalen: thank you for all that you do for us. Your kindness, organization, generosity with your time and resources, and your perpetual willingness to help—no matter the task—has not gone unnoticed over the last decade. Our department would not run without you.

To the research staff at McMaster facilities, Zoya Tabunshchyk at the McMaster Core Flow Facility; Chris Butcher, Jhoyner Martinez, and Andy Dufts at the Canadian Centre for Electron Microscopy; Mouhanad Babi and João Pedro Bronze de Firmino at the Centre for Advanced Light Microscopy; Zeynel Bayindir, Mehdi Keramane, Elna Luckham, and Marta Princz at the Biointerfaces Institute; John Colenbrander and Mark Mackenzie in the Department of Mechanical Engineering; Nidhi Jain and Rakesh Sahu at the Centre of Excellence in Protective Equipment and Materials: thank you for all that you have done to support my research program. The time, patience and expertise that you have shared with me is greatly appreciated and has markedly improved the quality of my research.

To collaborators outside of McMaster University, Dr. Bill Phillip and his team at the University of Notre Dame; Dr. Youliang He, Joselyne McPhedran, and Dan Walsh at CanmetMATERIALS; Jeffrey Parr and John Tomescu at Thetis Environmental; Beth Goodrich at EMD Millipore; Rocco Iannarelli and his team at the Dundas Wastewater Treatment Plant: thank you for allowing me to use your facilities, providing me with equipment and materials (Durapore® membranes), and for your sage advice. Your help and expertise have moved my research in new and interesting directions.

To “Team Supermask”, namely Patrick, Scott, Amin, Sarah, Charles, Catherine, João, and Chris: thank you for sharing the experience of performing purposeful work while the rest of the world ground to a halt due to the COVID-19 pandemic. I will never forget our odyssey which took us from that initial abominable mask-testing contraption to the sleek, bespoke “PFE” apparatus in which we now take pride. I would like to think that what we did provided a valuable contribution towards the betterment of public health. I am grateful for your camaraderie over this journey.

To those who have come before me, namely Amir, Carlos, Emily, Jake, Jeff, and Maddi: thank you for your wisdom, mentorship, and for inspiring me to become a better researcher. Your influence has positively impacted my growth as a chemical engineer and as a researcher.

To my funding sources, namely the Vanier Canada Graduate Scholarships, Canada Graduate Scholarships Master’s program, the Ontario Graduate Fellowships program, and McMaster University’s “Dean’s Excellence Engineering Doctoral Award” program: thank you for supporting me and ensuring that my quality-of-life was excellent during my doctoral research endeavours.

With regards to the software applications used in this work—BioRender, ChemDraw 22.0.0, FlowJo v10.8.1, ImageJ (Fiji) 1.53t, MATLAB R2022b, Microsoft Excel, Microsoft Visio, and L^AT_EX: I wish to acknowledge the role of these programs in bringing this manuscript to fruition.

To my colleagues in the Latulippe Research Group over the course of my doctoral degree—Abhishek, Adi, Alex, Amir, Ana, Anushree, Ashleigh, Blake, Brianna, Claire, Christophe, Danika, Eric, Evan, Graham, Ian, Indranil, Isabella, Jacob, Jacob, Jasmine, Jillian, Karina, Karl, Kelli-Anne, Kurt, Landon, Lauren, Lauren, Mehdi, Nathan, Nicole, Noel, Noelle, Matthew, Matthew, Melissa, Patrick, Reza, Sarah, Sarah, Salman, Samaneh, Samuel, Satyam, Shabnam, Shayna, Stephanie, Susan, and Yves: thank you for being a part of my PhD journey. I have enjoyed learning from you and collaborating with you. I wish you all the best—wherever you are in the world, now.

To my core “lab family”—Abhishek, Ana, Annika, Claire, Evan, Indranil, Karina, Landon, Nathan, Melissa, Patrick, Reza, the Sarahs, and Scott: thank you for the gift of friendship that you have given me over the last five-and-a-half years. I have thoroughly enjoyed that times that we have spent together: the various socials events, the games nights, the arms proliferation, the BBQs and dinner parties, FAFO, the camping trips, the venting, the softball team, the inevitable arms treaties, the late nights in JHE, the feral antics, and so on. I am extremely grateful for the wealth of happy memories that we have made. I look forward to our next five-and-a-half years.

*Last but not least, to my “actual family”—Karen, John, and Peter: thank you for your continuous love and support over the course of my PhD and over the last 28 years. I appreciate your words of encouragement, your confidence *in* me, and the pride that you show when you speak *of* me. Also, thank you for not asking *too many* questions about my work. You have made this journey appreciably more bearable, and know that I complete it as a better person than when I began.*

Table of Contents

Lay Abstract	iii
Abstract	iv
Acknowledgements	v
Table of Contents	viii
List of Figures	xv
List of Tables	xvi
List of Abbreviations & Symbols	xvii
Declaration of Academic Achievement	xxii
1 Microplastics: Small Particles, Big Problem?	1
1.1 Introduction to Microplastics	3
1.1.1 Classifications of Microplastics	4
1.1.2 Microplastics in the Aquatic Environment	7
1.1.3 Microplastics & Human Consequences	10
1.2 Municipal Wastewater Treatment Plants as a Source of Microplastics	13
1.2.1 MP Sampling & Quantification	15
1.2.2 Fate of Microplastics in Wastewater Treatment Plants	23
1.2.2.1 Fate by Facility	25
1.2.2.2 Fate by Treatment Stage & Technology	27
1.2.2.3 Fate by Microplastic Classification	36
1.2.2.4 Holistic Approaches to the Fate of Microplastics	40
1.3 Research Motivations	43
1.3.1 Microplastics Removal via Membrane Technologies	45
1.3.1.1 Removal Performance in Existing Wastewater Treatment Plants	45
1.3.1.2 Removal Performance in Laboratory Experiments	48
1.3.2 Opportunities for Novel Research	52
1.4 Works Cited	56
2 Membrane Theory & Wastewater Treatment	68
2.1 Introduction to Membrane Science	68
2.1.1 Classification Schemes for Membranes	69
2.1.1.1 Structure	69
2.1.1.2 Pore Size	71
2.1.1.3 Material	73
2.1.1.4 Geometry	74
2.1.1.5 Flow Path & Configuration	76
2.1.2 Metrics for Membrane Performance	77
2.1.2.1 Quantity-Based Analysis	78
2.1.2.2 Quality-Based Analysis	81
2.1.3 Membrane Fouling	86
2.1.3.1 Fouling Models	87
2.1.3.2 Reversible & Irreversible Fouling	91
2.1.3.3 Approaches to Fouling Mitigation	91
2.2 Introduction to Conventional Municipal Wastewater Treatment	93
2.2.1 Conventional Treatment Stages	94
2.2.1.1 Preliminary & Primary Treatment	94
2.2.1.2 Secondary Treatment	96
2.2.1.3 Tertiary Treatment	97
2.2.1.4 Solids Processing	98

2.2.2	Membranes in Municipal Wastewater Treatment	99
2.2.2.1	Membrane Bioreactors	99
2.2.2.2	Tertiary Wastewater Polishing	100
2.2.3	Analytical Techniques for Water/Wastewater Characterization	102
2.2.3.1	Solids Content	102
2.2.3.2	Total Organic Carbon	103
2.2.3.3	Chemical Oxygen Demand	105
2.2.3.4	pH and Conductivity	106
2.3	Works Cited	107
3	Assessment of Microplastic Particle Fouling of Ultrafiltration & Microfiltration Membranes	112
3.1	Motivations	112
3.2	Materials & Methods	115
3.2.1	Microplastic Particles	115
3.2.2	Membranes	116
3.2.3	Municipal Wastewater Effluent	116
3.2.4	Microplastic Suspensions	117
3.2.5	Filtration Experiments	118
3.2.6	Membrane Backwashing	119
3.3	Results & Discussions	120
3.3.1	Milled & Sieved Microplastic Particles	120
3.3.2	Filtration Experiments	122
3.3.3	Fouling Mechanisms	126
3.3.4	Filtration Experiments with Backwashing	128
3.4	Concluding Remarks	132
3.5	Works Cited	133
4	Evaluation of Microplastic Particle Transmission through Microfiltration Membranes	136
4.1	Motivations	136
4.2	Materials & Methods	138
4.2.1	Membranes	138
4.2.2	Microplastic Particles & Suspensions	138
4.2.3	Filtration Experiments	140
4.2.4	Focused Beam Reflectance Measurements	142
4.2.5	Confocal Laser Scanning Microscopy (CLSM)	142
4.3	Results & Discussions	143
4.3.1	Characterization of Irregularly-Shaped Microplastic Particles	143
4.3.2	Effect of Membrane Pore Size on MP Particle Transmission	145
4.3.3	Characterization of Microplastics in Permeate Samples	148
4.3.4	Spatial Analysis of Captured Microplastics via CLSM	154
4.3.5	Flux-Dependent Transmission of Microplastics	157
4.4	Concluding Remarks	160
4.5	Works Cited	161
5	Flow Cytometry for Quantifying Microplastic Particle Concentrations in Membrane Filtration Processes	164
5.1	Motivations	164
5.2	Materials & Methods	167
5.2.1	Chemicals & Membranes	167
5.2.2	Scanning Electron Microscopy	168

5.2.3	Filtration Experiments	169
5.2.4	Sample Analysis via Plate Reader	169
5.2.5	Sample Analysis via Flow Cytometer	170
5.2.6	Excitation-Emission Matrices of Microbead Suspensions	171
5.3	Results & Discussions	171
5.3.1	Flow Cytometry for Microbead Quantification	171
5.3.2	A Comparison of Microbead Quantification Techniques	173
5.3.3	Microbead Removal via Membrane Filtration	177
5.4	A Strategy to Estimate Microbead Size via Flow Cytometry	182
5.4.1	Model Formulation	183
5.4.2	Estimates of Particle Size	185
5.5	Concluding Remarks	188
5.6	Works Cited	190
6	Scaling-Up Microplastic Removal Studies to a Hollow Fiber Microfiltration Membrane Module	194
6.1	Introduction & Motivations	194
6.2	Materials & Methods	199
6.2.1	Chemicals & Wastewater	199
6.2.2	Preparation & Characterization of Microbeads	200
6.2.3	Filtration Experiments	202
6.2.3.1	Membrane Module Properties	202
6.2.3.2	Apparatus	202
6.2.3.3	Operational Protocol	204
6.2.3.4	Experiments Performed	207
6.2.4	Analysis via Flow Cytometry	207
6.2.5	Analysis via Confocal Laser Scanning Microscopy (CLSM)	209
6.3	Results & Discussions	209
6.3.1	Module Performance in the Filtration of Wastewater Only	209
6.3.2	Module Performance in the Filtration of Wastewater Containing Added Microbeads	212
6.3.3	Effect of Crossflow Velocity	217
6.3.4	Interpretation of a Curious Breakthrough Effect	222
6.3.5	Examination of Module Backwashing	225
6.3.5.1	Effect of Backwashing on Flux	225
6.3.5.2	Quantification of Microbeads in Backwashing Water	226
6.3.5.3	Visualization of Microbead Deposition via CLSM	228
6.4	Concluding Remarks	233
6.5	Works Cited	235
7	Conclusions & Recommendations for Future Work	239
7.1	Summary of Research	240
7.2	Opportunities for Future Study	243
7.3	Concluding Remarks	257
7.4	Works Cited	257
	Appendices	261
	Appendix A Supplementary Information for Chapter 3	262
A.1	Sample Calculations	262
A.2	Supplementary Tables	263
A.3	Supplementary Figures	264

Appendix B Supplementary Information for Chapter 4	271
B.1 Scanning Electron Microscopy	271
B.2 Membrane Surface Charge Measurements	272
B.3 Supplementary Results	273
Appendix C Supplementary Information for Chapter 5	283
C.1 Supplementary Figures	284
C.2 Data Tables for Microbead Size Estimation Experiments	288
Appendix D Supplementary Information for Chapter 6	289
D.1 Filtration Apparatus	289
D.2 Supplementary Results	291
D.3 Comprehensive Summary of Data from Filtration Experiments	294

List of Figures

1.1	Illustration of various transport pathways for plastic materials entering the natural environment.	2
1.2	Images of various morphologies of microplastics obtained via optical microscope.	7
1.3	Simplified flowchart which summarizes various methods documented in the literature for the collection, isolation, and characterization of microplastics in wastewater treatment plants.	17
1.4	Topical Web of Science search for publications, by year, involving microplastics and wastewater/sewage treatment from 2013–2022.	24
1.5	Overview of the fate of microplastics within wastewater treatment plants.	29
1.6	Summary of meta-analysis results performed by Liu <i>et al.</i> (2021), highlighting the effect of particle properties and specific treatment processes on the removal efficiency of the microplastics in wastewater treatment plants.	41
1.7	Illustration of the six critical thematic elements examined in this work which add value at the research nexus of membranes and microplastics.	53
2.1	Illustration of key terminology in a generic membrane filtration process using a porous membrane.	69
2.2	Cross-sectional sketches of various types of membrane structures.	70
2.3	Spectrum indicating the approximate pore sizes of different classifications of membranes used in liquid separations.	72
2.4	Chemical compositions of common membrane materials.	74
2.5	Illustration of the process for determining the pure water hydraulic permeability of three individual membrane samples.	80
2.6	Depiction of a stagnant film model for concentration polarization.	83
2.7	Plot of rejection coefficients as a function of $\lambda = a/r$ according to the Ferry Model.	85
2.8	Illustration of the four mechanisms of membrane fouling used in Hermia’s model.	90
2.9	Flowsheet of a conventional municipal wastewater treatment plant showing a series of possible unit operations.	95
2.10	The Shimadzu TOC-LCPH instrument with autosampler used in this work.	104
3.1	Diagram of the constant-pressure filtration setup.	119
3.2	Characterization of milled and sieved polyethylene microplastics.	121
3.3	Filtration of wastewater and polyethylene microplastics through the ultrafiltration and microfiltration membranes.	124
3.4	Electron microscopy images of the UB70 and V0.2 membranes used in this study: as-received and after the filtration of wastewater with/without added microplastics.	128
3.5	Filtration and backwashing cycles for the UB70 and V0.2 membranes.	129
3.6	Electron microscopy images of the UB70 and V0.2 membranes indicating the effect of backwashing on deposited foulants.	131

4.1	Electron microscopy images of the top surfaces and cross-sections of the Durapore® 0.45 µm- and 5 µm-rated membranes.	139
4.2	Schematic of the constant flux filtration system used in experiments to probe particle transmission.	141
4.3	Verification of the fluorescent behaviour of the milled/sieved microplastics used in filtration experiments.	144
4.4	Fluorescent intensities of permeate and feed samples filtered through 0.45 µm and 5 µm Durapore® membranes at a constant flux.	146
4.5	FBRM analysis of permeate and feed samples from filtration experiments with the 0.45 µm and 5 µm Durapore® membranes.	150
4.6	Top-down confocal laser scanning microscopy image montages of the 0.45 µm and 5 µm Durapore® membranes which were used in filtration experiments at a constant flux of 1,000 LMH.	155
4.7	The effect of flux on the fluorescent intensity of permeate samples over the course of filtrations using the 5 µm membrane.	158
5.1	Characterization of the 1–5 µm Cospheric microbeads used in experiments in this study.	169
5.2	Scatterplots and corresponding adjunct histograms for FSC-A versus FITC-A data collected using the flow cytometer.	172
5.3	Comparison of the solution matrix effects when quantifying microbead concentrations using the flow cytometer and plate reader.	174
5.4	Excitation-emission matrices illustrating the obscuring effect of humic acid when attempting to quantify microbead concentrations using the plate reader.	175
5.5	Comparison of the effect of pore size on microbead transmission and observed rejection using the Durapore® 0.45 µm and 5 µm membranes. Microbead concentrations were measured via flow cytometry.	178
5.6	Graphical illustration of the process used to estimate microbead particle sizes from flow cytometry FSC-A intensity measurements.	184
5.7	Estimation of microbead particle sizes in selected permeate samples for the filtration of microbeads in humic acid solution using the 5 µm membrane (Replicate #1).	186
6.1	Spectrum illustrating the two main “scales” of investigations involving microplastics and membranes and the opportunity for novel research that is created as a result.	196
6.2	Characterization of 0.5 and 2 µm <i>Invitrogen FluoSphere</i> microbeads used in this study.	201
6.3	Depiction of the <i>Cytiva Xampler</i> 0.65 µm microfiltration membrane module used in this study.	203
6.4	Simple piping and instrumentation diagram of the membrane module evaluation setup.	204
6.5	Transmembrane pressure and permeate flux during the filtration of wastewater only. . .	210
6.6	Transmembrane pressure, permeate flux, and particle rejection during the filtration of wastewater containing 1 mg/L (each) of 0.5 µm/2 µm microbeads.	212
6.7	Comparison of transmembrane pressure, permeate flux, and particle rejection during the filtration of wastewater with 1 mg/L (each) of 0.5 µm/2 µm microbeads at “high” and “low” levels of crossflow velocity.	221

6.8	Concentration of microbeads in the backwashing water that was collected after every sixth cycle for the two experiments run at Condition B.	227
6.9	Composite of confocal laser scanning microscopy images of hollow fiber half-sections following the culmination of all filtration experiments.	230
A.1	Electron microscopy images of the native membranes in top-down and cross-sectional profiles.	264
A.2	Diagram of the constant-pressure filtration setup, showing the construction of the membrane cells.	265
A.3	Comparison of particle sizes in the raw (unmilled) polyethylene feedstock and the milled/sieved microplastic particles	266
A.4	Comparison of filtration behaviour when two wastewater feeds collected on separate days were filtered using the UB70 membrane.	267
A.5	Comparison of the filtration of pure deionized water versus wastewater alone versus wastewater with 0.1 mg/L Tween 20 for the UB70 and V0.2 membranes.	267
A.6	Plots of permeate flux versus time for the UB70 and V0.2 membranes, showing the best-fit “cake filtration” fouling models.	268
A.7	Image of the backwashed V0.2 membrane which filtered wastewater containing 1 mg/L microplastics.	268
A.8	Camera images of native membranes and membranes fouled under various conditions.	269
A.9	Filtration of wastewater and polyethylene microplastic particles along with polystyrene microplastic fibers through the UB70 and V0.2 membranes.	270
B.1	Electron microscopy image of the as-purchased spherical microplastics from Cospheric.	271
B.2	Surface zeta potential of a Durapore® 5 µm membrane.	272
B.3	Example fluorescent intensity profiles for filtration experiments involving milled/sieved microplastics and the 0.45 µm and 5 µm Durapore® membranes. Results for the “rinse” and “filtration” experimental phases are shown.	273
B.4	Brightfield microscopy images of the as-received spherical microplastics and milled/sieved microplastics.	274
B.5	Pressure profiles for three filtration experiments using the 5 µm membrane at a flux of 1,000 LMH along with the best-fit model lines for compressible cake filtration.	276
B.6	Optical microscopy images of permeate samples from filtration experiments where the 5 µm membrane was used.	277
B.7	Optical microscopy image indicating the sizes of transmitted particles in one permeate sample from a filtration experiment where the 5 µm membrane was used.	278
B.8	Duplicate results from the focused beam reflectance measurement analysis of permeate and feed samples from filtration experiments with the 0.45 µm membrane.	279
B.9	Duplicate results from focused beam reflectance measurement analysis of permeate and feed samples from filtration experiments with the 5 µm membrane.	280
B.10	Confocal laser scanning microscopy orthogonal views of the 5 µm membrane taken at a depth of 20 µm from the upper surface, as defined in Figure 4.6.	281
B.11	3D views of the full confocal laser scanning microscopy z-stacks for the 0.45 µm and 5 µm Durapore® membranes.	282

C.1	Electron microscopy images of the Cospheric microbeads used in this study.	284
C.2	Excitation-emission matrices illustrating the obscuring effect of humic acid when attempting to quantify microbead concentrations using a fluorometric plate reader.	285
C.3	The effect of the diameter of ideal spherical microparticles on the number of particles per gram and the specific surface area.	285
C.4	The $\varphi(i)$ model relating FSC-A intensities to estimated microbead particle diameters.	286
C.5	Verification of the model relating flow cytometry FSC-A intensity measurements to microbead size.	286
C.6	Estimation of microbead particle sizes in selected permeate samples for the filtration of microbeads in humic acid solution using the 5 μm membrane (Replicate #2).	287
C.7	Estimation of microbead particle sizes from FSC-A intensity measurements in all of the filtration experiments involving the 5 μm membrane.	287
D.1	Comprehensive piping and instrument diagram which outlines the entire membrane module evaluation setup.	289
D.2	Example flow cytometry data for 1 mg/L of both 0.5 μm and 2 μm microbeads in milliQ water.	291
D.3	Comparison of permeate flux profiles for Modules A and B in the absence of, versus in the presence of added 0.5 $\mu\text{m}/2 \mu\text{m}$ microbeads.	292
D.4	Excitation-emission matrix illustrating the background autofluorescence of the natural solids in the wastewater that was used.	292
D.5	Summary of data collected during Experiment #1: Module A at Condition A.	294
D.6	Summary of data collected during Experiment #2: Module B at Condition A.	295
D.7	Summary of data collected during Experiment #3: Module A at Condition B.	296
D.8	Summary of data collected during Experiment #4: Module B at Condition B.	297
D.9	Summary of data collected during Experiment #5: Module A at Condition C.	298
D.10	Composite of all confocal laser scanning microscopy images taken of hollow fiber half-sections.	299

List of Tables

1.1	Summary of microplastic removal performance in 25 selected wastewater treatment plant studies.	28
1.2	The performance of membrane technologies towards the removal of microplastics, as reported in eleven research studies.	46
3.1	Summary of average water quality parameters for wastewater samples collected and used in filtration experiments.	117
3.2	Summary of “cake filtration” fouling model parameters for the two membranes challenged to wastewater suspensions containing various concentrations of microplastics.	127
5.1	Flow cytometry operational parameters and vertices of polygonal gates in FSC-A versus FITC-A plots.	170
6.1	Properties of wastewater samples used in this study.	200
6.2	Properties of the Cytiva membrane and module used in this study, as reported by the manufacturer.	202
6.3	List of experimental conditions and wastewater samples used in each experiment performed in this study.	207
6.4	Detailed list of flow cytometer operational parameters and polygonal gates used in quantifying microbead concentrations.	208
A.1	Detailed summary of wastewater properties used in membrane fouling experiments. . . .	263
A.2	Summary of the best-fit fouling model parameters for the mechanisms which most closely describe the flux decline data.	263
C.1	Summary of estimated size statistics of particles in feed/permeate samples taken during the filtration of microbeads in humic acid using the 5 μm membrane.	288
C.2	Comparison of solution conditions on the estimated size statistics of particles in the feeds/permeate samples of filtration experiments using the 5 μm membrane.	288
D.1	Summary of valves and instrumentation, as notated on the diagram in Figure D.1. . . .	290
D.2	Analysis of the variability of concentration measurements made via flow cytometry. . . .	291
D.3	Summary of the calculated volumes of feed wastewater required to produce the observed concentrations of MBs in the backwashing water from Experiments #3 and #4.	293

List of Abbreviations & Symbols

■ Abbreviations.

1°/2°/3°	primary/secondary/tertiary	EU	European Union
A ² O	anaerobic/anoxic/oxic	FBRM	focused beam reflectance measurement
AFM-IR	atomic force microscopy-infrared spectroscopy	FC	flow cytometry
Avg.	average	FESEM	field-emission scanning electron microscopy
ASM	activated sludge model	FITC	fluorescein isothiocyanate
ATR-FTIR	attenuated total reflectance-FTIR	FPA-FTIR	focal plane array-FTIR
BOD	biochemical oxygen demand	FSC	forward scattering by peak area (-A) or height (-H)
BW	backwashing	FTIR	Fourier transform infrared spectroscopy
CAS	conventional activated sludge	GC	gas chromatography
CDF	cumulative distribution function	HA	humic acid
CEB	chemically-enhanced backwashing	HRT	hydraulic retention time
CF	cake filtration	IB	intermediate blocking
CIP	cleaning-in-place	IC	inorganic carbon
COD	chemical oxygen demand	ICP-MS	inductively coupled plasma-MS
DAQ	data acquisition	IUCN	International Union for Conservation of Nature and Natural Resources
DI	deionized	LC	liquid chromatography
DLS	dynamic light scattering	LMH	L/m ² /h
DSC	differential scanning calorimetry	M/S-MP	milled/sieved-MP
DLVO	Derjaguin/Landau/Verwey/Overbeek	MB	microbead
DWTP	drinking water treatment plant	MBR	membrane bioreactor
EEM	excitation-emission matrix	MF	microfiltration
EPS	extracellular polymeric substances	MLD	million liters per day
Est.	estimated	MP	microplastic
		MS	mass spectrometry

MWCO	molecular weight cutoff	Py-GC-MS	pyrolysis-GC-MS
NOAA	National Oceanographic and Atmospheric Administration	RAS	return activated sludge
		Ref.	reference
NOM	natural organic matter	RO	reverse osmosis
NP	nanoplastic	RR	risk ratio
NTA	nanoparticle tracking analysis	SEM-EDS	scanning electron microscopy-energy dispersive spectroscopy
P&ID	pipng & instrumentation diagram	SLR	surface loading rate
PA	polyamide	Sph-MP	spherical MP
PAH	polycyclic aromatic hydrocarbon	SRT	solids retention time
PAN	polyacrylonitrile	SSC	side scattering by peak area (-A) or height (-H)
PARAFAC	parallel factor analysis	SSE	sum-of-squares of the errors
PC	polycarbonate	TC	total carbon
PCB	polychlorinated biphenyl	TDS	total dissolved solids
PE	polyethylene	TDS-GC-MS	thermal desorption-GC-MS
PEEK	polyether ether ketone	TED-GC-MS	thermal extraction desorption-GC-MS
PEI	polyetherimide		
PES	polyethersulfone	TGA-DSC	thermogravimetric analysis-DSC
PEst	polyester	TMP	transmembrane pressure
PET	polyethylene terephthalate	TOC	total organic carbon
Perm.	permeate	TS	total solids
PFAS	per- and polyfluoroalkyl substances	TSS	total suspended solids
PI	polyimide	UF	ultrafiltration
POP	persistent organic pollutant	UV	ultraviolet
PP	polypropylene	VFD	variable frequency drive
PR	plate reader	WAS	waste activated sludge
PS	polystyrene	WW	wastewater
PSf	polysulfone	WWTP	wastewater treatment plant
PU	polyurethane	XDLVO	extended DLVO
PVC	polyvinyl chloride		
PVP	polyvinyl pyrrolidone		

■ Symbols.

A	membrane area	i^*	FSC-A intensity of particle with diameter d^*
a	analyte particle diameter	j	arbitrary index variable
C	concentration	J_0	Hermia model initial flux
C_{eff}	effluent concentration	J_{BW}	backwashing flux
C_f	feed concentration	J_v	permeate volumetric flux
C_{inf}	influent concentration	\hat{J}_v	linear regression model for J_v vs. TMP
C_p	permeate concentration	K	flow meter K-value
C_w	concentration at membrane wall	K	Hermia model kinetic constant
D	diffusion coefficient	k	mass transfer coefficient
D_p	particle diameter	L	length (hollow fiber or pore)
d	microbead diameter	L_p	hydraulic permeability
d^*	particle diameter which produces i^*	M	permeate mass
\tilde{d}, d_{50}	median diameter	M	total number of FC events recorded
d_{10}, d_{90}	“size” below which 10% or 90% of particles fall	m	mass concentration of particles
$F(j)$	CDF of arbitrary variable j	m	mass (solids analysis)
$F_d(d)$	discrete CDF of particle diameter	N	number of hollow fibers per module
$\bar{F}_d(d)$	continuous CDF of particle diameter	N	total number of measurements/samples/etc.
$F_i(i)$	discrete CDF of FSC-A intensity	n	compressibility index
$\bar{F}_i(i)$	continuous CDF of FSC-A intensity	n	Hermia model parameter
$f(x)$	observed median frequency of chord length x via FBRM	n	number concentration of particles
$\hat{f}(x)$	log-normal distribution function fit to $f(x)$ data	n_{BW}	number concentration of particles in backwashing water
G	lag coefficient	n_f	number concentration of particles in feed
g	gravitational constant	$\tilde{n}_f(x)$	median number of counts in bin size x (feed sample)
h	height scaling parameter		
i	FSC-A intensity		

n_p	number concentration of particles in permeate	V	cumulative permeate volume (Hermia model)
$\tilde{n}_p(x)$	median number of counts in bin size x (permeate sample)	V	sample volume (solids analysis)
P	pressure	V_{BW}	volume of backwashing water
P_{feed}	feed pressure	V_f	volume of feed wastewater
P_{perm}	permeate pressure	v_{avg}	radially-averaged crossflow velocity
P_{ret}	retentate pressure	\bar{v}_{avg}	radially- and axially-averaged crossflow velocity
p	statistical p-value	v_t	terminal settling velocity
Q	volumetric flow rate entering bioreactor	X	biomass concentration in bioreactor
Q_{feed}	volumetric flow rate of feed	X_e	biomass concentration in effluent
Q_{HF}	volumetric flow rate through one hollow fiber	X_{RAS}	biomass concentration in RAS
Q_{perm}	volumetric flow rate of permeate	x	chord length size (bin)
Q_{WAS}	volumetric flow rate of WAS	x	distance along boundary layer
R	radius of hollow fiber lumen	x	distance along length of hollow fiber
R_0	observed rejection coefficient	\tilde{x}	chord length distribution median
R_a	actual rejection coefficient	z	depth in CLSM
R_c	cake resistance	α	specific cake resistance
R_f	foulant resistance	α	statistical level of significance
R_j	arbitrary resistance	α_c	specific cake resistance at reference pressure
R_m	intrinsic membrane resistance	β_0, β_1	compressible cake fouling model constants
R_n	number-based observed rejection coefficient	γ_0	shear rate at membrane interface
r	membrane pore radius	$\Delta(\cdot)$	change in (\cdot)
r	radial distance inside hollow fiber lumen	ΔP	pressure drop
Re	Reynolds Number		
S_0	observed sieving coefficient		
S_a	actual sieving coefficient		
t	time		
V	bioreactor volume		

ΔP_0	initial TMP
ΔP_c	pressure drop across cake
δ	boundary layer thickness
δ_c	cake layer thickness
ϵ	model residuals
ε	membrane (surface) pore density
ε_c	cake porosity
η	removal efficiency
λ	ratio of particle to pore radius
λ_{em}	emission wavelength
λ_{ex}	excitation wavelength
μ	fluid viscosity
ρ	density
ρ_f	fluid density
ρ_{MB}	microbead density
ρ_p	particle density
σ	standard deviation of log-normal distribution
φ	particle sizing model function

Declaration of Academic Achievement

This work has been written in the format of a “sandwich-style” thesis. The four research studies in Chapters 3–6 are either already in press, in submission, or in preparation for submission. The majority of efforts towards the completion of these works were my own: I was responsible for the conceptualization and planning of the research studies, the development and validation of new experimental methodologies, the collection, analysis, and visualization of data, the preparation and revision of manuscripts, and the supervision of undergraduate research assistants. This work was performed under the supervision of *David R. Latulippe* who contributed via the conceptualization and planning of the research studies, the review of results and project manuscripts, as well as the acquisition of resources and project funding. Other contributions are highlighted, below.

■ **Chapter 3:** Ryan J. LaRue, Blake Patterson, Susan O’Brien, and David R. Latulippe, “Evaluation of Membrane Fouling by Microplastic Particles in Tertiary Wastewater Treatment Processes,” *ACS ES&T Water*, vol. 2, no. 6, pp. 955–966. *In Press*.

Blake Patterson participated in the planning of this study, the development of experimental methodologies, and facilitated the collection of data from a portion of the filtration experiments. *Susan O’Brien* contributed to the collection of data from a portion of the filtration experiments. *Dan Walsh* and *Jocelyne McPhedran*, under the supervision of *Youliang He*, generously volunteered to mill/sieve the polyethylene feedstock according to the parameters which I derived.

■ **Chapter 4:** Ryan J. LaRue, Ashleigh Warren, and David R. Latulippe, “Effect of membrane pore size on the transmission of irregularly-shaped microplastic particles in a microfiltration process” *In Submission*.

Ashleigh Warren participated in the planning of this study and the development of experimental methodologies, plus contributed to the collection, analysis, and visualization of data from a portion of the filtration experiments. *Dan Walsh*, under the supervision of *Youliang He*, generously volunteered to mill/sieve the fluorescent polyethylene feedstock according to the parameters which

I derived. *Matthew McClure* performed data collection and analysis regarding the measurement of membrane surface charge.

■ **Chapter 5:** Ryan J. LaRue, Samuel Koo, Ashleigh Warren, Yves G. Mckay, and David R. Latulippe, “Flow Cytometry as a Powerful Tool for *In Situ* Quantification of Micrometer-Scale Microplastics in Membrane Filtration Processes” *In Preparation*.

Samuel Koo contributed to the conceptualization of the study and the development of the experimental methodologies. *Ashleigh Warren* contributed to the collection and visualization of a portion of the data from filtration experiments. *Yves G. Mckay* contributed to the analysis of data from microscopy experiments.

■ **Chapter 6:** Ryan J. LaRue and David R. Latulippe “Microfiltration Membrane Performance Assessment for the Removal of Microplastics from Tertiary Wastewater: Scaling-Up to a Hollow Fiber Module.” *In Preparation*.

Microplastics: Small Particles, Big Problem?

*F*OR BETTER OR FOR WORSE, the world has entered the “*Plasticene age*” [1] owing to the widespread use—and misuse—of synthetic plastic materials. It is hard to understate the ubiquity of these materials in modern life. Plastic products have seen an exponential increase since the 1950s, with the annual global output reaching approximately 300 million tons in 2013 [2]. A 2016 estimate of global plastic production yields a value exceeding 320 million tonnes [3], a figure which is expected to *double* over the next 20 years [4]. This sheer ubiquity stems for the low cost of plastics in conjunction with their wide range of advantageous physiochemical properties. Ironically, it is often the low cost and some of the advantageous properties engineered into these materials which are direct contributors of their negative consequences. One estimate suggests that 40% of the plastic that is produced is consumed in single-use applications [3], leading to an enormous amount of plastic waste. Unfortunately, it is estimated that only 6–26% of the plastic is recycled with the balance disposed of (*e.g.* landfills) or released into the environment through a large number of possible transport pathways [5]. Figure 1.1 summarizes various routes of transport of plastic materials into the environment. Plastic debris routinely enters the *aquatic* environment through either haphazard disposal or hydrological transport phenomena [6, 7]. Relative to the annual quantity of plastic produced annually, a significant fraction is believed to be lost to the aquatic environment where it persists for long periods of time; by 2025, it is estimated that a total of 250 million tonnes of plastic waste will have accumulated in this environmental compartment [8].

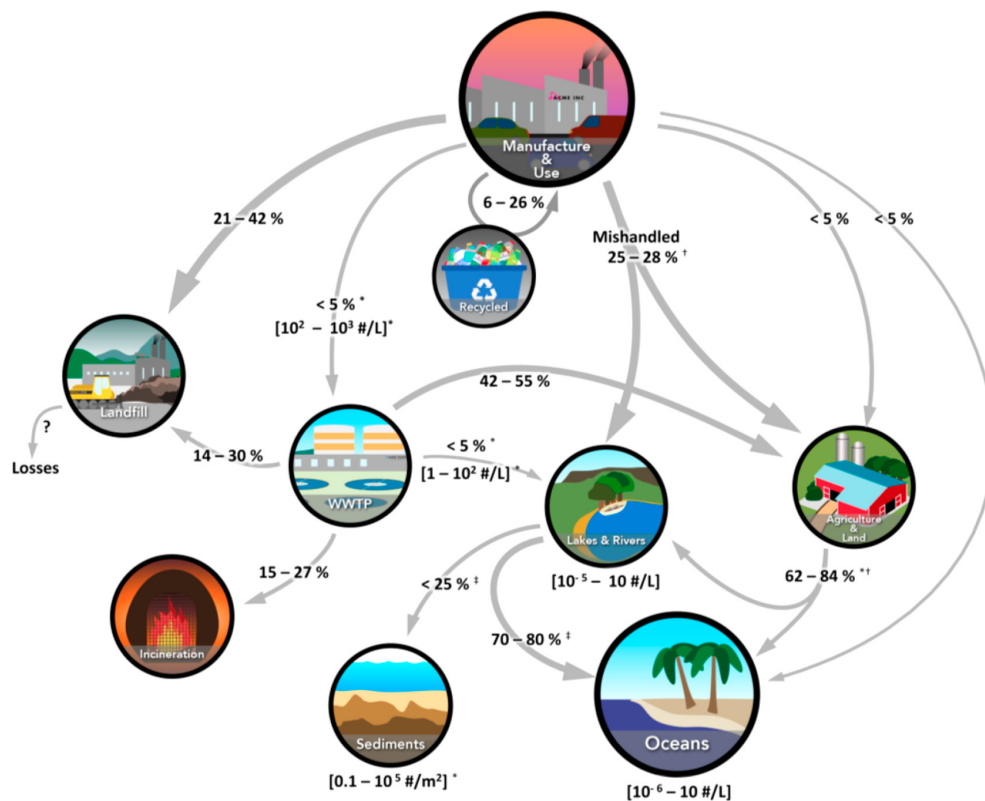


Figure 1.1: Illustration of various transport pathways for plastic materials entering the natural environment. *Only considers plastics < 5 mm in size. †Mishandled fractions are assumed to divide between two compartments. ‡Values presented are “best estimates” in the absence of concrete data. Figure reprinted with permission from O. S. Alimi, J. F. Budarz, L. M. Hernandez, and N. Tufenkji, “Microplastics and Nanoplastics in Aquatic Environments: Aggregation, Deposition, and Enhanced Contaminant Transport,” *Environmental Science & Technology*, vol. 52, pp. 1704–1724, 2018.

Initial concerns regarding plastic debris found in the oceans emerged in the early 1970s, but these first reports were largely ignored [6]. Since then, significant research has been undertaken to assess the ecological impact of plastic debris in the aquatic environment. Evidence has been produced which demonstrates that plastic pollution presents a substantial ecological threat on a global scale, partially owing to its poorly-degradable nature [2]. The consequences of marine “macroplastic” pollution—particles which are visible to the naked eye—are well-documented in the literature, and range from the effects of entanglement to the consequences of ingestion [6], among a large number of other effects. Some researchers suggest that this threat caused by mismanaged plastic waste in the aquatic environment shares a similar magnitude with the threat posed by climate change on ecological health moving into the future [9, 10].

While the field of aquatic *macroplastic* pollution is well-developed, Hidalgo-Ruz *et al.* (2012) note that additional concerns regarding *microplastic* pollution only recently gained serious attention—despite the fact that plastic “micro-debris” was documented in studies as early as the 1970s [11, 12]. In 2004, Thompson *et al.* termed the minute (*e.g.* sub-millimeter) plastic particulates in ocean water/sediments that they collected as “microplastics” [13] and accordingly, concern regarding these environmental microplastics as a *unique* form of pollution burgeoned. Since then, particles have been detected in both freshwater and seawater worldwide [9], along with other environmental compartments such as the atmosphere and soils [14]. Just like their larger macroplastic counterparts, microplastics are *ubiquitous* in the aquatic environment: they have been detected globally, from the most densely populated urban locations to the remotest arctic waters [15].

Concern regarding the *effects* of microplastic pollution has also proliferated since 2004, as will be detailed in §1.1.2–1.1.3. As a brief overview, it has been found that the size, properties, and ubiquity of these particles produce a persistent biological hazard in marine ecosystems. Numerous researchers have produced studies that document the wide-reaching negative ecological consequences that are associated with microplastic pollution [2, 6, 9, 11, 16–19]. These consequences also extend to humans. Microplastics have been found in the water that we drink and the seafood that we eat (*e.g.* shrimp and bivalves like mussels); as such, potential effects may impact human health, commercial interests such as fisheries, and the broader economy [2, 19–21]. To this end, efforts are underway to curb the introduction of microplastics into the aquatic environment.

1.1 Introduction to Microplastics

As is implied in the name, microplastics are small plastic particles. However, the *exact* size definition of what constitutes a “microplastic” is still up for debate. Disagreement runs rampant. For example, considering a small subset of review articles on the subject:

1. Various researchers such as Rocha-Santos *et al.* (2015), Eerkes-Medrano *et al.* (2015), Gatidou *et al.* (2019), and Sun *et al.* (2019) suggest that any plastic particle whose major dimension is smaller than 5 mm in size is a microplastic [7, 9, 16, 22]. This is ostensibly the most common definition when describing MPs.

2. In contrast to “common practice”, Avio *et al.* (2017) cite a different upper size limit: 1 mm [2].
3. Further, Enfrin *et al.* (2019) use a different definition with a fixed lower size limit: microplastics are 1 μm to 5 mm in size, whereas plastic particles smaller than 1 μm are “nanoplastics” [23]. A report by Koelmans *et al.* (2019) concurs with this assessment [20].
4. As a hybrid of the previous two approaches, Gao *et al.* (2023) write that microplastics are between 1 μm and 1 mm in size, whereas particles less than this 1 μm lower limit are referred to as nanoplastics [24].
5. Alimi *et al.* (2018) suggest additional size categories: *macroplastics* are greater than 25 mm in size, while *mesoplastics* are 5–25 mm, whereas *microplastics* fall in the range of 0.1 μm –5 mm [sic], and finally *nanoplastics* are less than 0.1 μm in size [5]. Bretas Alvim *et al.* (2020) agrees with the above definition of a “microplastic” [25].

Clearly, there are a variety of different possible definitions with respect to the size of a microplastic. In this work, pursuant to what appears to be “common practice”, all small plastic particles $\lesssim 5$ mm will be referred to as “microplastics” and abbreviated as “MPs”. While the upper size limit for MPs is fairly well established, the same cannot be said for the boundary between micro- and nanoplastics (NPs). As such, no particular distinction will be assumed in this work and the term “MP” will be used universally—*except* when a distinction between MPs and NPs is strictly necessary.

1.1.1 Classifications of Microplastics

Any given survey of the current literature will indicate that MPs vary drastically in size, shape (morphology), density, colour, and chemical composition/identity [25]. Critically, *there is no scientific consensus on the proper standards by which MPs are characterized*, from sample collection, to analysis, to the nomenclature used. Researchers such as Mintenig *et al.* (2017) invariably lament that a standardized system for sampling, isolating, and verifying the identity of MPs in samples is urgently required so that the results from individual studies can be effectively compared and summarized [26]. Contemporary studies of MPs in WWTPs often characterize these strongly heterogeneous particles based on some form of the following criteria:

■ **Morphology.** The appearance of the particle, namely its shape. There is no standardized nomenclature describing the shape of MPs and the assessment of MP morphology is subjective. A non-exhaustive series of MP morphology descriptors includes: fibers, particles, beads, pellets, ellipses, fragments, granules, lines, foams, films, sheets, and flakes [14, 16, 22]. While clearly a large number of descriptors exist, these terms can be reduced to the five “main” or most commonly used categories underlined above. *Fibers* are typically high-aspect-ratio thread-like MPs. *Beads* are (somewhat) smooth, rounded particles that approximate the shape of a sphere. In contrast, *fragments* are typically particles of irregular shape with faces and jagged edges. They can result from the breakdown of other particles like beads. *Foams* are like fragments or beads, but are porous in nature. *Films* are thin, flat MPs which approximate a two-dimensional surface. Finally, MP colour is also sometimes considered (*e.g.* [27]) as an adjunct descriptor of MP appearance.

■ **Size.** Characterization of the dimensions of the MP. In the majority of studies that are commissioned, the “size” refers to the *major dimension* of the MP. Categorizing MPs by a single dimension fails to consider that the particles are often highly irregular (*i.e.* long and narrow fibers; flat films), misrepresenting the nature of these particles. An exception to this common practice can be seen in a study by Simon *et al.* (2018) who considered both the major and minor dimensions of the MPs which were analyzed [28]. Like their shape, MPs tend to be polydisperse in terms of their size; measuring individual MPs in a given sample yields a distribution of sizes, as is clearly seen in the literature [16]. To this end, Kooi & Koelmans (2019) write that log-normal distributions are commonly applied to describe particle sizes in the aquatic environment, though they assert that MP particle size may be particularly well-approximated via a power-law distribution due to the propensity for the MPs to fragment into smaller sizes [29].

■ **Source.** Characterization of MPs based on where they are created. *Primary MPs* are manufactured to have a size in the “MP range”, while *secondary MPs* are generated when larger plastic particles are fragmented [11]. Prata *et al.* (2018) assert that common sources of primary MPs include abrasive microbeads found in toothpastes, body washes, exfoliant scrubs, cosmetics, airblasting abrasives, glitter, and raw plastic pellets from polymer manufacturing facilities [30]. For example, between roughly 4,000–94,500 microbeads can be released in a single use of exfoliating wash or

toothpaste [30–32]. Further, secondary MPs are created when fibers are shed from synthetic textiles such as during washing, or particles of macroplastics/other microplastics are degraded by physical (*i.e.* abrasive), chemical (*i.e.* thermooxidative, hydrolytic, photolytic), or biological means [6, 30]. A significant volume of research has been performed to understand the formation mechanisms of these secondary MPs. For example, research studies have suggested that a single synthetic garment can release anywhere from 1,900–1,000,000 MP fibers during washing; laundry loads roughly 5–6 kg in size have been found to release upwards of 6,000,000 fibers, depending on the properties of the textiles and the conditions at which the garments were washed [30]. Enfrin *et al.* (2019) provide an excellent summary of chemical mechanisms resulting in the formation of secondary MPs [23]: briefly, the exposure of polymers like polyethylene, polypropylene, polystyrene, and polyethylene terephthalate to UV light and/or water can cause oxidation of the plastic over time. These oxidative processes are accelerated by higher temperatures (*e.g.* hot weather) and solar irradiation [6]. Some polymers with heteroatoms like polyurethane and polyester are particularly susceptible decomposition via hydrolysis [23]. Enfrin *et al.* (2019) assert that hydrolysis/oxidation leads to cracks, fissures, and pits on the plastic particles which can propagate and cause embrittlement. Exposure to subsequent mechanical stresses such as friction, abrasion, or shear can induce the particles to break apart into MPs or even NPs. The formation of secondary MPs is a complex process, subject to prevailing environmental conditions and the physicochemical properties of the plastics, themselves [23].

■ **Composition.** The chemical identity of the MP particle. To this end, a large number of different polymers have been detected in samples. For example, Sun *et al.* (2019) documented that at least 31 MP polymers have been reported in municipal wastewater, alone [16]. The most commonly-seen polymers were found to be polyester (PEst), polyethylene (PE), polyethylene terephthalate (PET), and polyamide (PA); other MP polymers included polypropylene (PP), polystyrene (PS), polyurethane (PU), polyvinyl chloride (PVC) and polycarbonate (PC) [2, 16]. The morphology, source, and composition of MPs are often linked: polyester or polyamide (nylon) chemistries are often noted in MP fibers from textiles, and fragments from cosmetic products are often composed of polyethylene [30]. As will be made apparent, the specific surface chemistries of MPs are affected and altered by the adsorption of other species, weathering/aging, and other phenomena [5, 22, 24, 33].

From data and images collected by previous researchers (*e.g.* [27, 34–36]), it is critical to note that MPs are very often highly irregular in shape, and diverse in size/composition. Images of a diverse subset of MPs are shown in Figure 1.2.

1.1.2 Microplastics in the Aquatic Environment

The massive scale of MP pollution in the aquatic environment can be difficult to comprehend. MPs have been detected in surface waters, in pelagic/benthic zones, and directly in sediments [2]. One very recent estimate suggests that as of 2019, the surface layer of the world’s oceans contains 82–358 trillion plastic particles (average = 171 trillion particles), the majority of which are expected to be MPs [37]. From this study, the total amount of plastic is expected to weigh 1.1–4.9 million tonnes (average = 2.3 million tonnes). However, these figures are almost certainly gross underestimates of the *actual* amount of MPs present as they proceed from an array of studies which use sampling techniques that consider only the very surface of the ocean (*i.e.* < 1 m in depth). Via a similar set of

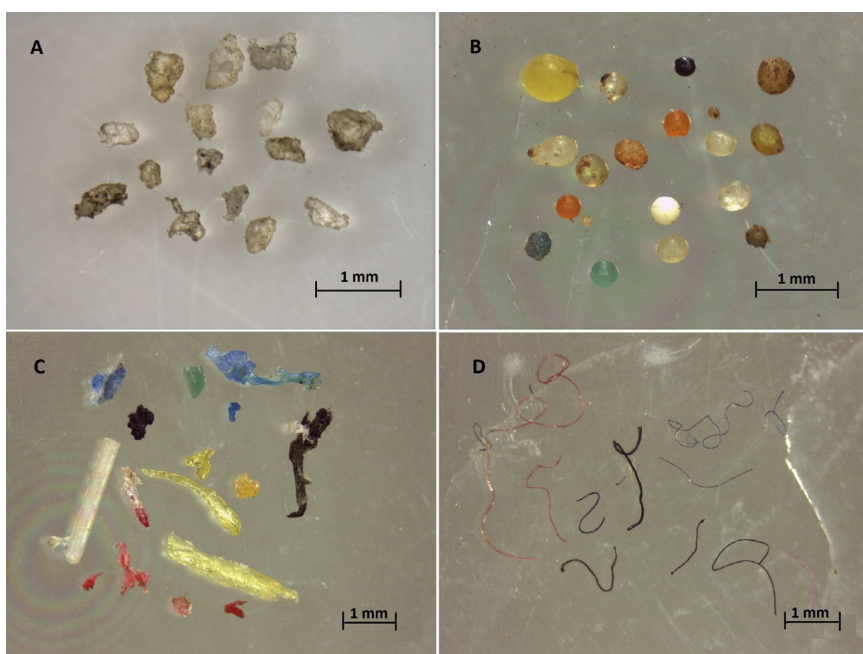


Figure 1.2: Images of various morphologies of MPs obtained via optical microscope. (A) Primary fragments/granules. (B) Primary beads/pellets/spheres. (C) Secondary films/sheets. (D) Secondary fibers. Image reproduced and used with permission from J. Talvitie, A. Mikola, A. Koistinen, and O. Setälä, “Solutions to microplastic pollution—Removal of microplastics from wastewater effluent with advanced wastewater treatment technologies,” *Water Research*, vol. 123, pp. 401–407, 2017.

measurements, significant quantities of MPs were observed in surface waters of the Great Lakes (average = 4.30×10^4 MPs/km²) [38] and within the water columns of various oceans/seas [39–42]. As another example, Zhao *et al.* (2014) recorded an average abundance of 4,137 MPs/m³ in the Yangtze Estuary which decreased to 0.167 MPs/m³ in the coastal waters of the East China Sea [43]. While these reports highlight the significant quantities of plastic particles present at the surfaces of water bodies, it is important to note that MPs have been measured in pelagic and benthic layers [11], in shallow estuary/subtidal sediments [13], in deep-sea sediments [44], as well as in shoreline sediments worldwide (*e.g.* 8–124 MPs/L of sediment) [17]. Transfer of MPs between zones is known to occur via various oceanographic processes, currents, wind, storms, and so on [2, 5]. As such, limitations imposed by the quantification techniques used lead to an incomplete picture of the amount of MPs present within the entire volumes of water bodies.

The release of MPs—or their *in situ* formation—in the aquatic environment is expected to cause significant environmental harm. A large body of research has been produced to document the negative potential ecological consequences of MPs [2, 6, 9, 11, 16]. To exacerbate the situation, the chemical stability of plastic materials means that they could be present in the environment for hundreds or even thousands of years [45], prolonging their ability to cause damage to aquatic ecosystems. The concerns are broadly associated with three main factors [46]:

1. MPs may be ingested if organisms confuse them with natural food sources;
2. Additives to the plastic materials can leach and affect exposed organisms; and
3. The particles can interact with a variety of environmental contaminants (*e.g.* via sorption).

Evidence exists demonstrating negative biological effects of MPs can result from both physical and chemical interactions with organisms. The ingestion of MPs (Factor 1) can directly lead to physical impacts and can also provide a route by which chemical impacts (Factors 2–3) can occur. The following is a brief summary of the consequences associated with MPs in the aquatic environment, although it must be disclosed that the risks associated with MP exposure towards various aquatic organisms remain poorly understood [46].

MPs relate to ecotoxicological effects in biota through direct ingestion as they can be a similar size as planktonic species—a common marine food source [7]. All else equal, smaller MPs are ex-

pected to be more harmful towards aquatic life than larger MPs [47, 48]. Ingestion of these MPs has been found to affect a wide range of species ranging from zooplankton, benthic vertebrates and molluscs, and even fish, amphibians, reptiles, and seabirds [25, 49, 50]. Negative effects directly stemming from the ingestion of MPs include: dilution of nutrients, alterations to feeding habits (*e.g.* pseudo-satiety), and physical damage via accumulation, blockages, and/or abrasion in the digestive tract [51]. Further research has shown that the presence of MPs can lead to inflammation and varied immune reactions. Even short-term exposure of some organisms to MPs (*e.g.* *Mytilus edulis*; 96 h; PE MPs) has shown to cause negative effects such as the growth of granulocytomas as a self-protection mechanism [52]. However, other organisms appear resistant to the effects of MPs. For example, isopods (*Idotea emarginata*) continuously exposed to three different types of MPs over a variety of concentrations saw no negative effects; no accumulation of the MPs in their digestive tracts was observed, either [53]. The consequences associated with the ingestion of MPs are exacerbated by the inclusion of additives which can leach into an organism's body. The polymers which make up MPs can release monomers or additives (*e.g.* plasticizers, fire retardants, antibacterials, etc.) such as phthalates, bisphenol A, polybrominated diphenyl esters, and alkyl phenols. These chemicals are known to be either toxic, endocrine-disrupting, carcinogenic, and/or mutagenic [5, 7, 46]. In addition to the aforementioned consequences, researchers have noted acute or chronic effects including, fertility problems, reproductive failure, oxidative stress, reduced growth rates, disturbances in the production of enzymes, and apoptosis [2, 18, 19, 50, 51, 54, 55]. Yet, Ziajahromi *et al.* (2016) rightly caution that experimental evidence with respect to the role of additive leaching on the health of organisms is limited [46]. Overall, it is expected that the observed consequences depend on type of organism, the concentration of MPs to which the organisms are exposed, the MP properties, and the exposure time [46, 51].

Alimi *et al.* (2018) write that MPs can act as both sources and sinks for environmental contaminants [5]. Due to their hydrophobic properties [56] and enormous surface area-to-volume ratios [23]—especially as particle size decreases—MPs can absorb and concentrate bioactive persistent organic pollutants (POPs). These include per- and polyfluoroalkyl substances (PFAS), polychlorinated biphenyls (PCBs), polycyclic aromatic hydrocarbons (PAHs), pharmaceuticals, antibiotics, heavy metals (*e.g.* Cd, Cr, Cu, Pb, Zn), pesticides, microbes, and a large number of other pollutants [5, 51, 56, 57]. In fact, MPs have shown to concentrate POPs by up to a factor of 10^6 [7].

The sorption (*i.e.* absorption and/or adsorption) and desorption characteristics of these contaminants is known to be a strong function of surface MP properties (*e.g.* hydrophobicity, specific surface area, etc.), solution conditions (*e.g.* salinity, temperature, etc.), and the presence of other substances such as natural organic matter [5, 56, 57]. For more information on the sorption of contaminants by MPs, the reader is referred to the plethora of studies in the contemporary literature which consider the subject [5, 56–58]. However, it should be noted that the literature currently lacks a good understanding of the *desorption* of contaminants from MPs. While it is well-understood that many contaminants can very readily partition onto MPs, some adsorption is found to actually be poorly reversible or completely irreversible [56]. For example, Razanajatovo *et al.* (2018) found that the antibiotic sulfamethoxazole bound irreversibly to PE MPs under the conditions that were tested [59]. Similarly, the desorption of various hexachlorocyclohexanes (*i.e.* POPs) was very slow in simulated intestinal fluids [60].

Overall, the contemporary literature suggests that there are serious consequences associated with MPs, their additives, and the pollutants which can use the MPs as vectors for transport within/between environmental compartments. Enfrin *et al.* write that such consequences are expected to be worse for NPs compared to MPs [23], though the concentrations of NPs in the environment are not yet definitively characterized [5]. Furthermore, the effects of long-term bioaccumulation and trophic transfer of MPs/NPs, their additives, and associated pollutants are concerning from an environmental perspective [9, 16, 17]. While there is substantial documentation in the literature regarding the negative effects of these particles on small groups of organisms, however, it not clear how these effects translate across entire species, ecosystems, and so on. Clearly, additional research is needed to investigate these concerns and address the large gaps in knowledge that still exist.

1.1.3 Microplastics & Human Consequences

In comparison with the effects of MPs in the environment, the health implications of MPs for humans is particularly poorly understood. Humans are exposed to MPs via inhalation and ingestion, though the consequences of this exposure are largely unknown, but expected to be dependent on the dose [20]. Wright and Kelly (2017) write that MPs may be inhaled via aerosols generated by coastal surf, via the wind-driven transport of MPs, from indoor exposure in polymer manufacturing,

and from the atmospheric fallout of MPs in the form of microfibers or particles from tires [3]. As previously stated, MPs are transferable between ecosystem trophic levels, [9, 17] and into seafood consumed by humans. Wright and Kelly (2017) summarize that the ingestion of MPs by fish—including commercial species—is widely reported in the literature, however, the mere existence of MPs in the gastrointestinal tract of fish is not immediately a cause for concern as humans do not typically consume these parts of the fish [3]. However, translocation of the MPs within the animal may be a greater cause for concern and could serve as a route by which humans could consume the MPs. Perhaps a more likely route of MP ingestion by humans is through the consumption of shellfish such as mussels. Again, the authors note that there is ample research which details how bivalves—including those intended for human consumption—capture and ingest MPs [3]. From the findings of one study, it is estimated that Chinese seafood consumers are exposed to hundreds of thousands of MPs annually [61]. Perhaps unsurprisingly, one study reported that certain store-bought sea salts contain up to 681 MPs/kg of salt [62]. Both samples of honey and sugar have been found to contain MPs [63] which may imply that the MPs in these foods are of atmospheric origin [3]. Tap water (< 61 MPs/L), bottled water (< 35,436 MPs/L), and unfortunately beer (< 109 MPs/L) have also been found to contain MPs of various sizes and shapes [20, 64–66], though the former two categories see a large variation in MP concentrations depending on the sample.

Determining the health effects of MPs on humans is difficult. The limited data that is available—often informed by animal models—suggests that likely effects from the accumulation of MPs would involve an immune response, inflammation, genotoxicity, oxidative stress, cell apoptosis, and/or necrosis [3, 20]. Perhaps though, the most likely source of harm to human health with respect to MPs involves the leaching of toxic additives or the desorption of contaminants from the particles, as described in §1.1.2. Briefly, it is known that many of the additives in plastics such as PVC cause health effects in humans, including reproductive harm (*e.g.* phthalates and bisphenol A), carcinogenicity (*e.g.* monomers like vinyl chloride), and mutagenicity (*e.g.* benzene) [3]. PVC is a particularly worrisome example as it can contain upwards of 80% plasticizer by weight, often di(2-ethylhexyl) phthalate, which can cause reproductive harm and disrupt hormones in the body [3]. However, the effects associated with these toxins are dose-dependent, and even a given person’s exposure to MPs is largely unknown.

MP transport from the digestive tract (or lungs) further into the body would facilitate both bioaccumulation and the potential for enhanced toxicity. Unfortunately, the use of animal models suggests that uptake in humans is plausible. In early research, ingested MPs such as PS latex particles (60 nm or 1–2.2 μm) have shown to undergo uptake and translocation into the lymphatic system via Peyer’s patches in the small intestines of rats and mice [3, 67, 68]. Furthermore, it has been noted that the persorption of microparticles up to 130 μm in size can occur whereby the particles are mechanically “kneaded” from the gastrointestinal tract into the circulatory system at desquamation zones [3]. For example, this phenomenon has been studied using probes such as PVC microparticles (*e.g.* 5–110 μm in size) in mammalian species including rats, rabbits, guinea pigs, dogs, and pigs [3, 69]. The ingestion of large quantities of PVC microparticles (~ 200 g) by dogs resulted in the detection of 10–15 particles/mL in blood as well as in various quantities in urine, bile, and cerebrospinal fluid; PVC microparticles were also isolated from the livers of rats following exposure [69]. In another study, PS particles (50 nm) ingested by rats were later found in their livers, spleens, and bone marrow [70]. Persorption of starch microparticles has even been shown in humans [3]. These results point to the transport of MPs within the body.

Recently, the development of sensitive MP quantification techniques has enabled researchers to search for the presence of MPs within the human body. A study by Ragusa *et al.* (2021) reported that a small number of MPs were detected in four of six human placentas that were analyzed [71]. A very recent study by Leslie *et al.* (2022) detected—for the first time—the presence of plastic particles in human blood: an average concentration of 1.6 $\mu\text{g}/\text{mL}$ was measured [72], although this value seems to be questionably high. Furthermore, the effects of NPs are starting to be considered. These particles may be particularly threatening due to their exceptionally small size and enormous specific surface areas; preliminary evidence suggests that some NPs are more toxic in the presence of organic materials [73, 74]. Currently, the pathways by which humans are exposed to MPs/NPs and their possible health consequences are just starting to be investigated. It is likely that any toxicity associated with the particles will occur cumulatively, which is fortunate because it is expected that the concentrations to which we are exposed remain relatively low [3]. Considerably more research is necessary with respect to the effects of these particles on humans.

From a contrasting purely economic standpoint, MP pollution presents significant negative consequences. The presence of MPs in seafood introduces uncertainty with respect to commercial interests [2, 19] due to the potential human health implications. By one estimate, the United Nations Environment Programme found that MP pollution is costing \$13 billion annually due to the outlays associated with shoreline clean-up, economic, and environmental damages [2]. Accordingly, there is *some* interest in combating MP pollution. As summarized by Avio *et al.* (2017), a wide range of organizations have commissioned programs to mitigate marine plastic debris, including the United States National Oceanographic and Atmospheric Administration (NOAA; *Marine Debris Program*), the European Union (EU; *European Marine Strategy Framework Directive 2008/56/EC*), the signatories of the Barcelona Convention (*2013 Marine Litter Regional Action Plan*), science ministers of the G7 nations (*Action Plan to Combat Marine Litter*), and so on. These initiatives are designed to address the complex ecological issues and uncertainties associated with plastic pollution with the goal of mitigating/remediating the potential environmental consequences [2]. The United States, United Kingdom, and Canada have all banned the manufacture and usage of microbeads in consumer products [50]. In Canada, current regulations have focused on merely limiting the consumption of single-use plastics and products that contain MPs (*e.g.* Canada’s *Microbeads in Toiletries Regulations* [75]) instead of regulating their discharge. However into the future, it is entirely foreseeable that fugitive MP emissions will be regulated.

1.2 Municipal Wastewater Treatment Plants as a Source of Microplastics

Pursuant to the diagram previously presented in Figure 1.1, MPs find their way into the aquatic environment from a variety of sources, typically classified as either “aquatic-based” or “land-based”. The former category describes the *in situ* formation of MPs (*i.e.* secondary MPs) from the breakdown of larger plastic objects such as fishing nets or other plastic debris like bags, bottles, and ropes [5, 46]. In terms of the land-based sources, terrestrial MPs, soil-bound MPs (*e.g.* in farm fields), or MPs from landfills may enter the aquatic environment from run-off following precipitation. MPs lifted by the wind may be blown into the water or settle via atmospheric deposition [14, 46, 51]. Notwithstanding these transport routes, *one major source of MPs in the aquatic environment is from the effluents of wastewater treatment plants* (WWTPs) [14, 16, 22, 24, 50, 57, 58], although the relative contributions of these routes is not settled science. For example, Krishnan *et al.* (2023) assert that the majority

of MPs that reach the environment originate from sewage water and wastewater [50]. Zhang *et al.* (2020) are more explicit and suggest that 80% of MPs in the aquatic environment originate from WWTPs [57], although their figure *cannot be verified*. However, a report commissioned by the International Union for Conservation of Nature and Natural Resources (IUCN) suggests that 25% of the primary MPs in the oceans originate from WWTP effluents [76]. This is perhaps a more reasonable estimate of the role of WWTPs in the efflux of MPs into the aquatic environment. However, the assertions of Ziajahromi *et al.* (2016) likely best describe the current state of knowledge: “there is a lack of quantitative estimation on the relative contribution of different sources to the total concentration of microplastics in the aquatic environment [and] the contribution of microplastics released via wastewater effluent compared to other sources is largely unknown” [46].

Part of the uncertainty surrounding the role of WWTPs on the occurrence of MPs in the aquatic environment may stem from the observation that studies on this subject are not definitive and results vary quite significantly. In their review of 17 such treatment facility studies, Barchiesi *et al.* (2021) noted the concentrations and characteristics of MPs upstream and downstream of WWTPs [21]: in 11 of the studies, there was a significant change in the abundance and/or type of the MPs downstream from the WWTP, providing a strong linkage between the facility and the environmental MPs. Three other studies—to some degree—demonstrated a linkage between the facility and the MPs in the aquatic environment, while in the last two studies, no linkage could be shown. In one of these last two studies, the MP concentration was actually higher upstream of the WWTP [21]; anecdotally, this may be a consequence of the dilution of natural waters by the WWTP effluent. While more research is clearly required, these results appear to indicate that certain WWTPs act as more of a source of MPs than others.

The importance of WWTPs as a route of MP transport into the aquatic environment is corroborated by MP efflux figures from studies of various facilities. Researchers have recorded the presence of MPs in the influents of all WWTPs that have been studied as well as the vast majority of WWTP effluents [16, 22, 24, 33, 77]. However, the quality of the incoming wastewater, the characteristics of the incoming MPs, the methods used to collect, identify, and quantify the MPs, in addition to other factors all drive the occurrence and fate of MPs within WWTPs [57]. In absolute terms, effluent MP concentrations from WWTPs may appear to be low ($\ll 1$ MP/L in some cases [78–81]),

but the considerable volumes of wastewater that are processed in many facilities means that the total *number* of MPs that are released into the aquatic environment can be substantial. For an idea of the magnitude of these numbers, the reader is referred to Table 1.1 later in this chapter. As a series of examples, a Canadian WWTP which treats 500 million liters of wastewater per day (MLD), on average, was estimated to release 32–97 million MPs/day (30 billion MPs/year) into the environment [80]. By contrast, a much smaller Chinese WWTP that treats 30 MLD was found to emit ~489 million MPs per day (~178 billion MPs/year), most of which were MP fibers [82]. Interestingly, an Israeli facility with the same average capacity was estimated to release only 59 million MPs per day (21.9 billion MPs/year)—a substantially lower efflux [48]. From the literature, reports assessing the daily emissions of MPs range from ~0 to almost 140 billion MPs/day [32, 83], though the reasonableness of this upper limit may be in question as one estimate of the efflux of MP particles from *all* American WWTPs ranges from 30–47 trillion particles per year (2,000–3,200 tonnes annually) [84]. Based on a study of an American WWTP, Conley *et al.* (2019) estimate that 0.34–0.68 g of MPs per capita are released into the aquatic environment each year [85]; this corresponding figure is 0.56 g of MPs per capita per year in a study by Simon *et al.* (2018) [28]. These last two estimates are one order in magnitude lower than a per capita estimate provided by Koutnik *et al.* (2021).

Despite the conflicting data depending on the study that is considered, on a global scale, this suggests that significant efforts are needed in order to limit the total quantity of MPs from entering the aquatic environment via WWTPs. As such, these facilities will be the focus of this work.

1.2.1 MP Sampling & Quantification

As was previously mentioned, there is substantial conflicting information in the literature regarding the effluxes of MPs into the environment. When attempting to understand the fate of MPs within WWTPs, it is crucial to understand how the measurements of MP abundances are obtained. This is because “current practice” in the field does not utilize an overarching standard for the proper, collection, isolation, identification, quantification, and description of MP concentrations in water, wastewater, and biosolids samples. Individual studies utilize their own methodologies and terminologies to report shapes and sizes of MPs. Even an agreed-upon lower boundary for the size of MPs does not exist [20, 35]. Perhaps humorously, almost every study and review paper laments

the lack of standardization, yet no standard has been implemented in the field. With observational studies of WWTPs spanning roughly the last decade, it is now more clear than ever that this lack of standardization means that these investigations are loosely comparable, at best. Koelmans *et al.* (2019) remark that such standardization is necessary from the standpoints of reproducibility and comparability so that high-quality data is produced in order to conduct risk assessments [20]. Barchiesi *et al.* (2021) agree and assert that methodological standardization is necessary to actually advance our knowledge of MP pollution [21]. Bretas Alvim *et al.* (2020) are even more explicit [25]:

“Despite the intense efforts that have been directed towards the elaboration of methodologies of separation, quantification and identification of these emerging contaminants, no standard protocol is still applied in WWTPs. These methodological differences [make] difficult the comparison of the results among researchers. Therefore, the determination of efficient and rapid protocols for the study of MPs is extremely important, always considering steps that evaluate cross-contamination, either in the transport of samples or during analysis. In addition, the standardization of sizes (sieving, nets and filters), chemical digestion (acidic, basic, peroxidation or other), density separation (best solution to be used), visual separation (addition of staining dyes) and analytical techniques for chemical identification of the polymer, need to be optimized and applied in a standard manner.”

As a consequence of the lack of standardization, the results from WWTP studies are *dependent on the methodologies* which were used to collect the results. This is likely a large factor in the conflicting results that are seen between the aforementioned studies! Whether they are investigating natural water sources, wastewater, or other media, most researchers follow a general a three-step procedure—sampling, processing, and analysis (plus reporting)—which is illustrated in Figure 1.3; an expanded version created by Zhang and Chen (2020) can be found externally in their review article [58].

■ **Sample collection.** In most cases, MPs are collected from WWTPs in containers (grab-sampling), using dedicated autosampler devices, surface filtration nets, or via a pump with an *in situ* filtration device [24, 25]. Collected wastewater samples are then typically passed through a cascade of online or offline mesh sieves of varying sizes, depending on the sizes of MPs that are desired by

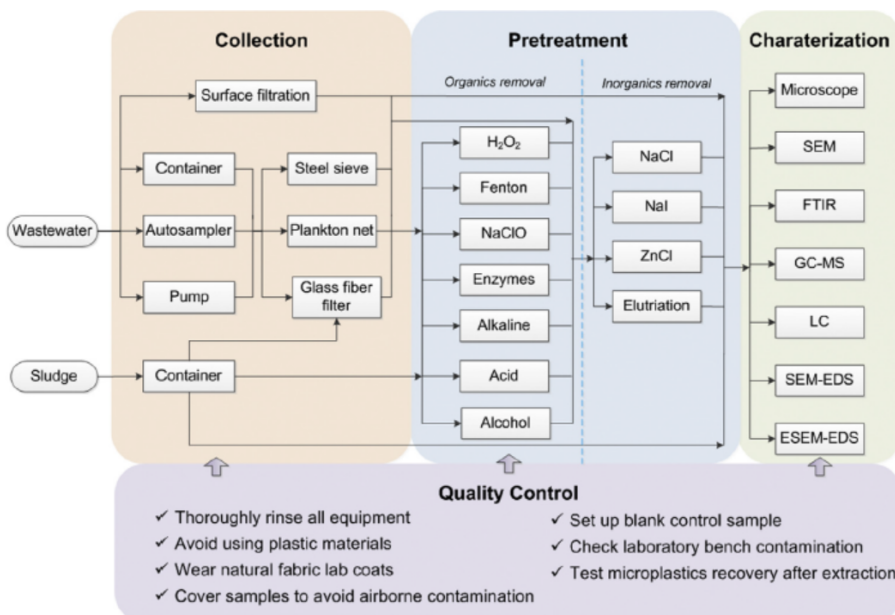


Figure 1.3: Simplified flowchart which summarizes various methods documented in the literature for the collection, isolation, and characterization of MPs in WWTPs. Image reproduced and used with permission from J. Sun, X. Dai, Q. Wang, M. C. van Loosdrecht, and B. J. Ni, “Microplastics in wastewater treatment plants: detection, occurrence and removal,” *Water Research*, vol. 152, pp. 21–37, 2019.

the researchers. Alvim Bretas *et al.* (2020) suggest that these sieves have openings roughly 38–4,750 μm in size, however, smaller sieve apertures are also seen (*e.g.* 10 μm [35]). Sun *et al.* suggest that the smallest sieve aperture is typically 20 μm [16]. Other studies by authors including Dris *et al.* (2015) and Leslie *et al.* (2017) directly filter the liquid through lab filters (*e.g.* a 0.7 μm Whatman glass filter) [86, 87], however these filters are significantly less porous and very susceptible to clogging via other organics in the wastewater. Clearly, the choice of the smallest sieve aperture and the other sieves in the stack affect the amount of MPs that are collected as well as how the MP size distributions can be reported.

The wastewater volumes collected also vary substantially, as reported by Bretas Alvim *et al.* (2020) who noted that sampled volumes could be as little as 0.05 L or as large as 21,000 L [25]. The danger with sampling very small volumes is that they may misrepresent MP concentrations in the large quantities of wastewater processed by these facilities, especially where the true MP concentrations are low [21]. The inherent limit of detection for MP analysis tools is improved when sample volumes are larger; Koelmans *et al.* (2019) recommends a minimum of 1 L of wastewater influent

and at least 500 L of sample for wastewater effluent to balance concerns related to the resolution of MP concentrations and the clogging of sampling apparatuses [20]. Intuitively, contamination by fugitive MPs [16] has a greater impact on small-volume samples, which is a substantial issue in MP quantification. To a similar end, the use of plastic vessels should be avoided when capturing and storing samples due to the possibility of contamination [20]; metal or glass vessels are good options. An excellent comparison of the advantages and drawbacks to MP sampling techniques in WWTPs is given by Gao *et al.* (2023) [24].

To illustrate the degree to which the sampling conditions can affect the results of MPs studies in WWTPs, Ben-David *et al.* (2021) analyzed wastewater samples from an Israeli WWTP using a “typical” process whereby the smallest-aperture sieve used was 20 μm , as well as an “extended” process where samples were passed through a 0.45 μm filter as the smallest-aperture collection device. Results indicate that 64.78 ± 18.88 and 1.97 ± 0.48 MPs/L were collected in the raw influent and plant effluent streams, respectively, under the “typical” sampling plan, while 129.67 ± 27.23 and 7.30 ± 1.08 MPs/L were collected in the raw influent and plant effluent streams, respectively, under the “extended” sampling plan [48].¹ This large difference in concentrations illustrates how the choice of sampling conditions can strongly affect the results of MP studies in terms of the number of MPs that are collected and their size distributions.

■ **Sample processing.** MPs suspended within the collected wastewater samples are distributed among other solids of both organic (*e.g.* cellulose, biopolymers, etc.) and inorganic (*e.g.* sand, clay) chemistries. In sample processing, the goal is to separate the MPs of interest from the other matter. Without such separations, the presence of contaminants can disguise the MPs, confound subsequent analytical techniques, or incorrectly contribute to the MP count if natural particles are not removed. Both physical and chemical extraction methods have been used [24].

Physical extraction can include a liquid-liquid extraction process using an oil, suitable to partition *hydrophobic* MPs [24, 80]. In tandem or as a separate process, a density gradient separation can be employed, using highly concentrated/saturated salt solutions like ZnCl_2 (density = 1.5–1.7 g/cm^3),

¹When quoting data in this work from Ben-David *et al.* (2021), “typical” MP concentrations are reported, unless specified otherwise.

NaI (density = 1.8 g/cm³), or less effectively, NaCl (density = 1.2 g/cm³) to float lighter MPs (typical densities = 0.90–1.6 g/cm³) to the top of the water column and settle denser sediments (~2.6 g/cm³) to the bottom of the water column [25, 26, 78, 81]. This is particularly effective for separating MPs from denser inorganics. During these processes, surfactants such as sodium dodecyl sulfate are sometimes used to help disaggregate suspended particles [26, 28]. Laboratory filtrations via filter papers, glass fibers, or membranes can be used at various times during processing to further isolate the solid MPs from the suspending water [25].

Chemical processes are also invaluable towards separating the MPs from organic matter by breaking down larger organic solids (while leaving the MPs intact), making it easier to isolate the MPs in later steps such as filtration. To this end, treatment of samples with acids, bases, oxidizing agents, and enzymes are all common methods by which MPs can be isolated [24, 25]. Acids such as HNO₃ and HCl have been employed (*e.g.* [49, 88, 89]); bases such as NaOH and KOH have similarly been used (*e.g.* [49, 89, 90]) during digestion steps. In a process sometimes termed wet peroxidation [16], oxidizing agents such as H₂O₂ (15–30%; *e.g.* [78, 91]) Fenton’s Reagent (H₂O₂ + Fe²⁺ @ pH ≈ 3; *e.g.* [35, 92]), or NaClO (*e.g.* [32]) are used for digestion instead [24, 25]. Finally, the treatment of samples via enzymes has been applied extensively [25], including: proteinase-K [49]; trypsin, collagenase, and papain [93]; cellulase [26, 28]; and protease with lipase [26]. Various combinations of these techniques can be used, where deemed effective or necessary [26, 28].

The effectiveness and suitability of these chemical techniques has been widely discussed in the literature. The goal of these techniques is to efficiently remove non-MP organic materials without substantially affecting the shape, size, chemistry, mass, or number of MPs present. However, studies have shown that chemical digestion of organics via acids/bases can damage or destroy the MPs, depending on the conditions that are used and the nature of the MPs. For example, various investigators have noted that while acids can be quite effective at destroying natural organic substances in samples, they can also damage the MPs by way of peak changes in Raman spectra, dissolution, loss of mass, colour changes, melting, and fragmentation [24, 25, 49]. Particularly affected plastics include PA, PU, PC, and expanded PS [25]. The specific chemistry and concentration of the acids used, the immersion time, and the digestion temperature are known to play a role in the damage to the MPs. Thus, care should be taken to verify that aggressive conditions are not used. Gao *et al.*

(2023) advocate against the use of acid treatments, suggesting that they are not even particularly effective [24], noting a study by Conley *et al.* (2019) whereby more than 80% of non-synthetic material was digested using 1 M HCl at 65°C but approximately 40% of PEst and 60% of PA (nylon) fibers were also destroyed in the process [24, 85]. In a similar manner, alkali solutions cause deleterious effects to the MP polymers; for example, Cole *et al.* (2014) noted that treating samples with 10 M NaOH at 60°C resulted in the partial degradation of PA fibers and the melding of PE fragments [49]. Hurley *et al.* (2018) further noted that KOH solutions were unsuitable for the destruction of organic matter [90]. In contrast, Gao *et al.* noted that peroxidation was more gentle on MP polymers, but good organics removal was still noted [24]. However in some cases, long reaction times ($O\{\text{days}\}$) affect the structures of some polymers (*e.g.* PA), but the use of Fenton’s reagent is a very effective method for achieving good rates of digestion at reasonable reaction times [25, 78, 80, 90, 92]. It is also noted that the elevated temperatures favoured in some of the peroxidation reactions are incompatible with polymers having low glass transition or melting temperatures (*e.g.* polylactic acid), meaning that these MPs are at risk of softening, changing shape, and/or agglomerating [24, 25]. Reaction temperatures should be kept below 40°C to minimize these negative effects [90]. Enzymatic treatment may be a feasible alternative or supplementary process with respect to more aggressive chemical digestion steps as the enzymes studied are effective towards organic matter removal, but are not known to have deleterious effects on the MPs. The downside to enzymatic treatment, however, is that it can be prohibitively expensive, requires very long reaction times (*e.g.* $O\{\text{days}\}$), and can be procedurally complex [24–26, 49].

In some studies, investigators eschew complex separation processes such as digestion whereby non-plastics are visually removed under an optical microscope (*e.g.* [79, 94]). While this is deemed acceptable for matrices like drinking water with few contaminants [20], Hidalgo-Ruz *et al.* (2012) advise that visual inspection is a very poor method for identifying which particles are plastic and which ones are not. An error rate of up to 70% is possible [11]; furthermore, fibrous materials are particularly problematic and other investigators reported that $\sim 50\%$ of visually-selected fibrous materials were miscategorized as plastic [26]. Regardless, the proper removal of inorganic and organic contaminants is a crucial step such that MPs can be properly identified and counted, subsequently. The reader is referred to one of the numerous review articles that summarize the advantages and drawbacks of MP sampling procedures [16, 20, 22, 24, 25].

■ **Sample analysis.** Following the removal of large fractions of organic and inorganic material, the particles that are left must be identified as MPs or rejected as some other material (*e.g.* remaining sediments, natural fibers, metal flakes, etc.). Typically, suspected MPs are submitted for further analysis to confirm/deny their nature. As was noted before, in the simplest of methods, a researcher can attempt to visually identify MPs versus non-MP particles under a microscope. Polarization microscopy has been shown to improve the identification process [95]. Furthermore, the use of stains or dyes like Nile Red (for staining plastic particles) [96, 97] or Rose-Bengal solution (for staining non-plastic particles) [48, 91, 98] also has shown to improve particle categorization.

To verify that these prospective MPs are indeed of plastic origin, a variety of chemical analytical techniques have been utilized, including various forms of Fourier transform infrared spectroscopy (FTIR) [26, 35, 99], various forms of Raman spectroscopy, atomic force microscopy-infrared spectroscopy (AFM-IR), and scanning electron microscopy-energy dispersive spectroscopy (SEM-EDS). Highly advanced thermoanalytical/spectrometric techniques have also been utilized such as forms of liquid chromatography (LC), pyrolysis-gas chromatography-mass spectrometry (Py-GC-MS), thermogravimetric analysis-differential scanning calorimetry (TGA-DSC), thermal desorption-gas chromatography-mass spectrometry (TDS-GC-MS), and thermal extraction desorption-gas chromatography mass spectrometry (TED-GC-MS) [24, 25, 58, 100–103]. Good comparisons of the advantages and drawbacks of some of these techniques are prepared by several investigators to which the reader is referred [7, 24]. Anecdotally, the most common techniques for the chemical identification of MPs appear to be the various forms of FTIR as they are relatively accessible to researchers, can sample very small particles (*i.e.* μ -FTIR) or larger-sized particles (*i.e.* attenuated total reflectance FTIR; ATR-FTIR), and are amenable to automation (*i.e.* focal plane array FTIR; FPA-FTIR) [24]. FTIR techniques collect absorbance or transmittance spectra of the samples that they analyze; as specific polymers absorb/reflect different wavelengths of infrared light due to various chemical groups/bonds, a (suspected) MP's infrared spectrum can be compared against spectral references in a database to determine the particle's chemical composition [16]. One commonly-used database is the *Hummel Polymer and Additives FT-IR Spectral Library* (ThermoFisher Scientific) [26, 91, 99].

While these techniques are inarguably useful for particle identification, they are still challenging in many cases. For example, they can be both labor- and time-consuming when large numbers of

particles (or large samples) must be processed [24]. Furthermore, spectral analysis is complicated by MP weathering due to hydrolysis, oxidation, UV photodegradation, etc. as these processes can change the chemical structure of the plastic (*e.g.* adding carbonyl/carboxyl groups) [5, 22, 24, 33] which can then modify the MP’s chemical spectrum [16, 48]. Other sources of interference include plastic additives [5], the presence of natural organics such as cellulose [104], sorbed organic/inorganic contaminants [5], and irremovable biofilm growth on the surface of the MPs [32]. Finally, Sun *et al.* (2019) note that particles smaller than 1 μm are especially difficult to characterize [16] as certain minimum sample quantities are necessary during analysis; for example, μ -FTIR and μ -Raman spectroscopy require particles greater than $\sim 10 \mu\text{m}$ and $\sim 1 \mu\text{m}$ in size, respectively [105]. To this end, the advancement of chemical identification techniques for small MPs and NPs is needed.

Finally, “confirmed” MPs may be resubmitted for visual analysis to document the MPs’ size, shape, colour, and other “visual” descriptors of interest to the researcher [16, 24].

■ **Reporting results.** Following the collection, processing, and analysis of MPs in samples, the results from the study are reported. Comprehensive analyses of the MPs in samples typically include information on the MP size, shape, and composition. See §1.1.1 for more information on MP classification schemes. Unfortunately, descriptors of morphology and MP irregularity are often subjectively assigned by the researcher according to their own criteria given that universal definitions are not yet standardized. To counteract these limitations, various metrics including the particle’s surface roughness, aspect ratio, equivalent spherical diameter, and/or various other “shape factors” related to MP dimensions, surface area, or perimeter are well-suited for quantifying (typically subjective) particle characteristics [29].

Of particular interest, MP *concentration* is typically reported by counting the number of collected MPs and dividing the count by the total volume of sample that was processed (typical units: MPs/L). However, MP weathering/fragmentation (or aggregation) is well-understood to occur in the environment and within WWTPs [23, 33, 84]. For example, MPs passing through WWTPs experience shearing due to mixing and pumping which cause break-up into smaller MPs [23]. As MP “counts” and “number concentrations” are not conserved quantities when MPs fragment, reporting number concentrations tends to misrepresent MP concentration variations in space or time; unfortunately,

most studies in the contemporary literature report *number* concentrations of MPs [7, 21, 24, 84]—likely for the purposes of convenience and the limitations of the available analytical equipment. A common chorus from researchers is that a more appropriate approach is to report *mass* concentration measurements of MPs in samples [14, 16, 84]. Accordingly, some investigators attempt to overcome the substantial disadvantages of MP number concentrations. For example, Simon *et al.* (2018) measured both major and minor dimensions of the MPs which they isolated and used a simple model to convert these dimensions to MP masses; it was found that a Danish WWTP released 0.5–12 μg MPs/L in its effluent [28]. Similarly, one German WWTP was found to release 0.13–0.18 mg MPs/L in its effluent [106]. Both Lv *et al.* (2019) and Conley *et al.* (2019) performed a similar analysis, converting MP number concentrations into mass concentrations in their studies [81, 85]. Other researchers have used more advanced techniques such as DSC [107], Py-GC-MS [108], and TED-GC-MS [101, 103] to quantify MP masses/mass concentrations. However, these advanced techniques are difficult to perform and may prove to be unsuitable for the average researcher.

Furthermore, the contamination of samples is known to be a significant concern in MP quantification. Robust research programs must consider the effects of fugitive airborne MPs, contamination from synthetic fibers in clothing, as well as other sources through the appropriate application of positive and negative controls [16, 20]. Overall, it is critical to note that the variety of methods used to collect, process, analyze and report information on MP samples have a direct impact on the nature of the results. As such, the comparison of results between studies should be done very cautiously, cognizant of the methodologies used. From a broader perspective, the lack of procedural standardization calls into question the quality of the data that is available regarding the occurrence and fate of MPs in the environment and man-made systems.

1.2.2 Fate of Microplastics in Wastewater Treatment Plants

As WWTPs are known to be sinks for MPs in urban environments [33], interest in the fate of MPs within these facilities has proliferated and consequently, the number research studies considering WWTPs has exploded over the last decade. As of 2023, studies into the removal effectiveness of WWTPs towards MPs have been conducted across the globe, including examples from Australia [91, 98], Eastern Asia [27, 81, 109–111], the Middle East [48, 92, 112], Europe

[26, 28, 36, 78, 79, 86, 113], and North America [32, 80, 85, 114, 115]. A topical *Web of Science* search for “microplastics AND (wastewater treatment OR sewage treatment)” finds only 3 records published in 2013, increasing dramatically to 459 records in 2022. This can be seen in Figure 1.4. These past studies have largely shown that the apparent removal of MPs varies widely—depending on the facility that is studied—due to differences in the treatment processes used: so-called primary (1°), secondary (2°), and/or tertiary (3° ; “polishing”) steps. A description of these contemporary municipal wastewater treatment processes can be found in §2.2.

A significant number of research studies have been performed which observe the effects of different facilities, stages, and unit operations on the removal of various types of MPs from influent wastewaters. Each individual study appears to add incremental additional value to the field; the implication of which is that the state of knowledge in the field appears to have remained largely unchanged over the last several years. To keep up with the increased number of original research studies produced, many review articles have also been written over that same time period (*e.g.* [14, 16, 21, 24, 25, 33, 45, 50, 51, 57, 77, 116, 117]). Like the studies which they summarize, these review articles add only a small amount of new insight to the academic discourse and largely seem to state/restate the same takeaways. Unfortunately, the process is also fraught with error. Even

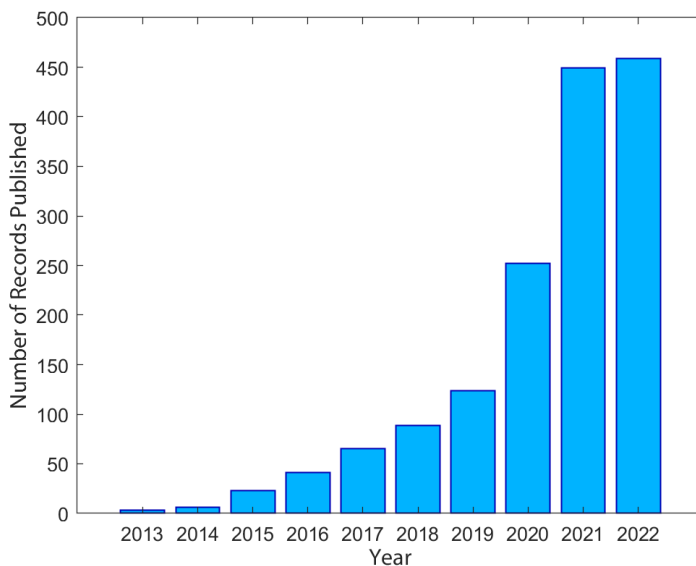


Figure 1.4: Topical *Web of Science* search for publications, by year, involving MPs and wastewater/sewage treatment from 2013–2022.

for reviews published in more reputable journals, a shocking number of these works include direct transcription errors of values or misrepresent the articles (*e.g.* report incorrect units) from which they draw upon. The problem is exacerbated by the lack of standardization in MP quantification techniques and inconsistent reporting of metrics such as MP concentrations. As such, developing a clear understanding of the effectiveness of WWTPs and WWTP technologies is a minefield for researchers. The following sections attempt to clearly synthesize what is known in the field and summarize the fate of MPs as a function of facility, treatment stage, and the unit operation(s) employed.

1.2.2.1 Fate by Facility

In consultation with the current literature, most WWTPs are quite effective at removing MPs from influent wastewater. MPs leaving WWTPs tend to do so either in the liquid effluent—the focus of this work—or in the solid fraction (*e.g.* sludge) which is out-of-scope, here. Many excellent articles exist (*e.g.* [84]) which consider the fate of MPs in WWTP sludge to which the reader is referred.

Concentrations of MPs in WWTP *influent* (C_{inf}) have been measured ranging from < 1 MP/L in a Chinese WWTP [81] to 18,285 MPs/L in a Danish WWTP [28].² A more recent study of three South Korean WWTPs disclosed an influent wastewater sample containing in excess of 31,400 suspected MP beads (70%), fibers (15%), fragments (11%), and sheets (4%) [83]. Variability in the composition of MPs—size, shape, chemical identity, etc.—in WWTP influents is also well-documented [24, 57], although strong emphasis is placed on the high abundance of PE (fragments) and PEst (fibers) within WWTPs [22, 58, 118]. Inevitably, the concentrations of MPs entering WWTPs globally vary significantly depending on the facility that is studied.

Research indicates that there are significant quantities of influent MPs, but the source of these MPs also bears considering. Barchiesi *et al.* (2021) write that variability in the influent MP characteristics is linked to factors external to the WWTP, such as the catchment area size from which the wastewater is drawn, the type of collection system (*i.e.* combined or separate sewers), the surrounding land use, along with a variety of socioeconomic factors relating to the population that is

²Interestingly, this value of C_{inf} is significantly underestimated (misrepresented) as 10,044 MPs/L by authors of several sequential review articles, *e.g.* [16, 22, 57, 77].

served [16, 21]. The load of MPs entering a WWTP can be correlated to the equivalent population served and the influent flow rate of wastewater [111]. Within these socioeconomic factors include the source of the wastewater (*e.g.* domestic, commercial, industrial, and/or combinations thereof) as this is known to contribute to the types (primary vs. secondary), compositions, morphologies, and abundances of the MPs which are fed to the WWTP [21, 92, 119]. For example, if the facility is fed by domestic sewers, MPs from personal care products/cosmetics and laundered textile fibers may be collected [51]. People’s preferences towards natural versus synthetic fibers in their clothing can contribute to the abundance of these fibers in received wastewater [16]. A WWTP that services an area with industrial installations (*e.g.* textile manufacturers) may see significant contributions of fibers or plastic powder feedstocks in its influent [51]. Furthermore, if the facility is fed by sewers that collect stormwater runoff, MPs originating from atmospheric debris, particles from construction, the breakdown of larger plastic parts (*e.g.* packaging), and dust generated by road wear on tires may also be input [51]. As a final example, a facility that also treats leachate from landfills may see MPs generated from plastic waste due to the harsh physicochemical conditions that exist [51].

The weather and season can—in some cases—affect the variety and abundance of MPs found in the WWTP influent. For example, Akarsu *et al.* (2020) note that significant concentrations of MPs in influent wastewater to rural WWTPs—as oppose to their more urban counterparts—can be attributed to agriculture and runoff during rain events [112]. In their evaluation of a Spanish WWTP, Bayo *et al.* (2020) found statistically higher concentrations of MPs in the summer as oppose to the winter; they also note the influence of runoff during wetter months [120]. Seasonal variability has been noted in studies of some additional facilities [48], but not in others [85, 113, 114]. In a similar fashion, variability within the day regarding MP concentrations and properties like size is seen in some facilities [47, 120]. For example, Bayo *et al.* (2020) saw a statistical increase in the size (but *not* in the concentration) of the influent MPs collected in the afternoon versus the morning over their lengthy sampling campaign; interestingly, no statistical variations in MP size were seen in the effluent [120]. In contrast, other researchers have found that rain events can increase the concentration of MPs in WWTP effluents [119, 121], explicated by Wolff *et al.* (2019) as the result of higher flow velocities within the facility which result in poorer particle settleability (see §2.2.1.1). Whereas there is evidence of some temporal patterns in research studies, no definite conclusions can be made here regarding the incidence and magnitudes of the effects [21].

Similarly to what is seen with wastewater influents, the concentrations of MPs in WWTP effluents can vary substantially, ranging from undetectable levels up to 447 MPs/L [16, 28]. The majority of facilities surveyed appear to produce effluent concentrations (C_{eff}) less than 10 MPs/L. To evaluate the ability of a facility to remove MPs from their influent wastewaters, MP removal efficiencies (η) can be computed as follows:

$$\eta = \left[1 - \frac{C_{\text{eff}}}{C_{\text{inf}}} \right] \times 100\% \quad (1.1)$$

The value of η can be calculated for an individual process or for an overall wastewater treatment facility. Data from a variety of WWTP studies in the current literature is self-tabulated in Table 1.1, including the type of facility,³ MP concentrations in the influent/effluent, and the overall MP removal efficiency, where applicable. Studies are organized by the country of origin, and every effort was made to include descriptive statistics which characterize the variability within the WWTPs such as the average \pm one standard deviation, or the range of values seen. However, there is no “standard” for the reporting of WWTP performance data, thus many studies often just report single values. As can be seen, while lower removal rates (*e.g.* $< 75\%$) are documented in some cases [81, 110, 122], the majority of studies have found that the overall removal of MPs in WWTPs is high (*e.g.* $> 90\%$). Overall, evidence suggests that contemporary WWTPs are found to be quite effective at removing MP from wastewater [16, 24, 33, 50, 77, 117], at least on a percentage basis.

1.2.2.2 Fate by Treatment Stage & Technology

Like in WWTPs as a whole, there is significant variability in the ability of these facilities to remove MPs based on the *treatment stage* that is considered. Refer to §2.2.1 for a primer on conventional WWTP treatment stages. As Michielssen *et al.* (2016) rightly state in the title of their research article: the “fate of microplastics [...] in wastewater treatment plants depends on the unit processes employed” [114]. The actual effectiveness of 1°, 2°, and 3° treatment stages is a function of the individual unit operations (*e.g.* settling, biological and chemical treatment, etc.) within these stages. Krishnan *et al.* (2023) note that the fraction of MPs removed in WWTPs is dependent upon both the treatment processes and the properties of the MPs found in the wastewater [50]. It cannot be emphasized enough that MP removal highly facility-dependent: what it receives and what processes

³That is, a “2°” WWTP has up to 2° treatment processes; a “3°” WWTP has up to 3° treatment processes.

Table 1.1: Summary of MP removal in 25 selected WWTP studies. Removal efficiencies η are reported for the entire facility based on MP number concentrations; “n/a” indicates data that is unavailable/unsuitable to report. *Indicates parallel treatment trains in the same WWTP.

Ref.	Location	WWTPs in Study	Type of Facility	Equivalent Population	Est. Flows (m ³ /year)	C_{inf} (MPs/L)	C_{eff} (MPs/L)	Est. Efflux (MPs/day)	η (%)
[91]	Australia	3	1°	1.23×10^6	1.12×10^8	n/a	1.5	4.60×10^8	n/a
			2°	6.71×10^4	6.21×10^6	n/a	0.48	8.16×10^6	n/a
			3°*	1.51×10^5	6.21×10^6	n/a	0.28	3.60×10^6	n/a
			3° (RO)*	1.51×10^5	1.75×10^7	n/a	0.21	1.00×10^7	n/a
[98]	Australia	1	3°	1.90×10^5	n/a	11.8 ± 1.10	2.76 ± 0.11	$(1.07-1.16) \times 10^8$	76.6
[80]	Canada	1	2°	1.30×10^6	1.64×10^8	31.1 ± 6.70	0.5 ± 0.2	$(32-97) \times 10^7$	97.1-99.1
[119]	China	7	2°	n/a	n/a	1-13.69	0.2-1.73	n/a	79.3-97.8
[27]	China	1	3°	2.40×10^6	3.65×10^8	12.03 ± 1.29	0.59 ± 0.22	$(5.9 \pm 2.2) \times 10^8$	95.2 ± 1.6
[81]	China	1	2°*	n/a	1.83×10^7	0.28-0.02	0.13-0.01	n/a	53.6
			2° (MBR)*	n/a	2.56×10^7	0.28-0.02	0.05-0.01	n/a	82.1
[110]	China	1	2°	n/a	7.30×10^6	79.9 ± 9.3	28.4 ± 7	5.70×10^8	64.4
[28]	Denmark	10	$9 \times 2^\circ / 1 \times 3^\circ$	n/a	n/a	2,223-18,285	29-447	n/a	99.3
[35]	Finland	1	2°*	n/a	$(3.93 \pm 0.18) \times 10^6$	57.6 ± 12.4	1 ± 0.4	1.0×10^7	98.3
			2° Pilot MBR*	n/a	1.10×10^3	57.6 ± 12.4	0.4 ± 0.1	n/a	99.4
[86]	France	1	2°	n/a	8.76×10^7	260-300	14-50	8.40×10^9	83-95
[26]	Germany	12	$8 \times 2^\circ / 4 \times 3^\circ$	n/a	$(1.9-130) \times 10^5$	n/a	0.08-7.52	$(4.19-1,240) \times 10^4$	n/a
[48]	Israel	1	3°	2.10×10^5	1.10×10^7	65 ± 19	1.97 ± 0.21	5.90×10^7	97
[78]	Italy	1	3°	1.20×10^6	1.46×10^8	2.5 ± 0.3	0.4 ± 0.1	1.60×10^8	84
[79]	Scotland	1	2°	6.50×10^5	9.52×10^7	15.7 ± 5.23	0.25 ± 0.04	6.52×10^7	98.4
[111]	S. Korea	50	Various	n/a	$(7.67-571) \times 10^6$	10-470	0.004-0.51	n/a	98.7-99.99
[83]	S. Korea	3	3°	n/a	$(9.69-171) \times 10^6$	4,200-31,400	33-297	$(8.8-1,390) \times 10^8$	98.9-99.2
[36]	Spain	2	2°	3.75×10^5	1.91×10^7	645 ± 182	16.4 ± 7.85	$(1.49-1.94) \times 10^9$	97.2
			2°	300	3.00×10^4	$1,567 \pm 413$	131 ± 95	$(1.07-2.64) \times 10^7$	91.6
[123]	Spain	1	2°	3.00×10^5	1.64×10^7	171 ± 43	10.7 ± 5.2	3.00×10^8	93.7
[120]	Spain	1	2°	2.10×10^5	1.28×10^8	3.2 ± 0.67	0.31 ± 0.06	6.70×10^6	90.3
[124]	Sweden	1	2°	1.20×10^4	1.88×10^6	15.1	0.00825	4.25×10^4	99.9
[125]	UK	8	$4 \times 2^\circ / 4 \times 3^\circ$	n/a	$(3.46-25.6) \times 10^7$	955-17,214	2-54	n/a	99.8
[85]	USA	3	2°	1.80×10^5	3.04×10^7	147	3.7	$(2.91-5.96) \times 10^8$	97.6 ± 1.2
			2°	5.30×10^4	6.90×10^6	126	17.6	$(1.04-5.87) \times 10^8$	85.2 ± 6
			2°	3.20×10^4	4.16×10^6	146	17.2	$(8.6-30.8) \times 10^7$	85.5 ± 9.1
[114]	USA	2	2°	2.40×10^6	9.13×10^8	133	5.9	1.48×10^9	95.6
			2° Pilot MBR*	n/a	n/a	91	0.5	n/a	99.4
			3°*	9.90×10^3	6.23×10^5	91	2.6	n/a	97.2
[104]	USA	1	2°	6.80×10^5	6.89×10^7	n/a	0.023	4.97×10^6	n/a
[122]	Vietnam	3	2°	n/a	$(2.63-18.3) \times 10^5$	183-443	138-340	$(3.8-150) \times 10^7$	21.8-25.5

it uses to perform the treatment. However, it has been found that some important generalizations can be made regarding MP removal at various stages in the treatment process. Sun *et al.* present a good summary of these removal characteristics, as represented in Figure 1.5. The following discussion features some of the main findings regarding the fate of MPs in WWTPs as a function of stage.

■ **A significant fraction of MPs are removed via preliminary/primary treatment steps.**

In many cases, the bulk of MPs can be removed via the initial treatment stage(s) in a WWTP. For example, in the studies which were analyzed by Sun *et al.* (2019), the authors found that 50–98% of MPs were removed in these stages. Similarly, in the 21 studies considered by Iyare *et al.* (2020), MP removal in preliminary/primary stages ranged 32–93% (average = 72%) [116]. Other audits of WWTPs and WWTP studies concur with this view [14, 21, 51, 126]. As examples of some of the facilities in these reviews, studies of WWTPs in Glasgow (Scotland) [79], Detroit (USA) [114], Vancouver (Canada) [80], and Helsinki (Finland) [94] saw 78%, 88%, 91.7%, and 97.9% decreases in MP concentrations on average, respectively, following preliminary plus 1° treatment. More conservatively, studies of WWTPs in Wuhan City (China) [110], Viikimäki (Finland) [127], and Paris (France) [86] saw 41%, 50%, and 60% decreases in MP concentrations on average, respectively. Investigations such as the one performed by Murphy *et al.* (2016) corroborate the removal of MPs in preliminary and primary treatment steps as significant concentrations of MPs are found in the solids drawn off these processes [79].

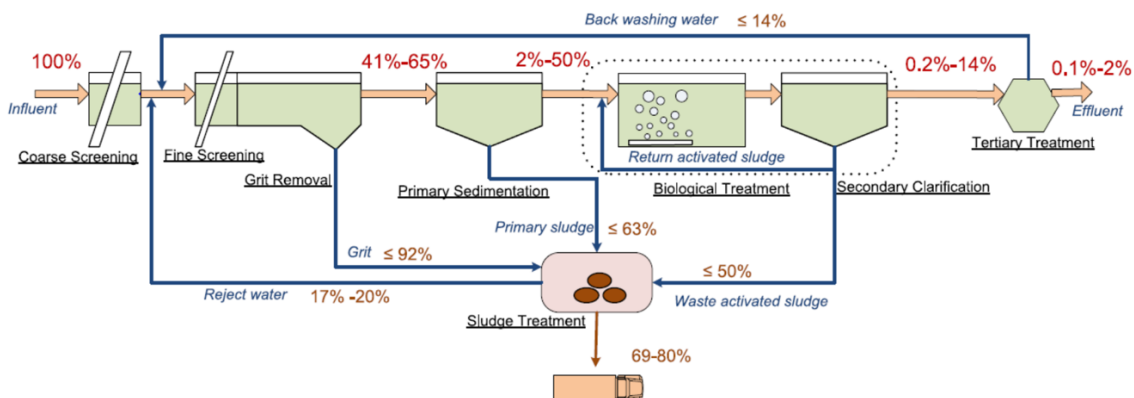


Figure 1.5: Overview of the fate of MPs within WWTPs. The percentage labels provide an estimate for the fraction of the MPs in the facility influent that remain at each stage. Image reproduced and used with permission from J. Sun, X. Dai, Q. Wang, M. C. van Loosdrecht, and B. J. Ni, “Microplastics in wastewater treatment plants: detection, occurrence and removal,” *Water Research*, vol. 152, pp. 21–37, 2019.

Recently, mechanisms for the removal of MPs in preliminary and primary treatment have been suggested. Trivially, some MPs can be individually caught or entrapped in larger aggregations; some MPs easily entangle in the solid matter (*e.g.* paper, food waste) which is captured by bar screens, grit/grease removal processes, and other preliminary unit operations [50, 57, 116]. Perhaps more interestingly, removal of MPs in primary treatment occurs due to particle settling *or* flotation as sedimentation processes are the dominant form of 1° treatment. The subset of particles less dense than the water (*e.g.* PP, PE [51]) are positively buoyant and can float to the surface of clarifiers where they are removed by surface skimming [16]. Conversely, the subset of particles more dense than water (*e.g.* PS, PEst [51]) are negatively buoyant and can sediment to the bottom of clarifiers where they are removed with the primary sludge [16]. The kinetics of the process (see §2.2.1.1 and Equation 2.15) are such that, all else equal, larger particles which are further away from the density of water settle/float faster and stand a greater chance of removal in clarifiers, as constrained by the overflow velocity/hydraulic retention time of the basin. The removal of MPs is known to be enhanced by entrapment in settling sludge flocs or rising greases/oils [23, 50] which act as MP collectors. Anecdotally, the importance of this mechanism of entrapment is highlighted in a study by Long *et al.* (2019) who noted a preferential removal of “rougher” so-called fragments and granules over “smoother” so-called fibers and pellets, where the “angular” and “twisted” nature of the former category enabled their capture [119].

■ **Secondary (biological) treatment processes can remove a significant fraction of the remaining MPs.** Considering the reviews by Sun *et al.* (2019) and Iyare *et al.* (2020), the researchers found that overall MP concentrations were reduced *cumulatively* to 86–99.8% and 53.6–99.9% (average = 88%) in the respective reviews [16, 116]. For the study by Iyare *et al.* (2020), a 72% reduction in MP concentrations following 1° treatment which improves to an overall 88% reduction in MP concentration following 2° treatment implies a 16% reduction due to 2° treatment alone ($88\% - 72\% = 16\%$): that is, a 16% reduction on an *absolute basis*. Reconsidering the example WWTP studies highlighted in the discussion on preliminary/primary treatment, the researchers in Glasgow [79], Detroit [114], Vancouver [80], and Helsinki [94] found that the absolute MP removals increased, on average, by 20%, 1.4%, 6.6%, and 1.2%, respectively, due to 2° treatment. This corresponds to average cumulative MP removals of 98%, 90%, 98.3% and 99.2%, respectively. In the other three facilities where 1° treatment was not quite as effective, by the end of 2° treatment, the cumu-

lative MP removal was found to have significantly improved. These WWTPs located in Wuhan City [110], Viikinmäki [127], and Paris [86] saw additional absolute removals averaging 16%, 36%, and 28%, raising the cumulative MP removals to 57%, 86%, and 88%, respectively, following 2° treatment.

Analyzing the *absolute basis* of MP removal, the contributions of the 2° processes appear to be less than the contributions of the 1° processes. However, it must be considered that the concentrations of MPs in the 2° process effluents are still compared to the concentrations of MPs in the WWTP influents. If *just* the effect of the 2° process is considered, the 2° process effluent should be compared relative to the 2° process influent. Using the “average” values reported by Iyare *et al.* (2020), the 16% absolute reduction reflects that the 2° processes actually removed an average of 57% of the MPs that were fed to them on a *relative basis*. This implies that the 2° treatment processes can also be quite effective in isolation.

MP removal mechanisms in 2° biological treatment processes leverage the proliferation of microorganisms as they consume substrates (*e.g.* organic material, nutrients). During their growth in the bioreactor, the microbes excrete extracellular polymeric substances (EPS): biopolymers which can form aggregates. MPs can also adsorb to the sticky aggregates which combine to form larger sludge flocs and entrap the MPs [16, 57]. The mechanisms of adsorption, aggregation, and entrapment which are facilitated in the bioreactor are key for encouraging the additional removal of MPs in 2° treatment: the sludge and sludge/MP flocs formed in the bioreactor are transported to 2° clarifiers where they further coalesce, settle, and are removed as waste activated sludge (WAS) [16, 57]. It has also been suggested that some microorganisms such as protozoa or metazoa may ingest small MPs [51, 116, 128], however, further research is needed to explore this possibility.

Researchers have documented the common presence of biofilms on MPs leaving 2° treatment processes [32]; in the broader aquatic environment, biofilms are ubiquitous and are found to readily form on the surfaces of moderately-sized (*e.g.* $O\{100\ \mu\text{m}\}$) MPs [5, 94, 129]. Research indicates that longer *retention times* in a WWTP’s bioreactor (see §2.2.1.2) promote the formation of biofilms which can dramatically alter the size and density of the particle along with its surface characteristics like hydrophilicity and roughness [21, 23, 50]. It has been found that the composition of these “bacterial assemblages” varies based on the water quality, the physiological properties of the bacterial

that colonize the MPs, and the MP's shape and surface properties [117, 130]. For example, bacteria have shown to preferentially colonize rougher, weathered MPs [117]. MPs with a biofilm may see their density and size increase which can lead to a higher settling rate for moderately-dense MPs; however, a decrease in density caused by the growth of biofilms on dense MPs (*e.g.* PESt [51]) may counteract an increase in MP size. In any case, neutrally-buoyant particles are more likely to evade removal via skimming or via settling in the sludge [16]. The natural organic matter (NOM) such as humic or fulvic acids present in the wastewater are also known to adsorb onto the surface of MPs. This can affect their surface properties as before, which in turn affects their stability in suspensions (*i.e.* their propensity to homo- or heteroaggregate) and their transport or deposition in aqueous environments [5]. Detailed research is ongoing which is necessary to provide the required level of understanding into these surface phenomena.

Poor MP removal in 2° treatment may be the result of the formation of unstable flocs which disintegrate under shear forces from mixing, aeration, and pumping; MPs released from unstable flocs may evade removal in the 2° clarifiers [32, 50, 116, 131]. The addition of chemicals such as coagulants (*e.g.* ferric sulfate) is suspected to enhance the formation of flocs [50, 116]. Furthermore, there is some evidence [27, 110] to suggest that 2° treatment variants like “A²O” processes (*i.e.* anaerobic/anoxic/oxic) demonstrate lower MP removal efficiencies than conventional activated sludge processes [50], however, there are far too few data points to make a definitive comparison at this time. See §2.2.1.2 for more information on types of 2° treatment. In spite of these considerations, research into the interactions between MPs, microorganisms, EPS, and their aggregates is sparse [116] and additional work is needed to elucidate these mechanisms and quantify the extent to which the aforementioned processes affect MP removal [51].

■ **Tertiary technologies can greatly improve the removal of MPs, especially when a significant portion of the MPs remain following secondary treatment.** In fact, WWTPs with dedicated 3° technologies have some of the highest MP removal efficiencies recorded (see Table 1.1). However, the magnitude of this MP removal in 3° processes can be variable given that this stage tends to see the greatest variety in technologies used—if and when this (optional) stage is present. Possible technologies include rapid sand, media, disc, or other types of filtration, membranes, and advanced oxidation processes [50, 57]. A more comprehensive list can be found in §2.2.1.2. Due

to the variety of technologies which are employed, a variety of MP removal mechanisms are seen such as interception and adhesion in adsorptive processes and media/sand filtration, degradation in oxidation processes, and various forms of rejection in membrane processes (§2.1.2.2) [34, 57].

Again considering the reviews by Sun *et al.* (2019) and Iyare *et al.* (2020), the researchers found that MP concentrations in 3° WWTPs saw overall (cumulative) reductions of 98–99.9% and 82–99% (average = 94%) in the respective works [16, 116]. For example, at a Chinese WWTP near Beijing, MP retention improved by ~16% in absolute terms from 79% to 95% (cumulatively) following a complex series of advanced 3° treatment processes including denitrification, ultrafiltration (UF), then ozonation and UV disinfection [27]. MP retention in the aforementioned Detroit WWTP increased by 7.2% in absolute terms from 90% to 97.2% as the result of a granular sand filtration process [114]. At a Los Angeles-area WWTP, MP concentrations decreased following a gravity filtration step such that effluent MP concentrations were undetectable with the methodologies used [32].

Like with 2° treatment, the reduction in MP concentrations via 3° technologies appear to be poor on an absolute basis (with respect to the 100% of MPs fed to the WWTP), but appear more substantial on a relative basis (with respect to the concentration of MPs entering the 3° process). In these relative terms, the Beijing-area and Detroit-area WWTPs saw 76% and 72% reductions in the MP concentrations across their 3° treatment processes, respectively. However as a cautionary note, where MP removals are already high due to 1°/2° technologies, the marginal value of adding a 3° technology decreases substantially, even in relative terms. For example, researchers studying an Israeli WWTP observed an overall 95.8% decrease in MP concentrations over the course of 1°/2° treatment, on average [48]. Cumulatively, this increases to an average of 97.0% removal following a 3° filtration process. While this final 97% MP removal efficiency places this facility among some the most effective in Table 1.1, the 3° process removed only 29% of the MPs fed to it, perhaps suggesting that the remaining fraction of MPs was the most difficult to remove. Furthermore, the researchers studying the Helsinki-area WWTP found no statistical difference in the average MP concentrations before and after a biologically-active 3° filter [94]. As the average MP removal following 2° treatment was *already high* (99.2%), any inherent MP removal in 3° treatment may have been masked via measurement noise, sample contamination, and natural variations in the low MP concentrations in the effluent. The overarching implication is that the marginal effect of adding additional (*e.g.* 3°)

treatment processes can see diminishing returns with respect to MP removal.

It has been shown that various facilities and treatment stages show different MP removal efficiencies, however, it is often the nature of the unit operation, itself, that truly governs the MP removal. Some unit operations are indeed more effective than others, and this variability in the effectiveness of unit operations is most clearly seen in 3° treatment processes. For example, the aforementioned 3° sand filtration system studied by Ben-David *et al.* (2021) caused, on average, a 28% decrease in MP concentrations which were already quite low following 2° treatment [48]. In their study of Finnish WWTPs, Talvitie *et al.* (2017) found that parallel rapid sand filtration, disc filters⁴ (10 µm or 20 µm pore size), and dissolved air flotation processes removed (in relative terms) 97%, 95%, and 40–98.5% of MPs which were fed to them via 2° effluents [34]. The significant variability in MP removal via disc filters was attributed to unfortunate processes disturbances; however, these sorts of real-world events and their effects must be considered, too. Findings are similar in other studies. In their investigation of three South Korean 3° WWTPs, Hidayaturrahman *et al.* (2019) found that following coagulation of 2° effluent wastewater, ozonation, disc filters (10 µm pore size), or rapid sand filtration processes removed (in relative terms) 89.9%, 79.4% and 73.8% of MPs, respectively, that were fed to these processes [83]. Interestingly, the coagulation step was found to remove considerably variable fractions of MPs (47.1%–81.6%), depending on the facility.

As a particularly frustrating example, in the Chinese WWTP which included a series of 3° treatment technologies (denitrification, UF membranes, ozonation, UV disinfection), the sequential processes removed $71.7 \pm 11.6\%$ of the MPs fed to the 3° stage [27]. For a single unit operation, this may be acceptable. However, several technologies were used in series which should theoretically result higher MP removals. Unfortunately, no attempts were made to disentangle the effects of the individual unit operations in 3° treatment, and no additional inferences can be made regarding the efficacy of individual unit operations, here. In other facilities where oxidation processes (*e.g.* UV, ozone, etc.) were specifically studied, mixed results have been obtained [14]. For example, following 3° UV treatment [81] and chlorination processes [110] in Chinese WWTPs, researchers noted apparent 25% and 17% reductions in the MP concentrations relative to what was fed to the stage. Ruan *et al.* (2019) even noted an *increase* in the number of MPs following chlorination in one WWTP in

⁴This technology operates by means of *cake filtration*, which some authors describe as “the formation of a dynamic membrane” [50, 58, 132].

Hong Kong which may have resulted from particle fragmentation, however, the MP concentrations were already quite low (< 1 MP/L) [133]. Thus, resolving differences in the concentrations may have been fraught with error. Other studies indicate that granular filtration, biologically-active filters, and maturation ponds appear to contribute little to MP removal [26, 115, 134].

At the aforementioned facility studied by Talvitie *et al.* (2017), the authors also analyzed MP concentrations leaving a membrane bioreactor (MBR), a unit operation which combines the biological processes of 2° treatment and membrane filtration commonly found in 3° treatment. Even though this unit operation was fed with 1° effluent having a substantial concentration of MPs (influent = 6.9 ± 1.0 MPs/L), the MBR still was the most effective technology for MP removal, where 99.9% of MPs that were fed to it were removed (effluent = 0.005 ± 0.004 MPs/L) [34]. In other facilities where membranes were used, researchers typically noted very high MP removals. For example, the MBR units studied by Lares *et al.* (2018) and Michielssen *et al.* (2016) demonstrated 99.4% and 99.1% removal efficiencies, respectively, relative to the MP concentrations fed to the units [35, 114]. Furthermore, the MBR treatment system used in a Chinese WWTP was reported to remove 82.1% of MPs on a number basis, but 99.5% of MPs on a mass basis, suggesting again that significant fragmentation of the MPs occurred; yet the MBR was still effective at removing a large amount of these fragments on the mass basis [81]. Additionally, Bayo *et al.* (2020) noted that the MBR studied in a Spanish WWTP removed 79% of MPs fed to it, producing a similar removal efficiency as a parallel “conventional” treatment system [113]. In contrast, the Dutch MBR studied by Leslie *et al.* (2017) found no significant removal of MPs. The use of 3° reverse osmosis (RO) membranes in an Australian WWTP studied by Ziajahromi *et al.* (2017) yielded surprisingly poor removal results: only 25% removal of the remaining 0.28 MPs/L was achieved [91]. In these studies, MPs concentrations are generally quite low and the “real” effect of MP removal may be obscured due to noise, sample contamination, or the resolution of the MP measuring technique.

Of course, 3° removal results must be compared cautiously as the (often) small concentration values of MPs are notoriously difficult to assess, and are thus prone to error (*e.g.* false zeros [116])—especially when small sample volumes are collected [16]. In addition, sample contamination and the effects of particle fragmentation tend to increase the MP concentrations in samples, so MP removal results should be considered with a healthy degree of skepticism.

1.2.2.3 Fate by Microplastic Classification

And just like there is significant variability in the removal of MPs by different facilities and different stages within these facilities, the degree to which different sizes, shapes, and chemical identities of MPs also varies substantially [51]. As before, removal strongly depends on the facility which is studied, the composition and quality of the wastewater that it receives, and the unit operations that are employed. While fate via MP classification is more convoluted than previous topics, a few generalizations can still be made.

■ **WWTPs are particularly effective at removing larger MPs.** Various contemporary reviews of studies of WWTPs tend to agree: larger MPs are easier to remove from wastewater than smaller MPs. Towards the effluent end of the process, larger MP size fractions (*e.g.* $> 500 \mu\text{m}$) are more likely to be absent [16, 26, 50] and consequentially, this can enrich the relative abundance of smaller size fractions along the course of the treatment train. Dris *et al.* (2015) noted that the largest MP size bin which was measured (1,000–5,000 μm) in their French 2° WWTP decreased monotonically from 49% to 0% from influent to effluent. Concurrently, MPs found in the smallest (100–500 μm) and middle (500–1,000 μm) bins increased in abundance, respectively, from 29% to 57%, and 26% to 43%. Similarly, Magni *et al.* (2019) found that removal efficiency increased with increasing particle size in an Italian WWTP: 94%, 94%, 77%, and 65% for size ranges of 1,000–5,000 μm , 500–1,000 μm , 100–500 μm , and 10–100 μm , respectively [78]. However, this observation is not universally true. Simon *et al.* (2018) could not statistically differentiate the median MP sizes in wastewater influent (48 μm) versus effluent (45 μm). Furthermore, Long *et al.* (2019) noticed the opposite trend: higher removal rates were seen in smaller MP size bins [119].

In particular, larger MPs are especially well-removed in preliminary and 1° processes, with these processes having the largest impact on the distribution of MP sizes over the course of the treatment train [16, 21, 50, 116]. As discussed in §1.2.2.2, larger particles have greater settling velocities which likely explains this phenomenon. As an example, in a Spanish WWTP, Bayo *et al.* (2020) noted a statistically-significant decrease in average MP size from the grit-and-grease removal step ($820 \pm 60 \mu\text{m}$) to the 2° bioreactor ($630 \pm 30 \mu\text{m}$) [120].

In 2° treatment processes, preferential removal of MP size fractions is more unclear. In their review of contemporary studies, Sun *et al.* (2019) found that overall, larger MPs are further removed in 2° processes and therefore were less abundant in the process effluents [16]. For example, in studies by Mintenig *et al.* (2017) and Ziajahromi *et al.* (2017), MPs larger than ~ 500 μm were almost completely absent in the effluent [26, 91]. Corroborating this finding, Talvitie *et al.* (2016) found that MPs larger than 300 μm comprised only 8% of all MPs after the 2° treatment process in the WWTP that they studied [134]. Lares *et al.* (2018) found that the largest MPs (1–5 mm) saw the greatest removal in the 2° treatment process that they studied [35]. On the contrary, in the facility studied by Dris *et al.* (2015), MPs 500–1,000 μm in size actually became enriched in relative abundance compared to MPs in the smaller 100–500 μm size range following 2° treatment [86]. The underlying rationale between the differences in MP removals in these various facilities remains unclear, however one hypothesis explicating the latter set of results suggests that the preferential removal of large particles in 1° treatment increases the relative abundance of smaller particles in 2° treatment which—from a basis of pure probability—stand a greater chance at removal. As another potential mechanism, Lee and Kim (2018) noted that MPs in the smallest measured size range (*i.e.* 106–300 μm) were removed more efficiently than MPs over 300 μm during 2° biological treatment due to their propensity to adsorb to “sticky” biofilms and flocs [135]. Liu *et al.* (2019) concur: during activated sludge treatment, the fraction of MPs smaller than 300 μm was most effectively removed in the biosolids [110]. Hidayaturrahman *et al.* (2019) suggest that surface-immobilized biofilms preferentially removal smaller MPs than those removed in activated sludge-based processes (*e.g.* flocs) [83]. Regardless, the results suggest that the intersection of the chemistries/surface properties of the biomass/MPs in the bioreactor play an important role in the capture of MPs in 2° treatment.

There is a paucity of evidence which definitely details the effect of 3° treatment on MP size. However, researchers have noted that the MPs found in the effluent tend to be in the smallest particle size bin(s) [50, 116]. For example, in the 3° WWTP studied by Ziajahromi *et al.* (2017), no MPs larger than 190 μm were found in the final effluent; similarly, the biofilter assessed by Liu *et al.* (2019) retained all particles larger than 100 μm [110]. As noted in §1.1.1, the particle size distribution in water samples (*i.e.* both influent and effluent) tends to see a pronounced skew towards smaller particle sizes: the smallest size bins often have the highest particle counts (*e.g.* [21, 98, 123, 136]).

This is especially notable in WWTP effluents, such as those following 3° treatment [35]. As always, exceptions exist to this common finding [112].

■ **The degree to which particular MP shapes and compositions are removed is heavily facility-dependent and not particularly well-understood.** The fate of MPs of different shapes and compositions is particularly complex, with little agreement in the literature regarding general trends on MP removal. One set of results produced by Long *et al.* (2019) show that the classifier which most strongly affects MP removal is MP size, then followed by composition or shape [119]. Similarly, Gao *et al.* (2023) note that MPs tend to be well-removed from WWTPs regardless of their shape, with the implication that the chemical identity of the MP is a more important consideration [24]. The specific chemical makeup of a MP affects its sedimentation or flotation rate, stemming from the inherent density of the polymer and its additives, as described in §1.2.2.2. Long *et al.* (2019) noted a slight increase in removal efficiency as particle density increased. Interestingly, the removal rate of PE—having a large range of possible densities (*e.g.* 0.91–0.97 g/cm³)—also exhibited the largest range of removal rates over the seven facilities that were studied [119]. In agreement, Raju *et al.* (2020) noted that denser polymers like PEst (~1.38 g/cm³) were found in greater amounts in settled sludge compared to less dense MP compositions like PE and PP (~0.90–0.94 g/cm³) [98]. Murphy *et al.* (2016) found that light PE microbeads were found only in the floated grease removed during the initial stages of treatment [79], emphasizing the importance of skimming in removing floatable MPs in 1° treatment steps.

Research studies of WWTPs tend to make distinctions between the fates of *fibers* versus *particles* (*i.e.* all non-fibers). While over 30 different MP polymers are compiled in review articles by Sun *et al.* (2019) and Liu *et al.* (2021), generally only a few different polymers are reported in a given WWTP study, which are often tied to the shape of the MP in the first place. For example, many MP fibers originate from textiles, therefore, many fibers are thus comprised of PEst or PA (nylon) [30]. One common observation in the literature is that MP fibers are present in significant concentrations in WWTP influents. Over the course of these facilities, fibers often continue to constitute a large fraction (or even majority) of the sampled MPs, and can even increase in relative abundance towards the facility effluent [16, 24, 34, 80, 91, 110, 119]. For example, Long *et al.* (2019) found that MP fibers were removed at a lower rate than non-fiber particles: 78.9%, versus 82.8%, 91.3%, and 91.4%

for fibers, pellets, fragments, and granules, respectively [119]. Ben-David *et al.* (2021) noted that the abundance of fibers dominated in the influent of their WWTP (74%) and their relative abundance was further enriched towards the effluent (91.6%) [48]. Bayo *et al.* (2020) also observed that the abundance of fibers was enriched in the effluent versus upstream samples in the WWTP that they studied [120], while Talvitie *et al.* (2017) also noted that fibers were particularly difficult to remove in the WWTP which they investigated [34].

However, there are many dissenting voices regarding the removal of fibers in WWTPs. For example, Lares *et al.* (2018) noted that 91% of MPs in a WWTP's influent were fibers, but in the effluent, the abundance of fibers was roughly equivalent to the abundance of particles, which implies a better relative removal of fibers in that facility [35]. Gies *et al.* (2018) also reported that fibers comprised the majority (69%) of MPs in their WWTP's influent; while the concentrations of fibers/particles decreased by 98.6%/98.8%, respectively, fibers still dominated in the (60%) in the effluent [80], albeit at a slightly lower abundance. Park *et al.* (2020) noted that 68.2% of MPs were particles in the influent of the WWTP that they studied, while in the effluent, 82.3% were particles, reinforcing the preferential removal of MP fibers in the facility [111]. Finally, Ngo *et al.* (2019) suggest that the high aspect ratio of fibers make them more difficult to remove in filtration operations [51].

Other authors have suggested that fibers are more easily removed in early treatment steps than particles. As noted by Sun *et al.* (2019), researchers have specifically found that the relative abundance of fibers declined following 1° treatment steps [80, 91, 124, 127]. One explanation for this finding is that the high-aspect-ratio fibers may find themselves more easily entrapped in sludge flocs which are removed via simple sedimentation [16]. Entering 2° treatment, the primary effluent may be enriched in particles as oppose to fibers; this may explain why MP *particles* are then preferentially removed in the subsequent unit operations [16]. This has been seen to re-enrich the relative abundance of fibers following 2° treatment [91, 127, 134]. For example, Raju *et al.* (2020) noted that PESt MPs (*i.e.* fibers) accounted for 27% of MPs entering 2° treatment, but became enriched to 46% abundance following treatment [98]. However, exceptions to the norm are found to exist, as usual. Zhang *et al.* (2020) assert that fibers and film-like particles can be well-removed in 2° treatment as they easily adsorb to EPS and settle with sludge in 2° clarification [57, 110, 136]. It is thought that these removal behaviours can stem from different surface characteristics of the MPs. Long *et*

al. (2019) assert that MPs with smoother or non-weathered surfaces (*e.g.* fibers and pellets) are more difficult to remove [119]. It is further stated that fragments and other irregular shapes can be removed more effectively during biological treatment as their angular surfaces are more conducive to microbial attachment which can aid in their removal [51, 119]. Overall, it is widely understood that MP compositions/shapes and their removal rates vary within and between facilities; however, no overarching explanation of the variations is accepted. To further elucidate the complexity of the fate of MP shapes and compositions, the reader is referred to several relevant review articles [14, 24, 77].

1.2.2.4 Holistic Approaches to the Fate of Microplastics

Until recently, works which study the fate of MPs in WWTPs were largely compared qualitatively, or one-to-one; there was a lack of a quantitative assessment of the field as a whole. This is understandable as the (previously) small number of studies commissioned, the broad range of methodologies used, and the lack of standardization in the reporting of results made robust, quantitative comparisons difficult to perform.

To this end, Liu *et al.* (2021) performed a meta-analysis on the compiled MP removal results of 38 facilities reported in 24 peer-reviewed studies [14]. The technique overrides findings which are true for individual studies and instead reports findings which are true for the body of studies as a whole. In their analysis, they computed the weighted-average “risk ratio” (RR), a value which describes the “effect size” of a single observation. Values of $RR < 1$ imply the removal of a particular subset of MPs by a particular facility or technology; the smaller the value of RR, the greater the magnitude of the removal. The reader is referred to the original publication for a description of the methodology [14]. A brief summary of their results is found, below, and is illustrated in Figure 1.6.

In their analysis of the effectiveness of different treatment stages, average RR values for 1° (including preliminary), 2°, and 3° treatment were 0.40, 0.39, and 0.48. On its face, this implies that 1° and 2° processes were both more effective, on average, towards the removal of MPs versus 3° treatment processes, however the statistical significance of these observations is questionable. As specific examples of unit operations, the average RRs for 1° clarification, bioreactors, and filtration technologies were calculated to be 0.39, 0.41, and 0.33, respectively. All three of these processes

are quite effective towards the removal of MPs. In contrast, A²O processes and grit and grease removal without 1° settling were found to be less effective with RRs of 0.73 and 0.61, respectively. Interestingly, the “advanced oxidation” processes have a particularly wide 95% confidence interval which reflects their variable effectiveness towards MP removal. The confidence interval about all 3° technologies is broadened for this reason.

In their analysis of the removal of different shapes of MPs—fibers, fragments, films, and pellets by their own classification—results are less definitive, though interesting findings are still gleaned. In 1° treatment, the RR values indicate that, on average, MP fibers were most likely to be removed

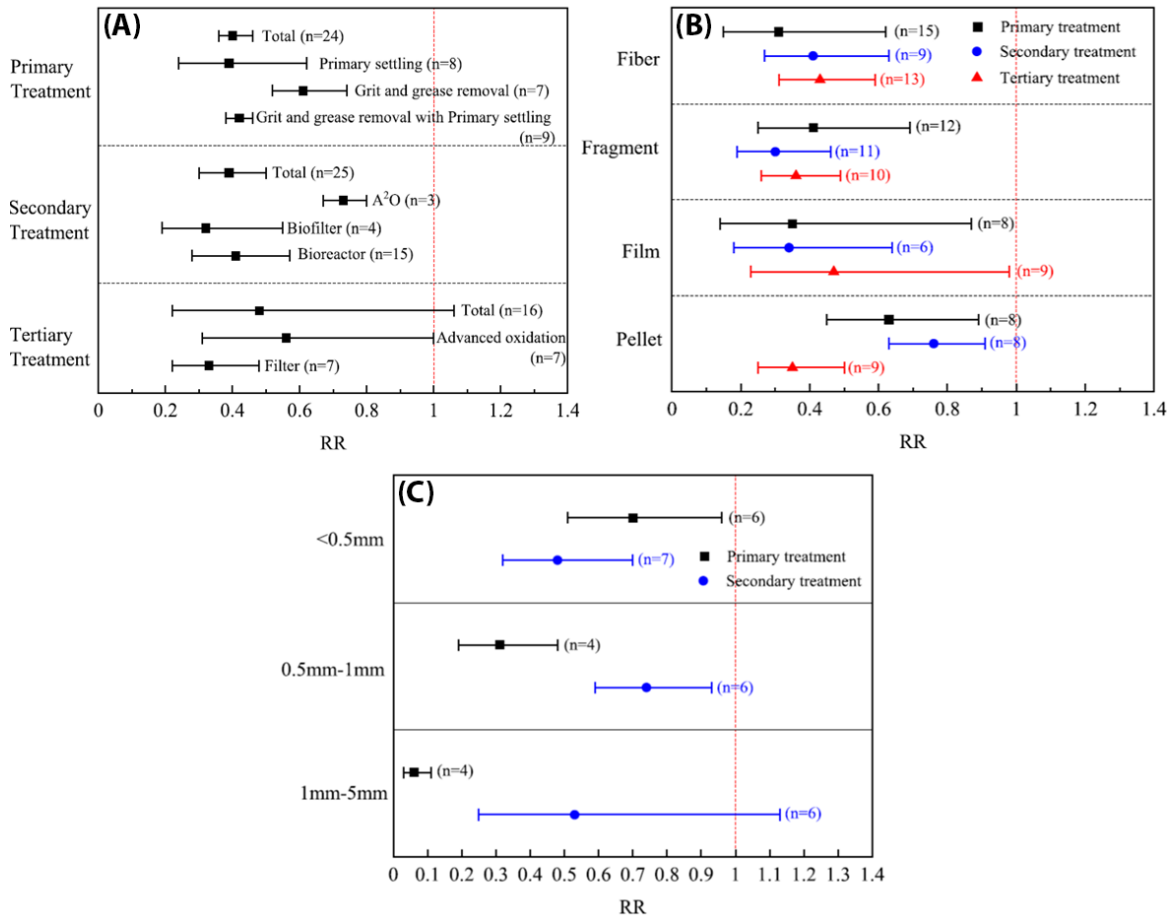


Figure 1.6: Summary of meta-analysis results performed by Liu *et al.* (2021), highlighting the effect of (A) specific treatment processes, (B) MP shape, and (C) MP size on the removal efficiency of the MPs in selected WWTPs [14]. The average risk ratios (RR) are shown along with 95% confidence intervals. Panels reused with permission from W. Liu, J. Zhang, H. Liu, X. Guo, X. Zhang, X. Yao, Z. Cao, and T. Zhang, “A review of the removal of microplastics in global wastewater treatment plants: Characteristics and mechanisms,” *Environment International*, vol. 146, p. 106277, 2021.

(RR = 0.31). In contrast, fragments were more likely to be removed in 2° treatment (RR = 0.30). These two findings are in line with the previous general discussions regarding the removal of different MP shapes. Finally, pellets (*i.e.* beads or spheres) saw the greatest removal in 3° treatment (RR = 0.35). Again, quantitative interpretations of the results should be handled cautiously due to the broad confidence intervals about the RRs. Due to a paucity of data, the removal of different size fractions of MPs was performed for just 1° and 2° treatment. Most evidently, the largest size fraction of particles (1–5 mm) demonstrated very effective removal (RR = 0.06) in primary treatment, but less so in 2° treatment (RR = 0.53; broad confidence interval). Similarly, the middle size fraction (0.5–1 mm) was most effectively removed in 1° treatment (RR = 0.31), but less so in 2° treatment (RR = 0.74). In line with some previous findings, the smallest particles (< 0.5 mm) were best captured in 2° treatment (RR = 0.48). However, the coarse size bins presented in this analysis make reporting meaningful conclusions difficult. Broadly speaking, these findings are in line what was seen in many of the individual results noted in §1.2.2.3.

Similarly, Azizi *et al.* (2020) performed their own meta-analysis on a heavily-pruned subset of 77 facilities in 18 peer-reviewed studies based on stringent selection criteria [45]. Their findings suggest that MP concentrations indeed decrease with every treatment step that is added to the train. On average, MP concentrations were calculated as 124.04, 20.67, 5.62, and 1.97 MPs/L in the influent, 1°, 2°, and 3° effluents, respectively. Perhaps surprisingly, their results suggest that MP shape was actually not an important characteristic in driving MP removal efficiency, although a significant degree in heterogeneity is noted between the studies that were included in the analysis [45].

While these meta-analyses are valuable in that they help to better quantify the fate of MPs in WWTPs, they are limited in several aspects. Most notably, they are completely reliant on the work performed by other researchers, their techniques, and their process of reporting results. As there is a grievous lack of standardization in this field, the comparison of results using different techniques is bound to introduce error in the composite results when the meta-analysis researchers attempt to aggregate the data. In several of the analyses performed by Liu *et al.* (2021) in particular, only a small number of studies were considered (*e.g.* $N = 3$ for A²O [14]) which is not necessarily a criticism of the researchers, but more a commentary on the availability of suitable data as a whole. Finally, the findings presented in the meta-analyses should be interpreted cautiously as the models

are purely explanative: they are not based in scientific/engineering theory and cannot be accurately predictive in nature. Regardless, it is clear that the removal of MPs in WWTPs is a complex topic and significant research is still required to understand the fate of these contaminants and to better design/optimize processes for their removal.

1.3 Research Motivations

In §1, it was introduced that MPs are a concerning new form of pollution. In §1.1.2, MP pollution in the aquatic environment was detailed along with evidence that this form of plastic debris presents a persistent ecological hazard. As an extension, §1.1.3 highlighted some potential health hazards associated with MPs and the human body. Then from §1.2, it is clear that WWTPs are a significant source of MPs despite the fact that—as seen in §1.2.2—many of these facilities are relatively effective towards the removal of the particles. Given the significant releases of MPs and the potential harms that researchers consider to be associated with them, technologies should be developed, installed, and/or optimized to maximize the removal of MPs from the effluents of WWTPs.

One possible approach to mitigating the efflux of MPs from WWTPs is through the use of *additional* technologies to remove the last traces of MPs prior to discharge. That is, polishing steps in the form of 3° treatments are a feasible way of achieving discharge objectives without drastically altering the layout of already-existing installations. Evidence in the current literature indicates that 3° treatment steps such as coagulation/flocculation, advanced oxidation processes, biofilters, particle/media filtration, and membrane technologies can be effective methods for removing residual MPs from wastewater effluents [23, 34, 50, 114, 116, 137–139]. To restate evidence described in §1.2.2.2, one estimate suggests that following 3° treatment steps, 98–99.9% of MPs were removed compared to only 86–99.8% removal of MPs following 2° treatment steps [16]. However, recall that the effectiveness of MP removal is a complex function of wastewater/MP properties and critically, the exact unit operations (*e.g.* particle/media filtration, biologically-active processes, oxidation, photodegradation, membranes, etc.) that are employed. Evidence from the field of drinking water treatment plants (DWTPs) can also be used, here, to provide insights into MP removal in WWTPs as both applications share some similar unit operations (*e.g.* media filtration). Evidently, the study of MPs in DWTPs appears less developed than the study of MPs in WWTPs [20]. As an example, Zhang *et*

al. (2020) assessed the removal of purchased MP beads via conventional drinking water treatment technologies including coagulation/flocculation combined with sedimentation as well as a granular filtration process using anthracite coal [140]. They lament that the former process was inadequate for the removal of the particles (*e.g.* $\sim 13.6\%$ removal rate for 45–53 μm particles). However, the latter process was effective at removing up to 99.9% of particles, though this effect was size dependent: large (*e.g.* $> 45 \mu\text{m}$) and very small (*e.g.* $\leq 1 \mu\text{m}$) particle size fractions were well-removed, but mid-sized particles in the range of 10–20 μm were more moderately removed (86.9%). Furthermore, in the three works reviewed by Barchiesi *et al.* (2021), a variety of coagulation, flocculation, sedimentation, granular activated carbon adsorption, sand filtration, and flotation processes are employed, however the total MP removal efficiencies only ranged from 70–88.6% using these technologies [21]. The authors of this review suggest that most filtration systems—*with the exception of membrane technologies*—are not dependable for comprehensive removal of MPs [21].

Evidence from the literature indeed points to the existence of significant variability in the efficacy of 3^o technologies towards MP capture, yet *membrane technologies appear to be particularly well-positioned for the removal of the MPs*. The ideality of membranes for this application is related to two important factors. Firstly, membranes have small pores—perhaps smaller than the MPs or NPs—which should be effective towards rejecting the MPs while allowing for the treated water to pass through. As such, an “ideal” membrane with small pores should act as a perfect barrier to the MPs and completely prevent their transmission into the facility effluent. Secondly, some WWTPs already employ membranes either in the form of MBRs or as a 3^o polishing step for the final removal of organic matter/nutrients to comply with discharge regulations (*e.g.* Canada’s *Wastewater Systems Effluent Regulations* [141]). Various membrane offerings are already validated for use in water and wastewater treatment applications, therefore, an “off-the-shelf” solution to the MP efflux problem may be inherently possible. To this end, many researchers specifically point to membrane-based technologies as perhaps the most promising MP removal candidates due to their high ($\geq 99\%$) potential MP recoveries [16, 21, 34, 50, 51, 56, 132, 142, 143]. The efficacy of MP removal via membranes will now be considered. For the edification of the reader, a primer on membrane science is presented in §2.1 in Chapter 2.

1.3.1 Microplastics Removal via Membrane Technologies

The contemporary literature contains a variety of evidence which documents (a) how MPs are removed by membrane operations in WWTPs, and (b) how membranes remove MPs under very controlled experimental conditions in the laboratory. To elaborate:

1.3.1.1 Removal Performance in Existing Wastewater Treatment Plants

There is good evidence in the contemporary literature from observational studies of WWTPs to suggest that membrane technologies perform well (*i.e.* high η) for the removal of MPs from wastewater effluents [32, 34, 35]. To begin, page 32 of §1.2.2.2 contains a discussion of findings from a variety of studies of WWTPs which utilize membrane technologies. A summary of these results, along with findings from other related studies, can be found in Table 1.2. The MP removal efficiencies are reported (based on MP number concentrations) for the unit operations containing the membranes and not for the whole plant—unlike previously seen in Table 1.1. It bears repeating that the findings of these studies should be compared cautiously due to differences in methodologies, the possibility of contamination of dilute samples, along with other aforementioned factors.

As is evident from Table 1.2, membranes have shown to be very effective for MP removal in some facilities; six of the eleven studies demonstrated over 95% removal of the particles by the membrane technologies, alone. Three of the other five facilities either show moderate removal of MPs by the membranes (*e.g.* 70–90%), whereas two facilities demonstrate poor 25% removal efficiencies. As additional corroborating evidence, a 2015 study by the New York Office of the Attorney General sampled the effluents of 34 WWTPs in the state and tested them for the presence of MP beads. Of these plants, nine were found to have no detectable trace of MP beads in their effluent, five of which use a microfiltration-based polishing step. However, as the study only accounted for MP beads, the effluent MP counts were almost certainly underestimated. Here, a few of the membrane processes from WWTPs highlighted in Table 1.2 will be considered in more detail.

Firstly, Baresel *et al.* (2019) noted that they did not find any MPs in effluent samples obtained from a Swedish MBR (reported pore size = 0.2 μm) [144]. However, they did not elaborate on their methodology, therefore, this result must be interpreted very cautiously. Further, Michielssen *et al.*

Table 1.2: The performance of membrane technologies towards the removal of MPs, as reported in eleven research studies, ordered by decreasing average MP removal efficiency η . The value of η is reported for the specific unit operation, and not the facility as a whole.

Ref.	Location	Membrane Process	Process η
[144]	Sweden	Submerged MBR; flat-sheet UF [†] membranes (<i>Alfa Laval MFM 100</i>); reported pore size = 0.2 μm	~100%
[34]	Finland	Submerged pilot MBR; flat-sheet UF [†] membranes (<i>Kubota</i>); reported pore size = 0.4 μm	99.9%
[35]	Finland	Submerged pilot MBR; flat-sheet membranes (<i>Kubota</i>); reported pore size = 0.4 μm	99.9%
[114]	USA	MBR; ceramic disc membranes (<i>Grundfos BioBooster MFU</i>); reported pore size = 0.2 μm	99.1%
[145]	Italy	Externally-submerged sidestream pilot MBR; hollow fiber UF membranes (<i>Koch Puron</i>); reported pore size = 0.03 μm	97%
[146]	Spain	Unspecified MBR	96.2%
[81]	China	Unspecified submerged MBR; hollow fiber membranes; reported pore size = 0.1 μm	82.1%
[113]	Spain	Submerged MBR; flat-sheet membranes (<i>Kubota EK-400</i>)	79%
[27]	China	Unspecified UF membranes in series with other 3 ^o treatment processes	71.7%
[91]	Australia	Unspecified UF/RO polishing processes	25%
[87]	Netherlands	Unspecified MBR; reported pore size = 0.08 μm	25% [‡]

[†]This “UF” label reported by the authors does not fit the “typical” definition of this type of membrane with respect to the reported pore size. [‡]MP removal efficiency is not statistically-significant.

(2016) evaluated the effectiveness of an American pilot-scale MBR unit [114]. This system contained a ceramic disc microfiltration (MF) membrane (pore size = 0.2 μm). The MBR alone removed 99.1% of MPs which were sent to it, while 88.9% of MPs still in the MBR effluent were found to be fibers (0.47 MPs/L). This membrane also appears to allow the preferential transmission of fibers over fragments. While the overall removal of MPs is impressive, the incomplete retention of the MPs leads to the possibility that some particles are able to pass through the membrane due to their morphologies, or due to a broad membrane pore size distribution. A Finnish pilot-scale MBR that was studied by Talvitie *et al.* (2017) was found to remove 99.9% of MPs, most of which were fibers [34]. The unit contained 8 m² of Kubota flat-sheet chlorinated PE membrane (nominal pore size = 0.4 μm). Notably, the membrane retained MPs of all shapes, sizes and compositions, with the exception of a small number of PEst fibers. A more comprehensive study by Lares *et al.* (2018) using the same

MBR unit further elucidated the membrane’s effectiveness: 99.8% and 99.6% of particles and fibers, respectively, were removed [35]. Roughly 40% of the particles in the permeate stream were above 1,000 μm in size, another $\sim 40\%$ were 250–1,000 μm in size, while the remaining $\sim 20\%$ were below 250 μm . It is perplexing that the larger particles (particle size \gg pore size) may have passed through the membrane. A similar result was observed by researchers studying the poorest-performing unit in Table 1.2, whose Dutch pilot-scale MBR (undisclosed membrane; stated pore size = 0.08 μm) transmitted 51 MP/L, on average [87]. The authors, here, suggest that fiber transmission may occur longitudinally through the membrane pores, a phenomenon which has been observed elsewhere [147]. In each of these studies, other possible explanations for MPs in permeate samples include membrane defects or gaps in the modules, the likely contamination of the dilute samples, or fragmentation of the MPs during pumping. The hypothesis of fragmentation is shared by researchers studying a Chinese MBR [81]. The system used was reported to remove 82.1% of MPs on a *number basis*, but 99.5% of MPs on a *mass basis*, suggesting again that significant fragmentation of the MPs occurred which increased the overall *number* of MPs across the process.

Instead of using MBR technologies, the facility studied by Ziajahromi *et al.* (2017) utilized sequential UF and RO membranes as a high-quality final polishing step [91]. In theory, RO membranes should produce effluent that is devoid of MPs or any other suspended solids due to the very tight solute cutoff. However, a MP concentration of 0.21 MP/L was detected in the permeate water, the vast majority of which were fibers. The authors explicate that the RO membranes are not always perfect separators and surmise that membrane defects or “larger size pores” may be to blame [91]. While the premise and the former interpretation are viable, the latter explanation misrepresents the mechanism by which these membranes separate particles from water: a preferential diffusion of water through a dense polymer film as oppose to the sieving of solutes in a porous network [148]. (See §2.1.1 for information on types of membrane transport.) A more reasonable possible explanation may involve imperfect sealing around membrane units, or mere sample contamination. This explanation is particularly likely due to the low MP concentrations and the nature of the MPs (fibers) which may have originated from the experimenters’ clothes. Membrane defects and leaks in seals may be present, especially with wear-and-tear over time, though additional research is needed to confirm or deny this hypothesis. In the other study which utilized 3^o membrane technologies, the authors did not provide a good explanation for the poor membrane performance and merely suggested that the

results were on par with other studies and 3° technologies [27].

From Table 1.2, it is evident that most of the facilities studied utilized various models of MBRs. As such, there is a good opportunity to perform novel research regarding membranes and membrane modules designed for 3° treatment stages instead—even at a laboratory scale. Furthermore, the installation 3° polishing technologies at the end of poorly-performing WWTPs appears to be less invasive/complex than retrofitting MBRs to replace/augment 2° or 3° treatment processes. *With this in mind, the research in this work seizes this opportunity and will focus on providing insights into the performance of MF and UF membrane systems for these 3° effluent polishing applications.*

1.3.1.2 Removal Performance in Laboratory Experiments

In contrast, there are fewer studies in the contemporary literature that contain laboratory experiments designed to assess the MP removal abilities of membranes under controlled conditions. To clarify, there are *plenty* of studies (*e.g.* [149–151]) that use *microparticles* or *nanoparticles* in the context of studying membrane filtration phenomena. While these sorts of investigations can serve as a guide to predict the physicochemical interactions between MPs and membranes, they do not tell the “full story” as the solution conditions (*e.g.* “pristine” buffers, ultrapure water), microparticles (*e.g.* spherical microbeads), membranes (*e.g.* bioseparations membranes), and operating conditions (*e.g.* dead-end filtration) are not necessarily representative of what is seen in actual WWTPs (*e.g.* complex solution matrices like wastewater with ample suspended/dissolved solids, irregular MPs, crossflow filtration, backwashing, etc.). While more representative conditions have been considered at various points in isolation, research at the intersection of these conditions is still needed. To this end, controlled laboratory studies which consider MP/membrane interactions have been performed, including the following investigations.

In novel laboratory-scale research involving coagulants and membranes, Ma *et al.* (2019) investigated the removal of PE MPs from freshwater in drinking water applications in back-to-back studies [152, 153]. The investigations used flat sheet polyvinylidene fluoride (PVDF) UF membranes obtained from Tianjin Motimo Membrane Technology Ltd. and Ande Membrane Separation Technology & Engineering. Both membranes were reported to have 30 nm nominal pore sizes. It was

found that the membranes were able to retain all PE MPs to which the membranes were challenged. However, the authors did not characterize the particle size sufficiently for the significance of this result to be elucidated; the smallest size fraction was nominally “< 500 μm ”. As perhaps a more important limitation to this study, it would be expected that the MPs used by Ma *et al.* would be largely removed by 1°/2° treatment stages and therefore the membranes would not see, many particles of this large size ($\sim 500 \mu\text{m}$), in actuality. Considering this lower size bound, the implication is that the major dimension of these MPs would be almost 17,000 \times larger than the stated pore size, and in the absence of leaks or defects, the complete rejection of individual non-coagulated MPs could be almost guaranteed. When either FeCl_3 or AlCl_3 coagulants were added to the prepared suspensions of MPs, the permeate flux declined significantly due to the formation of a MP cake layer on the membrane. This layer was much less prominent when the MPs were in suspension without any coagulant. Findings suggest that the addition of coagulant to MP suspensions may hinder the performance of a downstream UF step by creating a dense, resistive cake layer. A substantive discussion on membrane fouling theory can be found in §2.1.3.

Providing more value to the field, in a very recent work, Pizzichetti *et al.* (2023) performed a mechanistic analysis on MP fouling of cellulose acetate MF membranes (Mervilab; stated pore size = 5 μm) by PA and PS MPs with average sizes of $41 \pm 16 \mu\text{m}$ and $109 \pm 74 \mu\text{m}$, respectively [154]. The MPs were suspended in pure water at concentrations from 1–20 mg/L and filtered at transmembrane pressures from 0.1–0.7 bar in hour-long experiments. In constant-pressure filtration tests, it was found that higher MP concentrations (regardless of material) induced greater flux declines due to membrane fouling. Similarly, when varying the applied transmembrane pressure with the MP concentrations held constant, higher pressures were associated with greater magnitudes of flux declines, presumably because these higher pressures resulted in a greater accumulation of MPs on the membrane surfaces. A maximum transmembrane pressure threshold was seen, between 0.3–0.5 bar, which balanced the productivity of permeate water and the magnitude of fouling effects. The researchers also noted that the neutrally-charged PA MPs caused a greater degree of fouling which was attributed to their smaller size, resulting in denser cake layer formed on the membrane surface. In contrast, they noted that the larger, negatively-charged PS MPs with highly-irregular shapes formed a looser cake layer which was less resistive to the flow of water and therefore saw a lower magnitude of flux decline [154]. While this study provides valuable mechanistic insights into MF

membrane performance in the presence of MPs, it is limited in that the solution conditions do not mimic the complexity of real wastewater and the stated membrane pore size is an order of magnitude larger than what is typically used in these applications.

Similarly, Pramanik *et al.* (2021) considered the filtration of fragmentable MPs via MF and UF membranes, namely 0.1 μm PVDF (*Millipore VVLP*) and 100 kDa molecular weight cutoff polyethersulfone (*Millipore PBHK*) flat sheet models [155]. 75–300 μm primary particles having PE, PVC, and PEst chemistries were fragmented in water via shear forces induced by mixing and were used in subsequent 24-hour filtration experiments. These experiments were carried out in pure water (again) in an *Amicon*® stirred cell device (membrane area = 13.4 cm^2) at 70 kPa of transmembrane pressure. Nanoparticle tracking analysis (NTA) was performed to quantify the presence of the MPs in feed and permeate samples. Rejection was found to be somewhat size-dependent for both types of membranes, with the UF membrane providing a greater degree of particle rejection than the MF membrane. Maximum particle rejections of 96% and 91% were recorded for the UF and MF, respectively, which is unexpected given that the MPs were significantly larger (0.74–1.88 μm) than the UF membrane’s pores. This may be an indicator of leakage or broad pore size distributions. The UF membrane was also found to have a higher rate of flux decline due to fouling than the MF membrane, though the authors suggest that a better understanding of the fouling mechanisms and kinetics are necessary to understand the phenomenon.

To this end, in a series of well-received research papers, Enfrin *et al.* considered various aspects of membrane fouling via MPs [156]. Initially, they studied the fouling of 30 kDa molecular weight cutoff polysulfone (PSf) UF membranes (area = 33.5 cm^2). Fouling was induced by very small, irregularly-shaped MPs (size = 13–690 nm; concentration = 10 mg/L) isolated from a facial scrub. Permeate flux decline experiments were conducted at constant pressure (1 bar) in a *Sterlitech CF042AC* crossflow filtration cell. Over 48 hours, a permeate flux decline of 38% was recorded in the presence of the added particles, compared to 15% when only pure water was filtered. Intermediate pore blocking and subsequent cake filtration mechanisms (see §2.1.3.1) were proposed due to the deposition of the hydrophobic particles onto the membrane. While the crossflow filtration mode used in this study was more amenable to real wastewater treatment processes—as oppose to the study by Pramanik *et al.* (2021)—this study is similarly limited in that the solution

conditions do not well reflect those found in WWTPs. The presence of organic matter or other suspended/dissolved solids would ameliorate the quality of this research, though giving credit to the authors, their choices of solution conditions were justified using drinking water treatment as an end application. In subsequent investigations, Enfrin *et al.* probed the fouling behaviour of PET nanofibers (length = 13 ± 7 μm ; concentration = 10 mg/L) filtered with the same membranes in the same crossflow configuration [157]. The solution with the fibers also contained model organic contaminants (polyvinyl alcohols and polyethylene glycols; concentrations = 0.01–1 mg/L). During filtration experiments, the organic contaminants contributed to a 50% flux decline due to internal pore fouling versus only 10% attributed to the loose mat of entangled fibers which deposited on the membrane surfaces. This entanglement was found to occur at low shear rates; in contrast, greater degrees of turbulence were found to reduce the adsorption of the fibers. Overall, the organic molecules were a far stronger contributor to the membrane fouling than the fibers, themselves. Adding these organic molecules into the feed solution helps to simulate the dissolved solids found in wastewater, though better analogues can be found (*e.g.* humic acids from NOM). Additional work regarding the fouling of membranes via PS fibers as well as the quantification of fiber transmission can be found in the investigations presented by B. Patterson (2021) [147].

To mitigate the effects of MP fouling, Enfrin *et al.* also investigated the effectiveness of techniques such as surface modification [158] and physical cleaning via air scouring [159]. For example, plasma polymerization of hydrophilic monomers (acrylic acid and cyclopropylamine) onto the surface of the aforementioned hydrophobic PSf membranes was performed. Compared to the original unmodified membranes, the researchers found that these surface treatments reduced the adsorption of the irregular PE MP particles obtained from facial scrubs (93 ± 1 nm; 10 mg/L) by more than 60% [158], demonstrating that hydrophilic membranes have a lower propensity for fouling due to hydrophobic particles. As an extension of this technique, even with UF membranes that were specifically treated with a hydrophobic hexamethyldisiloxane coating, gas scouring limited the MP-induced flux decline to 23% versus 38% when no cleaning was performed; simultaneously, the adsorption of the particles was roughly halved [159]. The results of these studies indicate that chemical properties (*e.g.* hydrophilicity) play an important role in governing the MP/membrane interactions that cause fouling and affirm that data-driven selection, design, and operation of membranes/membrane systems can improve the performance of the processes.

While all these studies have provided insights on the interactions between membranes and MPs, in particular, the solution conditions used (pure water and model organic foulants) to suspend the particles do not represent well the solution conditions of effluent wastewater. Further research is needed to quantify these effects in more complex solution chemistries that adequately represent the wastewater fed to 3° membrane polishing operations: this consideration will be an important focus of this work.

1.3.2 Opportunities for Novel Research

It has been established that membrane technologies are prime candidates to mitigate the efflux of MPs from WWTPs. However, the membranes that are currently used in WWTPs are *not designed, tested, and implemented for the explicit removal of MPs* [132]. Initial anecdotal and deliberate investigations suggest that membranes are at least effective—but not necessarily perfect—in this application. From a survey of the literature, it can be seen that efforts are still needed to comprehensively characterize the performance of these technologies (*e.g.* rejection, throughput, lifespan, etc.), especially at the intersection of membrane/MP properties, solution conditions, and system operating parameters. *Addressing this knowledge gap is the overall goal of this work*—specifically, elucidating the interactions between MP particles and MF/UF membranes in the application of 3° wastewater polishing. As a note to the reader, *focus in this work is given to MP particles* which are a very common MP morphology in WWTPs. While MP fibers are also commonplace and present their own challenges, they are out-of-scope, here.

As a result of the synthesis of various contemporary literature sources and my own insights, I have developed a list of six thematic elements to guide novel research involving the removal of MPs via membrane technologies. Descriptions of the shortfalls addressed by these elements originate from the discussions in §1.1–1.3. While this list is not comprehensive, it serves as a basis for guiding the selection of experimental parameters with the goal of producing research which is valuable to the field. The thematic elements are represented in the infographic in Figure 1.7 and described below:

1. **Irregular-shaped microparticles.** As noted in §1.1.1, the MPs found in WWTPs vary widely in their shape, but overall, they tend to be irregular in nature. That is, a variety of angular particles (fragments) and high-aspect-ratio fibers are often seen, as oppose to perfectly

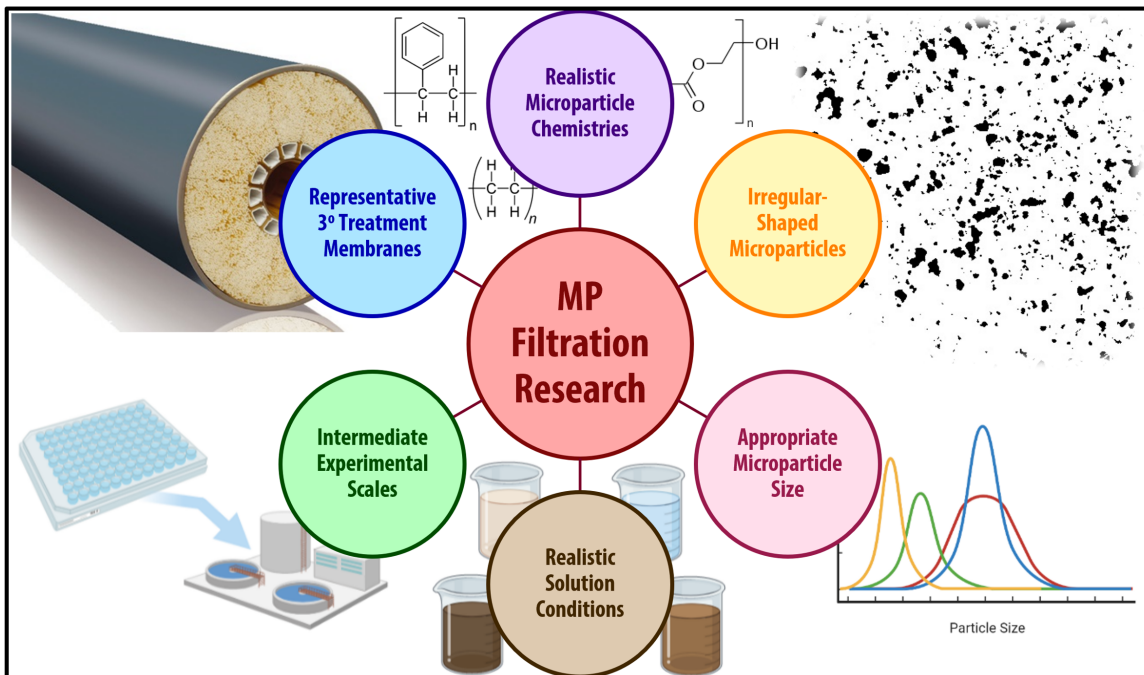


Figure 1.7: Illustration of the six critical thematic elements examined in this work which add value at the research nexus of membranes and MPs.

spherical beads. Spherical microparticles are easily purchased (*e.g.* Cospheric’s lines of polymer microspheres), however, monodisperse spheres do not adequately represent the most common types of MPs found in WWTPs. Like with the irregular MPs used by researchers such as Enfrin *et al.* (2020) or Pizzichetti *et al.* (2023) [154, 156], efforts should be made—where possible—to use irregular-shaped microparticles in MP filtration experiments to ensure that the obtained results are realistic in nature. The importance of appropriate MP shape is reinforced by previous fundamental filtration studies; it is well-understood that geometric factors such as the aspect ratio of analytes (*e.g.* Au nano-rods; capsular bacteria) and their conformation within membrane pores can significantly affect their rejection [160, 161]. It is hypothesized that the rejection of MPs in tortuous porous networks is significantly influenced by their high degree of irregularity and heterogeneity.

2. **Appropriate microparticle sizes.** As noted in §1.2.2.3, larger MPs tend to be well-removed in early stages of WWTPs. This enriches smaller size fractions which are discharged in the effluents. As such, there is little value in performing membrane filtration research using large size fractions of MPs (*e.g.* 1–5 mm, or even perhaps 0.1–1 mm). Instead, focus should rest on smaller size fractions. Of particular interest are MPs smaller than the narrowest commonly-

used sieve aperture (20 μm) for collecting MPs in WWTPs, as indicated in §1.2.1. There is a dearth of research involving the fate of these very small MPs. This represents a significant opportunity to perform research that adds substantial value to the field. Furthermore, it is evident that MPs in WWTPs are polydisperse in terms of their size, though the breadth of which is dependent on the facility that is studied. This should be taken into consideration when MP feedstocks are considered for filtration research. Whereas monodisperse populations of particles are easier to work with, polydisperse populations better represent the actual nature of MPs in WWTPs.

3. **Realistic solution conditions.** The current literature contains two contrasting bodies of research studies involving particles which can be construed as MPs: there exist many large-scale observational studies of WWTPs where investigators passively assess the ability of the facilities to remove MPs; and, there exist many laboratory-scale experimental studies of fundamental filtration phenomena using polymer nano- and microparticles. The former case involves complex water matrices, whereas the latter case involves relatively pure solutions. As a particularly important factor, investigators should choose solution compositions that represent those seen in WWTPs (*e.g.* actual wastewater) or closely mimic it, if necessary, such that interactions between the solution matrix, MP particles, and membrane process can be elucidated.
4. **Intermediate experimental sizes and time-scales.** The aforementioned divide between large-scale observational studies versus laboratory-scale experimental studies continues. The former case involves very large volumes of water observed over extended timescales (*e.g.* $\sim 10^8$ L per day), whereas the latter case involves very small volumes and short timescales (*e.g.* $\sim 10^{-1}$ L per hour-long experiment). As such, there is a tremendous opportunity to bridge these two regimes and perform research at moderate (reasonable) experimental sizes, time scales, and operating conditions, all while using realistic experimental conditions.
5. **Representative 3^o treatment membranes.** Membranes can be purchased or synthesized in a variety of pore sizes and chemistries and operated in various geometries and flow paths. Discussions of membrane properties are covered, in depth, in §2.1.1; discussions of the types of membranes used in municipal WWTPs are covered in §2.2.2. Briefly, focus should be on hollow fiber/flat sheet UF/MF membranes operated in a crossflow mode which all tend to be found in wastewater treatment applications. PVDF membrane chemistries should be targeted

for the same reason. To address the paucity of research in this area, the membranes which are evaluated should be specifically designed for use in 3° wastewater treatment applications, where possible. This factor also encompasses the “realistic” operation of these representative membranes, such as the use of backwashing and cleaning processes (see §2.1.3.3) which are commonplace in actual membrane installations.

6. **Realistic microparticle chemistries.** While it has been noted in §1.2.2.3 that > 30 MP polymers have been identified in samples taken from WWTPs, certain polymers have been recorded much more frequently than others: PE, PEst, PET, PA, PS, and PP. MPs consisting of “rarer” polymers (*e.g.* polysulfone [16]) could be found in a WWTP, however more prevalent compositions should be targeted. MPs of different chemical identities have differing surface properties—hydrophobicity/hydrophilicity, surface charge, etc.—which govern their interactions with other MPs (*e.g.* homoaggregation), other species like NOM (*e.g.* heteroaggregation), and critically, membrane surfaces (*e.g.* fouling and rejection phenomena). Via §1.2.2.3/§1.3.1.2, it is seen that chemical composition (MP *and* membrane material) influences MP removal, thus the choice of MP chemistry should be carefully considered.

■ **Research objectives in this work.** With this in mind, four individual research studies were commissioned to help understand the performance of these membranes and to guide the *intelligent design and operation of 3° treatment membrane processes*. These investigations are guided by surveys of the literature, especially the discussions in §1.3.1. To this end, the high-level research objectives of these studies are stated, below, along with the thematic elements which are most overtly considered:

- ▶ **Chapter 3.** To what extent does the presence of irregular and polydisperse MP particles affect the fouling of UF and MF membranes when 2° effluent wastewater is filtered? (*Elements 1–4 & 6*)
- ▶ **Chapter 4.** How does the pore size of a MF membrane affect the transmission of irregularly-shaped, polydisperse MP particles over a range of permeate fluxes? (*Elements 1–2 & 6*)
- ▶ **Chapter 5.** What value can the technique of flow cytometry provide towards “non-bulk” quantification of individual (fluorescent) MPs suspended in membrane feed and permeate samples? (*Elements 2–3*)

- **Chapter 6.** When 2° effluent wastewater containing MPs is processed via microfiltration, what insights can be obtained regarding membrane performance (*e.g.* fouling behaviour, MP rejection) when the process is scaled up to the “module” level and operated over repeated filtration/cleaning cycles? (*Elements 2–6*)

These four research studies are presented in Chapters 3–6. But first, the subsequent chapter summarizes background theory on membrane science (§2.1) and municipal wastewater treatment (§2.2) to contextualize the information that was presented in Chapter 1 and to provide a theoretical foundation for the included research studies.

1.4 Works Cited

- [1] C. Reed, “Dawn of the plasticene age,” *New Scientist*, vol. 225, pp. 28–32, 2015.
- [2] C. G. Avio, S. Gorbi, and F. Regoli, “Plastics and microplastics in the oceans: From emerging pollutants to emerged threat,” *Marine Environmental Research*, vol. 128, pp. 2–11, 2017.
- [3] S. L. Wright and F. J. Kelly, “Plastic and Human Health: A Micro Issue?” *Environmental Science & Technology*, vol. 51, pp. 6634–6647, 2017.
- [4] “The New Plastics Economy: Rethinking the Future of Plastics,” World Economic Forum, 2016. [Online]. Available: https://www3.weforum.org/docs/WEF_The_New_Plastics_Economy.pdf
- [5] O. S. Alimi, J. F. Budarz, L. M. Hernandez, and N. Tufenkji, “Microplastics and Nanoplastics in Aquatic Environments: Aggregation, Deposition, and Enhanced Contaminant Transport,” *Environmental Science & Technology*, vol. 52, pp. 1704–1724, 2018.
- [6] A. L. Andrady, “Microplastics in the marine environment,” *Marine Pollution Bulletin*, vol. 62, pp. 1596–1605, 2011.
- [7] T. Rocha-Santos and A. C. Duarte, “A critical overview of the analytical approaches to the occurrence, the fate and the behavior of microplastics in the environment,” *Trends in Analytical Chemistry*, vol. 65, pp. 47–53, 2015.
- [8] J. R. Jambeck, R. Geyer, C. Wilcox, T. R. Siegler, M. Perryman, A. Andrady, R. Narayan, and K. L. Law, “Plastic waste inputs from land into the ocean,” *Science*, vol. 347, pp. 768–771, 2015.
- [9] D. Eerkes-Medrano, R. C. Thompson, and D. C. Aldridge, “Microplastics in freshwater systems: A review of the emerging threats, identification of knowledge gaps and prioritisation of research needs,” *Water Research*, vol. 75, pp. 63–82, 2015.
- [10] W. J. Sutherland, S. Bardsley, L. Bennun, M. Clout, I. M. Côté, M. H. Depledge, L. V. Dicks, A. P. Dobson, L. Fellman, E. Fleishman, D. W. Gibbons, A. J. Impey, J. H. Lawton, F. Lickorish, D. B. Lindenmayer, T. E. Lovejoy, R. M. Nally, J. Madgwick, L. S. Peck,

- J. Pretty, S. V. Prior, K. H. Redford, J. P. Scharlemann, M. Spalding, and A. R. Watkinson, “Horizon scan of global conservation issues for 2011,” *Trends in Ecology & Evolution*, vol. 26, pp. 10–16, 2011.
- [11] V. Hidalgo-Ruz, L. Gutow, R. C. Thompson, and M. Thiel, “Microplastics in the Marine Environment: A Review of the Methods Used for Identification and Quantification,” *Environmental Science & Technology*, vol. 46, pp. 3060–3075, 2012.
- [12] D. G. Shaw and R. H. Day, “Colour- and form-dependent loss of plastic micro-debris from the North Pacific Ocean,” *Marine Pollution Bulletin*, vol. 28, pp. 39–43, 1994.
- [13] R. C. Thompson, Y. Olson, R. P. Mitchell, A. Davis, S. J. Rowland, A. W. John, D. McGonigle, and A. E. Russell, “Lost at Sea: Where Is All the Plastic?” *Science*, vol. 304, p. 838, 2004.
- [14] W. Liu, J. Zhang, H. Liu, X. Guo, X. Zhang, X. Yao, Z. Cao, and T. Zhang, “A review of the removal of microplastics in global wastewater treatment plants: Characteristics and mechanisms,” *Environment International*, vol. 146, p. 106277, 2021.
- [15] L. D. K. Kanhai, K. Gardfeldt, T. Krumpfen, R. C. Thompson, and I. O’Connor, “Microplastics in sea ice and seawater beneath ice floes from the arctic ocean,” *Nature Scientific Reports*, vol. 10, pp. 1–11, 2020.
- [16] J. Sun, X. Dai, Q. Wang, M. C. van Loosdrecht, and B. J. Ni, “Microplastics in wastewater treatment plants: detection, occurrence and removal,” *Water Research*, vol. 152, pp. 21–37, 2019.
- [17] M. A. Browne, P. Crump, S. J. Niven, E. Teuten, A. Tonkin, T. Galloway, and R. Thompson, “Accumulation of Microplate on Shorelines Worldwide: Sources and Sinks,” *Environmental Science & Technology*, vol. 45, pp. 9175–9179, 2011.
- [18] M. A. Browne, S. J. Niven, T. S. Galloway, S. J. Rowland, and R. C. Thompson, “Microplastic moves pollutants and additives to worms, reducing functions linked to health and biodiversity,” *Current Biology*, vol. 23, no. 23, pp. 2388–2392, 2013.
- [19] L. Van Cauwenberghe and C. R. Janssen, “Microplastics in bivalves cultured for human consumption,” *Environmental Pollution*, vol. 193, pp. 65–70, 2014.
- [20] A. A. Koelmans, N. H. M. Nor, E. Hermsen, M. Kooi, S. M. Mintenig, and J. D. France, “Microplastics in freshwaters and drinking water: Critical review and assessment of data quality,” *Water Research*, vol. 155, pp. 410–422, 2019.
- [21] M. Barchiesi, A. Chiavola, C. D. Marcantonio, and M. R. Boni, “Presence and fate of microplastics in the water sources: focus on the role of wastewater and drinking water treatment plants,” *Journal of Water Process Engineering*, vol. 40, p. 101787, 2021.
- [22] G. Gatidou, O. S. Arvaniti, and A. S. Stasinakis, “Review on the occurrence and fate of microplastics in Sewage Treatment Plants,” *Journal of Hazardous Materials*, vol. 367, pp. 504–512, 2019.
- [23] M. Enfrin, L. F. Dumée, and J. Lee, “Nano/microplastics in water and wastewater treatment processes—origin, impact and potential solutions,” *Water Research*, vol. 161, pp. 621–638, 2019.
- [24] Z. Gao, L. Chen, J. Cizdziel, and Y. Huang, “Research progress on microplastics in wastewater treatment plants: A holistic review,” *Journal of Environmental Management*, vol. 325, 2023.

- [25] C. Bretas Alvim, J. A. Mendoza-Roca, and A. Bes-Piá, “Wastewater treatment plant as microplastics release source—Quantification and identification techniques,” *Journal of Environmental Management*, vol. 255, p. 109739, 2020.
- [26] S. M. Mintenig, I. Int-Veen, M. G. J. Löder, S. Primpke, and G. Gerdtts, “Identification of microplastic in effluents of waste water treatment plants using focal plane array-based micro-Fourier-transform infrared imaging,” *Water Research*, vol. 108, pp. 365–372, 2017.
- [27] L. Yang, K. Li, S. Cui, Y. Kang, L. An, and K. Lei, “Removal of microplastics in municipal sewage from China’s largest water reclamation plant,” *Water Research*, vol. 155, pp. 175–181, 2019.
- [28] M. Simon, N. van Alst, and J. Vollertsen, “Quantification of microplastic mass and removal rates at wastewater treatment plants applying Focal Plane Array (FPA)-based Fourier Transform Infrared (FT-IR) imaging,” *Water Research*, vol. 142, pp. 1–9, 2018.
- [29] M. Kooi and A. A. Koelmans, “Simplifying microplastic via continuous probability distributions for size, shape, and density,” *Environmental Science & Technology Letters*, vol. 6, no. 9, pp. 551–557, 2019.
- [30] J. Correia Prata, “Microplastics in wastewater: State of the knowledge on sources, fate and solutions,” *Marine Pollution Bulletin*, vol. 129, pp. 262–265, 2018.
- [31] I. E. Napper, A. Bakir, S. J. Rowland, and R. C. Thompson, “Characterisation, quantity and sorptive properties of microplastics extracted from cosmetics,” *Marine Pollution Bulletin*, vol. 99, pp. 178–185, 2015.
- [32] S. A. Carr, J. Liu, and A. G. Tesoro, “Transport and fate of microplastic particles in wastewater treatment plants,” *Water Research*, vol. 91, pp. 174–182, 2016.
- [33] X. Wu, X. Zhao, R. Chen, P. Liu, W. Liang, J. Wang, M. Teng, X. Wang, and S. Gao, “Wastewater treatment plants act as essential sources of microplastic formation in aquatic environments: A critical review,” *Water Research*, vol. 221, 2022.
- [34] J. Talvitie, A. Mikola, A. Koistinen, and O. Setälä, “Solutions to microplastic pollution—Removal of microplastics from wastewater effluent with advanced wastewater treatment technologies,” *Water Research*, vol. 123, pp. 401–407, 2017.
- [35] M. Lares, M. C. Ncibi, M. Sillanpää, and M. Sillanpää, “Occurrence, identification and removal of microplastic particles and fibers in conventional activated sludge process and advanced MBR technology,” *Water Research*, vol. 133, pp. 236–246, 2018.
- [36] A. A. Franco, J. M. Arellano, G. Albendín, R. Rodríguez-Barroso, J. M. Quiroga, and M. D. Coello, “Microplastic pollution in wastewater treatment plants in the city of Cádiz: Abundance, removal efficiency and presence in receiving water body,” *Science of The Total Environment*, vol. 776, p. 145795, 2021.
- [37] M. Eriksen, W. Cowger, L. M. Erdle, S. Coffin, P. Villarrubia-Gómez, C. J. Moore, E. J. Carpenter, R. H. Day, M. Thiel, and C. Wilcox, “A growing plastic smog, now estimated to be over 170 trillion plastic particles afloat in the world’s oceans—Urgent solutions required,” *PLOS ONE*, vol. 18, p. e0281596, 2023.
- [38] M. Eriksen, S. Mason, S. Wilson, C. Box, A. Zellers, W. Edwards, H. Farley, and S. Amato, “Microplastic pollution in the surface waters of the Laurentian Great Lakes,” *Marine Pollution Bulletin*, vol. 77, pp. 177–182, 2013.

- [39] A. Collignon, J.-H. Hecq, F. Glagani, P. Voisin, F. Collard, and A. Goffart, “Neustonic microplastic and zooplankton in the north western Mediterranean Sea,” *Marine Pollution Bulletin*, vol. 64, no. 4, pp. 861–864, 2012.
- [40] A. L. Lusher, V. Tirelli, I. O’Connor, and R. Officer, “Microplastics in Arctic polar waters: the first reported values of particles in surface and sub-surface samples,” *Scientific Reports*, vol. 5, pp. 1–9, 2015.
- [41] J. A. I. do Sul, M. F. Costa, M. Barletta, and F. J. A. Cysneiros, “Pelagic microplastics around an archipelago of the Equatorial Atlantic,” *Marine Pollution Bulletin*, vol. 75, pp. 305–309, 2013.
- [42] M. Eriksen, L. C. Lebreton, H. S. Carson, M. Thiel, C. J. Moore, J. C. Borerro, F. Galgani, P. G. Ryan, and J. Reisser, “Plastic Pollution in the World’s Oceans: More than 5 Trillion Plastic Pieces Weighing over 250,000 Tons Afloat at Sea,” *PLOS ONE*, vol. 9, p. e111913, 2014.
- [43] S. Zhao, L. Zhu, T. Wang, and D. Li, “Suspended microplastics in the surface water of the Yangtze Estuary System, China: First observations on occurrence, distribution,” *Marine Pollution Bulletin*, vol. 86, pp. 562–568, 2014.
- [44] L. Van Cauwenberghe, A. Vanreusel, J. Mees, and C. R. Janssen, “Microplastic pollution in deep-sea sediments,” *Environmental Pollution*, vol. 182, pp. 495–499, 2013.
- [45] N. Azizi, S. Nasser, R. N. Nodehi, N. Jaafarzadeh, and M. Pirsahab, “Evaluation of conventional wastewater treatment plants efficiency to remove microplastics in terms of abundance, size, shape, and type: A systematic review and Meta-analysis,” *Marine Pollution Bulletin*, vol. 177, 4 2022.
- [46] S. Ziajahromi, P. A. Neale, and F. D. Leusch, “Wastewater treatment plant effluent as a source of microplastics: review of the fate, chemical interactions and potential risks to aquatic organisms,” *Water Science & Technology*, vol. 74, pp. 2253–2269, 2016.
- [47] R. M. Blair, S. Waldron, and C. Gauchotte-Lindsay, “Average daily flow of microplastics through a tertiary wastewater treatment plant over a ten-month period,” *Water Research*, vol. 163, p. 114909, 2019.
- [48] E. A. Ben-David, M. Habibi, E. Haddad, M. Hasanin, D. L. Angel, A. M. Booth, and I. Sabbah, “Microplastic distributions in a domestic wastewater treatment plant: Removal efficiency, seasonal variation and influence of sampling technique,” *Science of The Total Environment*, vol. 752, p. 141880, 2021.
- [49] M. Cole, H. Webb, P. K. Lindeque, E. S. Fileman, C. Halsband, and T. S. Galloway, “Isolation of microplastics in biota-rich seawater samples and marine organisms,” *Scientific Reports*, vol. 4, pp. 1–8, 2014.
- [50] R. Y. Krishnan, S. Manikandan, R. Subbaiya, N. Karmegam, W. Kim, and M. Govarthanam, “Recent approaches and advanced wastewater treatment technologies for mitigating emerging microplastics contamination—A critical review,” *Science of The Total Environment*, vol. 858, p. 159681, 2023.
- [51] P. L. Ngo, B. K. Pramanik, K. Shah, and R. Roychand, “Pathway, classification and removal efficiency of microplastics in wastewater treatment plants,” *Environmental Pollution*, vol. 255, p. 113326, 2019.

- [52] N. Von Moos, P. Burkhardt-Holm, and A. Köhler, “Uptake and Effects of Microplastics on Cells and Tissue of the Blue Mussel *Mytilus edulis* L. after an Experimental Exposure,” *Environmental Science & Technology*, vol. 46, pp. 11 327–11 335, 2012.
- [53] J. Hämer, L. Gutow, A. Köhler, and R. Saborowski, “Fate of Microplastics in the Marine Isopod *Idotea emarginata*,” *Environmental Science & Technology*, vol. 48, pp. 13 451–13 458, 11 2014.
- [54] C. M. Rochman, R. L. Lewison, M. Eriksen, H. Allen, A.-M. Cook, and S. J. Teh, “Polybrominated diphenyl ethers (PBDEs) in fish tissue may be an indicator of plastic contamination in marine habitats,” *Science of the Total Environment*, vol. 476, pp. 622–633, 2014.
- [55] C. G. Avio, S. Gorbi, M. Milan, M. Benedetti, D. Fattorini, G. d’Errico, M. Pauletto, L. Bargelloni, and F. Regoli, “Pollutants bioavailability and toxicological risk from microplastics to marine mussels,” *Environmental Pollution*, vol. 198, pp. 211–222, 2015.
- [56] S. H. Joo, Y. Liang, M. Kim, J. Byun, and H. Choi, “Microplastics with adsorbed contaminants: Mechanisms and Treatment,” *Environmental Challenges*, vol. 3, p. 100042, 2021.
- [57] X. Zhang, J. Chen, and J. Li, “The removal of microplastics in the wastewater treatment process and their potential impact on anaerobic digestion due to pollutants association,” *Chemosphere*, vol. 251, p. 126360, 2020.
- [58] Z. Zhang and Y. Chen, “Effects of microplastics on wastewater and sewage sludge treatment and their removal: A review,” *Chemical Engineering Journal*, vol. 382, p. 122955, 2020.
- [59] R. M. Razanajatovo, J. Ding, S. Zhang, H. Jiang, and H. Zou, “Sorption and desorption of selected pharmaceuticals by polyethylene microplastics,” *Marine Pollution Bulletin*, vol. 136, pp. 516–523, 2018.
- [60] H. Lee, H. J. Lee, and J. H. Kwon, “Estimating microplastic-bound intake of hydrophobic organic chemicals by fish using measured desorption rates to artificial gut fluid,” *Science of The Total Environment*, vol. 651, pp. 162–170, 2019.
- [61] J. Li, D. Yang, L. Li, K. Jabeen, and H. Shi, “Microplastics in commercial bivalves from China,” *Environmental Pollution*, vol. 207, pp. 190–195, 2015.
- [62] D. Yang, H. Shi, L. Li, J. Li, K. Jabeen, and P. Kolandhasamy, “Microplastic Pollution in Table Salts from China,” *Environmental Science & Technology*, vol. 49, pp. 13 622–13 627, 2015.
- [63] G. Liebezeit and E. Liebezeit, “Non-pollen particulates in honey and sugar,” *Food Additives & Contaminants: Part A*, vol. 30, pp. 2136–2140, 2013.
- [64] G. Liebezeit and E. Liebezeit, “Synthetic particles as contaminants in German beers,” *Food Additives & Contaminants: Part A*, vol. 31, pp. 1574–1578, 2014.
- [65] B. E. Oßmann, G. Sarau, H. Holtmannspötter, M. Pischetsrieder, S. H. Christiansen, and W. Dicke, “Small-sized microplastics and pigmented particles in bottled mineral water,” *Water Research*, vol. 141, pp. 307–316, 2018.
- [66] M. Kosuth, S. A. Mason, and E. V. Wattenberg, “Anthropogenic contamination of tap water, beer, and sea salt,” *PLOS ONE*, vol. 13, p. e0194970, 2018.

- [67] A. Hillery, P. Jani, and A. Florence, “Comparative, Quantitative Study of Lymphoid and Non-Lymphoid Uptake of 60 nm Polystyrene Particles,” *Journal of Drug Targeting*, vol. 2, pp. 151–156, 1994.
- [68] M. LeFevre, A. Boccio, and D. Joel, “Intestinal uptake of fluorescent microspheres in young and aged mice,” in *Proceedings of the Society for Experimental Biology and Medicine*, vol. 190, no. 1, 1989, pp. 23–27.
- [69] G. Volkheimer, “Hematogenous dissemination of ingested polyvinyl chloride particles,” *Annals of the New York Academy of Sciences*, vol. 246, pp. 164–171, 1975.
- [70] P. Jani, G. W. Halbert, J. Langridge, and A. T. Florence, “Nanoparticle uptake by the rat gastrointestinal mucosa: quantitation and particle size dependency,” *Journal of Pharmacy and Pharmacology*, vol. 42, no. 12, pp. 821–826, 1990.
- [71] A. Ragusa, A. Svelato, C. Santacroce, P. Catalano, V. Notarstefano, O. Carnevali, F. Papa, M. C. A. Rongioletti, F. Baiocco, S. Draghi, E. D’Amore, D. Rinaldo, M. Matta, and E. Giorgini, “Plasticenta: First evidence of microplastics in human placenta,” *Environment International*, vol. 146, p. 106274, 2021.
- [72] H. A. Leslie, M. J. M. van Velzen, S. H. Brandsma, A. D. Vethaak, J. J. Garcia-Vallejo, and M. H. Lamoree, “Discovery and quantification of plastic particle pollution in human blood,” *Environment International*, vol. 163, p. 107199, 2022.
- [73] K. E. Peiponen, J. Rätty, U. Ishaq, S. Péliisset, and R. Ali, “Outlook on optical identification of micro- and nanoplastics in aquatic environments,” *Chemosphere*, vol. 214, pp. 424–429, 2019.
- [74] A. A. Mohana, S. M. Farhad, N. Haque, and B. K. Pramanik, “Understanding the fate of nano-plastics in wastewater treatment plants and their removal using membrane processes,” *Chemosphere*, vol. 284, p. 131430, 2021.
- [75] “Microbeads in Toiletries Regulations,” Government of Canada, 2018. [Online]. Available: <https://laws-lois.justice.gc.ca/PDF/SOR-2017-111.pdf>
- [76] J. Boucher and D. Friot, “Primary Microplastics in the Oceans: A Global Evaluation of Sources,” International Union for Conservation of Nature and Natural Resources (IUCN), 2017.
- [77] A. Yaseen, I. Assad, M. S. Sofi, M. Z. Hashmi, and S. U. Bhat, “A global review of microplastics in wastewater treatment plants: Understanding their occurrence, fate and impact,” *Environmental Research*, vol. 212, 2022.
- [78] S. Magni, A. Binelli, L. Pittura, C. G. Avio, C. Della Torre, C. C. Parenti, S. Gorbi, and F. Regoli, “The fate of microplastics in an Italian Wastewater Treatment Plant,” *Science of the Total Environment*, vol. 652, pp. 602–610, 2019.
- [79] F. Murphy, C. Ewins, F. Carbonnier, and B. Quinn, “Wastewater Treatment Works (WwTW) as a Source of Microplastics in the Aquatic Environment,” *Environmental Science & Technology*, vol. 50, pp. 5800–5808, 2016.
- [80] E. A. Gies, J. L. LeNoble, M. Noël, A. Etemadifar, F. Bishay, E. R. Hall, and P. S. Ross, “Retention of microplastics in a major secondary wastewater treatment plant in Vancouver, Canada,” *Marine Pollution Bulletin*, vol. 133, pp. 553–561, 2018.

- [81] X. Lv, Q. Dong, Z. Zuo, Y. Liu, X. Huang, and W. M. Wu, “Microplastics in a municipal wastewater treatment plant: Fate, dynamic distribution, removal efficiencies, and control strategies,” *Journal of Cleaner Production*, vol. 225, pp. 579–586, 2019.
- [82] X. Xu, Q. Hou, Y. Xue, Y. Jian, and L. Wang, “Pollution characteristics and fate of microfibers in the wastewater from textile dyeing wastewater treatment plant,” *Water Science and Technology*, vol. 78, no. 10, pp. 2046–2054, 2018.
- [83] H. Hidayatullah and T. G. Lee, “A study on characteristics of microplastic in wastewater of South Korea: Identification, quantification, and fate of microplastics during treatment process,” *Marine Pollution Bulletin*, vol. 146, pp. 696–702, 2019.
- [84] V. S. Koutnik, S. Alkidim, J. Leonard, F. DePrima, S. Cao, E. M. V. Hoek, and S. K. Mohanty, “Unaccounted Microplastics in Wastewater Sludge: Where Do They Go?” *ACS ES&T Water*, vol. 1, pp. 1086–1097, 2021.
- [85] K. Conley, A. Clum, J. Deepe, H. Lane, and B. Beckingham, “Wastewater treatment plants as a source of microplastics to an urban estuary: Removal efficiencies and loading per capita over one year,” *Water Research X*, vol. 3, p. 100030, 2019.
- [86] R. Dris, J. Gasperi, V. Rocher, M. Saad, N. Renault, and B. Tassin, “Microplastic contamination in an urban area: a case study in Greater Paris,” *Environmental Chemistry*, vol. 12, no. 5, pp. 592–599, 2015.
- [87] H. A. Leslie, S. H. Brandsma, M. J. M. Van Velzen, and A. Vethaak, “Microplastics en route: Field measurements in the Dutch river delta and Amsterdam canals, wastewater treatment plants, North Sea sediments and biota,” *Environment International*, vol. 101, pp. 133–142, 2017.
- [88] M. Claessens, L. Van Cauwenberghe, M. B. Vandegheuchte, and C. R. Janssen, “New techniques for the detection of microplastics in sediments and field collected organisms,” *Marine Pollution Bulletin*, vol. 70, pp. 227–233, 2013.
- [89] A. I. Catarino, R. Thompson, W. Sanderson, and T. B. Henry, “Development and optimization of a standard method for extraction of microplastics in mussels by enzyme digestion of soft tissues,” *Environmental Toxicology and Chemistry*, vol. 36, pp. 947–951, 2017.
- [90] R. R. Hurley, A. L. Lusher, M. Olsen, and L. Nizzetto, “Validation of a method for extracting microplastics from complex, organic-rich, environmental matrices,” *Environmental Science & Technology*, vol. 52, pp. 7409–7417, 2018.
- [91] S. Ziajahromi, P. A. Neale, L. Rintoul, and F. D. L. Leusch, “Wastewater treatment plants as a pathway for microplastics: development of a new approach to sample wastewater-based microplastics,” *Water Research*, vol. 112, pp. 93–99, 2017.
- [92] S. Gündoğdu, C. Çevik, E. Güzel, and S. Kilercioğlu, “Microplastics in municipal wastewater treatment plants in Turkey: a comparison of the influent and secondary effluent concentrations,” *Environmental Monitoring and Assessment*, vol. 190, pp. 1–10, 2018.
- [93] W. Courtene-Jones, B. Quinn, F. Murphy, S. F. Gary, and B. E. Narayanaswamy, “Optimisation of enzymatic digestion and validation of specimen preservation methods for the analysis of ingested microplastics,” *Analytical Methods*, vol. 9, pp. 1437–1445, 2017.
- [94] J. Talvitie, A. Mikola, O. Setälä, M. Heinonen, and A. Koistinen, “How well is microlitter purified from wastewater?—A detailed study on the stepwise removal of microlitter in a tertiary level wastewater treatment plant,” *Water Research*, vol. 109, pp. 164–172, 2017.

- [95] I. Sierra, M. R. Chialanza, R. Faccio, D. Carrizo, L. Fornaro, and A. Pérez-Parada, “Identification of microplastics in wastewater samples by means of polarized light optical microscopy,” *Environmental Science and Pollution Research*, vol. 27, pp. 7409–7419, 2020.
- [96] T. Maes, R. Jessop, N. Wellner, K. Haupt, and A. G. Mayes, “A rapid-screening approach to detect and quantify microplastics based on fluorescent tagging with Nile Red,” *Nature Scientific Reports*, vol. 7, pp. 1–10, 2017.
- [97] G. Erni-Cassola, M. I. Gibson, R. C. Thompson, and J. A. Christie-Oleza, “Lost, but Found with Nile Red: A Novel Method for Detecting and Quantifying Small Microplastics (1 mm to 20 μm) in Environmental Samples,” *Environmental Science & Technology*, vol. 51, pp. 13 641–13 648, 2017.
- [98] S. Raju, M. Carbery, A. Kuttykattil, K. Senthirajah, A. Lundmark, Z. Rogers, S. SCB, G. Evans, and T. Palanisami, “Improved methodology to determine the fate and transport of microplastics in a secondary wastewater treatment plant,” *Water Research*, vol. 173, p. 115549, 2020.
- [99] A. S. Tagg, M. Sapp, J. P. Harrison, and J. J. Ojeda, “Identification and quantification of microplastics in wastewater using focal plane array-based reflectance micro-FT-IR imaging,” *Analytical Chemistry*, vol. 87, no. 12, pp. 6032–6040, 2015.
- [100] E. Dümichen, A. K. Barthel, U. Braun, C. G. Bannick, K. Brand, M. Jekel, and R. Senz, “Analysis of polyethylene microplastics in environmental samples, using a thermal decomposition method,” *Water Research*, vol. 85, pp. 451–457, 2015.
- [101] E. Dümichen, P. Eisentraut, C. G. Bannick, A. K. Barthel, R. Senz, and U. Braun, “Fast identification of microplastics in complex environmental samples by a thermal degradation method,” *Chemosphere*, vol. 174, pp. 572–584, 2017.
- [102] A. M. Elert, R. Becker, E. Duemichen, P. Eisentraut, J. Falkenhagen, H. Sturm, and U. Braun, “Comparison of different methods for mp detection: what can we learn from them, and why asking the right question before measurements matters?” *Environmental Pollution*, vol. 231, pp. 1256–1264, 2017.
- [103] M. Funck, M. M. Al-Azzawi, A. Yildirim, O. Knoop, T. C. Schmidt, J. E. Drewes, and J. Tuerk, “Release of microplastic particles to the aquatic environment via wastewater treatment plants: The impact of sand filters as tertiary treatment,” *Chemical Engineering Journal*, vol. 426, p. 130933, 2021.
- [104] A. Dyachenko, J. Mitchell, and N. Arsem, “Extraction and identification of microplastic particles from secondary wastewater treatment plant (WWTP) effluent,” *Analytical Methods*, vol. 9, no. 9, pp. 1412–1418, 2017.
- [105] F. Caputo, R. Vogel, J. Savage, G. Vella, A. Law, G. D. Camera, G. Hannon, B. Peacock, D. Mehn, J. Ponti, O. Geiss, D. Aubert, A. Prina-Mello, and L. Calzolari, “Measuring particle size distribution and mass concentration of nanoplastics and microplastics: addressing some analytical challenges in the sub-micron size range,” *Journal of Colloid and Interface Science*, vol. 588, pp. 401–417, 2021.
- [106] C. G. Bannick, R. Szewzyk, M. Ricking, S. Schniegler, N. Obermaier, A. K. Barthel, K. Altmann, P. Eisentraut, and U. Braun, “Development and testing of a fractionated filtration for sampling of microplastics in water,” *Water Research*, vol. 149, pp. 650–658, 2019.
- [107] H. Bitter and S. Lackner, “First quantification of semi-crystalline microplastics in industrial wastewaters,” *Chemosphere*, vol. 258, p. 127388, 2020.

- [108] L. Hermabessiere, C. Himber, B. Boricaud, M. Kazour, R. Amara, A. L. Cassone, M. Laurentie, I. Paul-Pont, P. Soudant, A. Dehaut, and G. Duflos, “Optimization, performance, and application of a pyrolysis-GC/MS method for the identification of microplastics,” *Analytical and Bioanalytical Chemistry*, vol. 410, pp. 6663–6676, 2018.
- [109] X. Li, L. Chen, Q. Mei, B. Dong, X. Dai, G. Ding, and E. Y. Zeng, “Microplastics in sewage sludge from the wastewater treatment plants in China,” *Water Research*, vol. 142, pp. 75–85, 2018.
- [110] X. Liu, W. Yuan, M. Di, Z. Li, and J. Wang, “Transfer and fate of microplastics during the conventional activated sludge process in one wastewater treatment plant of China,” *Chemical Engineering Journal*, vol. 362, pp. 176–182, 2019.
- [111] H.-J. Park, M.-J. Oh, P.-G. Kim, G. Kim, D.-H. Jeong, B.-K. Ju, W.-S. Lee, H.-M. Chung, H.-J. Kang, and J.-H. Kwon, “National Reconnaissance Survey of Microplastics in Municipal Wastewater Treatment Plants in Korea,” *Environmental Science and Technology*, vol. 54, pp. 1503–1512, 2020.
- [112] C. Akarsu, H. Kumbur, K. Gökdağ, A. E. Kideys, and A. Sanchez-Vidal, “Microplastics composition and load from three wastewater treatment plants discharging into Mersin Bay, north eastern Mediterranean Sea,” *Marine Pollution Bulletin*, vol. 150, p. 110776, 2020.
- [113] J. Bayo, J. López-Castellanos, and S. Olmos, “Membrane bioreactor and rapid sand filtration for the removal of microplastics in an urban wastewater treatment plant,” *Marine Pollution Bulletin*, vol. 156, p. 111211, 2020.
- [114] M. R. Michielssen, E. R. Michielssen, J. Ni, and M. B. Duhaime, “Fate of microplastics and other small anthropogenic litter (SAL) in wastewater treatment plants depends on unit processes employed,” *Environmental Science: Water Research & Technology*, vol. 2, no. 6, pp. 1064–1073, 2016.
- [115] S. A. Mason, D. Garneau, R. Sutton, Y. Chu, K. Ehmann, J. Barnes, P. Fink, D. Papazissimos, and D. L. Rogers, “Microplastic pollution is widely detected in US municipal wastewater treatment plant effluent,” *Environmental Pollution*, vol. 218, pp. 1045–1054, 2016.
- [116] P. U. Iyare, S. K. Ouki, and T. Bond, “Microplastics removal in wastewater treatment plants: a critical review,” *Environmental Science: Water Research & Technology*, vol. 6, pp. 2664–2675, 2020.
- [117] A. H. Hamidian, E. J. Ozumchelouei, F. Feizi, C. Wu, Y. Zhang, and M. Yang, “A review on the characteristics of microplastics in wastewater treatment plants: A source for toxic chemicals,” *Journal of Cleaner Production*, vol. 295, p. 126480, 2021.
- [118] S. Freeman, A. M. Booth, I. Sabbah, R. Tiller, J. Dierking, K. Klun, A. Rotter, E. Ben-David, J. Javidpour, and D. L. Angel, “Between source and sea: The role of wastewater treatment in reducing marine microplastics,” *Journal of Environmental Management*, vol. 266, p. 110642, 2020.
- [119] Z. Long, Z. Pan, W. Wang, J. Ren, X. Yu, L. Lin, H. Lin, H. Chen, and X. Jin, “Microplastic abundance, characteristics, and removal in wastewater treatment plants in a coastal city of China,” *Water Research*, vol. 155, pp. 255–265, 2019.
- [120] J. Bayo, S. Olmos, and J. López-Castellanos, “Microplastics in an urban wastewater treatment plant: The influence of physicochemical parameters and environmental factors,” *Chemosphere*, vol. 238, p. 124593, 2020.

- [121] S. Wolff, J. Kerpen, J. Prediger, L. Barkmann, and L. Müller, “Determination of the microplastics emission in the effluent of a municipal waste water treatment plant using Raman microspectroscopy,” *Water Research X*, vol. 2, p. 100014, 2019.
- [122] V. D. Manh, X. T. L. Thao, D. V. Ngo, and T. D. Thom, “Distribution and occurrence of microplastics in wastewater treatment plants,” *Environmental Technology & Innovation*, vol. 26, p. 102286, 2022.
- [123] C. Edo, M. González-Pleiter, F. Leganés, F. Fernández-Piñas, and R. Rosal, “Fate of microplastics in wastewater treatment plants and their environmental dispersion with effluent and sludge,” *Environmental Pollution*, vol. 259, p. 113837, 2020.
- [124] K. Magnusson and F. Norén, “Screening of microplastic particles in and down-stream a wastewater treatment plant,” IVL Swedish Environmental Research Institute, 2014.
- [125] A. A. Horton, R. K. Cross, D. S. Read, M. D. Jürgens, H. L. Ball, C. Svendsen, J. Vollertsen, and A. C. Johnson, “Semi-automated analysis of microplastics in complex wastewater samples,” *Environmental Pollution*, vol. 268, p. 115841, 2021.
- [126] S. Ziajahromi, P. A. Neale, I. T. Silveira, A. Chua, and F. D. Leusch, “An audit of microplastic abundance throughout three Australian wastewater treatment plants,” *Chemosphere*, vol. 263, p. 128294, 2021.
- [127] J. Talvitie, M. Heinonen, J. P. Pääkkönen, E. Vahtera, A. Mikola, O. Setälä, and R. Vahala, “Do wastewater treatment plants act as a potential point source of microplastics? Preliminary study in the coastal Gulf of Finland, Baltic Sea,” *Water Science & Technology*, vol. 72, pp. 1495–1504, 2015.
- [128] C. Scherer, A. Weber, S. Lambert, and M. Wagner, “Interactions of microplastics with freshwater biota,” *Handbook of Environmental Chemistry*, vol. 58, pp. 153–180, 2018.
- [129] C. D. Rummel, A. Jahnke, E. Gorokhova, D. Kühnel, and M. Schmitt-Jansen, “Impacts of Biofilm Formation on the Fate and Potential Effects of Microplastic in the Aquatic Environment,” *Environmental Science & Technology Letters*, vol. 4, no. 7, pp. 258–267, 2017.
- [130] K. Parrish and N. L. Fahrenfeld, “Microplastic biofilm in fresh- and wastewater as a function of microparticle type and size class,” *Environmental Science: Water Research & Technology*, vol. 5, pp. 495–505, 2019.
- [131] C. Sun, L. Fiksdal, A. Hanssen-Bauer, M. B. Rye, and T. Leiknes, “Characterization of membrane biofouling at different operating conditions (flux) in drinking water treatment using confocal laser scanning microscopy (CLSM) and image analysis,” *Journal of Membrane Science*, vol. 382, no. 1–2, pp. 194–201, 2011.
- [132] T. Puerio, E. Piacentini, and R. Mazzei, “Membrane processes for microplastic removal,” *Molecules*, vol. 24, p. 4148, 2019.
- [133] Y. Ruan, K. Zhang, C. Wu, R. Wu, and P. K. S. Lam, “A preliminary screening of *HBCD* enantiomers transported by microplastics in wastewater treatment plants,” *Science of The Total Environment*, vol. 674, pp. 171–178, 2019.
- [134] J. Talvitie, A. Mikola, O. Setälä, M. Heinonen, and A. Koistinen, “How well is microlitter purified from wastewater?—a detailed study on the stepwise removal of microlitter in a tertiary level wastewater treatment plant,” *Water Research*, vol. 109, pp. 164–172, 2016.
- [135] H. Lee and Y. Kim, “Treatment characteristics of microplastics at biological sewage treatment facilities in Korea,” *Marine Pollution Bulletin*, vol. 137, pp. 1–8, 2018.

- [136] X. Xu, Y. Jian, Y. Xue, Q. Hou, and L. P. Wang, “Microplastics in the wastewater treatment plants (WWTPs): Occurrence and removal,” *Chemosphere*, vol. 235, pp. 1089–1096, 2019.
- [137] M. Lapointe, J. M. Farner, L. M. Hernandez, and N. Tufenkji, “Understanding and improving microplastic removal during water treatment: Impact of coagulation and flocculation,” *Environmental Science & Technology*, vol. 54, pp. 8719–8727, 2020.
- [138] X.-S. Wang, H. Song, Y.-L. Liu, X.-R. Pan, H.-C. Zhang, Z. Gao, D.-Z. Kong, R. Wang, L. Wang, and J. Ma, “Quantitatively analyzing the variation of micrometer-sized microplastic during water treatment with the flow cytometry-fluorescent beads method,” *ACS ES&T Engineering*, vol. 1, pp. 1668–1677, 2021.
- [139] I. A. Ricardo, E. A. Alberto, A. H. S. Júnior, D. L. P. Macuvele, N. Padoin, C. Soares, H. G. Riella, M. C. V. Starling, and A. G. Trovó, “A critical review on microplastics, interaction with organic and inorganic pollutants, impacts and effectiveness of advanced oxidation processes applied for their removal from aqueous matrices,” *Chemical Engineering Journal*, vol. 424, p. 130282, 2021.
- [140] Y. Zhang, A. Diehl, A. Lewandowski, K. Gopalakrishnan, and T. Baker, “Removal efficiency of micro- and nanoplastics (180 nm–125 µm) during drinking water treatment,” *Science of The Total Environment*, vol. 720, p. 137383, 2020.
- [141] “Wastewater Systems Effluent Regulations SOR/2012-139,” Government of Canada, 2012. [Online]. Available: <https://laws-lois.justice.gc.ca/eng/regulations/sor-2012-139/fulltext.html>
- [142] M. Henze, W. Gujer, T. Mino, and M. van Loosedrecht, *Activated Sludge Models ASM1, ASM2, ASM2d and ASM3*. IWA Publishing, 2006.
- [143] S. Raju, M. Carbery, A. Kuttykattil, K. Senathirajah, S. Subashchandrabose, G. Evans, and P. Thavamani, “Transport and fate of microplastics in wastewater treatment plants: implications to environmental health,” *Reviews in Environmental Science and Biotechnology*, pp. 1–17, 2018.
- [144] C. Baresel, M. Harding, and J. Fång, “Ultrafiltration/Granulated Active Carbon-Biofilter: Efficient Removal of a Broad Range of Micropollutants,” *Applied Sciences*, vol. 9, p. 710, 2019.
- [145] A. Foglia, G. Cipolletta, N. Frison, S. Sabbatini, S. Gorbi, A. L. Eusebi, and F. Fatone, “Anaerobic membrane bioreactor for urban wastewater valorisation: Operative strategies and fertigation reuse,” *Chemical Engineering Transactions*, vol. 74, pp. 247–252, 2019.
- [146] S. Olmos, J. López-Castellanos, and J. Bayo, “Are advanced wastewater treatment technologies a solution for total removal of microplastics in wastewater effluents?” *WIT Transactions on Ecology and the Environment*, vol. 229, pp. 109–116, 2019.
- [147] B. Patterson, “Membrane Filtration of Microplastic Fibers: Assessment of Membrane, Microplastic, and Solution Properties,” Master’s thesis, McMaster University, Hamilton ON, 2021. [Online]. Available: <http://hdl.handle.net/11375/26932>
- [148] W. J. Koros, G. K. Fleming, S. M. Jordan, T. H. Kim, and H. H. Hoehn, “Polymeric membrane materials for solution-diffusion based permeation separations,” *Progress in Polymer Science*, vol. 13, no. 4, pp. 339–401, 1988.
- [149] K. Trzaskus, M. Elshof, A. Kemperman, and K. Nijmeijer, “Understanding the role of nanoparticle size and polydispersity in fouling development during dead-end microfiltration,” *Journal of Membrane Science*, vol. 516, pp. 152–161, 2016.

- [150] M. Pazouki, A. N. Wilton, and D. R. Latulippe, “An experimental study on sterile filtration of fluorescently labeled nanoparticles—the importance of surfactant concentration,” *Separation and Purification Technology*, vol. 218, pp. 217–226, 2019.
- [151] N. Taylor, W. J. Ma, A. Kristopeit, S. C. Wang, and A. L. Zydney, “Retention characteristics of sterile filters—Effect of pore size and structure,” *Journal of Membrane Science*, vol. 635, p. 119436, 2021.
- [152] B. Ma, W. Xue, C. Hu, H. Liu, J. Qu, and L. Li, “Characteristics of microplastic removal via coagulation and ultrafiltration during drinking water treatment,” *Chemical Engineering Journal*, vol. 359, pp. 159–167, 2019.
- [153] B. Ma, W. Xue, Y. Ding, C. Hu, H. Liu, and J. Qu, “Removal characteristics of microplastics by Fe-based coagulants during drinking water treatment,” *Journal of Environmental Sciences*, vol. 78, pp. 267–275, 2019.
- [154] A. R. P. Pizzichetti, C. Pablos, C. Álvarez-Fernández, K. Reynolds, S. Stanley, and J. Marugán, “Kinetic and mechanistic analysis of membrane fouling in microplastics removal from water by dead-end microfiltration,” *Journal of Environmental Chemical Engineering*, vol. 11, p. 109338, 2023.
- [155] B. K. Pramanik, S. K. Pramanik, and S. Monira, “Understanding the fragmentation of microplastics into nano-plastics and removal of nano/microplastics from wastewater using membrane, air flotation and nano-ferrofluid processes,” *Chemosphere*, vol. 282, p. 131053, 2021.
- [156] M. Enfrin, J. Lee, P. Le-Clech, and L. F. Dumée, “Kinetic and mechanistic aspects of ultrafiltration membrane fouling by nano- and microplastics,” *Journal of Membrane Science*, vol. 601, p. 117890, 2020.
- [157] M. Enfrin, C. Hachemi, D. L. Callahan, J. Lee, and F. Dumée, “Membrane fouling by nanofibres and organic contaminants-mechanisms and mitigation via periodic cleaning strategies,” *Separation and Purification Technology*, vol. 278, pp. 1383–5866, 2022.
- [158] M. Enfrin, J. Wang, A. Merenda, L. F. Dumée, and J. Lee, “Mitigation of membrane fouling by nano/microplastics via surface chemistry control,” *Journal of Membrane Science*, vol. 633, p. 119379, 2021.
- [159] M. Enfrin, J. Lee, A. G. Fane, and L. F. Dumée, “Mitigation of membrane particulate fouling by nano/microplastics via physical cleaning strategies,” *Science of The Total Environment*, vol. 788, p. 147689, 2021.
- [160] B. Agasanapura, R. E. Baltus, C. Tanneru, and S. Chellam, “Membrane rejection of nonspherical particles: Modeling and experiment,” *AIChE Journal*, vol. 59, pp. 3863–3873, 2013.
- [161] B. Agasanapura, R. E. Baltus, C. T. Tanneru, and S. Chellam, “Effect of electrostatic interactions on rejection of capsular and spherical particles from porous membranes: Theory and experiment,” *Journal of Colloid and Interface Science*, vol. 448, pp. 492–500, 2015.

Membrane Theory & Wastewater Treatment

2.1 Introduction to Membrane Science

In the most general sense, a membrane is a thin film which controls the transfer of mass between two bulk phases. These bulk phases can be either mixtures (multiple components) or pure (single component). As part of a separation process, a permselective membrane allows for the preferential transfer of a component from one phase to the other [1]. This transfer of mass between phases is facilitated by one or more driving forces: commonly, a chemical potential gradient (*e.g.* concentration, pressure, or both) serves this purpose [2]. There are a multitude of different membranes in existence, having a variety of characteristics, and designed for a wide range of separation applications. Example applications include: seawater desalination, gas separations, hemodialysis, bioprocessing, dairy filtration, and so on. For purposes of brevity, only a subset of membrane offerings will be considered in detail, here—namely synthetic polymeric microfiltration and ultrafiltration membranes for use in water and wastewater treatment.

■ **Key Terminology.** In a membrane filtration process, the feed enters the membrane unit. The portion of the feed that passes through the membrane is termed the permeate or filtrate stream and the portion that does not pass through is termed the retentate, reject, or concentrate stream [2]. This is illustrated in Figure 2.1. For a pressure-driven membrane process, an approximation for the magnitude of the *pressure driving force* across the membrane is captured by the average *transmembrane*

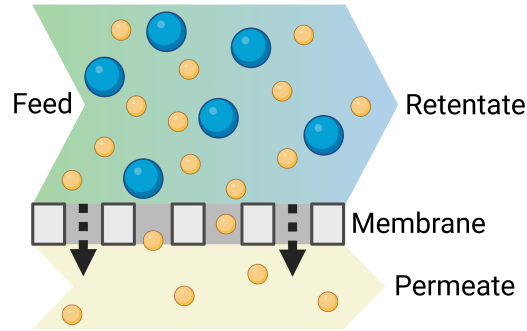


Figure 2.1: Illustration of key terminology in a generic membrane filtration process using a porous membrane.

pressure (TMP) metric:

$$TMP = \frac{P_{feed} + P_{ret}}{2} - P_{perm} \quad (2.1)$$

where P_{feed} , P_{ret} , and P_{perm} are the feed, retentate, and permeate pressures [3].

2.1.1 Classification Schemes for Membranes

Various classification schemes can be proposed to characterize the nature and function of a membrane, depending on the application. While other schemes exist, the most useful categories when considering water/wastewater treatment are: structure, pore size, material, geometry, and flow path.

2.1.1.1 Structure

A representation of different membrane structures can be found in Figure 2.2 and are described below [1]:

■ **Porous & dense membranes.** Firstly, the membranes used in water and wastewater treatment can either be *porous* or *dense*. Briefly, whether a membrane is porous versus dense affects the type of transport that occurs across it. Porous membranes (*e.g.* microfiltration and ultrafiltration) rely on the so-called “pore-flow” model whereby permeant is transported across the membrane through fluid-filled pores. A separation occurs when one or more components in the feed mixture are excluded from the volume occupied by the pores and thus cannot pass across the membrane. In contrast, dense membranes (*e.g.* reverse osmosis) rely on the “solution-diffusion” model whereby the permeant must first dissolve in the material that comprises the membrane, then diffuse away down a concentration

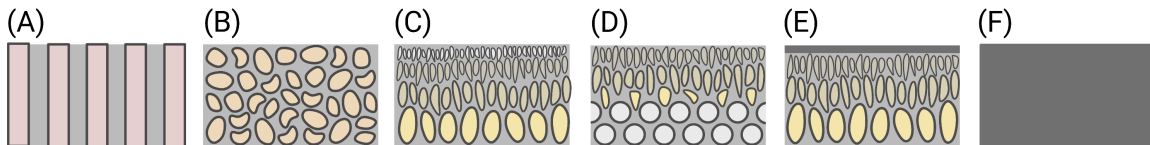


Figure 2.2: Cross-sectional sketches of various types of membrane structures. (A) Porous track-etched membrane. (B) Porous symmetric membrane. (C) Porous asymmetric membrane. (D) Composite membrane with an asymmetric porous layer cast onto a woven support. (E) Composite membrane with a dense skin over a porous asymmetric supporting layer. (F) Dense membrane.

gradient to the other side of the film. A separation occurs due to preferential solubility of components in the membrane material over others, as well as the relative rates of diffusion of components across the film [4, 5].

■ **Isotropic & anisotropic membranes.** Secondly, the polymeric membranes used in water and wastewater treatment can either be *isotropic* or *anisotropic*. Isotropic membranes are symmetrical through their cross-sections and can be either wholly porous or dense. Porous isotropic membranes have a structure consisting of a random interconnecting network of pores [4] whereby permeants traverse the void space of the membrane from the feed side to the permeate side. A special exception to this description is a track-etched membrane (*e.g.* the *EMD Millipore Isopore™* line) which consists of parallel cylindrical pores which traverse the cross-section of the membrane. In contrast, dense isotropic membranes have no definable pores and rely on the transport of dissolved permeants via diffusion from the feed side to the permeate side.

Conversely, anisotropic membranes are not symmetrical in nature. They can be further divided into asymmetric and composite membranes. Often prepared via a phase inversion technique [1], the former category describes a membrane which is comprised of a single material, but has a porous structure that varies through its cross-section. The latter category describes a membrane that is comprised of layers of different materials and therefore varies through its cross-section. A common manifestation of a composite membrane involves a thin film that is cast onto a woven substrate for mechanical support [1]; an example of a membrane with this structure is *EMD Millipore's* 5 μm *Durapore®* membrane, seen in Figure 4.1. Another common manifestation of a composite membrane is a hybrid between a dense and a porous membrane, whereby a thin, dense film is formed on the surface of a thicker, porous membrane; this is the case with some reverse osmosis membranes [1].

As the rate of transport of permeant through a membrane is inversely proportional to its thickness, enhancing the productivity of a membrane can be accomplished by minimizing the membrane thickness. Anisotropic membranes with very thin selective skin layers (*e.g.* $O\{1\ \mu\text{m}\}$) over very porous supporting layers are highly desirable. This is advantageous as the thicker porous layers contribute to the mechanical strength of the membrane but do not contribute significantly towards the mass transfer resistance which is dominated by the very thin skin layer [1]. This is such a great advantage that most commercial membranes are now anisotropic in structure [4].

2.1.1.2 Pore Size

Perhaps the most common method of categorizing membranes is through their pore size. For liquid separations, there are four main types of membranes with relation to pore size, some of what have already been mentioned. From the largest to smallest pore size, they are:

- ▶ **Microfiltration (MF).** MF membranes are porous in structure; they generally have the largest pores in liquid filtration applications, ranging from approximately 0.1–10 μm [5]. They can retain many colloidal or fine particulates [6], depending on the membrane that is used.
- ▶ **Ultrafiltration (UF).** UF membranes are porous in structure and tend to have pores roughly 2–100 nm in size; they are effective at retaining and/or separating macromolecules such as proteins, sugars, and biopolymers [5]. The separation ability of an UF membrane is often expressed as its molecular weight cutoff (MWCO), the molecular weight of an analyte of which 90% is retained by the membrane [7].
- ▶ **Nanofiltration (NF).** NF membranes have very small pores roughly 0.5–2 nm in size and are effective at withholding components down to the size of multivalent ions [5].
- ▶ **Hyperfiltration or reverse osmosis (RO).** RO membranes are quoted as having the smallest of pore sizes, roughly less than 0.5 nm. However, they are unique among the four categories here in that the separation layer is dense and does not have definable pores. The “pores” are really transient statistically-distributed free volumes between polymer chains which molecules can occupy. These volumes are created and destroyed due to the thermal motion of the polymer chains on the same timescales as the diffusion of the analyte species [4]. Modern RO membranes are often produced in the form of “thin-film composites” [3].

As informed by Van der Bruggen *et al.* (2003), an *approximate* comparison of the pore size ranges of these four main categories is illustrated in Figure 2.3 [5].

Manufacturers of membranes will often state the membrane type (MF/UF/etc.) and quote a “nominal” pore size or MWCO. It is a well-known secret in the field of membrane science that this value may or may not reflect the “true size” the pores or the “actual” ability of the membrane to retain a solute of a certain size. As a first consideration, assume that a manufacturer offers an UF membrane with a 50 kDa MWCO. However, manufacturers rarely state their choice of molecular analyte (*e.g.* a specific protein, bacterium, polyethylene glycol, dextran, etc.) and the conditions (*e.g.* pressure, flux, time, etc.) under which the rejection experiment was performed. The chemical makeup, shape, and conformation of the analyte as well as the experimental “challenge conditions” affect analyte rejection [8], thus, it is impossible to ascertain what exactly “50 kDa MWCO” actually means. For a given membrane process application, it is therefore important to validate the separation performance of the membrane (*e.g.* via analyte rejection tests) against the actual feed that is used to ascertain whether the required degree of separation can be attained. Furthermore with few exceptions, membranes do not have a single pore size, but a distribution thereof [8]. Due to the manufacturing processes used (*e.g.* phase inversion), a range of pore sizes and shapes are created. Any attempt to distill the pore size distribution of a membrane down to a single number oversimplifies the actual nature of the membranes pores. A well-controlled membrane manufacturing process will attempt to minimize the pore size distribution, however in reality, some spread will be seen, though rarely reported [8]. Techniques such as porosimetry can be used to ascertain the pore size distribution of a membrane of interest. Overall, a membrane’s quoted nominal pore size or MWCO are merely marketing descriptors used by manufacturers and may not be reflective of the actual performance of the membrane in its desired application.

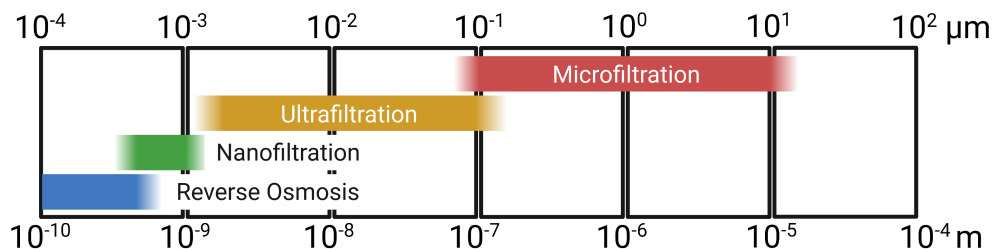


Figure 2.3: Spectrum indicating the approximate pore sizes of different classifications of membranes used in liquid separations.

2.1.1.3 Material

Most membranes that are used in commercial water/wastewater treatment applications consist of organic polymers [5], although examples of ceramic or metal membranes can be found [1, 4]. The membrane material can affect its pore structure, its separation performance, its surface properties (*e.g.* hydrophobicity/hydrophilicity), and its resilience towards process conditions (*e.g.* temperature, pressure, presence of chlorine), among other factors. Van der Bruggen *et al.* (2003) state that the most commonly-used polymeric materials for MF membranes include polyvinylidene fluoride (PVDF), polytetrafluoroethylene (PTFE), polypropylene (PP), polyethylene (PE), polysulfone (PSf) or polyethersulfone (PES), polyimide (PI) or polyetherimide (PEI), polyamide (PA), polyether ether ketone (PEEK), and cellulose esters [5]. Membranes of this type are typically produced via phase inversion, track-etching, stretching, or sintering processes. Like microfiltration membranes, UF membranes are typically synthesized via phase inversion from polyacrylonitrile (PAN), PES, PVDF, PI or PEI, PA, PEEK, or cellulosic materials [5]. Chemical structures of some common membrane polymers [1] are illustrated in Figure 2.4.

Membrane materials are chosen due to considerations (*i.e.* tradeoffs) such as cost, usable lifespan, and performance towards their end-use applications (*e.g.* separation ability, anti-fouling behaviour, free chlorine tolerance). For example, PES and PSf are chemically-stable, have good mechanical strength, and are heat-tolerant despite the fact that they are fairly hydrophobic and prone to fouling via adsorption [1]. Notwithstanding the multitude of other options, PVDF is a very common membrane chemistry in water and wastewater treatment owing to its chemical inertness and resistance to oxidation, thermal stability, mechanical strength, and ability to form well-structured membranes—in spite of its hydrophobic nature, too [9, 10]. Compensating for the hydrophobicity of membrane polymers is a common theme across the field of membrane science as hydrophobicity contributes to significant fouling behaviour (see §2.1.3). To mitigate this fouling, hydrophobic polymers can be blended with more hydrophilic materials (*e.g.* polyvinyl pyrrolidone; PVP) to improve the performance of the final product [1, 5]. A variety of other techniques have been successfully applied such as the incorporation of hydrophilic “blocks” in block co-polymers, surface modifications like plasma treatment, physisorption of hydrophilic species to the membrane surface, and the graft polymerization of hydrophilic monomers [5, 11].

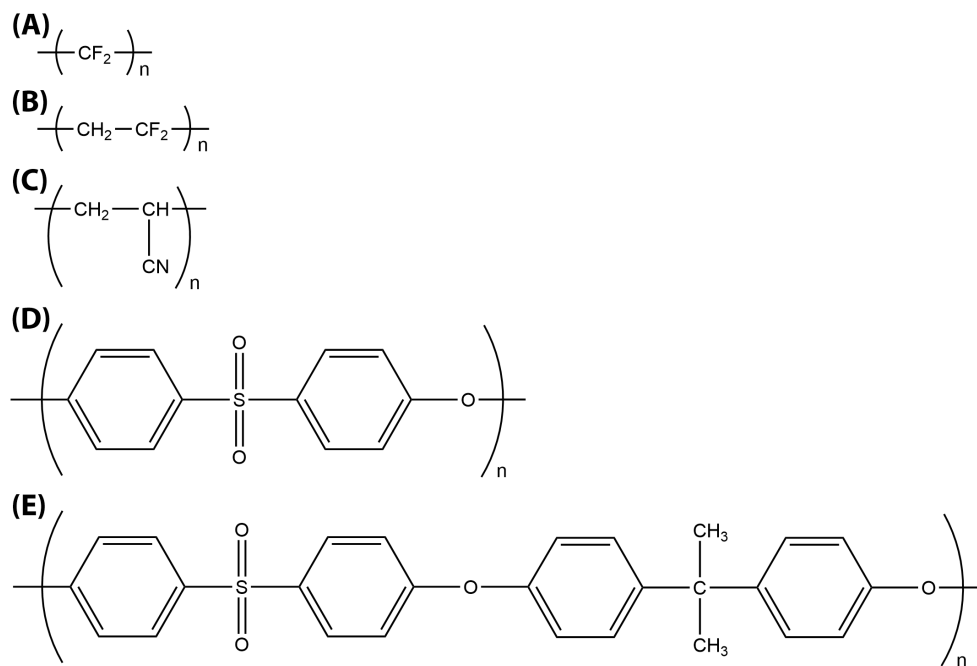


Figure 2.4: Chemical compositions of common membrane materials. (A) PTFE. (B) PVDF. (C) PAN. (D) PES. (E) PSf.

2.1.1.4 Geometry

For most commercial applications, membranes are constructed in two general formats: flat and cylindrical [1]. These formats are assembled into modules of different geometries, namely flat-sheet, spiral-wound, hollow fiber, and tubular. Below, a good comparison of these geometries is prepared by Zeman & Zydney (1996) [8]:

- **Flat Sheet.** These membranes are akin to a sheet of paper, where feed fluid approaches one side of the sheet and permeates through to the other side. In small-scale applications such as laboratory filtration experiments, individual flat sheet membrane coupons are very commonly used, temporarily sealed into membrane test devices such as the ubiquitous *EMD Millipore Amicon*® stirred cell, the *Sterlitech SEPA* cell, or various filter holders (*e.g.* from Cole-Parmer). In larger commercial applications, multiple large rectangular sheets of membrane are sandwiched between alternating porous supports (for mechanical strength) and feed channel spacers/turbulence promoters. This arrangement of membranes gives rise to the term “flat plate” membrane or “plate-and-frame” membrane modules. These units tend to be middle-

ground options in terms of energy requirements and fouling propensity, however some flat sheet modules can be difficult to backwash if they are not supported on the feed side [8].

- ▶ **Spiral Wound.** These modules take flat sheet membranes and pack them into a more efficient volume. The flat sheet membranes sandwich a porous permeate spacer which is sealed in at three of the edges. The fourth edge is attached to a central permeate collection tube. A feed spacer is placed against the membrane sandwich and all of the layers are rolled around the tube in a spiral fashion. The entire spiral wound membrane is then fit into a pressure vessel. The feed to the spiral wound membrane is introduced parallel to permeate collection tube such that the feed passes tangentially over the membrane surface in the volume created by the feed spacer. Fluid permeates across the membrane, passes along the permeate spacer and leaves from the permeate collection tube. While spiral wound membranes are advantageous from the perspectives of packing density and mass transfer, they are highly susceptible to particulate fouling, are particularly hard to clean, and cannot be easily backwashed [8].

- ▶ **Hollow Fiber.** Hollow fiber or capillary membranes are akin to a drinking straw, where feed fluid can flow outside of the fiber and permeate radially through the wall of the membrane into the inner cylindrical channel (“lumen”), then exit through one or both ends of the fiber. Or, the feed can flow through the lumen and permeate through the wall of the membrane to the outside of the fiber. In the former case, the membrane skin layer is typically on the outside surface of the hollow fiber and the process is termed “outside-in filtration”; the opposite is true for the latter case which is termed “inside-out filtration”. Hollow fiber or capillary membranes are roughly 0.05–2 mm in diameter, though various sources (*e.g.* [1, 8, 12]) disagree on the exact size ranges which constitute “hollow fibers” or “capillaries”. The terminology is immaterial and perhaps outdated; henceforth “hollow fiber membrane” will be used, here. In commercial applications, bundles of fibers (roughly in the thousands [1]) are sealed together at their ends and packed into pressure vessels, analogous to shell-and-tube heat exchangers [8]. This leads to excellent packing densities. Hollow fibers are advantageous as they have reasonable manufacturing and pumping costs and they are self-supporting so they can be effectively cleaned by backwashing. This is an important consideration as they are susceptible to fouling and especially particulate plugging. Even though the fibers have good mechanical strength, fiber breakage can be an issue which leads to high replacement costs [8].

- **Tubular.** Tubular membranes are very similar to hollow fibers except that they are much larger in diameter—roughly 3 to 25 mm—and always operate in inside-out configuration. The large inner bore is an advantage as it enables the membrane to be resistant to particle plugging and foulants can be easily cleaned via chemical or physical means. Also, high circulation velocities and shear rates can be obtained which is amenable for preventing fouling in the first place. However, the significant space requirements/capital costs and high energy (pumping) costs are a significant disadvantage to tubular membranes [8].

As is noted, each geometry has its advantages and disadvantages and the use of one geometry over another is generally application-specific.

2.1.1.5 Flow Path & Configuration

The flow path of fluid in the membrane geometries and modules described in §2.1.1.4 is an important driver of filtration performance, especially with respect to mass transfer characteristics [8, 13]. For reference, the process illustrated in Figure 2.1 shows a membrane operated in a *crossflow* configuration. Eliminating flow through the retentate stream, the process becomes a *dead-end* filtration.

■ **Dead-end filtration configuration.** In dead-end filtration, the feed enters the membrane module. Any matter leaving the module must pass through the membrane and into the permeate stream [8]. When the feed flow path is orthogonal to the membrane's surface, it is called normal flow. As components that cannot pass through the membrane accumulate over time in the fluid upstream of the membrane, generally, dead-end processes must be run where the concentration of these rejected components is low to avoid excessive fouling [9, 12]. Examples of dead-end filtration occur in sterilization processes in the pharmaceutical industry or in laboratory separations [8].

■ **Crossflow filtration configuration.** In crossflow filtration, the feed enters the membrane module and flows across the membrane surface. The fluid can either pass through the membrane into the permeate stream, or leave via the retentate/concentrate/reject stream [8]. When the feed flow path is parallel to the membrane's surface, it is called tangential flow. Zeman and Zydney write that most large-scale MF/UF processes operate in the crossflow configuration; the main advantage

to this configuration is that high rates of mass transfer away from the feed-membrane interface can be achieved via elevated crossflow velocities, shear rates, and induced turbulence which mitigates the negative effects of concentration polarization and fouling [8]. See §2.1.2.2 and §2.1.3 for an in-depth discussion on these phenomena.

The use of one flow configuration versus another presents a series of tradeoffs [8]. Whereas cross-flow filtration is desirable to achieve high rates of mass transfer, a significant portion of the feed fluid does not pass through the membrane. This retentate stream can be recirculated to the start of the process, if desired, or treated as a waste stream—both of which incur additional capital and operating costs. In contrast, dead-end processes do not require fluid recirculation which reduces operational (pumping) and capital costs (pumping equipment). However, very significant costs can be incurred with dead-end filtration processes if excessive concentration polarization and fouling occur.

2.1.2 Metrics for Membrane Performance

Chew and colleagues write that for a synthetic membrane to operate successfully in a particular application, three critical “legs” of the process must be considered: (1) the capacity of the membrane, (2) the selectivity of the membrane, and (3) the mass and momentum transport to/from the membrane. The *capacity* of a membrane refers to the *quantity* of fluid that it can filter, meaning its throughput or yield. The *selectivity* of a membrane refers to the *quality* of the separation that can be achieved, or its ability to transmit (or reject) one particular component in the feed over another. *Mass and momentum transport* serve to govern the incidence and severity of *concentration polarization* and *membrane fouling*, phenomena which can undermine the efficacy of the other two “legs” of the process. As the “legs” are inherently interconnected, omitting one in the analysis of a membrane process can present an incomplete or misleading picture of the system [14]. The various quantity- and quality-based analyses to be described in the following two subsections (§2.1.2.1–2.1.2.2) serve as metrics by which membrane performance can be evaluated or analyzed. As membrane fouling is such a complex consideration, interwoven with almost all other aspects of membrane science, it has been given its own section (§2.1.3) where it can be described in greater depth.

2.1.2.1 Quantity-Based Analysis

First, *flux* and *permeability* are two critical metrics for quantifying a membrane’s performance and are ubiquitous in the field of membrane science and engineering. In general, they describe the quantity of fluid that can pass through a given membrane. These values are also important as the flux/permeability of “new” or “pristine” membrane materials can be compared to the flux/permeability of “used” membrane materials, whereby these metrics may vary drastically over time. All else equal, processes such as fouling or compaction are expected to reduce the flux/permeability of a membrane, whereas processes such as abrasion or damage may do the opposite. For water/wastewater treatment membranes, perhaps the most useful flux/permeability metrics are the “pure water flux” or “pure water hydraulic permeability”. Here, pure water is passed through the membrane as a baseline indicator of performance in the absence of solutes or other performance-affecting components.

■ **Flux.** A flux is simply a quantity which passes through a cross-sectional area in a given amount of time. In particular, the permeate volumetric flux J_v expresses the volume of fluid per unit area per time passing through a membrane. It can have SI units of $\text{m}^3/\text{m}^2/\text{s} \leftrightarrow \text{m}/\text{s}$, but is often expressed in terms of $\text{L}/\text{m}^2/\text{h}$ (“LMH”). J_v can be computed as the volumetric flow rate of fluid Q_{perm} (m^3/s or L/h) permeating through a membrane of surface area A (m^2) normal to the flow of the fluid:

$$J_v = \frac{Q_{perm}}{A} \quad (2.2)$$

For an “ideal” membrane with identical, straight, cylindrical pores of radius r (m), the pressure-driven permeate flux across this membrane can be estimated via the Hagen-Poiseuille Equation, as follows [8]:

$$J_v = \frac{\varepsilon \pi r^4 \Delta P}{8 \mu L} \quad (2.3)$$

where ΔP is the pressure difference across the pores (Pa) of length L (m), μ is the fluid’s dynamic viscosity ($\text{Pa}\cdot\text{s}$), and ε is the (surface) pore density of the membrane (m^{-2}). As is visible for an ideal membrane, permeate flux is proportional to the fourth power of pore radius which, *ceteris paribus*, means that membranes with large pore sizes have much greater fluxes than membranes with small pore sizes (*e.g.* MF versus NF in §2.1.1.2).

■ **Permeability.** Permeability is related to the flux of fluid through a membrane. It takes into account the fact that flux is pressure-dependent: higher TMPs result in higher permeate fluxes. The permeability of a membrane L_p is its volumetric flux normalized by the TMP, however the *proper* calculation of this value is nuanced and non-trivial.

To determine the pure water permeability of a membrane sample, pure water is passed at a known and constant TMP through a membrane coupon having a surface area A (m^2). The TMP is recorded along with the change in collected permeate water mass ΔM (kg) over the duration of the test, Δt (s). Using a reasonable density of the water (*e.g.* $\rho = 1,000 \text{ kg/m}^3$), a permeate volumetric flow rate Q_{perm} (m^3/s) can be easily calculated:

$$Q_{perm} = \frac{1}{\rho} \cdot \frac{\Delta M}{\Delta t} \quad (2.4)$$

Via Equation 2.2, a permeate volumetric flux J_v (m/s) can be computed at that value of *TMP*.

Now to determine the hydraulic permeability, the process above should be repeated several times at different TMPs such that several (J_v , *TMP*) pairs are recorded. In this work, a minimum of four (J_v , *TMP*) pairs were used, though five pairs were sought in most cases. Where possible, values of *TMP* were chosen to be less than or equal to the maximum TMP seen under normal experimental conditions to avoid unnecessary membrane compaction. Mathematically, the pure water hydraulic permeability of a membrane L_p is described as the linear slope of J_v versus *TMP* data. For the robust determination of L_p , two criteria should be satisfied:

1. The J_v versus *TMP* data should follow a linear relationship. That is, the residuals $\epsilon = J_v - \hat{J}_v$ between the permeate water flux data points J_v and the linear model \hat{J}_v should be randomly-distributed (*i.e.* no “trend” in ϵ vs. *TMP*).
2. The intercept of the regression of J_v versus *TMP* should be statistically indistinguishable from zero (*i.e.* $\alpha = 0.05$). That is to say, at a *TMP* value of 0, there should be no permeate flow.

If these criteria are satisfied, the slope of the regression is the pure water hydraulic permeability with units of flux per pressure. L_p can be reported in SI units of $\text{m}^3/\text{m}^2/\text{s}/\text{Pa}$, or equivalently, $\text{m}/\text{s}/\text{Pa}$. Often, a simple unit conversion is performed to express L_p in units of $\text{L}/\text{m}^2/\text{h}/\text{bar}$ (*i.e.* “LMH/bar”).

A second method of measuring pure water hydraulic permeability involves driving water through the membrane at a known and constant volumetric flow rate Q_{perm} , and thus, a known and constant permeate flux J_v . The TMP that results is recorded. This process is repeated over a range of Q_{perm} values such that a series of J_v versus TMP values is produced and L_p can again be calculated as the linear slope of J_v versus TMP .

Figure 2.5 features an example of the process to calculate membrane pure water permeability using real experimental data from Chapter 3. The reader is referred there for more information on the experimental setup. A series of three coupons was cut from the same membrane (Synder V0.2) and secured in parallel membrane test cells. The determination of L_p proceeded as follows: Pure water in a feed vessel was pressurized to give a constant TMP was fed to the membrane cells. The system was given time to reach steady state such that the flow rates of water permeating through the membranes were deemed to be constant. At that point, permeate water was collected on a series of load cells for two minutes. The accumulated mass-versus-time data that was produced along with Equations 2.4 and 2.2 were used to calculate J_v . The value of TMP used was averaged over the two minutes where the permeate water was collected. This process was repeated at four new TMP

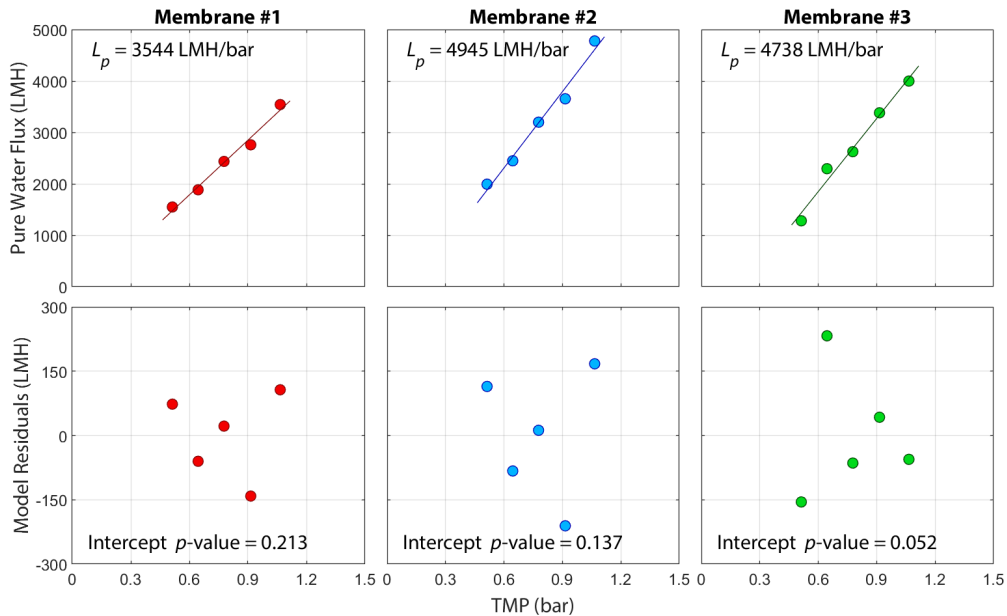


Figure 2.5: Illustration of the process for determining the pure water hydraulic permeability of three individual membrane samples (Synder V0.2). **(Top Row)** Graphs of J_v versus TMP where the slope of the regression (—) is L_p . **(Bottom Row)** Residual plots for the linear regression model fit to the J_v versus TMP data.

levels in a randomized pattern to reduce the effects of hysteresis. In Figure 2.5, the values of L_p for the three membrane coupons are easily determined from the regression of J_v versus TMP data. The model residuals ϵ show no trend and $p > \alpha$ for the regression line intercepts (*i.e.* the intercepts are statistically indifferent from zero). Thus the values of L_p that were produced are robust.

2.1.2.2 Quality-Based Analysis

In a simple filtration process, a fluid containing an analyte molecule is sent to a membrane in order to separate that analyte from the fluid. Examples include the removal of salt molecules from water in seawater reverse osmosis, the separation of an undesirable protein from a mixture containing a valuable protein in biotherapeutic manufacturing, or the removal of suspended solids from a mixed liquor in a wastewater treatment process. Rejection can occur due to various mechanisms, and the extent to which the separations are performed can be reported via several common metrics including the sieving coefficient and the rejection coefficient.

■ **Observed sieving & rejection coefficients** The *sieving* or *rejection* coefficients are very common metrics for reporting the quality of a separation. These two quantities relate the concentrations of the analyte in the bulk feed (C_f) and in the permeate stream (C_p). The observed sieving (S_0) and rejection coefficients (R_0) are interrelated and defined as follows [8]:

$$S_0 = \frac{C_p}{C_f} \quad (2.5a)$$

$$R_0 = 1 - \frac{C_p}{C_f} = 1 - S_0 \quad (2.5b)$$

By inspection, it is elementary to see that the sieving coefficient describes the fraction of the analyte that passes into the permeate stream from the bulk feed; conversely, the rejection coefficient describes the fraction of the analyte that is withheld by the membrane. In the case of an analyte that is completely withheld by the membrane, $S_0 = 0$ and $R_0 = 1$ as $C_p = 0$. Conversely, where a membrane allows the complete transmission of the analyte, $S_0 = 1$ and $R_0 = 0$ as $C_p = C_f$. As such, it is visible that $0 \leq S_0 \leq 1$ and $0 \leq R_0 \leq 1$. Instead of working in “absolute” concentrations, sieving/rejection coefficient ratios are valuable in that they are expressed in relative terms which

permits better comparability between experiments, membranes, and systems as different feed concentrations can directly impact the quality of the separations.

■ **Film Theory & concentration polarization** During the filtration of a fluid containing a suspended or dissolved analyte, there is a coexistence of transport processes which affect the filtration dynamics. Typically, convective drag due to the flow of permeate fluid transports the analyte towards the membrane [15]. In an idealized dead-end filtration, this convective transport is solely opposed by the Brownian back-diffusion of the analyte away from the membrane surface towards the bulk fluid. In crossflow filtration or where the bulk fluid is mixed, other forces can be present such as shear-induced diffusion, inertial lift, or lateral migration. The magnitude of these forces are found to be strong functions of the shear rate, as well as the size and concentration of the particles [15, 16]. When the rate of convective transport exceeds the rate of all the back-transport to the bulk, there is a transient accumulation of analyte at the feed-membrane interface, assuming that a significant fraction of analyte is rejected by the membrane. Over time, this accumulation of analyte can arrest if the convective and back-transport rates reach a balance [17], for example, due to increased hydrodynamic forces as the so-called “concentration polarization” layer of analyte thickens in crossflow filtration. The hydrodynamic forces, here, play a significant role in governing the thickness of the concentration polarization layer [16].

A simple “stagnant” Film Theory model can be used to describe the mass transport behaviour in the boundary layer film at steady state when the mass transport comprises of convection and back-diffusion [4, 18]. Using a simple mass balance over the boundary layer [4]:

$$J_v C_p = J_v C - D \frac{dC}{dx} \quad (2.6)$$

Here, J_v is the volumetric flux of fluid across the membrane, C_p is the analyte concentration in the permeate, D is the diffusion coefficient of the analyte, and $C = C(x)$ is the concentration of analyte in the stagnant film boundary layer lying between the bulk feed ($C = C_f$ at $x = 0$ m) and the membrane surface/wall ($C = C_w$ at $x = \delta$ m) [4]. An illustration of the Film Theory model can be seen in Figure 2.6. Integrating over the thickness of the boundary layer ($x \in [0, \delta]$) produces the

well-known equation:

$$J_v = k \ln \left[\frac{C_w - C_p}{C_f - C_p} \right] \quad (2.7)$$

where k is the mass transfer coefficient of the analyte (m/s) [4, 19].

With the effects of concentration polarization, the value of C_f is unrealistically low to accurately describe the quantity of analyte to which the membrane is challenged. There is a much higher concentration of analyte, $C_w > C_f$, which is withheld by the membrane. Thus, C_f can be replaced by C_w in the formulas for the sieving and rejection coefficients to yield the following:

$$S_a = \frac{C_p}{C_w} \quad (2.8a)$$

$$R_a = 1 - \frac{C_p}{C_w} = 1 - S_a \quad (2.8b)$$

S_a and R_a are called the *actual* sieving/rejection coefficients, respectively [8]. These “actual” coefficients are mathematically related to the “observed” coefficients through a rearrangement of the Film Theory model in Equation 2.7 [19]:

$$S_a = \frac{S_0}{(1 - S_0) \exp(J_v/k) + S_0} = 1 - R_a \quad (2.9)$$

As C_w requires a mass transfer model to estimate, observed rejection coefficients are reported in this work as opposed to actual rejection coefficients.

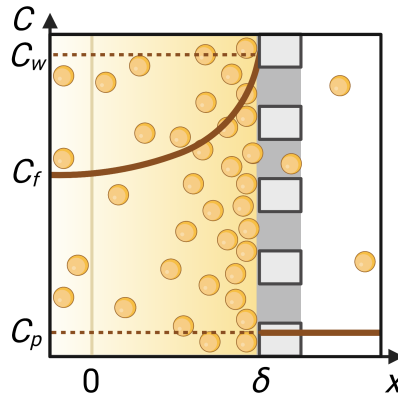


Figure 2.6: Depiction of a stagnant film model for concentration polarization. The physical significance of concentrations used to calculate sieving/rejection coefficients is illustrated.

■ **Rejection Mechanisms** The dominant mechanism by which an analyte is rejected by a membrane can vary widely depending on the type of membrane (*e.g.* MF versus RO) and the properties of analyte in question (*e.g.* bacterial cells versus sodium ions); it can change even over the course of a filtration. For example, Wiesner & Buckley (1996) state that parameters that affect the rejection of analytes like organic molecules include the conformation of the molecule, its polarity, dielectric constant, and its hydrophobicity/hydrophobicity [20]. As the focus of this work is on MF/UF membranes, this section will consider “pore-flow model” mechanisms [4] most applicable to these types of membranes.

Wiesner & Buckley (1996) write that suspended particles are separated from fluids via *mechanical sieving* (steric rejection) which is a result of size differences between the particle and pore [20]. Rejection via sieving dominates analyte removal in MF/UF processes [5, 20]. In its simplest form: if a particle that approaches a membrane pore is smaller than that pore, it can pass through, while if the particle is larger than the pore, it cannot pass through [21]. Of course, reality is not as simple as this statement. It has been found that particles much smaller than the pore size are more likely to pass through the pore while larger particles (still smaller than the pore size) are less likely to pass through. A simple model to describe this phenomenon was created by J. D. Ferry in 1936 [20, 22]. This model considers particle sieving through a *straight cylindrical pore* of radius r . Given a monodisperse feed of solid spherical particles of radius a , the fraction of particles that permeate through the pore—that is, the sieving coefficient S_0 —can be assessed in terms of the dimensionless ratio $\lambda = a/r$ [20]:

$$S_0 = \begin{cases} (1 - \lambda)^2(2 - [1 - \lambda]^2)G & \lambda \leq 1 \\ 0 & \lambda > 1 \end{cases} \quad (2.10a)$$

$$G = \exp(-0.7146\lambda^2) \quad (2.10b)$$

where G is an experimentally-derived “lag coefficient” proposed by Zeman and Wales (1981) [23]. As is visible in Figure 2.7, particle rejection via sieving increases as the ratio of particle to pore size increases. Where $a \geq r$, the particles are completely rejected as they cannot fit inside the pore. This model is oversimplified with respect to the actual nature of membranes (*e.g.* non-cylindrical pores, surface charge, etc.) and the particles that they typically filter (*e.g.* non-spherical shape, polydispersity in size). Various researchers have worked to produce other refined expressions of this

model (*e.g.* the Ferry-Renkin Model [12]) which attempt to capture real factors that affect rejection, including electrostatic and dispersive forces between the particles and the pore walls, particle drag during advection and diffusion, and the flexibility of some macromolecules [20, 24, 25].

The presence of a surface charge on a membrane can affect the rejection of a charged analyte in the feed. Wiesner & Aptel (1996) note that the presence and magnitude of these charges can produce a variety of complex phenomena which alter the pore “size” of the membrane that is accessible to the analyte. They also state that the effects of solvation also reduce the pore size seen by an analyte due to the additional bound layers of structured water molecules. Therefore electrostatic interactions and hydration effects create a smaller “effective” pore size which can help to increase the observed particle rejection beyond solely mechanical means. Overall, the magnitude of the charges on the membrane and analyte govern the degree of rejection by this mechanism [20].

Analytes can also be “rejected” via physical capture on the membrane surface. This can happen via interception, diffusion, or other phenomena [26]—the first two of which are particle size-dependent [20]. However, analyte-membrane interfacial interactions regulate whether the analyte can approach the membrane surface and adhere/adsorb once it is in sufficiently close proximity. The combination of phenomena which describe this behaviour can be modelled by the powerful extended Derjaguin/Landau/Verwey/Overbeek Theory (XDLVO) [14, 26, 27]. XDLVO Theory describes the net interaction energy that arises from the various attractive and repulsive potentials, including the

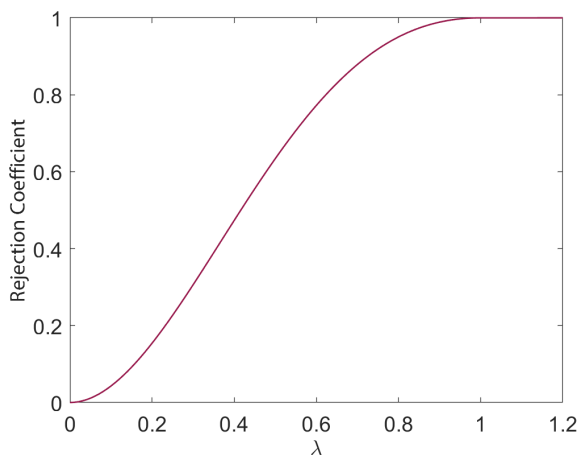


Figure 2.7: Plot of rejection coefficients as a function of $\lambda = a/r$ according to the Ferry Model.

energy barrier that must be overcome to bring an analyte particle close enough to the membrane surface whereby attractive forces dominate and the interaction energy is minimized [26]. These include the basic “DLVO forces” (Lifshitz-van der Waals/dipole interactions; electrostatic/electrical double layer interactions) plus additional “XDLVO” considerations (hydrogen bonding; steric forces; hydrophobic and hydration effects, *i.e.* Lewis acid-base interactions) [14, 27]. The Lewis acid-base interactions are a key driving force governing interactions between hydrophobic analytes/surfaces which comprise a significant portion of the interactions in membrane separations [14].

Furthermore, over the course of a filtration, the rejection of analyte particles can lead to the build-up of a “cake” layer on the membrane surface. Analyte particles which approach or enter the cake layer can be removed by previously-deposited particles in a mechanism that is well-described by packed-bed filtration [20]. As in particle capture, interception can occur when a particle which follows a streamline is brought into the proximity of the membrane or another particle. Diffusion or gravitation can lead to analyte particles leaving their streamline and colliding with immobile particles that are already part of the cake. In this manner, the cake can actually function as its own “dynamic membrane” which governs the rejection of further analytes: in some cases, to a greater extent than rejection due to the membrane, itself [20].

2.1.3 Membrane Fouling

Membrane fouling is a complex process from a physicochemical standpoint and as such, predicting, preventing, and treating its occurrences consumes significant time, energy and money. Chew *et al.* (2020) write that membrane fouling is the “Achilles’ heel” of liquid membrane separations processes [14] due to the decline in throughput for a given membrane. The term “fouling” is used to describe all root causes of this decline (*e.g.* pore plugging, cake formation, etc.) excluding membrane compaction or structural changes over the course of filtration [28]. For a membrane process run at constant pressure, fouling causes a decline in the permeate flux over time; for a membrane run at constant flux, an increase in the TMP results due to fouling.

The process of fouling is complex, originating from interactions between components in the feed water (“foulants”) and the membrane interface. Simply said, the process of fouling inhibits the

ability of a fluid to transport across a porous membrane as the foulants occlude and/or constrict the membrane's pores, or hinder transport through the formation of a cake layer which can act as its own dynamic membrane [20]. These foulants can manifest as particulates (*e.g.* clay particles, cellular aggregates), colloidal matter (*e.g.* proteins, polysaccharides, humic substances), dissolved substances, as well as microorganisms which can proliferate and form biofilms on membrane surfaces [15, 29]. Foulants that are transported to the feed-membrane interface via convection, gravitation, or other means can interact with the membrane, of course subject to the attractive and repulsive forces described via XDLVO Theory (§2.1.2.2). Ironically, the same mechanisms which aid in rejecting analytes can contribute to membrane fouling. If the foulant-membrane or foulant-foulant interfacial energies are conducive, foulant adsorption, deposition, adhesion, or even chemical bonding to the membrane can occur [14]. Depending on the strength of the interactions, the fouling may or may not be reversible.

Previous studies have found that the incidence and severity of the fouling are complex functions of feed water chemistry (*e.g.* pH, ionic strength, temperature), the physicochemical properties of the foulants (*e.g.* size, charge, molecular conformation, hydrophobicity), the physicochemical properties of the membrane (*e.g.* surface morphology, pore structure, surface energies, charge, molecular weight cut-off), and the hydraulic operating conditions of the system (*e.g.* transmembrane pressure, initial permeate flux, mode of operation, crossflow velocity, hydrodynamics) [14, 15, 20, 28, 30]. All these factors can influence how foulants interact with, and accumulate on the membrane surface.

2.1.3.1 Fouling Models

The concentration polarization phenomenon discussed in §2.1.2.2 not only affects the rejection of analytes, but also affects the propensity for the membrane to foul. Here, it can be assumed that the “analyte” rejected by the membrane also has a tendency to foul it. Via the stagnant film model, the *increasing concentration gradient* of the foulant in the boundary layer approaching the feed-membrane interface increases foulant/membrane interactions. In addition, this elevated concentration at the interface (C_w) can sometimes exceed the foulant's solubility, causing precipitation, scaling, or gelation [31]. The multitude of details regarding the Film Theory implications of fouling are well-described in detail in various external sources [4, 15, 16, 18, 28, 32, 33]. While it is well-

understood that concentration polarization can lead to membrane fouling, it does not describe the *mechanism(s)* by which the fouling occurs.

Various models have been proposed over the years to describe different mechanisms of membrane fouling. Empirically, fouling behaviour manifests as a decline in permeate flux (in constant-pressure filtration) or an increase in TMP (in constant-flux filtration). The nature of these changes can be used to ascertain a “dominant” fouling mechanism at a particular time during the filtration by attempting to fit one or more models to the filtration performance data.

■ **Hermia Fouling Models.** Hermia (1982) proposed a differential equation to describe the rate of flux decline during constant-pressure filtration due to different forms of membrane fouling [14, 34]. The model shown in Equation 2.11 describes a *transient* process, where t is the elapsed time and V is the cumulative permeate volume [35].

$$\frac{d^2t}{dV^2} = K \left(\frac{dt}{dV} \right)^n \quad (2.11)$$

Parameters K and n are model constants, both of which have a physical meaning. The value of n corresponds to one of the four “classical” fouling mechanisms—complete blocking, intermediate blocking, standard blocking, and cake filtration [14]—which are simplifications used to describe actual empirical phenomena. According to Vela *et al.* (2008) [34]:

- ▶ **Complete blocking** ($n = 2$). Particles that reach the membrane surface deposit and fully block the entrances of pores. Monolayer deposition is assumed, and the particle size is much larger than the pore size.
- ▶ **Intermediate blocking** ($n = 1$). In a less restrictive analogue to complete blocking, particles that approach the membrane surface either directly block pores or settle on other particles which have previously deposited. The sizes of the particles and pores are similar.
- ▶ **Standard blocking** ($n = 1.5$). Particles which approach the membrane deposit on the interior surfaces of the pores, implying that the particle size is smaller than the pore size. This causes the pores to narrow, leading to the alternate name of this model: pore constriction. This model assumes that the pores are of constant radius and length.

- **Cake filtration** ($n = 0$). Particles which approach the membrane surface deposit in layers over the surface, but do not penetrate inside the membrane. Over time, multiple layers of deposited particles can build up, forming a “cake”.

An illustration of these four mechanisms can be seen in Figure 2.8. The integrated solutions to Equation 2.11 relate the permeate flux $J_v(t)$ passing through a dead-ended membrane over time t and can be seen in Equations 2.12a–2.12d for the complete blocking (a), intermediate blocking (b), standard blocking (c), and cake filtration (d) models [34]:

$$J_v(t) = \exp[\ln J_0 - Kt] \quad (2.12a)$$

$$J_v(t) = \left[\frac{1}{J_0} + Kt \right]^{-1} \quad (2.12b)$$

$$J_v(t) = \left[\frac{1}{J_0^{0.5}} + Kt \right]^{-2} \quad (2.12c)$$

$$J_v(t) = \left[\frac{1}{J_0^2} + Kt \right]^{-0.5} \quad (2.12d)$$

The $J_v(t)$ models contain J_0 , the initial permeate flux ($t = 0$), as well as the parameter K , a mechanism-specific kinetic constant which describes the rate of flux decline. As such, the units of K depend on the mechanism and on the units of “flux” and “time”. As is unsurprising on the inspection of Figure 2.8 that the presence of fouling can reduce the throughput of fluid that can pass through the membrane as well as increase the rejection of analytes due to the reduction in the pore size “seen” by the analytes [36].

■ **Cake filtration & the sum-of-resistances approach.** In the initial stages of a filtration, and especially when particle sieving occurs (*e.g.* in microfiltration) [37], pore blocking mechanisms tend to dominate; this is particularly the case when foulant is dilute [21]. As the filtration proceeds and particles continue to deposit, a cake layer can build up over time and the dominant fouling mechanism can change. The cake layer can act as a secondary membrane, controlling the transport of permeate fluid and the removal of analytes; it can even supersede the role of the actual membrane in governing filtration behaviour [15]. Here, a “resistances-in-series” model can be used to relate the volumetric flux J_v (m/s) to the (constant) transmembrane pressure TMP (Pa) according to Darcy’s

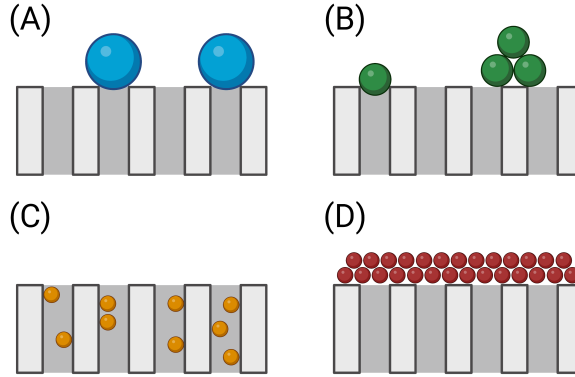


Figure 2.8: Illustration of the four mechanisms of membrane fouling used in Hermia’s model: (A) complete blocking, (B) intermediate blocking, (C) standard blocking, and (D) cake filtration.

Law [15] when cake filtration is the dominant mechanism of membrane fouling:

$$J_v = \frac{TMP}{\mu \left(\sum_j R_j \right)} \quad (2.13)$$

Here, μ is the dynamic viscosity of the fluid (Pa·s) and $\sum_j R_j$ is the total resistance to flow during filtration (m^{-1}). Individual resistances in series R_j which can contribute to this total resistance include the intrinsic resistance of the membrane (R_m), the resistance of reversibly/irreversibly-deposited foulants (R_f), and/or the resistance of the cake layer (R_c) [38]. This model does not explicitly consider a time dependency and thus is valid for systems at steady-state, where the rate of cake formation equals the rate of foulant re-entrainment. In transient processes, note that the individual resistances such as R_c are liable to change over time as the cake accumulates. A simple expression for R_c proceeds from the Kozeny Equation, where the cake is *incompressible* and composed of identical spherical particles of diameter D_p [29]:

$$R_c = \frac{180(1 - \varepsilon_c)^2 \delta_c}{D_p^2 \varepsilon_c^3} \quad (2.14)$$

Here, ε_c is the cake porosity (unitless) and δ_c (m) is the cake thickness. Due to the complexity of membrane fouling, many other models—or variations of the ones described—have been developed by researchers for a variety of systems under investigation. Still, Chew *et al.* (2020) lament that current theory for predicting the fouling behaviour of real solutions/suspensions is critically lacking and therefore, experimentation is required to optimize systems with respect to the membrane used and the operating conditions employed [14].

2.1.3.2 Reversible & Irreversible Fouling.

In concentration polarization, the gradient in increasing concentration towards the feed-membrane interface is the result of a balance of dynamic transport processes. As such, it can be interrupted by arresting the permeate flow and replacing the feed fluid within the membrane module [15]. Processes can be designed to do just that. Concentration polarization, itself, is *reversible*, but its consequences are not necessarily so. *Reversible fouling* can also result from the accumulation of a labile foulant/cake layer on the membrane surface. According to Guo *et al.* (2012), physico-chemical cleaning procedures like backwashing, hydrodynamic/air scouring, or chemical cleaning can remove loose or lightly-adsorbed materials from the membrane’s surface and/or from inside its pores. Conversely, *irreversible fouling* tends to occur due to pore plugging or strong chemisorption [15]. Whereas proper cleaning can restore a reversibly-fouled membrane’s permeate flux (or permeability) to its pre-fouled levels, the presence of irreversible fouling limits the degree to which the flux can be recovered. However, whether fouling is “reversible” versus “irreversible” depends entirely on the nature of the processes available for cleaning the membrane [15]. What proves to be reversible fouling in one process may not feasibly constitute reversible fouling in another process.

2.1.3.3 Approaches to Fouling Mitigation

Due to the substantial negative consequences associated with membrane fouling, various fouling mitigation techniques have been proposed and evaluated with varying levels of success. Some techniques involve periodic cleaning processes to attempt to return the permeate flux to pre-fouled levels, while others attempt to slow the rate at which fouling occurs to maximize the membrane yield. These techniques include the use of fouling-resistant membranes, feed water pretreatment (*e.g.* pH adjustment), exploiting hydrodynamics, and the techniques described when reversible fouling was considered [39].

A very common process to mitigate membrane fouling is through *backwashing* which involves flowing clean water through the membrane in the backwards direction: from permeate to feed. Doing so is fundamental for controlling reversible membrane fouling whereby labile foulants are loosened and/or dislodged, including particulate cake foulants [40]. An additional benefit from backwashing is that the concentration polarization layer formed at the feed-membrane interface is disrupted [14].

As backwashing interrupts the operation of the membrane, it is important to optimize the frequency and duration of the backwashing process. As the backwashing frequency increases, membrane productivity decreases [40]. Typically, the backwashing frequency depends on the permeate flux, the design and configuration of the membrane process, and quality parameters of the feed water [41]. While the frequency/duration is heavily dependent on external factors, one rough estimate suggests that backwashing is performed every 30–90 minutes with a duration of 1–3 minutes [40]. Basu (2015) further notes that during these processes, the backwashing flux J_{BW} should be at least as high as a cycle's initial permeate flux $J_v(t = 0)$, if not higher. It is noted that backwashing can be enhanced through the use of an air scour (*i.e.* bubbling air through the module) and a high-velocity forward flush of the module [40]. A second tier of cleaning can be periodically instituted by performing a chemically-enhanced backwashing (CEB) process whereby oxidants (*e.g.* sodium hypochlorite), acids, and/or bases (*e.g.* citric acid, sodium hydroxide) are used to help solubilize and remove additional foulants [40]. A third tier of cleaning that can be used involves a chemical cleaning-in-place (CIP) whereby a module is taken offline and left to soak in a chemical solution similar to that used in CEB processes [41].

In a review of wastewater polishing installations, Raffin *et al.* (2013) provide a glimpse into the actual operation of nine water reclamation plants that use membrane technologies [41]. The study's authors listed a variety of design and operational parameters including membrane type, operating flux, TMP, as well as backwashing and CEB parameters. For the MF/UF stages of these facilities, backwashing frequency ranged from 8–38 minutes (average = 22 min). While the forward permeate fluxes ranged 28–65 LMH (average = 46 LMH), the backwashing fluxes ranged 100–300 LMH (average = 230 LMH): 2.5–6.8 \times greater (average = 5 \times) than the forward permeate fluxes, on average. CEB frequency ranged from three times daily to twice monthly (mode = daily) using chemicals such as sodium hypochlorite (for the removal of organics) and citric acid (for the removal of inorganics). CIP frequency ranged from once every 21 days to yearly (mode = monthly), using chemicals such as sodium hypochlorite, citric acid, oxalic acid and sodium hydroxide. The reader is referred to this article for a detailed list of process design and operating parameters [41].

2.2 Introduction to Conventional Municipal Wastewater Treatment

Communities produce liquid wastes that result from the consumption of water for domestic, institutional, and industrial uses, along with water collected incidentally from natural sources (*e.g.* runoff, stormwater). This untreated wastewater can contain a variety of components which are hazardous to humans and the environment [42]. Contaminants can include organic and inorganic species, pathogenic microorganisms, toxic chemicals including those which are mutagenic/carcinogenic, and substrates/nutrients which can dramatically alter the ecosystems of receiving water bodies. Examples of hazardous species of concern in wastewater include pathogens originating from human or animal waste, detergents, pesticides, pharmaceuticals, endocrine-disrupting substances, and industrial chemicals [3, 43]. Many of these species are harmful to humans and aquatic organisms even in very low concentrations [43]. Substrates/nutrients in wastewater refer to carbonaceous molecules, nitrogen-containing species (*e.g.* ammonia, nitrate), and phosphorus-containing species (*e.g.* phosphate)—all which stimulate excessive biological growth (*e.g.* algae, microorganisms, etc.) in the receiving water body [3]. The United States Environmental Protection Agency writes that accelerated growth of algae blocks the penetration of sunlight and suffocates aquatic plants and animals by consuming dissolved oxygen in the water. The term “eutrophication” is used to describe these consequences when an excess of nutrients is released into the water—greater than the ecosystem’s ability to assimilate them [43]. This is one possible negative outcome of poor wastewater management practices.

In the modern model of centralized municipal wastewater treatment, wastewater collected from producers via the municipal sewer system is diverted to a local wastewater treatment plant (WWTP). The goal of these facilities is to protect public health in a manner which considers the prevailing environmental, economic, social, and political norms [3]. Physically speaking, this involves removing undesirable components from the wastewater, discharging the treated water into a receiving body, and/or reusing the water/removed solids in other applications [9, 44, 45].

It should be noted that the properties of the wastewater received by these facilities such a flow rates and composition vary significantly based on factors including [3]:

- **Location.** What households, businesses, institutions, natural processes, etc. contribute to the wastewater inflows? What is in the waste that is discharged and what regulations govern what

can be accepted?

- ▶ **Collection system design.** Are the sewage and stormwater sewer systems combined or separate?
- ▶ **Temporal factors.** What is the time of day? What season is it? What is the prevailing weather and climate?

As such, it can be hard to define a “typical” wastewater composition. The result of this variability is that wastewater treatment processes must be designed based on the particular needs of the community such as the expected range of the inflow rates, the range of wastewater compositions, and discharge regulations/requirements.

2.2.1 Conventional Treatment Stages

Krishnan *et al.* (2023) write that globally, municipal WWTPs share a fundamental structure, notwithstanding the exact choice and arrangement of the unit processes varies from facility to facility [46]. The following sections contain a brief description of “typical” major stages and key unit operations in conventional municipal wastewater treatment. To accompany, a schematic of a generic conventional WWTP is shown in Figure 2.9. The information presented in the following sections is largely reiterated from the textbook “*Wastewater Engineering: Treatment and Reuse*” which provide excellent in-depth perspectives of wastewater treatment processes [3]. The reader is referred to the cited sources to learn more about the nuances of the large variety of wastewater treatment processes that are available.

2.2.1.1 Preliminary & Primary Treatment

The purpose of preliminary treatment unit operations is to remove large solids from the influent to avoid inhibiting or impairing the efficacy of downstream processes [47]. Devices such as grit traps [3] and coarse (*e.g.* 6–150 mm) or fine (*e.g.* < 6 mm) screens are employed to remove grit/grease along with large objects like rags, branches, large plastic particles, and rocks [47, 48].

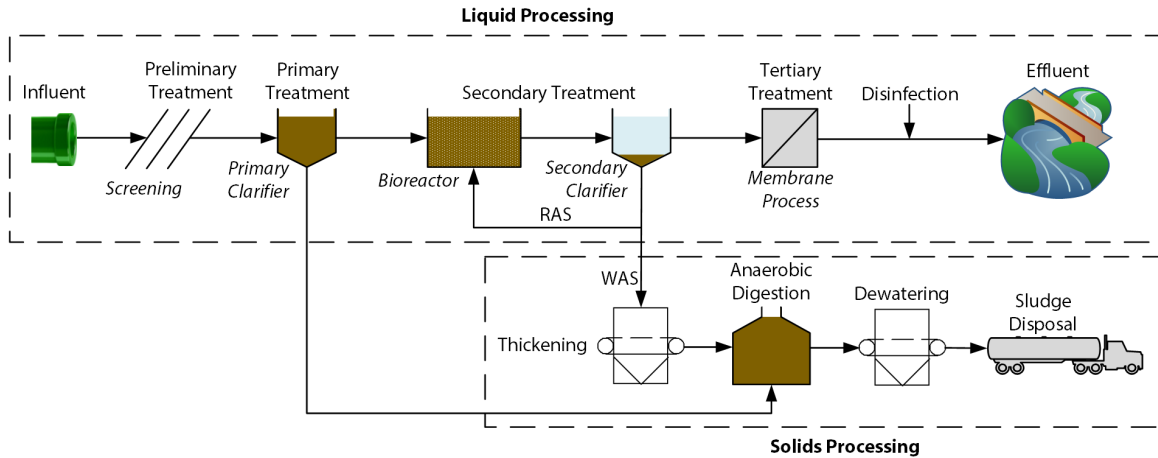


Figure 2.9: Flowsheet of a conventional municipal wastewater treatment plant showing a series of possible unit operations.

Primary (1°) treatment directly follows preliminary treatment; these processes are sometimes even considered as a single entity. Entering a 1° treatment process, the wastewater contains substantial quantities of suspended solids and dissolved matter. The 1° treatment unit operations aim to capture the easily-removable matter from the wastewater to reduce the suspended solids concentration by roughly 50–70% for well-designed and efficient unit operations [3]. As such, 1° treatment often consists of a density-driven sedimentation process which removes settleable (or floatable) solids. The wastewater is transferred to large basins termed “clarifiers” whereby solids are left to settle due to gravity. Polymer flocculants and/or coagulants may be added to accelerate this process. The settled solids—primary sludge—are collected from the bottom of the clarifier and sent for further treatment in solids processing unit operations. A common design parameter of clarifiers is the surface loading rate (SLR) or “overflow velocity” (units: volume/area/time, *e.g.* m³/m²/day or m/s) which expresses the average flow rate of wastewater processed by the clarifier normalized by its surface area. Typical SLRs in 1° clarifiers range from 30–50 m³/m²/day for average flow conditions, with retention times on order of hours (*e.g.* 1.5–2.5 hours) [3, 47]. Where the terminal settling velocity v_t (m/s) of a particular particle is *greater* than the SLR, the particle is assumed to be removed by the clarifier. The value of v_t can be calculated as follows [3]:

$$v_t = \frac{gD_p^2(\rho_p - \rho_f)}{18\mu} \quad (2.15)$$

Here, g is the gravitational constant (m/s), ρ_p/ρ_f are the densities of the particle/fluid (kg/m³), D_p

is the particle diameter (m), and μ is the fluid viscosity (Pa·s). Equation 2.15 assumes steady-state, unhindered gravitational settling of small spheres under Stokes' Flow such that the Reynolds Number Re is less than one [3, 49, 50]. The implication, here, is that when $v_t < SLR$, the particle is not removed by the clarifier. As $v_t \propto D_p^2$, Equation 2.15 implies that 1° treatment preferentially captures and removes larger suspended solids, leaving smaller suspended/dissolved matter in the wastewater, all else equal. The liquid overflow is then sent on to the next stage in the treatment train.

2.2.1.2 Secondary Treatment

Secondary (2°) treatment processes attempt to remove leftover wastewater components, in particular, well-suspended or dissolved biodegradable matter. This is typically performed via biological processes. A common manifestation of 2° treatment is the inclusion of a “conventional activated sludge” (CAS) process involving three features: a bioreactor for the growth of microorganisms, a liquid-solid separation process such as a sedimentation tank, and a recycle stream to return some of the settled biosolids to the bioreactor [3]. Microorganisms growing in the bioreactor are especially good at consuming and removing soluble/colloidal organic matter and nutrients, collectively termed as “substrate”. The growth kinetics of these microorganisms and the corresponding removal rates of substrate is well-described by the series of “activated sludge models” (ASMs); additional information on these complex models is detailed elsewhere [51]. In large volumes of the bioreactor (*e.g.* *oxic* zones), effective aeration is needed to provide oxygen to the microorganisms to promote substrate removal [3]. In other systems related to the CAS process including so-called “A²O” (*i.e.* anaerobic/anoxic/oxic) processes, aeration is required in *oxic* zones, but is contraindicated in sequential *anaerobic* and *anoxic* zones to promote specific nutrient removal processes. Other innovative biological unit operations may be incorporated such as biological contactors, sequencing batch reactors, biofilters, or fluidized/moving bed bioreactors which are described elsewhere [3, 47, 52].

Following the bioreactor, a separation process is employed to remove the biomass (“mixed liquor suspended solids”) from the water, particularly the microorganisms and the extracellular substances that they produce. These are often easier to remove from the wastewater than the substrates left over from 2° treatment. The separation process is often another set of clarifiers, termed “secondary clarifiers”. As before, the 2° clarifiers are designed such that particles have enough time to settle

(*e.g.* $v_t > SLR$). Here, the SLRs range from 16–28 m³/m²/day for average flow conditions [3]. The sludge collected from the bottom of the clarifier basins is split into two fractions: a “waste” fraction that is disposed (“waste activated sludge”; WAS), and a fraction that is “returned” to the bioreactor (“return activated sludge”; RAS) to allow the continued growth of the microorganisms. The liquid overflow from the 2° clarifiers can be sent for further (tertiary) treatment or discharged if the effluent water quality is suitable.

As described via ASMs [51], the removal of substrate in the 2° bioreactor is a complex function of physical, chemical, and biological parameters such as the temperature, the nature and concentrations of the microorganisms/substrates/inhibitors that are present, the availability of oxygen, and the solids retention time (SRT). The SRT is an estimate for the average length of time that sludge resides in 2° treatment. This value typically ranges from 3–6 days but can be longer (~40 days) in specific processes if nitrogen/phosphorus removal processes are performed [3]. For reference, the average SRT (days) can be estimated as follows via a material balance:

$$SRT = \frac{VX}{(Q - Q_{WAS})X_e + Q_{WAS}X_{RAS}} \quad (2.16)$$

Here, V is the bioreactor volume (L); X , X_{RAS} , and X_e are the average biomass concentrations (mass/L) in the bioreactor, RAS, and liquid effluent leaving the 2° treatment system, respectively; whereas Q and Q_{WAS} are the material flow rates (L/day) entering the system and leaving in the WAS, respectively [3]. An average hydraulic retention time (HRT) for the *liquid* can also be simply estimated:

$$HRT = \frac{V}{Q} \quad (2.17)$$

Values of the HRT typically range from 0.5–12 hours [3, 52] depending on the facility; at the extreme end of the spectrum, it is known that the HRT can approach even 40 hours when specific nitrogen/phosphorus removal processes are employed [3].

2.2.1.3 Tertiary Treatment

While the CAS process can be quite effective at removing organic matter from wastewater (~90% [43]), certain locations and facilities may require additional polishing to remove residual organics, solids and nutrients (*e.g.* ammonia) so that the effluent complies with government policy (*e.g.* Canada’s

Wastewater Systems Effluent Regulations [53]). Typically, the goal is to minimize the effluent concentrations of substrate and other contaminants. This is especially true for the nutrients and hazardous components (*e.g.* heavy metals or pharmaceuticals) which are not adequately removed in previous treatment stages [3]. Therefore, additional tertiary (3^o) treatment “polishing” steps are required.

Residual components in the influent to 3^o processes can be a consequence of the feed wastewater composition *and* the effectiveness of previous unit operations. Depending on the needs of the facility, a variety of unit operations can be applied to remove remaining components from the wastewater, including depth/media (*e.g.* sand) filtration, oxidation processes, chemical precipitation, adsorption/ion exchange, biological processes, and membrane technologies (MF/UF/NF/RO) [3]. For example, the removal of residual colloidal/suspended organic or inorganic solids can be accomplished via various filtration technologies; dissolved organic species are often removed via adsorption, oxidation, chemical precipitation, or membrane filtration; dissolved inorganic species can be targeted via membrane filtration, ion exchange, or chemical precipitation. Biological methods for substrate removal may be used, such as rotating biological contactors or trickling bed filters [3].

Following the last unit operation in the treatment train, the treated wastewater is often disinfected to inactivate disease-carrying microorganisms. This is often performed with chlorine and related compounds, ozone, or UV radiation [3, 43]. If chlorine-related compounds are used, dechlorination is important as even low concentrations of chlorine are strongly detrimental to aquatic life [43]. At this point, the treated wastewater is ready for discharge.

2.2.1.4 Solids Processing

Municipal wastewater treatment is designed to separate suspended and dissolved contaminants from the water. The contaminants that are removed leave the liquid treatment train mainly as sludge. The term “sludge” describes the solids and *biosolids* that are produced in the processes, where the term “biosolids” reflects the biological nature and value of these products. As the sludge contains only ~0.5–12% solids on a mass basis, substantial separations still need to be performed to recover water and reduce the volume of sludge to be disposed [3].

Briefly to this end, a variety of solids processing unit operations can be employed. Sludge thickening processes can be used to reduce the volume of the sludge to be treated; specific unit operations include centrifugation, and gravity-belt or rotary-drum thickening [3]. Following thickening, sludge stabilization is performed in many facilities to inactivate pathogens, reduces odors, and inhibit the process of putrefaction. Alkaline stabilization (commonly using lime) increases the sludge pH to 12 or higher, rendering it unable to support microbial life. In another process termed anaerobic digestion, the sludge is fermented at elevated temperatures (typically 30–38°C) in the absence of oxygen to convert some of the organic matter into methane and carbon dioxide. As an added benefit, methane is also evolved which can be used as biogas to generate heat or electricity [3]. Following stabilization, the sludge can be sent for additional mechanical dewatering to further reduce the volume of the sludge via similar techniques as in sludge thickening. At this point, polymer flocculants may be added to substantially increase solids capture during dewatering. In the end, the solids content can be increased to 10–35%, dependent on the nature of the sludge and processes employed [3]. The solids may be further dried prior to disposal.

The significant costs associated with disposing sludge require that the volume/mass of waste must be minimized. Depending on the method of disposal, costs can be incurred due to trucking the solids off-site, landfilling, or the energy associated with incineration. The reject water removed from the sludge is typically sent back to the liquid treatment train for reprocessing [3].

2.2.2 Membranes in Municipal Wastewater Treatment

There are two main implementations of membrane processes in municipal wastewater treatment facilities: membrane bioreactors which serve as hybrid 2°/3° processes, or membrane processes as a final polishing step in 3° treatment.

2.2.2.1 Membrane Bioreactors

Membrane bioreactors (MBRs) can be considered as the amalgamation of a standard WWTP bioreactor and a membrane separation step (*i.e.* combining 2° and 3° technologies) whereby microorganisms in the bioreactor grow and consume substrate from the influent while the water is continuously drawn

off through the membrane. The sludge which accumulates in the bioreactor settles within and is drawn off from the bottom of the basin. Such a system can be used to reduce the footprint of conventional WWTPs as it eliminates the need for 2° clarifiers or other 2° treatment processes, all while producing very high quality effluent (*e.g.* ~98% suspended solids removal) [38].

According to Manem & Sanderson (1996), MBRs use either MF or UF membranes in hollow fiber, flat sheet, or tubular geometries [38]. In practice, typically the first two geometries are seen [54]. MBRs are designed and operated in one of two configurations: external or submerged. In the former case, a series of membrane modules are located external to the bioreactor and the mixed liquor is pumped under pressure from the bioreactor to the membrane. The permeate water is discharged while the retentate—enriched in suspended solids—is recycled back to the bioreactor. This is also termed a *recirculated* MBR [38]. In the latter case, also called an *integrated* MBR, the membrane module is submerged directly into the bioreactor such that the membranes are in direct contact with the mixed liquor [4]. Flow through the membrane is induced by vacuum suction from the permeate side of the membrane. In this configuration, there is no retentate stream.

Fouling in MBRs is a constant concern, due to the high concentration of solids in the mixed liquor; depending on the installation, this is often in the range of 6,000–10,000 mg/L [55, 56]. In addition, microorganisms in the bioreactor contribute to the formation of tenacious biofilms on a membrane’s surface and within its pores which can contribute to permeate flux decline [57, 58]. Regular backwashing and other periodic cleaning processes can help control this fouling and in immersed MBRs, air sparging can be used to significantly mitigate fouling while concurrently aerating the mixed liquor [4].

2.2.2.2 Tertiary Wastewater Polishing

Some wastewater treatment facilities opt to use membrane technologies as a 3° treatment unit operation for the removal of residual components not captured during conventional 1° or 2° methods. MF, UF, NF, and/or RO are employed as they prove to be highly effective barriers against these residual species [41], especially with the emergence of contaminants of concern [3]. From a wastewater treatment perspective, MF membranes should strongly reject most residual suspended solids

and bacteria, whereas UF is similarly effective but should also reject some organic pollutants and viruses, whereas NF and RO membranes will reject almost all remaining contaminants down to heavy metals [3]. Like in recirculated MBRs, various membrane geometries can be used in 3^o wastewater polishing, such as hollow fiber and spiral wound.

Perhaps the main advantage of the various membrane technologies is that consistently, a very high quality of effluent water is produced [3] which is especially amenable to water reuse applications or where receiving water bodies are fragile. For example, in a case study of the Dublin San Ramon Sanitary District facility, the use of a MF process¹ reduced, on average, the suspended solids content by 97%, the chemical oxygen demand by 75%, and the total organic carbon content by 57%; as expected, the dissolved solids content was not reduced [3]. Due to problems associated with fouling, NF and RO membranes require pretreatment via MF/UF membranes to ensure a suitable feed water quality. This is the case in the aforementioned facility where the MF process fed into a RO process. There, the RO membranes² reduced, on average, the *remaining* suspended solids content by > 99%, the chemical oxygen demand by > 91%, the total organic carbon content by > 94%, and the dissolved solids content by roughly [sic] 97% [3]. One other benefit to using membrane technologies in 3^o wastewater treatment is that they can also rid the water of natural organic matter (NOM) which can lead to the creation of hazardous disinfection byproducts during downstream chlorination [59, 60].

However, the use of membranes presents a few drawbacks which can include required pretreatment (*e.g.* chemical addition) and various operational costs. In crossflow filtration, the flow rate of feed wastewater exceeds the flow rate of the permeate water due to the existence of the retentate stream, implying that very large volumes of fluid need to be pumped to feed the membrane systems. In addition, the retentate stream can be mixed with fresh feed and recirculated through the membrane module in order to maintain high crossflow rates [3]. Significant pumping costs are involved. Then due to the accumulation of rejected matter, a bleed stream containing these solids (“residuals”) must also be removed from the membrane process and either sent for further treatment via some other technology (*e.g.* evaporation ponds), or be recycled back to earlier stages in the treatment process such as the plant headworks [3, 61] or 2^o treatment [62, 63]. In a similar fashion, backwashing

¹Study conducted over eight months in 2000; average flux = 67 LMH; other process conditions and membrane units not specified.

²Study conducted over eight months in 1999; average flux = 14.5 LMH; other process conditions and membrane units not specified.

water from external MBRs and 3rd membrane operations also contains residuals and therefore requires further treatment [64]. All of this additional treatment incurs operational costs and capital expenditures. However, continued innovation in the area of membranes for wastewater treatment will bring down the costs associated with these technologies; in some cases, using membranes is already competitive with conventional wastewater treatment processes from a cost perspective [3].

2.2.3 Analytical Techniques for Water/Wastewater Characterization

In this section, bulk analyses for measuring the properties of water and wastewater samples are described. Due to the complex compositions of waters/wastewaters, *bulk measurements* are often necessary to provide useful descriptors of the quality of samples. For example, some of the metrics are used to quantify the amount of solids—including organic material (*e.g.* total solids, total organic carbon)—that are present in a sample. In terms of membrane filtration, the concentration and makeup of the solids that are present can contribute to the incidence and severity of membrane fouling [15]. The pH of the wastewater can affect the surface charge on molecules or membranes while the conductivity of the wastewater sample is related to the concentration of ions that are present. Both of these considerations can influence electrostatic interactions between particles and govern phenomena such as adsorption and coagulation. Therefore, the characterization of wastewater is critical to provide adequate benchmarking of the results of filtration experiments using wastewater. Comprehensive examples of such characterizations performed in this work can be found in Tables 6.1 and A.1.

2.2.3.1 Solids Content

The solids content of wastewater can refer to the amount of dissolved, colloidal, and/or suspended solid matter present [65]. Measurements of the solids content can serve to monitor the amount of organic material, microorganisms, etc. that are present in samples.

The solids content of wastewater samples was measured as follows, approximating a method recorded by the United States Environmental Protection Agency [66]: an aluminum dish having a mass of m_0 (g) is pre-weighed and filled with ~ 25 mL of wastewater, giving a total mass of m_1 (g). The dish and wastewater are then left in an oven at 104°C until the water completely evaporates,

leaving the dried solids behind. After letting the dish cool completely in a desiccator, it is reweighed, giving a mass of m_2 (g). The total solids TS (mg/L) is then calculated as follows:

$$TS = \frac{m_2 - m_0}{m_1 - m_0} \times 10^6 \quad (2.18)$$

where a water density of $\rho = 1$ g/mL is assumed and 10^6 is a unit conversion factor. Extending this method, the total *suspended* solids TSS (mg/L) and total *dissolved* solids TDS (mg/L) comprise two fractions of the total solids present in a wastewater sample according to the following simple relationship:

$$TS = TSS + TDS \quad (2.19)$$

Practically speaking, the suspended solids fraction is retained by a filter with a 0.45 μm pore size while the dissolved solids fraction will pass through that filter [65]. To measure the TSS fraction of the wastewater, a known volume of wastewater V (L) is vacuum-filtered through a pre-weighed glass fiber filter (mass = m_0 ; g) having a 0.45 μm pore size. The filter is then dried in the oven at 104°C and weighed as before (mass = m_2 ; g). The TSS (mg/L) can then be calculated as follows:

$$TSS = \frac{m_2 - m_0}{V} \times 10^3 \quad (2.20)$$

The TDS can then be simply calculated using Equation 2.19. In cases where $TDS \gg TSS$, the method used to calculate TS can be applied instead, where the wastewater added to the tray is simply the wastewater that passes *through* the glass fiber filter. Equation 2.18 is then applicable in this scenario, substituting TDS for TS . As the nature of the individual species present in TS/TSS/TDS analyses cannot be ascertained, solids analysis is clearly a bulk characterization method. In this work, measurements were performed in triplicate, requiring ~ 25 mL of wastewater per replicate.

2.2.3.2 Total Organic Carbon

Total organic carbon (TOC) is a commonly-assessed water quality parameter in water/wastewater treatment and environmental sciences. It acts as a “surrogate” metric to describe the concentrations of NOM molecules in samples [67]. It provides similar information to lengthier biochemical oxygen demand (BOD; $O\{\text{days}\}$) and chemical oxygen demand (COD; $O\{\text{hours}\}$) testing in a shorter time-

span ($O\{\text{minutes}\}$). Again, it should be noted that these methods only provide a *bulk estimate* of the concentrations of species and do not provide insights into the identities of the species [67].

In this work, TOC was measured using a *Shimadzu TOC-LCPH* instrument equipped with an autosampler, as seen in Figure 2.10. According to the manufacturer, it employs a 680°C combustion furnace packed with a catalytic bed to decompose and oxidize carbonaceous molecules in water samples [68]. This oxidation process converts substances to gaseous carbon dioxide which is read using a non-dispersive infrared detector. The manufacturer states that the analysis process relies on a distinction between “types” of carbon within a sample: the “total carbon” (TC) is divided into total “organic” (TOC) and total “inorganic” (IC) carbon fractions. These three fractions are related by the following simple equation, and thus measuring *any two* of the quantities in Equation 2.21 would result in the calculation of the third quantity [68]:

$$TC = TOC + IC \quad (2.21)$$

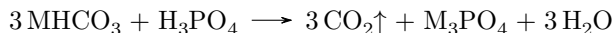
Here, the distinction between types of carbonaceous molecules relies on the chemical definition of “organic” versus “inorganic” molecules which contain carbon. For example, ethanol, sucrose, polysaccharides, and proteins all constitute organic molecules and would all comprise a part of the TOC



Figure 2.10: The Shimadzu TOC-LCPH instrument with autosampler used in this work.

fraction in a sample. Similarly, dissolved carbon dioxide, carbonic acid, metal bicarbonates, and metal carbonates would all comprise a part of the IC fraction in a sample.

To determine the TOC of a sample (mg/L), a two-step “TC-IC” protocol was employed, as recommended by the manufacturer [68]. Here, the TOC is *indirectly obtained* via TC and IC measurements.³ First, the TC is determined by combusting and oxidizing a known volume of the sample and analyzing the amount of carbon the in gas that is produced. Subsequently, the IC portion is measured by injecting another known volume of sample into a reaction chamber which receives a dose of ~25% phosphoric acid (Caledon Laboratories Ltd.). The acidified environment aids in converting the inorganic carbon into carbon dioxide, and the quantity of carbon in the CO₂ gas that is evolved is analyzed. An example of a complete reaction involving a metal bicarbonate (MHCO₃) is seen below:



Given the TC/IC measurements, the TOC can be computed using the relationship in Equation 2.21.

During analysis, carbon dioxide passing through the non-dispersive infrared detector creates a voltage peak (mV) and the area under this peak is proportional to the concentration of carbon in the sample. As such, the instrument requires calibration curves to map peak areas to carbon concentrations. General-purpose aqueous calibration curves based on standards (Ricca Chemical Company) containing potassium hydrogen phthalate (TOC) or sodium carbonate/sodium bicarbonate (IC) were used to measure carbon concentrations in the range of 0–1,000 mg/L. For organic carbon analyses, measurements were performed in triplicate, requiring approximately 7 mL of sample per replicate.

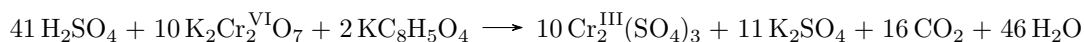
2.2.3.3 Chemical Oxygen Demand

The degradation of organic species utilizes oxygen: the more organic matter that is present, the more oxygen that is needed. In the aquatic environment, the requirement for oxygen in the decomposition of organic matter (*e.g.* from wastewater effluents) depletes the oxygen that is available. This is detrimental to the ecosystem. However in the laboratory, the demand for oxygen required in

³This protocol is preferred where $TOC > IC$ as the absolute uncertainties associated with measuring TC and IC sum to an overall uncertainty which is *lower* than if TOC is measured directly by the instrument.

the degradation of samples can also be used as an indicator of the concentration of organic matter that is present [69–72]. The chemical oxygen demand (COD) of a sample is the amount of oxygen required to chemically oxidize an organic sample to carbon dioxide and water. This is typically done using acidified potassium dichromate, a strong oxidizer [73]. One standardized method of doing so is outlined in *ASTM A-1252-06(2020)* [74].

In this work, COD was measured using commercial vials (*Hach HR COD*) in accordance with the method detailed by the manufacturer. In their product documentation, the manufacturer states that the COD is calculated by heating a known volume of sample in the presence of concentrated sulfuric acid, potassium dichromate, and a silver catalyst. A redox reaction occurs, which (almost completely) oxidizes the organic matter and reduces the Cr^{6+} ion (orange) to the Cr^{3+} ion (green). The COD is determined by measuring the orange-to-green colour change using a spectrophotometer (*Hach DR 3900*) at a wavelength of $\lambda = 620$ nm via a pre-programmed calibration curve. An example reaction involving the oxidation of potassium hydrogen phthalate ($\text{KC}_8\text{H}_5\text{O}_4$) is shown below [74]:



As a disclaimer, it is well-known that the chloride ion is also oxidized by the dichromate ion and therefore its presence artificially elevates the COD. As such, Hach adds a mercury salt to complex with, and remove chloride ions. In a similar fashion, certain inorganic ions like Fe^{2+} and NO_2^- are also oxidizable and will artificially elevate the COD [74]. Overall, COD measurements were performed in duplicate or triplicate, requiring 2 mL of wastewater per replicate.

2.2.3.4 pH and Conductivity

Water and wastewater aliquots, mixed on a magnetic stirrer, were analyzed for their pH and solution conductivity using a *Hanna Instruments HI5522* analyzer with pH and conductivity probes. The probes were calibrated using standard solutions provided by the manufacturer. All pH and conductivity measurements were performed in triplicate.

2.3 Works Cited

- [1] P. Aptel and C. A. Buckley, “Categories of Membrane Operations,” in *Water Treatment Membrane Processes*, J. Mallevalle, P. R. Odendall, and M. R. Wiesner, Eds. McGraw-Hill, 1996.
- [2] W. W. Ho and K. K. Sirkar, “Overview,” in *Membrane Handbook*, W. W. Ho and K. K. Sirkar, Eds. Van Nostrand Reinhold, 1992.
- [3] Metcalf & Eddy Inc., G. Tchobanoglous, F. Burton, and H. Stensel, *Wastewater Engineering: Treatment and Reuse*, 4th ed. McGraw-Hill, 2003.
- [4] R. Baker, *Membrane Technology and Applications*. John Wiley & Sons Ltd., 2012.
- [5] B. Van der Bruggen, C. Vandecasteele, T. V. Gestel, W. Doyen, and R. Leysen, “A review of pressure-driven membrane processes in wastewater treatment and drinking water production,” *Environmental Progress*, vol. 22, pp. 46–56, 2003.
- [6] R. H. Davis, “Definitions,” in *Membrane Handbook*, W. W. Ho and K. K. Sirkar, Eds. Van Nostrand Reinhold, 1992.
- [7] S. S. Kulkarni, E. W. Funk, and N. N. Li, “Theory for Deadend Microfiltration,” in *Membrane Handbook*, W. W. Ho and K. K. Sirkar, Eds. Van Nostrand Reinhold, 1992.
- [8] L. J. Zeman and A. L. Zydney, *Microfiltration and Ultrafiltration: Principles and Applications*. Marcel Dekker, 1996.
- [9] D. M. Warsinger, S. Chakraborty, E. W. Tow, M. H. Plumlee, C. Bellona, S. Loutatidou, L. Karimi, A. M. Mikelonis, A. Achilli, A. Ghassemi, L. P. Padhye, S. A. Snyder, S. Curcio, C. D. Vecitis, H. A. Arafat, and J. H. Lienhard, “A review of polymeric membranes and processes for potable water reuse,” *Progress in Polymer Science*, vol. 81, p. 209, 2016.
- [10] E. Yuliwati and A. F. Ismail, “Effect of additives concentration on the surface properties and performance of PVDF ultrafiltration membranes for refinery produced wastewater treatment,” *Desalination*, vol. 273, pp. 226–234, 2011.
- [11] B. Van der Bruggen, “Chemical modification of polyethersulfone nanofiltration membranes: A review,” *Journal of Applied Polymer Science*, vol. 114, pp. 630–642, 2009.
- [12] H. Strathmann, *Introduction to Membrane Science and Technology*, 1st ed. Wiley-VCH Verlag GmbH & Co. KGaA, 2011.
- [13] U. Beuscher, E. J. Kappert, and J. G. Wijmans, “Membrane research beyond materials science,” *Journal of Membrane Science*, vol. 643, 2022.
- [14] J. W. Chew, J. Kilduff, and G. Belfort, “The behavior of suspensions and macromolecular solutions in crossflow microfiltration: An update,” *Journal of Membrane Science*, vol. 601, p. 117865, 2020.
- [15] W. Guo, H.-H. Ngo, and J. Li, “A mini-review on membrane fouling,” *Bioresource Technology*, vol. 122, pp. 27–34, 2012.
- [16] G. Belfort, R. H. Davis, and A. L. Zydney, “The behavior of suspensions and macromolecular solutions in crossflow microfiltration,” *Journal of Membrane Science*, vol. 96, pp. 1–58, 1994.

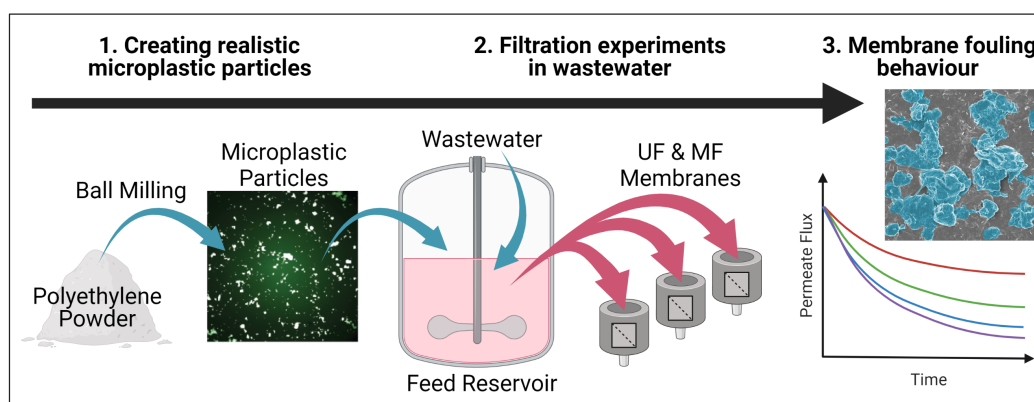
- [17] R. Bai and H. F. Leow, “Microfiltration of activated sludge wastewater—The effect of system operation parameters,” *Separation and Purification Technology*, vol. 29, pp. 189–198, 2002.
- [18] S. Sablani, M. Goosen, R. Al-Belushi, and M. Wilf, “Concentration polarization in ultrafiltration and reverse osmosis: a critical review,” *Desalination*, vol. 141, pp. 269–289, 2001.
- [19] W. Opong and A. Zydney, “Diffusive and convective protein transport through asymmetric membranes,” *AIChE Journal*, vol. 37, pp. 1497–1510, 1991.
- [20] M. R. Wiesner and C. A. Buckley, “Principles of Rejection in Pressure-Driven Membrane Processes,” in *Water Treatment Membrane Processes*, J. Mallevalle, P. R. Odendall, and M. R. Wiesner, Eds. McGraw-Hill, 1996.
- [21] S. Kosvintsev, I. Cumming, R. Holdich, D. Lloyd, and V. Starov, “Sieve mechanism of microfiltration separation,” *Physicochemical Engineering Aspects*, vol. 230, pp. 167–182, 2004.
- [22] J. D. Ferry, “Statistical evaluation of sieve constants in ultrafiltration,” *Journal of General Physiology*, vol. 20, pp. 95–104, 1936.
- [23] L. Zeman and M. Wales, “Polymer solute rejection by ultrafiltration membranes,” in *Synthetic Membranes: Volume II*, A. F. Turbak, Ed. American Chemical Society, 1981, vol. 154.
- [24] W. M. Deen, “Hindered transport of large molecules in liquid-filled pores,” *AIChE Journal*, vol. 33, pp. 1409–1425, 1987.
- [25] M. G. Davidson and W. M. Deen, “Hydrodynamic theory for the hindered transport of flexible macromolecules in porous membranes,” *Journal of Membrane Science*, vol. 35, pp. 167–192, 1988.
- [26] R. H. Davis and D. C. Grant, “Theory for Deadend Microfiltration,” in *Membrane Handbook*, W. W. Ho and K. K. Sirkar, Eds. Van Nostrand Reinhold, 1992.
- [27] C. J. V. Oss, “The Extended DLVO Theory,” in *The Properties of Water and Their Role in Colloidal and Biological Systems*. Elsevier, 2008.
- [28] C. Anselme and E. P. Jacobs, “Ultrafiltration,” in *Water Treatment Membrane Processes*, J. Mallevalle, P. R. Odendall, and M. R. Wiesner, Eds. McGraw-Hill, 1996.
- [29] M. R. Wiesner and P. Aptel, “Mass Transport and Permeate Flux and Fouling in Pressure-Driven Processes,” in *Water Treatment Membrane Processes*, J. Mallevalle, P. R. Odendall, and M. R. Wiesner, Eds. McGraw-Hill, 1996.
- [30] Q. Li and M. Elimelech, “Organic fouling and chemical cleaning of nanofiltration membranes: measurements and mechanisms,” *Environmental Science & Technology*, vol. 38, no. 17, pp. 4683–4693, 2004.
- [31] W. Zhang, J. Luo, L. Ding, and M. Y. Jaffrin, “A review on flux decline control strategies in pressure-driven membrane processes,” *Industrial and Engineering Chemistry Research*, vol. 54, pp. 2843–2861, 2015.
- [32] K. J. Hwang and Y. H. Cheng, “The role of dynamic membrane in cross-flow microfiltration of macromolecules,” *Separation Science and Technology*, vol. 38, pp. 779–795, 2003.
- [33] J. S. Taylor and E. P. Jacobs, “Reverse Osmosis and Nanofiltration,” in *Water Treatment Membrane Processes*, J. Mallevalle, P. R. Odendall, and M. R. Wiesner, Eds. McGraw-Hill, 1996.

- [34] M. C. V. Vela, S. A. Blanco, J. L. García, and E. B. Rodríguez, “Analysis of membrane pore blocking models applied to the ultrafiltration of PEG,” *Separation and Purification Technology*, vol. 62, no. 3, pp. 489–498, 2008.
- [35] J. Hermia, “Constant pressure blocking filtration laws-application to power-law non-Newtonian fluids,” *Chemical Engineering Research and Design*, vol. 60, pp. 183–187, 1982.
- [36] A. J. Schäfer, A. G. Fane, and T. D. Waite, “Fouling effects on rejection in the membrane filtration of natural waters,” *Desalination*, vol. 131, pp. 215–224, 2000.
- [37] G. Belfort and N. Nagata, “Fluid mechanics and cross-flow filtration: some thoughts,” *Desalination*, vol. 53, pp. 57–79, 1985.
- [38] J. Manem and R. Sanderson, “Membrane Bioreactors,” in *Water Treatment Membrane Processes*, J. Mallevalle, P. R. Odendall, and M. R. Wiesner, Eds. McGraw-Hill, 1996.
- [39] N. Hilal, O. O. Ogunbiyi, N. J. Miles, and R. Nigmatullin, “Methods employed for control of fouling in MF and UF membranes: a comprehensive review,” *Separation Science & Technology*, vol. 40, no. 10, pp. 1957–2005, 2005.
- [40] O. D. Basu, “Backwashing,” in *Encyclopedia of Membranes*, E. Drioli and L. Giorno, Eds. Springer Berlin Heidelberg, 2016.
- [41] M. Raffin, E. Germain, and S. Judd, “Wastewater polishing using membrane technology: a review of existing installations,” *Environmental Technology*, vol. 34, no. 5, pp. 617–627, 2013.
- [42] P. L. Ngo, B. K. Pramanik, K. Shah, and R. Roychand, “Pathway, classification and removal efficiency of microplastics in wastewater treatment plants,” *Environmental Pollution*, vol. 255, p. 113326, 2019.
- [43] “Primer for Municipal Wastewater Treatment Systems EPA 832-R-04-001,” United States Environmental Protection Agency—Office of Water and Office of Wastewater Management, 2004.
- [44] T. Wintgens, T. Melin, A. Schäfer, S. Khan, and M. Muston, “The role of membrane processes in municipal wastewater reclamation and reuse,” *Desalination*, vol. 178, pp. 1–11, 2005.
- [45] L. Yang, J. Hur, and W. Zhuang, “Occurrence and behaviors of fluorescence EEM-PARAFAC components in drinking water and wastewater treatment systems and their applications: A review,” *Environmental Science and Pollution Research*, vol. 22, pp. 6500–6510, 2015.
- [46] R. Y. Krishnan, S. Manikandan, R. Subbaiya, N. Karmegam, W. Kim, and M. Govarthan, “Recent approaches and advanced wastewater treatment technologies for mitigating emerging microplastics contamination—A critical review,” *Science of The Total Environment*, vol. 858, p. 159681, 2023.
- [47] P. U. Iyare, S. K. Ouki, and T. Bond, “Microplastics removal in wastewater treatment plants: a critical review,” *Environmental Science: Water Research & Technology*, vol. 6, pp. 2664–2675, 2020.
- [48] M. Enfrin, L. F. Dumée, and J. Lee, “Nano/microplastics in water and wastewater treatment processes—origin, impact and potential solutions,” *Water Research*, vol. 161, pp. 621–638, 2019.
- [49] C. Nicolella, M. M. C. van Loosdrecht, R. Di Felice, and M. Rovatti, “Terminal settling velocity and bed-expansion characteristics of biofilm-coated particles,” *Biotechnology and Bioengineering*, vol. 62, no. 1, pp. 62–70, 1999.

- [50] P. J. Pritchard, *Fox and McDonald's Introduction to Fluid Mechanics*, 8th ed. John Wiley & Sons, 2011.
- [51] M. Henze, W. Gujer, T. Mino, and M. van Loosdrecht, *Activated Sludge Models ASM1, ASM2, ASM2d and ASM3*. IWA Publishing, 2006.
- [52] X. Zhang, J. Chen, and J. Li, "The removal of microplastics in the wastewater treatment process and their potential impact on anaerobic digestion due to pollutants association," *Chemosphere*, vol. 251, p. 126360, 2020.
- [53] "Wastewater Systems Effluent Regulations SOR/2012-139," Government of Canada, 2012. [Online]. Available: <https://laws-lois.justice.gc.ca/eng/regulations/sor-2012-139/fulltext.html>
- [54] P. Le-Clech, V. Chen, and T. A. Fane, "Fouling in membrane bioreactors used in wastewater treatment," *Journal of Membrane Science*, vol. 284, pp. 17–53, 2006.
- [55] W. Liu, J. Zhang, H. Liu, X. Guo, X. Zhang, X. Yao, Z. Cao, and T. Zhang, "A review of the removal of microplastics in global wastewater treatment plants: Characteristics and mechanisms," *Environment International*, vol. 146, p. 106277, 2021.
- [56] L. Dvořák, J. Svojitka, J. Wanner, and T. Wintgens, "Nitrification performance in a membrane bioreactor treating industrial wastewater," *Water Research*, vol. 47, pp. 4412–4421, 2013.
- [57] M. F. A. Goosen, S. S. Sablani, H. Al-Hinai, S. Al-Obeidani, R. Al-Belushi, and A. D. Jackson, "Fouling of reverse osmosis and ultrafiltration membranes: a critical review," *Separation Science and Technology*, vol. 39, no. 10, pp. 2261–2297, 2005.
- [58] Y. Miura, Y. Watanabe, and S. Okabe, "Membrane biofouling in pilot-scale membrane bioreactors (MBRs) treating municipal wastewater: impact of biofilm formation," *Environmental Science & Technology*, vol. 41, no. 2, pp. 632–638, 2007.
- [59] O. Kaarela, M. Koppanen, T. Kesti, R. Kettunen, M. Palmroth, and J. Rintala, "Natural organic matter removal in a full-scale drinking water treatment plant using ClO₂ oxidation: Performance of two virgin granular activated carbons," *Journal of Water Process Engineering*, vol. 41, p. 102001, 2021.
- [60] A. Bhatnagar and M. Sillanpää, "Removal of natural organic matter (NOM) and its constituents from water by adsorption—A review," *Chemosphere*, vol. 166, pp. 497–510, 2017.
- [61] S. de Boer, J. González-Rodríguez, J. J. Conde, and M. T. Moreira, "Benchmarking tertiary water treatments for the removal of micropollutants and pathogens based on operational and sustainability criteria," *Journal of Water Process Engineering*, vol. 46, p. 102587, 2022.
- [62] R. A. Bergman, R. Porter, D. Joffe, and E. Minchew, "Commissioning and Operation of a 50 MGD Ultrafiltration Advanced Reclamation Facility for Gwinnett County, Georgia," in *Proceedings of the Water Environment Federation*, vol. 2006, no. 10, 2006, pp. 2698–2715.
- [63] W. A. Mitch and D. L. Sedlak, "Characterization and Fate of *N*-Nitrosodimethylamine Precursors in Municipal Wastewater Treatment Plants," *Environmental Science and Technology*, vol. 38, pp. 1445–1454, 2004.
- [64] J. Sun, X. Dai, Q. Wang, M. C. van Loosdrecht, and B. J. Ni, "Microplastics in wastewater treatment plants: detection, occurrence and removal," *Water Research*, vol. 152, pp. 21–37, 2019.
- [65] E. I. P. Volcke, K. Solon, Y. Comeau, and M. Henze, *Biological Wastewater Treatment*, 2nd ed., G. H. Chen, M. C. M. Loosdrecht, G. A. Ekama, and D. Brdjanovic, Eds. IWA Publishing, 2020.

- [66] “Methods for Chemical Analysis of Water and Wastes EPA/600/4-79/020,” United States Environmental Protection Agency—Office of Research and Development, 1983.
- [67] X. Wang, J. Wang, K. Li, H. Zhang, and M. Yang, “Molecular characterization of effluent organic matter in secondary effluent and reclaimed water: Comparison to natural organic matter in source water,” *Journal of Environmental Sciences*, vol. 63, pp. 140–146, 2018.
- [68] “Total Organic Carbon Analyzer TOC-LCPH/CPN User’s Manual,” Shimadzu Corporation, 2014.
- [69] Y.-C. Kim, K.-H. Lee, S. Sasaki, K. Hashimoto, K. Ikebukuro, and I. Karube, “Photocatalytic sensor for chemical oxygen demand determination based on oxygen electrode,” *Analytical Chemistry*, vol. 72, 2000.
- [70] M. L. Balconi, M. Borgarello, R. Ferraroli, and F. Realini, “Chemical oxygen demand determination in well and river waters by flow-injection analysis using a microwave oven during the oxidation step,” *Analytica Chimica Acta*, vol. 261, pp. 295–299, 1992.
- [71] K. H. Lee, T. Ishikawa, S. McNiven, Y. Nomura, S. Sasaki, Y. Arikawa, and I. Karube, “Chemical oxygen demand sensor employing a thin layer electrochemical cell,” *Analytica Chimica Acta*, vol. 386, pp. 211–220, 1999.
- [72] A. Cuesta, J. L. Todoli, and A. Canals, “Flow injection method for the rapid determination of chemical oxygen demand based on microwave digestion and chromium speciation in flame atomic absorption spectrometry,” *Spectrochimica Acta Part B: Atomic Spectroscopy*, vol. 51, pp. 1791–1800, 1996.
- [73] M. Kolb, M. Bahadir, and B. Teichgräber, “Determination of chemical oxygen demand (COD) using an alternative wet chemical method free of mercury and dichromate,” *Water Research*, vol. 122, pp. 645–654, 2017.
- [74] “ASTM D1252-06(2020) - Standard Test Methods for Chemical Oxygen Demand (Dichromate Oxygen Demand) of Water,” ASTM International, 2020.

Assessment of Microplastic Particle Fouling of Ultrafiltration & Microfiltration Membranes



The work presented in this chapter is adapted with permission from R. J. LaRue, B. Patterson, S. O'Brien, and D. R. Latulippe, "Evaluation of Membrane Fouling by Microplastic Particles in Tertiary Wastewater Treatment Processes," *ACS ES&T Water*, vol. 2, 2022. Copyright 2023 American Chemical Society.

3.1 Motivations

Despite the use of membrane processes in some wastewater treatment plants (WWTPs), there has been little research aimed at quantifying the impact of microplastics (MPs) on membrane

performance—particularly their role in the fouling of ultrafiltration (UF) and microfiltration (MF) membranes. As is discussed in detail in §2.1.3, fouling is the process whereby the permeation of water through a membrane is inhibited due to the accumulation of solids (*e.g.* organics, colloidal matter) on its surface or within its pores. Despite being a critical issue in the design and operation of membrane systems, fouling induced via MPs has been largely overlooked in the MP filtration literature, until recently [1]. As the small size of MPs increases the influence of particle-particle and particle-membrane surface interactions during filtration [2], it is necessary to develop a strong understanding of the occurrence and mechanisms of MP fouling (*e.g.* cake filtration, pore blocking) if we are to understand the impacts of MPs on membrane processes.

Various researchers have attempted to address the gap in the literature regarding the fouling behaviour of MPs with respect to membranes in wastewater treatment, as was discussed in detail in §1.3.1, to which the reader is referred. In a series of articles, Enfrin *et al.* highlighted this knowledge gap and subsequently published research regarding the fouling of UF membranes by MP particles and fibers. Firstly, very small polyethylene (PE) particles (size = 13–690 nm; concentration = 10 mg/L) in pure water were filtered using 30 kDa molecular weight cutoff polysulfone UF membranes and permeate flux measurements were periodically taken. Over 48 h, a permeate flux decline of 38% was recorded, compared to only 15% when just pure water was filtered [3]. In subsequent investigations, the authors probed the fouling behaviour of MP nanofibers (length = 13 ± 7 μm ; concentration = 10 mg/L) filtered using the same UF membranes, but also in the presence of model organic contaminants (polyvinyl alcohols and polyethylene glycols). They determined that these contaminants actually contributed to the overall flux decline significantly more than the fibers did [4], underscoring the importance of relevant solution conditions when performing filtration experiments with MPs. To complement this work, the researchers then evaluated the effectiveness of MP fouling mitigation techniques such as surface modification via hydrophilic and hydrophobic monomers [5], and physical cleaning via air scouring [6], where both techniques could be tuned to drastically mitigate the severity of membrane fouling by particulate MPs suspended in pure water. In another example, Ma *et al.* (2019) evaluated the removal of large PE MPs (smallest size fraction: < 500 μm) using polyvinylidene fluoride (PVDF) UF membranes with a focus on drinking water applications [7, 8]. Their investigation revealed that coagulated PE particles often induced more significant fouling than uncoagulated particles; however, lower magnitudes of fouling were seen when larger particles were

filtered. While all these studies have provided insights on membrane fouling via MPs, the solution conditions used (pure water or model organic foulants) to suspend the particles/fibers do not accurately represent wastewater properties in a WWTP. Further research is needed to quantify the effect of MP fouling in the complex solution chemistries associated with the wastewater fed to 3rd membrane polishing unit operations in WWTPs.

When considering the morphologies of MPs typically found in WWTPs, it is clear that there is value in performing filtration research with irregularly-shaped, polydisperse MP particles as oppose to the fairly monodisperse, “regularly-shaped” microparticles (*e.g.* latex spheres, gold nanorods, silica micro/nanoparticles, etc.) which have been used in filtration research for a number of decades (*e.g.* [2, 9–12]). While it is relatively easy to purchase or synthesize “regular” micro/nanoparticles, it is more difficult to acquire representative “irregular” particles. To this end, three alternatives have been identified. Firstly, MP particles could be purchased. However, it is difficult to find suppliers who offer irregularly-shaped particles at the size scales (*i.e.* $O\{1\ \mu\text{m}\}$) required for research focusing on MP filtration phenomena. Even for a common polymer such as PE which has *substantial research value*, I am not aware of commercial sources for PE MP particles. Secondly, MPs could be isolated from WWTP effluents, the environment, or from personal care products (*e.g.* [3]). This method is challenging as it requires the collection of large samples as well as the use of intensive procedures to isolate the MPs from other naturally-occurring substances. For example, the technique developed by Mintenig *et al.* [13] to isolate, identify, and quantify MPs in WWTPs required a minimum of 18 days. Also, temporal variations in the effluents from WWTPs result in MPs of varying sizes, shapes, and chemistries, which is inadvisable for the sake of consistency between experiments. Thirdly, MPs could be directly created in the laboratory by breaking down a plastic feedstock, such as through a milling process (*e.g.* Eitzen *et al.*'s MP particles [14]), or by directly synthesizing microparticles, such as through a electrospinning process (*e.g.* B. Patterson's MP fibers [15]). This third option is particularly promising for producing PE MP particles for filtration research as particle size, shape, and chemistry could be feasibly controlled or tailored towards a particular experiment or application.

To this end, PE was selected as an appropriate chemistry for laboratory-synthesized MPs as it is one of the most commonly-encountered polymers in WWTP (effluent) samples, and is often measured in high relative abundances [13, 16–18]. For comparison, PE MPs have been used in other

membrane-based studies [5, 6]. Non-spherical MPs $\sim 10\ \mu\text{m}$ in size were produced in a fairly simple two-step process involving a planetary ball mill and sieves. The MPs were suspended in wastewater, and UF/MF flat-sheet membranes were used in constant pressure filtration experiments to study the effects of MP concentrations on membrane fouling.

3.2 Materials & Methods

3.2.1 Microplastic Particles

Linear low-density PE was obtained in powder form (particle size $\sim 0.5\text{--}1\ \text{mm}$) from Exxon Mobil (LL 8460). PE MP particles were generated using a planetary ball mill (*Retsch PM100*) equipped with a 250 mL stainless steel grinding jar and spherical zirconia milling media (diameter = 3 mm). Initially, the jar was charged with 7.25 g of PE and 290 g of the milling media, satisfying the manufacturer's recommended 1:40 ratio of feedstock to media. The mill was operated in intervals of 5 minutes at 500 rpm followed by 5 seconds at 0 rpm for a total of 6 hours. Then, the milled PE was transferred to a 25 μm sieve which was manually agitated. To disaggregate the particles, ethanol was added to the milled PE on the sieve. The particles that passed through the sieve were placed in an oven at 40°C overnight to evaporate away the ethanol, leaving only the virgin MPs of interest behind.

The size and shape properties of milled and sieved MP particles were characterized in two ways. The first method was via optical microscopy. To this end, a sparse dispersion of MP powder was aspirated onto double-sided tape affixed to a clean glass slide. The particles were immobilized using a cover slip and imaged against a black background using a *Nikon Eclipse LV100* optical microscope with a 10 \times objective lens (0.65 $\mu\text{m}/\text{pixel}$) and a *pco.panda* black-and-white camera. Images were acquired from areas of the slide with a fine particle dispersion using Nikon's *NIS-Elements AR* software. No attempts were made to disaggregate or differentiate between individual and overlapping particles. The particles were characterized using the built-in particle analysis functionality in the *Fiji* distribution of the *ImageJ* software program.

The second method was via focused beam reflectance measurement (FBRM), a technique which uses a rotating laser beam that is periodically backscattered as it reflects off particles in a suspen-

sion. As the orientation of a given particle is essentially random, therefore, so is the straight-line path that the laser spot takes across that particle, from one side to the other. This arbitrary distance is termed a “*chord length*”, while the collection of chord lengths obtained by the instrument over time is termed the “chord length distribution”. While they are not necessarily equivalent, the chord length distribution via FBRM can serve as an approximation to the particle size distribution in a sample [19]. To this end, a 100 mL suspension consisting of 10 mg/L of PE MPs suspended in 100 mg/L of Tween 20 non-ionic surfactant (VWR International) was created and immersed in an ultrasonication bath (Branson) for one hour to disperse the particles. The dispersion was then continuously agitated via a magnetic stirrer while the FBRM probe (Mettler-Toledo) was immersed in the suspension, with chord length measurements obtained every two seconds for 180 seconds, total.

3.2.2 Membranes

PVDF flat-sheet UF (*TriSep UB70*; 0.03 μm pore size) and MF (*Synder V0.2*; 0.2 μm pore size) membranes were used in this study. Both membranes are recommended for wastewater treatment applications by their respective manufacturers. The membranes were first rinsed with copious amounts of deionized water to remove any preservative and then soaked for at least 24 hours to ensure full hydration. Following soaking, the membranes were kept wet until they were required for use.

The membranes were imaged via field-emission scanning electron microscopy (FESEM). Prior to imaging, the membrane coupons were left to air-dry on the benchtop. Small subsections ($\sim 9 \text{ mm}^2$) were taken from the center of each coupon and mounted on aluminum stubs which were subsequently sputter-coated with 5 nm of platinum. These samples were then imaged using a *JEOL 7000F* instrument at a 5.0 kV acceleration voltage. Multiple locations on each of the mounted membranes were viewed to verify that the acquired micrographs were reasonably representative of the sample. Refer to Figure A.1 for electron microscopy images of the native membranes.

3.2.3 Municipal Wastewater Effluent

Effluent wastewater was collected in five-gallon buckets from the surface of a 2° clarifier tank at the Dundas Wastewater Treatment Plant (Hamilton, Canada), as needed. Solid aggregates were al-

lowed to settle, then the supernatant water was carefully decanted. Prior to further use, wastewater from each bucket was comprehensively characterized (“pre-screened”), where the measured water quality parameters included the total solids (TS) content, chemical oxygen demand (COD), total carbon/total organic carbon (TC/TOC), and conductivity. Excluding the COD tests which were performed in duplicate, all analyses were performed in triplicate. The test methodologies are noted in §2.2.3.

As wastewater properties are known to vary substantially with time in a WWTP, incoming buckets—collected on different days—were screened to verify that the water quality parameters (TS, COD, TOC, TC, and conductivity) were reasonably consistent. By performing a qualitative comparison against previous wastewater samples, inconsistent buckets were discarded and not used in the subsequent filtration experiments. Over this study, eleven buckets of wastewater were collected, analyzed, and deemed acceptable for use. Table 3.1 summarizes the *average* water quality parameters \pm one standard deviation, where the latter value is a metric describing the accepted variability between samples. Detailed wastewater properties of *each bucket* are summarized in Table A.1.

3.2.4 Microplastic Suspensions

The MP particles created via ball-milling and sieving were suspended into pre-screened wastewater. Due to the (impractically) low concentration of MPs in WWTP effluent (see §1.2), a base-case concentration of 1 mg MPs/L was chosen for use in 24-hour filtration experiments. This value scales a 24-hour experiment in the laboratory to roughly three months of WWTP operation via previously-reported effluent MP *mass* concentrations [17]. The corresponding calculations are seen in §A.1. Similarly, Enfrin *et al.* chose MP concentrations of 10 mg/L as a “reasonable” approximation of MP concentrations in water reclamation plants [4–6]. Further, Ziajahromi *et al.* (2016) estimate that the expected concentration MPs in municipal wastewater *influent* collected the United Kingdom ranges

Table 3.1: Summary of average water quality parameters for wastewater samples collected and used in filtration experiments ($N = 11$ buckets).

TS (mg/L)	TOC (mg/L)	TC (mg/L)	COD (mg/L)	Conductivity (μ S/cm)
737 ± 80	6.0 ± 2.0	33 ± 7	41 ± 5	$1,102 \pm 140$

from 0.27–1.4 mg/L [20], though this range would be expected to be significantly lower at the ends of the processes. Thus, the selection of MP mass concentrations used in this study are reasonable in comparison with previous studies. Finally, it should be noted that no attempts were made to characterize the “natural” concentrations of MPs, here, as it was reasonably anticipated that the MPs doped into the wastewater would significantly outnumber any that were already present.

For filtration experiments involving MP particles, concentrated suspensions of 0.1, 1, or 10 mg/mL of PE were doped into a solution consisting of Tween 20 and deionized water. The Tween concentration was always set as one-tenth of the MP concentration as previous experiments (not shown) determined that this ratio permits the PE to remain reasonably-well suspended. MP suspensions were sonicated for one hour to disperse the particles prior to filtration experiments.

3.2.5 Filtration Experiments

A constant-pressure apparatus was constructed for the filtration experiments; a diagram of the apparatus is displayed in Figure 3.1. The bottom of the aluminum feed reservoir (21.8 L capacity) was outfitted with a magnetic stir bar to ensure that the wastewater was well-mixed. Three custom-built aluminum dead-end filtration cells were connected to the reservoir via stainless steel tubing. Inside each of the cells, a flat-sheet membrane coupon, cut to 25 mm in diameter (active area = 347 mm²), was placed on top of a coarse stainless steel mesh spacer which, in turn, sat atop a grooved permeate carrier disc. Finally, a Buna-N O-ring (McMaster-Carr; 1.004” OD, 0.864” ID) was placed atop the membrane coupon and each cell was sealed tightly using machine screws. Great care was taken to ensure that the apparatus was constructed from non-plastic materials, wherever possible.

To eliminate compaction during wastewater filtration, the membrane coupons were pre-compacted at 103 kPa (15 psi) for one hour prior to conducting filtration experiments. To do so, the reservoir was charged with deionized water and flow was achieved by pressurizing the vessel using nitrogen gas. Following this compaction step, the deionized water was completely replaced with either wastewater or a mixture of wastewater and MPs. In experiments with MPs, a small volume of concentrated MP suspension was added to the wastewater in the reservoir to achieve final MP concentrations of 0.1, 1 or 10 mg/L. In experiments without MPs, Tween was added to the wastewater as a control

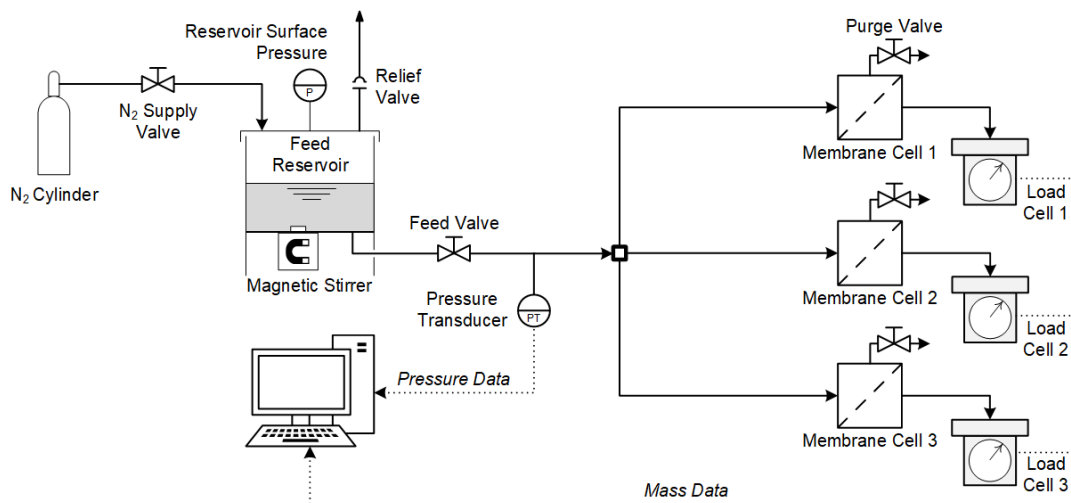


Figure 3.1: Diagram of the constant-pressure filtration setup. See Figure A.2 for a schematic of the membrane cells.

(final concentration = 0.1 mg/L corresponding to the “base case” scenario) as experiments with the MPs required the surfactant to suspend the particles. Filtration experiments proceeded at a surface pressure of 69 kPa (10 psi) for a total of 24 hours. During the experiments, permeate water from each filter cell was collected atop a custom-built scale consisting of a 3 kg load cell and an amplifier circuit (*Creatron HX711*). The mass data was sent to a computer via an *Arduino Uno 3* module. Mass data points were recorded every 30 seconds using *RsMulti* software (A&D Company), while the feed pressure was continuously monitored by a USB pressure transducer (*Omega PX409*; *Digital Transducer Application* software) located upstream of the membrane cells.

3.2.6 Membrane Backwashing

A select number of experiments were conducted with a modified version of the filtration setup shown in Figure 3.1 to study the effect of backwashing (BW) on flux recovery. A syringe pump (*Harvard Apparatus PHD ULTRA*) was outfitted with three 60 mL syringes containing 0.1% sodium hypochlorite (bleach) solution in deionized water. BW was achieved by closing the feed valve on the filtration apparatus and connecting each syringe to the permeate port of a membrane cell via silicone tubing. Purge valves at the top of the membrane cells were opened to evacuate the BW solution. Following the forward filtration of the wastewater for one hour at 69 kPa (10 psi), the membranes were backwashed by injecting the bleach solution backwards through the membranes at constant

flux for three minutes. A BW flux J_{BW} approximately twice the initial wastewater flux was used, which corresponded to $J_{BW} = 1,000 \text{ L/m}^2/\text{h}$ (LMH) and $J_{BW} = 3,000 \text{ LMH}$ for the UB70 and V0.2 membranes, respectively. After each BW step, wastewater was reintroduced into the membrane cells to displace the bleach solution. In total, three filtration/BW cycles were performed per experiment.

3.3 Results & Discussions

3.3.1 Milled & Sieved Microplastic Particles

The particle sizes of the powdered PE feedstock procured for this study were somewhat large ($\sim 0.5\text{--}1 \text{ mm}$). Previous studies have shown that a great fraction of these “larger” MPs are removed early in typical wastewater treatment processes (*e.g.* during primary clarification, skimming), and thus, smaller MP particles are present in the effluent [18, 21, 22]. In accordance with prior studies, a ball-milling process was used to convert the larger PE grains into smaller MP particles. For example, Eitzen *et al.* (2019) used a cryogenic ball mill to convert macroscopic polystyrene (PS) pellets into smaller-sized MP particles in the size range of 1–200 μm , depending on the milling conditions [14]. Similarly, Pizzichetti *et al.* (2023) used a cryogenic ball mill to break down polyamide (PA) and PS particles which were then captured between 20 μm - and 300 μm -aperture sieves to produce irregular MP particles for filtration experiments. Evidently, these processes present inherent challenges for producing usable quantities of very small (*i.e.* $O\{1 \mu\text{m}\}$) MPs stemming from limitations in the possible reduction in particle size, the aggregation of milled particles because of heating, difficulties in fractionating (*e.g.* sieving) the milled product, and/or low overall yields of particles of interest. Despite the use of milling instruments to produce plastic microparticles in several other previous studies [14, 23–26], to my knowledge, researchers had not produced or used irregular microparticles specifically having an appropriate size to interact with MF membrane pores.

As shown in Figure 3.2, the processing conditions employed in the present study were successful in creating suitable PE MPs. An optical microscopy image of the milled and sieved PE MPs is displayed in Panel A. It is clear that milling/sieving effectively reduced the particle size of the powdered PE feedstock. Furthermore, the irregular shape (*i.e.* not perfectly circular or spherical) of the particles is clearly visible, which means that the milling process was successful in creating

MP particles that are representative of those found in the effluents of actual WWTPs [16]. The top-down image in Panel A was analyzed to determine the average “size” of the milled particles ($N = 724$). The minimum and maximum Feret diameters (*i.e.* “caliper sizes”) of each particle were extracted, with the true particle “size” being reported as the arithmetic average of these two values. In a similar fashion, Simon *et al.* (2018) characterized particles based on their major and minor axes [17]. The histogram in Panel B illustrates the distribution of the minimum, maximum, and average Feret diameters in the microscope image. As can be seen, the most prevalent particle sizes were just under 10 μm . From this distribution, the mean and median sizes of the particles can be calculated as $14.5 \pm 13.9 \mu\text{m}$ (average \pm standard deviation) and 9.5 μm , respectively. Furthermore, the mean aspect ratio of the particles was 1.67 ± 0.51 which confirms that the milling/sieving process was effective at creating irregular-shaped MPs, whereby aspect ratios further from unity correspond to more elongated and therefore less regular particles.

It should be noted that particle images were taken from regions with a low surface density of immobilized particles. However for reasons of feasibility and to avoid neglecting “large” MPs, no attempts were made to exclude aggregates from the image analysis performed in Fiji. Additionally,

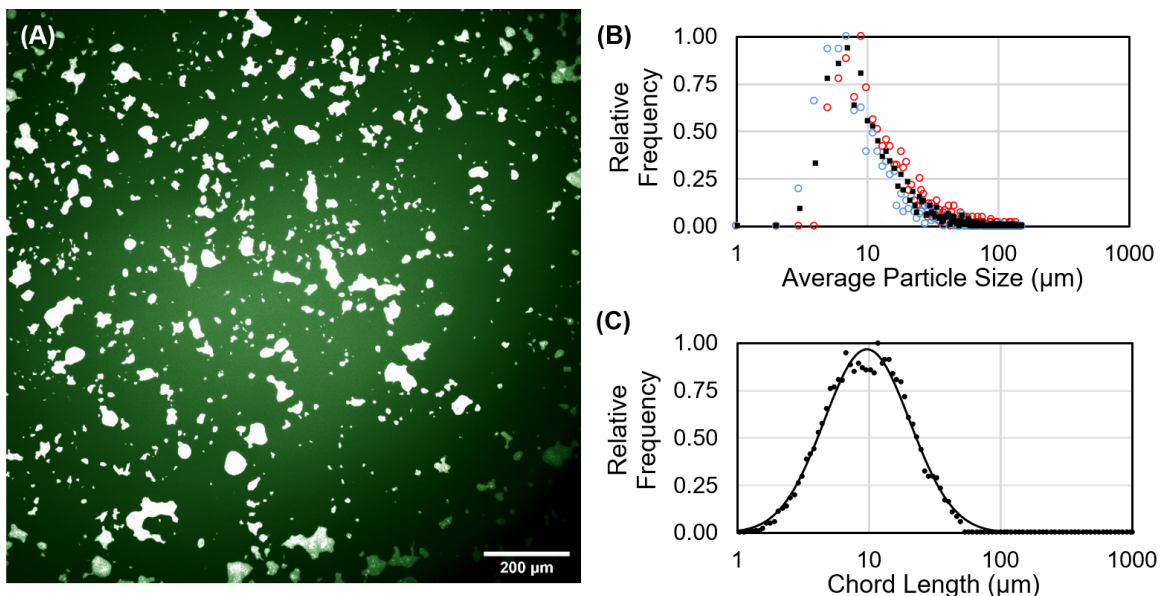


Figure 3.2: Characterization of milled and sieved PE MPs. (A) False-colour optical microscopy image of the MPs. (B) Distributions of the minimum (\circ), maximum (\circ), and average (\blacksquare) Feret diameters from the image analysis. (C) Particle chord length distribution via FBRM. Data points (\bullet) and the best-fit log-normal distribution ($—$) are shown. A more detailed characterization of the feed particles and the milled and sieved MPs is shown in Figure A.3.

to avoid counting small image artefacts and pixelation, the software was programmed to arbitrarily ignore any “particles” smaller than $4 \mu\text{m}^2$, corresponding to artefacts consisting of < 9 pixels. These artefacts were thus excluded from the particle analysis, albeit, at the expense of any very small micro- or nanoplastics (*i.e.* $< 1 \mu\text{m}$) that may have been produced, but not detected. Furthermore, particle sizes were measured after *manual thresholding* of the acquired images which introduces an unquantified element of uncertainty in the particle sizing estimates. As such, the limitations of the image analysis procedure mean that the particle size distribution is potentially smaller than reported.

A histogram of the chord length distribution of milled/sieved MPs from FBRM measurements is displayed in Panel C. A sample of chord lengths was taken every two seconds for a 180-second period, with the median frequency $f(x)$ at which each chord length x appeared over time was used to create the histogram. The log-normal distribution function $\hat{f}(x)$ shown in Equation 3.1 was then fit to the chord length frequency data [27]:

$$\hat{f}(x) = \frac{h}{x\sigma\sqrt{2\pi}} \exp\left(-\frac{[\ln(x/\tilde{x})]^2}{2\sigma^2}\right) \quad (3.1)$$

where \tilde{x} and σ are the median and standard deviation (on the log-scale) of the chord length distribution, and h is a “height” scaling parameter used to match the frequency data. The sum-of-squares of the errors between the model $\hat{f}(x)$ and the actual frequency data $f(x)$ was minimized to obtain the values of m , σ , and h . As can be seen in Panel C, the log-normal function is a reasonable representation of the chord length distribution; the most frequent chord length (mode) corresponds to $9.7 \mu\text{m}$ while the distribution’s median chord length is $17.5 \mu\text{m}$. It should be noted that the FBRM may tend to underestimate the true “size” of a particle [19] as the measured chord lengths do not necessarily pass from one side of the particle to its opposite side. While suspended aggregates are not differentiated from single particles, the mode chord length obtained via FBRM is in excellent agreement the most commonly seen average particle sizes ($\sim 9 \mu\text{m}$) obtained via image analysis.

3.3.2 Filtration Experiments

The effects of the concentration of MPs in a wastewater feed on membrane filtration performance during constant pressure operation are shown in Figure 3.3. The results in Panel A are the cumulative mass of permeate water collected during the 24 hour experiments with the UB70 UF membrane.

For the control experiment with a wastewater solution containing just Tween (0.1 mg/L) but no MPs, the average amount of wastewater collected over a 24-hour period was 622 ± 55 g. Due to the significant presence of suspended solid material in the wastewater that was obtained from the 2° clarifier tank at the local WWTP, the filtration results obtained for wastewater with Tween were substantially different than those obtained from similar experiments conducted with deionized water. This reinforces the need to conduct filtration experiments in water matrices that are representative of those seen in WWTPs. Furthermore, it was found that the addition of MPs to the wastewater solution had a noticeable effect on the filtration performance of the UB70 membrane. For concentrations of 0.1, 1, and 10 mg/L of PE MPs in the wastewater feed, the average mass of collected permeate from the UB70 membrane decreased to 483 ± 25 g, 352 ± 30 g, and 293 ± 15 g, respectively. Thus, the addition of even the lowest concentration of PE MPs in the feed solution resulted in a 23% decline in total permeate mass collected compared to a 53% decline when the greatest concentration of MPs was added.

In contrast, when the V0.2 MF membrane was used, the average mass of collected permeate during the 24-hour filtration of wastewater containing Tween but no MPs (943 ± 70 g) was 52% higher than that obtained with the UB70 UF membrane. This is not surprising given that the reported pore size of the MF membrane ($0.2 \mu\text{m}$) is much larger than that of the UF membrane ($0.03 \mu\text{m}$). Pure water permeability measurements for the two membranes corroborate the finding: the permeability value of the V0.2 MF membrane ($3,788 \pm 1,015$ LMH/bar) was approximately six times greater than that of the UB70 UF membrane (618 ± 77 LMH/bar), on average. Refer to §2.1.2.1 for information regarding permeability measurements. When PE MPs were filtered along with the wastewater at concentrations of 0.1, 1, and 10 mg/L, the average mass of collected permeate from the V0.2 membrane MF decreased to 709 ± 34 g, 644 ± 67 g, and 322 ± 12 g respectively. It is interesting to note that at the highest MP concentration used in this study, for example, the percentage decrease in filtration capacity for the V0.2 MF membrane (66%) was higher than that for the UB70 UF membrane (53%), potentially due to the MPs embedding themselves in the larger pore openings of the MF membrane.

Furthermore, the cumulative permeate mass results in Panels A and C were translated into permeate volumetric flux profiles ($J_v(t)$; LMH) in Panels B and D, respectively, using Equations 2.2–2.4.

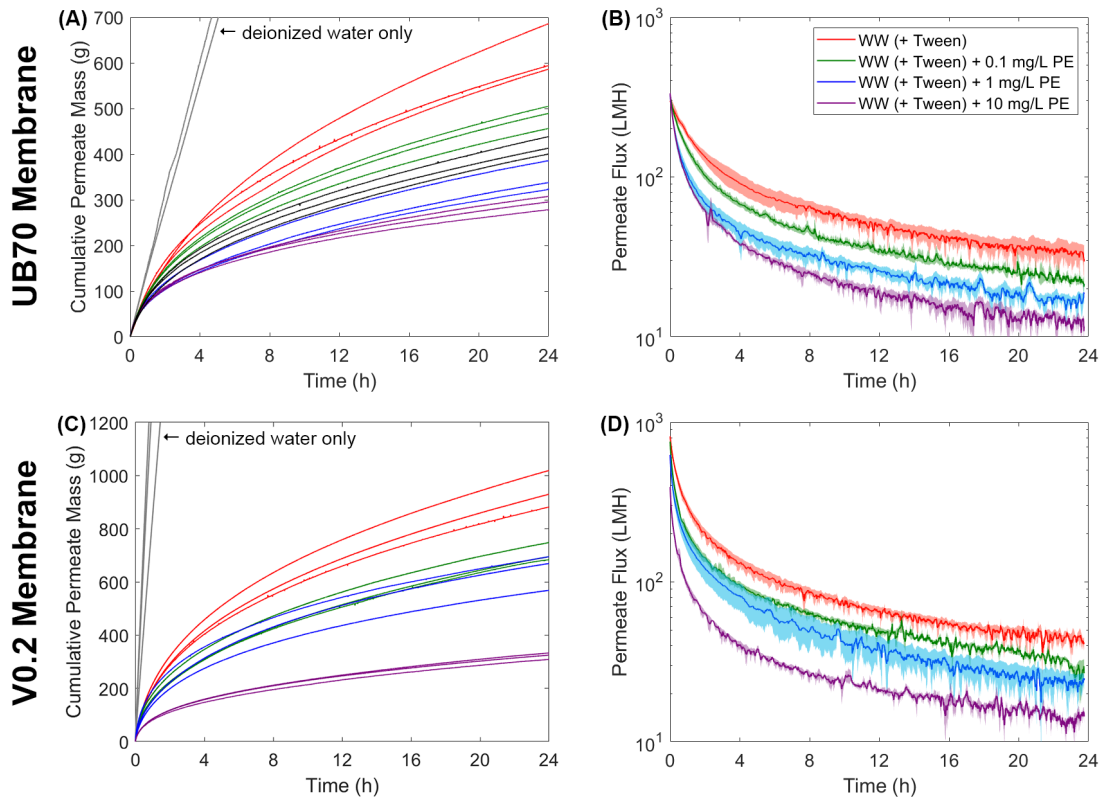


Figure 3.3: Filtration of wastewater and PE MPs through the UB70 UF (Panels A and B) and V0.2 MF (Panels C and D) membranes. Panels A and C display the cumulative permeate water mass collected over the 24-hour filtration tests; the three lines in each data series reflect the triplicate measurements. Panels B and D display a transformation of the results in Panels A and C into permeate fluxes. The colour band around each data series indicates the range of values experienced in that experimental condition, while the solid line at its center is the average of the three measurements.

$\Delta M/\Delta t$ —the rate of change in the mass of the permeate collected—was approximated using a forward-differences numerical method. A wastewater density of $\rho = 1,000 \text{ kg/m}^3$ was used and Δt was set at 0.25 h in order to balance resolution and smoothing of the $J_v(t)$ function. As shown in Panel B, the average permeate flux through the UB70 membrane (averaged over triplicate experiments) decreased from approximately 320 LMH to 30 LMH during filtration of the wastewater without MPs. By comparison, the permeate flux decreased (on average) to 21 LMH, 18 LMH, and 12 LMH after 24 hours of filtration of wastewater solutions containing 0.1 mg/L, 1 mg/L, and 10 mg/L of PE MPs, respectively. Similarly, the results shown in Panel D indicate that the average permeate flux for the V0.2 MF membrane decreased from approximately 800 LMH to 41 LMH for the filtrations using only wastewater and Tween. By comparison, the average flux decreased to 27 LMH,

23 LMH, and 15 LMH when 0.1 mg/L, 1 mg/L and 10 mg/L of wastewater and MPs were filtered, respectively. Thus, despite the two membranes having significantly different initial fluxes (320 versus 800 LMH), there was little difference in their filtration performance at the *end* of the 24-hour filtration period. While it might be predicted *a priori* that 3^o wastewater treatment processes using MF membranes (versus UF membranes) might be more resistant to wastewater and MP fouling over time, it is evident from this study that laboratory-scale experiments with real wastewater and MPs are needed in order to elucidate the true filtration phenomena.

The flux decline results from this investigation are reasonable in context of other MP fouling experiments in the literature. In the *substantially similar* work performed by Pizzichetti *et al.* (2023)—but published *after* the work described in this chapter—PS and PA MPs were suspended in pure water (1–20 mg/L) and filtered at a constant transmembrane pressure (30 kPa/4.35 psi) over hour-long experiments [28]. The results obtained also suggest that higher MP concentrations (regardless of chemistry) induced greater flux declines due to the effects of membrane fouling. However, a denser cake layer was observed with the smaller PA MPs that were used, resulting in greater flux declines than when the larger, more irregularly-shaped PS MPs were used (*i.e.* $41 \pm 16 \mu\text{m}$ versus $109 \pm 74 \mu\text{m}$). Additional discussions regarding the findings of this work can be found in §1.3.1.2. Further, in the study performed by Enfrin *et al.* (2020) where very small PE MPs suspended in pure water were filtered in crossflow configuration using polysulfone UF membranes, significant flux declines were also seen due to the adsorption of the particles onto the membranes [3]. However, these declines are much less in magnitude (38% over 48 h) than those seen in this study with the UB70 and V0.2 membranes: 91%–98% and 95%–99%, respectively, over 24 hours. This discrepancy is attributable to the presence of the suspended/dissolved solids in the wastewater which contributed to the fouling-induced flux decline. In another study which investigated membrane fouling phenomena caused by plastic nanofibers in the presence of model organic foulants (polyethylene glycol and polyvinyl alcohol), the magnitudes of the flux declines increased from roughly 25% to 85% when the model foulant concentrations increased from 0.01 to 1 mg/L [4]. This finding substantiates what is reported in this study. In reality, the flux declines seen in this study would normally be less drastic due to mitigating processes (*e.g.* crossflow filtration, backwashing, cleaning-in-place, scouring), yet the results demonstrate that MP particles contribute to flux decline during wastewater filtration.

Finally, it is understood that the properties of 2° clarifier effluent wastewater (*i.e.* water quality) can vary significantly over time. However great effort was taken to ensure that the wastewater feed that was obtained and used in filtration experiments (*i.e.* Figure 3.3) maintained reasonably consistent properties. This was done by assessing quality parameters of the wastewater collected from the WWTP and accepting or rejecting the samples based on the results of these measurements. Even though there was still some variability in the “accepted” pre-screened wastewater, initial experiments were performed which indicated that filtering wastewater from buckets collected on different days—but using the same membrane—yielded reasonably similar results. Refer to Figure A.4 for an illustration of the filtration behaviour when two different (but “accepted”) wastewater feeds were filtered with the UB70 membrane. Thus, variations in the cumulative permeate masses/permeate fluxes over time can be attributed to the presence and concentration of the MPs. Similarly, no appreciable difference was observed in the cumulative permeate masses over time for experiments conducted with wastewater alone and those conducted with wastewater plus Tween (see Figure A.5).

3.3.3 Fouling Mechanisms

In order to determine the most probable fouling mechanism(s) that caused the significant decline in permeate flux at the various conditions shown in Figure 3.3, the four fouling models developed by Hermia [29] were fit to the flux-versus-time data in Figure 3.3. See §2.1.3.1 for an explanation of these models. To obtain the model constants J_0 and K , the sum-of-squares of the errors (SSE) between the model and the flux-versus-time data (averaged over the three replicates) was minimized. The model with the lowest SSE was considered to provide the “best” description of the data. For both membranes, “cake filtration” proved to be the dominant fouling mechanism. The exceptions to this result were the 0.1 mg/L and 10 mg/L cases for the UB70 membrane, which were described marginally better by the “intermediate blocking” model. For the sake of comparison, the cake filtration model was fit to all of the data series; graphs of the flux decline data overlaid with the “cake filtration” fouling models are shown in Figure A.6.

The best-fit parameters for the “cake filtration” model are also summarized in Table 3.2; alternatively, the parameters for the cases where “intermediate blocking” is actually dominant are given in Table A.2. The rate of flux decline increased with increasing MP concentration, which is evidenced

Table 3.2: Summary of “cake filtration” fouling model parameters for the two membranes challenged to wastewater suspensions containing various concentrations of MPs.

mg/L PE	UB70				V0.2			
	0	0.1	1	10	0	0.1	1	10
J_0 (LMH)	348	276	378	282	939	834	694	449
$K \times 10^5$ (h ⁻¹)	2.92	5.03	10.6	13.5	1.37	2.66	3.81	12.5

by the increase in K values. In the absence of added MPs, solids carried via the convective flux of wastewater are deposited onto the membrane surface, creating a cake layer that inhibits filtration. When MPs are added, they are also carried to the membrane surface where they accumulate and contribute to an increased resistance towards the flow of water through the membrane. Assuming a well-mixed feed, the accumulation of MPs on the membrane surface can be approximated as 140 mg/m², 1,000 mg/m², and 8,400 mg/m² for the 0.1 mg/L, 1 mg/L, and 10 mg/L suspensions, respectively. This cake layer became more resistive as the MP concentration (and surface accumulation) increased, as evidenced by sharper flux decline profiles—indicated by larger K values—and a lower cumulative permeate mass. This trend was also seen by Pizzichetti *et al.* (2023) in their similar MP fouling experiments whereby higher MP loadings resulted in greater kinetic constants in their fouling models, though they noted that the flux decline profiles were best-described by sequential “complete blocking” followed by “cake filtration” [28]. Furthermore, the model values in this work for J_0 also decrease as the concentration of MPs increases for the V0.2 membrane. This trend likely does not hold for the UB70 membrane due to a few limitations: the cake filtration models were not dominant for describing the filtrations using 0.1 mg/L or 10 mg/L of PE. Considering the observations made by Pizzichetti *et al.* (2023), it is possible that sequential mechanisms may better describe the fouling kinetics. It should be noted that the models and calculated parameters are descriptive—not explanative—of the process.

In the aforementioned study performed by Enfrin *et al.* (2020), fouling models were also fit to the flux decline data. In the early stages of the filtrations, the mechanism of surface (intermediate) pore blocking was most appropriate, however the authors found that a cake filtration cake model became more appropriate as the filtration progressed due to the accumulation of the particles on the surfaces of the membranes [3]. These results are in good agreement with the findings from this study.

The effects of fouling on the membrane surfaces are depicted in Figure 3.4. Initially, the pore structure is clearly visible on the native membranes. However as shown in the middle panels, the pore structure becomes obscured by a textured cake of organic material that accumulates on the membrane surface following wastewater filtration. Similarly, MPs that were added to the wastewater are visibly embedded in the cake of organics. As a result, the water must pass through the cake and around the dense PE particles that coat the membrane's surface and remain there due to interactions between the PE and PVDF membrane. Cake layer formation is undesirable from a design and operations standpoint as it either reduces the volume of water that can be treated which necessitates greater capital investment in membrane area, or results in greater utility costs due to the higher pressures required to permeate the desired volume of water. Overall, MPs in wastewater inherently lead to increased cake fouling with both the UF and MF membranes.

3.3.4 Filtration Experiments with Backwashing

BW processes are commonly used to mitigate cake formation on the surfaces of membranes. In general, these processes loosen surface deposits by forcing clean water at high flux from the per-

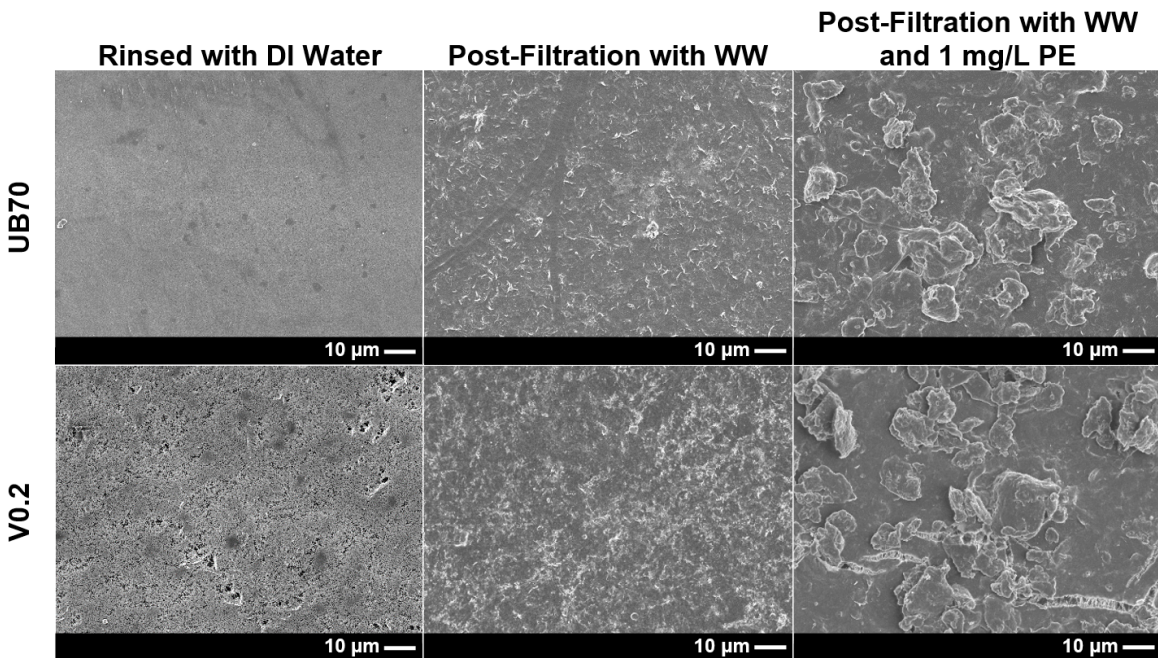


Figure 3.4: FESEM images of the two types of membranes used in this study at three different conditions: as-received and rinsed with DI water; after 24 hours of filtration with wastewater containing no MPs; and after 24 hours of filtration with wastewater containing 1 mg/L of MPs.

meate side of the membrane towards the feed. In theory, a “perfect” BW process will restore the membrane’s permeate flux to its initial value, $J_v(0)$. Using additive chemicals during BW processes (*i.e.* chemically-enhanced backwashing; CEB) such as bleach [30, 31] can help to achieve this goal. In the BW experiments, wastewater (no Tween) and wastewater with 1 mg/L MP suspensions (plus 0.1 mg/L Tween) were filtered for one-hour intervals. These intervals were followed by three-minute BW cycles where a 0.1% bleach solution was injected at high flux. Figure 3.5 shows the results of this BW scheme. Note that the flux values $J_v(t)$ were normalized by the initial flux measurement $J_v(0)$ for comparative purposes. For both membranes and all solution chemistries, permeate flux increased substantially after BW at $t = 1$ and 2 hours. However, the flux did not necessarily recover to its initial state (*i.e.* $J_v(t)/J_v(0) \neq 1.0$) which suggests that the foulants were not completely removed from the surface or from within the pores of the membrane.

When no MPs were added to the wastewater, the relative flux of the UB70 membrane recovered to average values of 0.85 and 0.81 after the first and second BW, respectively. In contrast, the presence of 1 mg/L of PE resulted in lower flux recoveries of 0.74 and 0.71, respectively. This lower flux recovery after the second BW process indicates that it was unable to remove foulant matter from the membrane’s surface, and solids continued to accumulate as additional wastewater was filtered. Increasing the number of filtration/BW cycles could help determine the extent of this phenomenon.

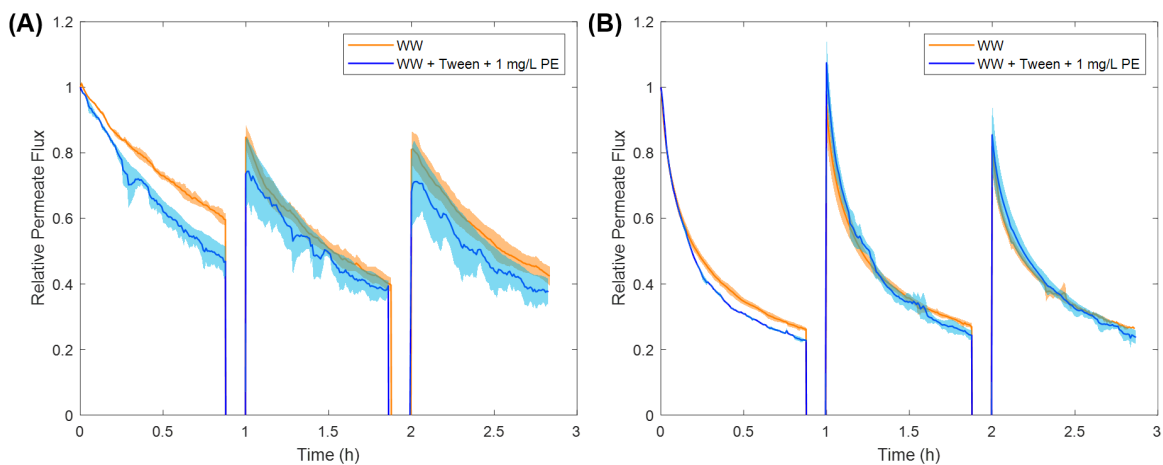


Figure 3.5: Filtration and BW cycles for the (A) UB70 and (B) V0.2 membranes. Filtrations of wastewater and wastewater with 1 mg/L of PE MPs were performed in one-hour intervals followed by BW processes at $t = 1$ and 2 hours. The colour band around each data series refers to the range of values experienced in that experimental condition while the solid line at its center (—) is the average of the three replicates.

The permeate flux recoveries for the V0.2 membrane exhibited a different trend. With wastewater only, the average relative flux recovered to approximately 0.94 and 0.82 after the first and second BW, respectively. When MPs were added, these values increased to 1.06 and 0.85, respectively. Note that the one recovery above 1.0 cannot be differentiated from a “full” flux recovery (*i.e.* $J_v(t)/J_v(0) = 1.0$) due to the variance in the individual measurements. Interestingly, the flux recovery for the V0.2 membrane was greater when MPs were present versus with wastewater alone. This result is potentially attributable to MPs dislodging portions of the organic foulant layer as they were stripped from the membrane surface. This likely did not occur with the UB70 UF membrane due to its much lower BW flux ($J_{BW} = 1,000$ LMH vs. 3,000 LMH) and thus weaker hydrodynamic forces. Although greater average relative flux recoveries occurred when MPs were present, the *flux declines* during these filtrations were still more substantial where MPs were added—as expected given the results from Figure 3.3. In addition, the average flux recovery decreased after subsequent filtrations due to imperfect regeneration and the continued accumulation of foulants.

Figure 3.6 presents FESEM images of the membranes used in the BW experiments. Membranes that were subjected to all three BW cycles were compared with those that were removed from the apparatus at the end of third filtration cycle, but prior to the third BW. The additional BW cycle appears to dislodge a significant portion of MPs from the membrane’s surface. In the experiments with MPs, the images following BW have a lower density of MPs (and perhaps smaller MPs) compared to those that did not undergo the BW. The process also appears to disturb the organic cake layer on the surfaces of the membranes. This observation was particularly apparent with the V0.2 MF membrane: it experienced a higher, more turbulent BW flux which was particularly effective according to the flux recovery values. Note that the pores of the *backwashed* V0.2 membranes re-emerge through the cracks in the cake layers, but remain covered in the *non-backwashed* membranes. A magnified view showing the re-emergence of the membrane surface is shown in Figure A.7. The results clearly indicate that the BW process was effective at removing a significant portion of the solids/MPs from the surfaces of the membranes, in particular, the V0.2 MF membrane. For reference, macro-scale images of the entire membranes (native/fouled/backwashed) are shown in Figure A.8.

In addition to BW, other fouling mitigation strategies (*e.g.* physical cleaning, surface chemistry control) have been considered with respect to MPs. In a study by Enfrin *et al.* (2021), it was found

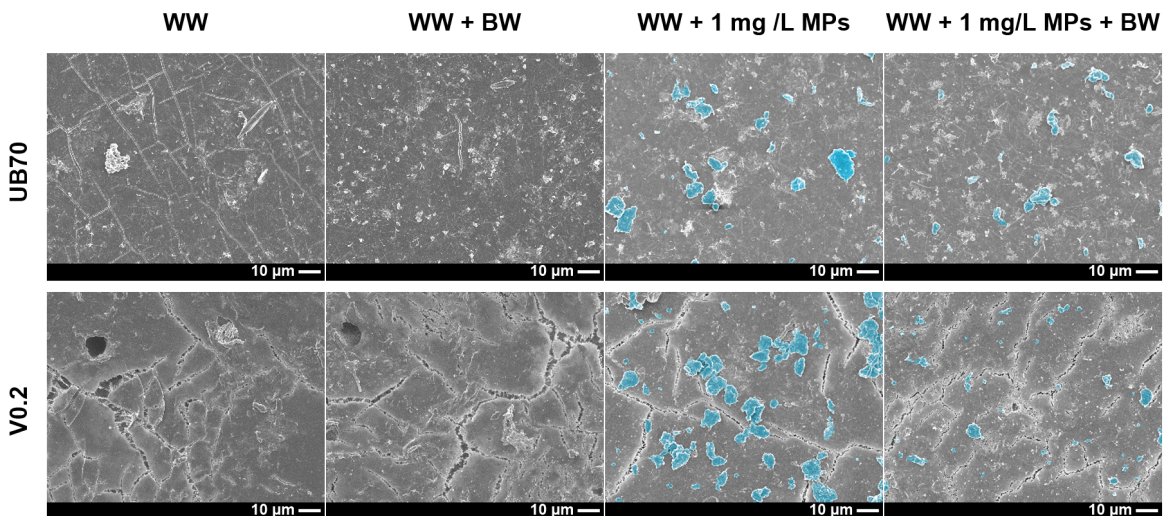


Figure 3.6: FESEM images of the UB70 and V0.2 membranes indicating the effect of BW on deposited foulants. The membranes filtered wastewater and wastewater with MPs for three one-hour cycles interspersed with BW steps. In the columns labelled with “BW”, one last BW step was performed after the final filtration. In experiments with MPs, raised areas on the micrographs (*i.e.* potential MPs) were coloured during image processing. The bottom-right panel is magnified in Figure A.7.

that air scouring limited flux decline to only 22% (versus 38% without scouring) over the course of a filtration experiment involving very small PE MPs [6]. While it is not a perfect head-to-head comparison, the BW process in the work described herein appears to be more effective for removing MPs from the surfaces of the membranes than the one described by Enfrin and colleagues. In a similar manner, the authors also demonstrated that surface chemistry modifications can inhibit the adsorption of MPs [5]. The use of hydrophilic coatings such as acrylic acid and cyclopropylamine reduced the adsorption of the PE MPs by greater than 60%, limiting flux decline to only 8% over the course of the 6 h filtration experiment. A combination of informed membrane design (*e.g.* surface modifications) and membrane process operation (*e.g.* BW processes, physical cleaning) will likely best serve to maximize membrane performance and preserve the lifespan of these technologies.

Due to the scaling-up of the MP concentrations, every hour of filtration in the BW process from this work reflects approximately four days of operation in a real WWTP. For perspective, in a review of WWTPs conducted by Raffin *et al.* (2013), the BW frequency ranged from every 8 minutes to every 38 minutes, and the addition of chemicals (*e.g.* NaOCl, NaOH) via CEB ranged from three times daily to twice per month in the nine facilities studied [32]. Clearly, BW processes are highly dependent on the system and wastewater characteristics. While the scaling of experiments

in the laboratory can create a rough representation of the wastewater treatment process in real life, bench-scale experiments such as the ones presented in this investigation are critical for advancing our knowledge of the interactions between MPs and membrane systems. If the accumulation of MPs on the surface of membranes in WWTPs occurs as observed in this study, then facilities will have to take certain design/operational considerations into account. For example, while BW processes can mitigate the flux decline caused by MPs, they should still be ameliorated (*e.g.* higher flux, longer BW, CEB, etc.) to address MP fouling and to prolong the membrane's life. Contemporary research has shown techniques such as using crossflow filtration [3], plasma surface modification of membranes [5] and physical cleaning via periodic air scouring [4, 6] can be effective at mitigating the effects of MP fouling. However, further research is needed to understand how MPs with different sizes, shapes, and chemistries (*e.g.* polypropylene, polyester, etc.) affect the fouling of membranes made of different materials (*e.g.* PVDF, polyethersulfone, etc.), possessing different pore sizes, and having different geometries (*e.g.* flat-sheet, hollow-fiber, spiral-wound).

3.4 Concluding Remarks

In this study: a planetary ball-milling and sieving process was developed to create sufficient amounts of irregularly-shaped MPs for membrane filtration studies. The conditions used in this study produced particles approximately 10 μm in size. Subsequently, constant-pressure filtration experiments were conducted using *TriSep UB70* UF and *Synder V0.2* MF membranes. The cumulative volume of permeate water collected over time was significantly less when wastewater was filtered (versus pure water) because of membrane fouling. Pursuant to this finding, it is important to consider the effects of complex solution matrices such as actual wastewater when performing MP fouling studies. For both of the membranes, the presence of MPs—even in small concentrations relative to the solids in the WW—increased the magnitude of flux decline over 24 hours when compared to wastewater alone. Increasing the concentration of MPs also increased the flux decline, as evidenced by the application of the cake filtration fouling model. While the initial flux of the MF membrane was significantly higher than that of the UF membrane, the “fouled” flux values of both were remarkably similar following 24 hours of filtration. Finally, both membranes were backwashed at high flux using a bleach solution. The UF membrane showed lower flux recovery in the presence of MPs than when only wastewater was filtered. In contrast, the MF membrane showed higher flux recovery when MPs

were present than when only wastewater was filtered. However, the overall flux decline for the MF membrane was significantly higher when MPs were present.

Overall, there is a clear need to design and implement validated WWTP technologies that can effectively remove MPs from wastewater. While this study provides important insights into the fouling of dead-end membranes by MPs suspended in actual wastewater, it is limited in that it does not concurrently consider the *rejection* of those MPs. That is, no relationship between MP fouling behaviour and particle transmission for the two membrane pore sizes was developed. MP transmission was excluded from the scope of this work due to the inherent difficulties associated with quantifying MP concentrations (see §1.2.1 for more details), especially in complex solution matrices such as wastewater. As the MPs were not particularly distinct from other solids that were present—as is often the case—careful work would be needed to isolate and identify MPs in samples. For this study, MP concentration measurements would require the development of a robust separation procedure to isolate the MPs from the wastewater solids (*e.g.* [13]), followed by a MP counting procedure using an optical microscope. Both the separation and counting procedures would be expected to be thoroughly laborious tasks. Without automation, counting the MPs using a microscope is especially challenging given the large numbers of particles in feed samples: assuming monodisperse spherical PE MPs having diameters of 10 μm a mass concentration of 1 mg MPs/L corresponds to a number concentration of approximately 2×10^6 MPs/L. Acknowledging this overall shortcoming, the next chapter in this work describes an improved method for MP quantification using *fluorescent* PE MP particles and a standard laboratory fluorometric plate reader. To this end, the concentration of MPs in aqueous suspensions was quantified and MP rejection/transmission measurements were performed.

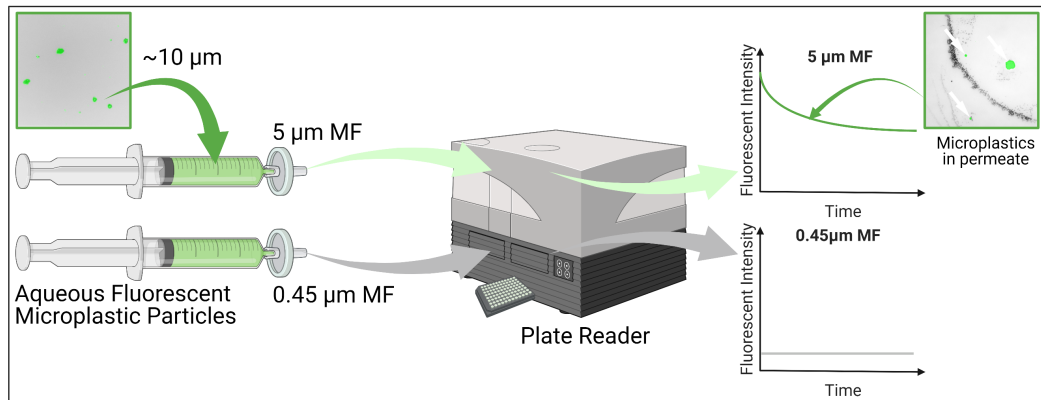
3.5 Works Cited

- [1] R. J. LaRue, B. Patterson, S. O'Brien, and D. R. Latulippe, "Evaluation of Membrane Fouling by Microplastic Particles in Tertiary Wastewater Treatment Processes," *ACS ES&T Water*, vol. 2, 2022.
- [2] K. W. Trzaskus, W. M. de Vos, A. Kemperman, and K. Nijmeijer, "Towards controlled fouling and rejection in dead-end microfiltration of nanoparticles—role of electrostatic interactions," *Journal of Membrane Science*, vol. 496, pp. 174–184, 2015.

- [3] M. Enfrin, J. Lee, P. Le-Clech, and L. F. Dumée, “Kinetic and mechanistic aspects of ultrafiltration membrane fouling by nano- and microplastics,” *Journal of Membrane Science*, vol. 601, p. 117890, 2020.
- [4] M. Enfrin, C. Hachemi, D. L. Callahan, J. Lee, and F. Dumée, “Membrane fouling by nanofibres and organic contaminants-mechanisms and mitigation via periodic cleaning strategies,” *Separation and Purification Technology*, vol. 278, pp. 1383–5866, 2022.
- [5] M. Enfrin, J. Wang, A. Merenda, L. F. Dumée, and J. Lee, “Mitigation of membrane fouling by nano/microplastics via surface chemistry control,” *Journal of Membrane Science*, vol. 633, p. 119379, 2021.
- [6] M. Enfrin, J. Lee, A. G. Fane, and L. F. Dumée, “Mitigation of membrane particulate fouling by nano/microplastics via physical cleaning strategies,” *Science of The Total Environment*, vol. 788, p. 147689, 2021.
- [7] B. Ma, W. Xue, C. Hu, H. Liu, J. Qu, and L. Li, “Characteristics of microplastic removal via coagulation and ultrafiltration during drinking water treatment,” *Chemical Engineering Journal*, vol. 359, pp. 159–167, 2019.
- [8] B. Ma, W. Xue, Y. Ding, C. Hu, H. Liu, and J. Qu, “Removal characteristics of microplastics by Fe-based coagulants during drinking water treatment,” *Journal of Environmental Sciences*, vol. 78, pp. 267–275, 2019.
- [9] K. Trzaskus, M. Elshof, A. Kemperman, and K. Nijmeijer, “Understanding the role of nanoparticle size and polydispersity in fouling development during dead-end microfiltration,” *Journal of Membrane Science*, vol. 516, pp. 152–161, 2016.
- [10] B. Agasanapura, R. E. Baltus, C. T. Tanneru, and S. Chellam, “Effect of electrostatic interactions on rejection of capsular and spherical particles from porous membranes: Theory and experiment,” *Journal of Colloid and Interface Science*, vol. 448, pp. 492–500, 2015.
- [11] H. Nazem-Bokaei, F. Fallahianbijan, D. Chen, S. M. O’Donnell, C. Carbrelo, S. Giglia, D. Bell, and A. L. Zydney, “Probing pore structure of virus filters using scanning electron microscopy with gold nanoparticles,” *Journal of Membrane Science*, vol. 552, pp. 144–152, 2018.
- [12] M. Pazouki, A. N. Wilton, and D. R. Latulippe, “An experimental study on sterile filtration of fluorescently labeled nanoparticles—the importance of surfactant concentration,” *Separation and Purification Technology*, vol. 218, pp. 217–226, 2019.
- [13] S. M. Mintenig, I. Int-Veen, M. G. J. Löder, S. Primpke, and G. Gerdt, “Identification of microplastic in effluents of waste water treatment plants using focal plane array-based micro-Fourier-transform infrared imaging,” *Water Research*, vol. 108, pp. 365–372, 2017.
- [14] L. Eitzen, S. Paul, U. Braun, K. Altmann, M. Jekel, and A. S. Ruhl, “The challenge in preparing particle suspensions for aquatic microplastic research,” *Environmental Research*, 2019.
- [15] B. Patterson, “Membrane Filtration of Microplastic Fibers: Assessment of Membrane, Microplastic, and Solution Properties,” Master’s thesis, McMaster University, Hamilton ON, 2021. [Online]. Available: <http://hdl.handle.net/11375/26932>
- [16] J. Sun, X. Dai, Q. Wang, M. C. van Loosdrecht, and B. J. Ni, “Microplastics in wastewater treatment plants: detection, occurrence and removal,” *Water Research*, vol. 152, pp. 21–37, 2019.

- [17] M. Simon, N. van Alst, and J. Vollertsen, “Quantification of microplastic mass and removal rates at wastewater treatment plants applying Focal Plane Array (FPA)-based Fourier Transform Infrared (FT-IR) imaging,” *Water Research*, vol. 142, pp. 1–9, 2018.
- [18] M. Lares, M. C. Ncibi, M. Sillanpää, and M. Sillanpää, “Occurrence, identification and removal of microplastic particles and fibers in conventional activated sludge process and advanced MBR technology,” *Water Research*, vol. 133, pp. 236–246, 2018.
- [19] M. Li, D. Wilkinson, and K. Patchigolla, “Comparison of Particle Size Distributions Measured Using Different Techniques,” *Particulate Science and Technology*, vol. 23, pp. 265–284, 2007.
- [20] S. Ziajahromi, P. A. Neale, and F. D. Leusch, “Wastewater treatment plant effluent as a source of microplastics: review of the fate, chemical interactions and potential risks to aquatic organisms,” *Water Science & Technology*, vol. 74, pp. 2253–2269, 2016.
- [21] R. Dris, J. Gasperi, V. Rocher, M. Saad, N. Renault, and B. Tassin, “Microplastic contamination in an urban area: a case study in Greater Paris,” *Environmental Chemistry*, vol. 12, no. 5, pp. 592–599, 2015.
- [22] S. Magni, A. Binelli, L. Pittura, C. G. Avio, C. Della Torre, C. C. Parenti, S. Gorbi, and F. Regoli, “The fate of microplastics in an Italian Wastewater Treatment Plant,” *Science of the Total Environment*, vol. 652, pp. 602–610, 2019.
- [23] Y. Dong, M. Gao, Z. Song, and W. Qiu, “As(III) adsorption onto different-sized polystyrene microplastic particles and its mechanism,” *Chemosphere*, 2020.
- [24] J. Schmidt, M. Plata, S. Tröger, and W. Peukert, “Production of polymer particles below 5 μm by wet grinding,” *Powder Technology*, vol. 228, pp. 84–90, 2012.
- [25] J. Hwang, D. Choi, S. Han, J. Choi, and J. Hong, “An assessment of the toxicity of polypropylene microplastics in human derived cells,” *Science of the Total Environment*, 2019.
- [26] A. Jemec, P. Horvat, U. Kunej, M. Bele, and A. Kržan, “Uptake and effects of microplastic textile fibers on freshwater crustacean *Daphnia magna*,” *Environmental Pollution*, 2016.
- [27] J. Gubicza, J. Szépvölgyi, I. Mohai, L. Zsoldos, and T. Ungár, “Particle size distribution and dislocation density determined by high resolution x-ray diffraction in nanocrystalline silicon nitride powders,” *Materials Science and Engineering A*, 2000.
- [28] A. R. P. Pizzichetti, C. Pablos, C. Álvarez-Fernández, K. Reynolds, S. Stanley, and J. Marugán, “Kinetic and mechanistic analysis of membrane fouling in microplastics removal from water by dead-end microfiltration,” *Journal of Environmental Chemical Engineering*, vol. 11, p. 109338, 2023.
- [29] J. Hermia, “Constant pressure blocking filtration laws-application to power-law non-Newtonian fluids,” *Chemical Engineering Research and Design*, vol. 60, pp. 183–187, 1982.
- [30] T. Zsirai, P. Buzatu, P. Aerts, and S. Judd, “Efficacy of relaxation, backflushing, chemical cleaning and clogging removal for an immersed hollow fibre membrane bioreactor,” *Water Research*, vol. 46, pp. 4499–4507, 2012.
- [31] S. K. Lateef, B. Z. Soh, and K. Kimura, “Direct membrane filtration of municipal wastewater with chemically enhanced backwash for recovery of organic matter,” *Bioresour. Technology*, vol. 150, pp. 149–155, 2013.
- [32] M. Raffin, E. Germain, and S. Judd, “Wastewater polishing using membrane technology: a review of existing installations,” *Environmental Technology*, vol. 34, no. 5, pp. 617–627, 2013.

Evaluation of Microplastic Particle Transmission through Microfiltration Membranes



4.1 Motivations

As is recounted in §1.3.1.1, membrane filtration processes are used in some 3^o treatment stages in wastewater treatment plants (WWTPs), and several studies have reported results related to removal of microplastics (MPs) via these processes. The majority of these studies have focused on membrane bioreactors (MBRs) that employ ultrafiltration (UF) or microfiltration (MF) membranes [1–8], however there are other studies that have focused on the staged use of UF and reverse osmosis (RO) membranes [9]. While these investigations demonstrate the role that membrane technologies can play in limiting the release of MPs into the environment, analyses were performed at a “facility level” and

often failed to disclose important technical information regarding the membrane filtration processes. For example, a 2017 study by Leslie *et al.* on the fate of MPs in Dutch municipal WWTPs [10] reported that one facility used a 0.08 μm pore size membrane in the MBR, however no information was given regarding the membrane geometry, chemistry, or manufacturer. Similarly, a 2019 study by Olmos *et al.* [3] on WWTPs in Spain contained no details on the pore size, chemistry, or manufacturer of the membrane that was used in the MBR. Finally, the 2017 study by Ziajahromi *et al.* WWTPs in Australia [9] on gave no technical information (*e.g.* pore size, manufacturer, chemistry, area, geometry, operating conditions) for the UF and RO membranes that were employed.

Adding to the confusion of literature results, Leslie *et al.* (2017) reported that a MBR containing a membrane with a 0.08 μm pore size demonstrated no additional ability to remove MPs from wastewater [10]. Ziajahromi *et al.* (2017) reported that permeate from the staged UF-RO process contained detectable levels (0.21 MPs/L) of MPs that were greater than 100 μm in size [9]; no explanation was given for how these large MPs transmitted through the dense separation layer of the RO membrane. However, some evidence exists regarding more consistent MP removal efficiencies. For example, Talvitie *et al.* (2017) reported 99.9% removal of MPs (feed concentration = 6.9 ± 1.0 MPs/L; permeate concentration = 0.005 ± 0.004 MPs/L) for a MBR containing a MF membrane with 0.4 μm pore size [7]. A subsequent study by Lares *et al.* (2018) considering the same MBR reported a 99.4% removal of MPs (feed concentration = 57.6 ± 12.4 MPs/L; permeate concentration = 0.4 ± 0.1 MPs/L) [1]. The removal efficiencies are quite similar in these two studies despite the differences in MP feed concentrations. Interestingly, even though the membranes used in the latter two studies have nominal pore sizes five times greater than the poorly-performing unit studied by Leslie *et al.*, the MP removal efficiencies were comparatively excellent.

There is poor understanding of the factors that affect MP removal (*i.e.* rejection) by membranes in WWTPs, including the effects of membrane pore size. This study aims to obtain quantitative data detailing MP rejection/transmission through commercial MF membranes of varying pore sizes. To this end, Durapore® polyvinylidene fluoride (PVDF) membranes (nominal pore sizes = 0.45 μm and 5 μm) were used to filter irregularly-shaped *fluorescent* polyethylene (PE) MPs created via the milling/sieving process developed in Chapter 3. Constant-flux filtration experiments were conducted and the presence of MPs in feed/permeate samples was quantified using a fluorescence assay.

4.2 Materials & Methods

4.2.1 Membranes

Flat sheet Durapore® PVDF membranes (EMD Millipore) with rated pore sizes of 5 μm (Lot R1AB88861) and 0.45 μm (Lot R9PA28407) were obtained. As shown in Figure 4.1, top-down field-emission scanning electron microscopy (FESEM) images of the two membranes gave the expected result of smaller pores and a tighter pore structure for the 0.45 μm membrane. In addition, the cross-sectional images revealed that while the 0.45 μm membrane is symmetrical and homogeneous in structure, the 5 μm membrane contains a fibrous support layer in the center of the membrane. At solution pHs above ~ 3 , the membranes possess net negative surface charges, as measured using an Anton Parr SurPASS 3 electrokinetic analyzer for solid surfaces. Via Figure B.2 (*i.e.* the 5 μm membrane), the surface charge is stable at -29 ± 3 mV (average \pm standard deviation) from pH 5–10. Refer to §B.1–B.2 for details on FESEM imaging and surface charge measurements.

4.2.2 Microplastic Particles & Suspensions

Spherical PE MPs (hereafter referred to as Sph-MPs) with a nominal density of 1.00 g/cm³ were obtained from Cospheric (*UVPMS-BG-1.00*; Santa Barbara, California). According to the manufacturer, these microspheres contain a proprietary fluorescent (green) tag which is evenly distributed throughout the polymer matrix and cannot leach out. To corroborate, preliminary tests (not shown) using the Sph-MPs indicate no evidence of leaching of the fluorescent dye from the particles into aqueous solutions. The measured sizes of the Sph-MPs obtained from FESEM imaging (*i.e.* via Figure B.1) was in good agreement with manufacturer-reported size of 53–63 μm .

Irregularly-shaped MPs were created using a milling and sieving procedure which was previously developed [11] and described in §3.2.1. Briefly, a planetary ball mill (*Retsch PM100*) was charged with 290 g of spherical zirconia milling media (3 mm diameter) and 7.25 g of Sph-MPs. The mill was run for 6 hours (total) using intervals of 5 minutes at 500 rpm followed by 5 seconds at 0 rpm to facilitate for modest cooling. The milled product was wet-sieved (25 μm aperture) using ethanol and the particles which passed through the sieve were collected and dried. These fluorescent milled and sieved MPs—hereafter referred to as M/S-MPs—were subsequently used in filtration experiments.

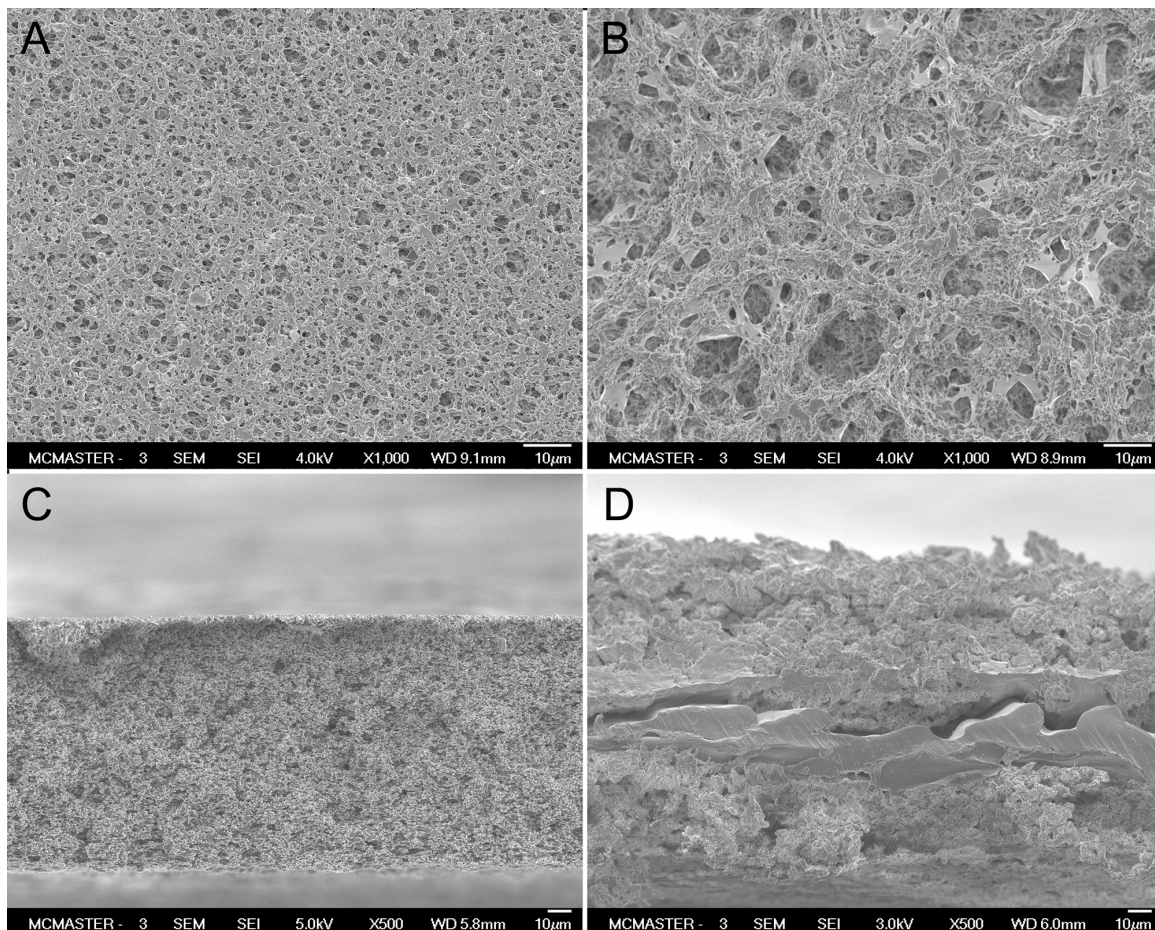


Figure 4.1: FESEM images of the top surfaces (A & B) and cross-sections (C & D) of the Durapore® 0.45 µm-rated membrane (A & C) and Durapore® 5 µm-rated membrane (B & D). The scale bars at the bottom-right of each image are 10 µm in length.

Stock suspensions (100 mg/L) of M/S-MPs or Sph-MPs were prepared in a solution of Tween 20 (VWR Canada; 100 mg/L) in milliQ water (*Millipore milliQ Reference* system; resistivity = 18.2 MΩ·cm). This use of surfactant was recommended by the manufacturer of the microparticles. Suspensions were sonicated in a bath (Branson) for a minimum of 30 minutes to facilitate the dispersion of the MPs. As needed for filtration experiments, stock suspensions were diluted with milliQ water to a final concentration of 10 mg/L, followed by sonication for a minimum of 30 minutes. The transfer of MP suspensions was performed using a clean 10 mL glass pipette to avoid MP particles partitioning onto the plastic pipette tips. Similarly, all suspensions were kept in glass labware. Unused solutions were stored in glass bottles wrapped in aluminum foil at 4°C; additional sonication was needed to redistribute pre-made MP suspensions.

Dry feedstocks of Sph-MPs and M/S-MPs were imaged using an optical microscope to elucidate their size and shape. To do so, double-sided tape was affixed to a glass microscope slide and a fine dispersion of the particles was aspirated onto the tape via a glass Pasteur pipette. Furthermore, samples of permeate water were also imaged to confirm the presence or absence of MPs in later filtration experiments (see §4.2.3). 10 μL aliquots of permeate water were pipetted onto clean glass microscope slides which were then set aside to dry overnight. Microscopy images were obtained using a *Nikon Eclipse LV100* optical microscope equipped with a *pco.panda* black-and-white camera and acquired using Nikon’s NIS Elements-AR software. Samples of MPs in the dry feedstocks were imaged using a 10 \times objective lens (0.65 $\mu\text{m}/\text{pixel}$) while samples of MPs in the (dried) permeate water were imaged using a 40 \times objective lens (0.16 $\mu\text{m}/\text{pixel}$). Brightfield images were first acquired of regions of interest. Then, images of the same regions were obtained through a FITC (fluorescence) filter to highlight the fluorescent particles against the non-fluorescing background. Finally, new images of the same regions were obtained through a rhodamine filter which served to provide a measurement of the background noise and to verify that no other contaminating fluorescent particles were present (*i.e.* a negative control). The acquired images were processed in the Fiji distribution of the ImageJ software program. To clearly visualize the fluorescent MPs, images obtained via the FITC filter with the background subtracted were overlaid as “masks” onto the brightfield images.

4.2.3 Filtration Experiments

MF membranes were first immersed in milliQ water for a minimum of 30 minutes and cut to a diameter of 13 mm using an arch punch. Wetted membrane discs were assembled into 13 mm-diameter filter holders (Cole-Parmer) giving an estimated active membrane area of 75 mm^2 . The filter cell, a pressure transducer (*Omega PX409-030GV*), and an adjoining stainless steel tee fitting were assembled and affixed to a 60 mL syringe (BD) on a syringe pump (*Harvard Apparatus PHD ULTRA*); a diagram of this system setup can be found in Figure 4.2. Prior to assembly, all components in the filtration apparatus were first thoroughly rinsed with ethanol and milliQ water to dislodge any possible remnant MPs from previous filtration experiments.

Prior to the filtration of MPs, milliQ water was permeated through the filtration setup and membrane for a minimum of 10 minutes, whereby permeate samples of approximately 250 μL were

collected in glass vials every two minutes. These samples were subsequently aliquoted into a UV-compatible half-area 96-well microplate (PerkinElmer) and analyzed via a fluorescent plate reader (specified below) to verify that no MPs were present in the permeate before a filtration experiment was performed (*i.e.* as a “rinse test” step). Only then could the actual filtration of fluorescent microparticles proceed. For illustration, the results from several “rinse test” steps at a permeate flux of $1,000 \text{ L/m}^2/\text{h}$ (LMH) are shown in Figure B.3 for both membranes.

Subsequently, the syringe was filled with 10 mg/L suspension of Sph-MPs or M/S-MPs and the apparatus was purged with a small volume ($\sim 3 \text{ mL}$) of this suspension. For experiments with fluxes ranging from $J = 250\text{--}1,000 \text{ LMH}$, a single 60 mL syringe was used. For higher fluxes ranging from $J = 4,000\text{--}8,000 \text{ LMH}$, two syringes injecting in parallel were used in order to provide enough MP suspension for full experiments. The syringes were wrapped in aluminum foil (to reduce photobleaching of the MPs) and permeate samples of $\sim 250 \mu\text{L}$ were again collected in glass vials for the duration of the experiment. Filtration experiments at each individual condition (*e.g.* membrane pore size, flux, etc.) were performed in triplicate to verify the reliability of the data.

Permeate and feed samples were analyzed using a *Tecan Spark 10M* microplate reader. Small-volume aliquots ($150 \mu\text{L}$) of each sample were transferred into microplates, as before. A fluorescence intensity detection protocol was performed using excitation/emission wavelengths of $\lambda_{ex} = 485 \text{ nm}$ / $\lambda_{em} = 485 \text{ nm}$ and corresponding bandwidths of $20 \text{ nm}/25 \text{ nm}$, respectively. A gain of “50” was used, obtained from an optimization experiment to maximize the fluorescence signal (data not shown).

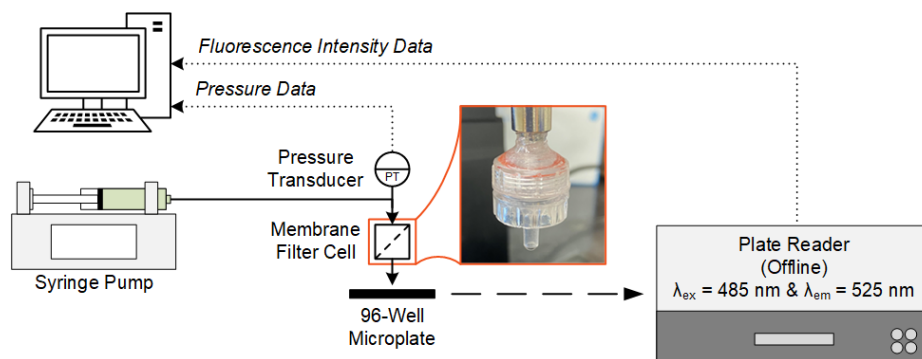


Figure 4.2: Schematic of the constant flux filtration apparatus used in particle transmission experiments in this study. The syringe pump was used to deliver the MP suspensions at constant flux into the filter cell containing the Durapore® PVDF membranes.

4.2.4 Focused Beam Reflectance Measurements

A focused beam reflectance measurement (FBRM) instrument (Mettler-Toledo) was used to measure the chord length distribution of MPs samples. Before each analysis, the FBRM probe was immersed in milliQ water and then under vigorous stirring (via a magnetic stir bar) the chord length distribution was measured every two seconds for five minutes as a control test. Due to the fairly large sample volume requirements of the FBRM instrument (typically 100 mL), the *entire permeate sample* from an hour-long filtration experiment had to be collected and analyzed. Chord length distributions were again recorded every two seconds for another five minutes to quantify the size of the MPs in the bulk sample (range = 1–1,000 μm). The median frequency $f(x)$ at which each chord length of size x was seen was calculated to obtain a (median) frequency distribution of chord lengths over the five-minute data collection periods where the probe was immersed in the sample jar.

4.2.5 Confocal Laser Scanning Microscopy (CLSM)

After a limited number of filtration experiments, the MF membranes were removed from the filtration cell, cut into small square sections (roughly 5×5 mm), and then immersed overnight in solutions of Nile Red (10 mg/L; Sigma-Aldrich) in 95% ethanol (Caledon Laboratories Ltd.). Previous studies have shown that Nile Red can improve the visibility of PVDF in confocal laser scanning microscopy (CLSM) experiments [12, 13]. Dried dyed samples were mounted on glass microscopy slides and sandwiched under glass slide covers prior to imaging using a *Nikon A1R* confocal laser scanning microscope with a $20\times$ objective lens and mounted on a *Nikon Ti2* inverted microscope base. Dual lasers were used to excite the fluorescent Nile Red which stained the membranes and fluorescent M/S-MPs which were embedded in the membrane structures during the filtration experiments. Excitation/emission wavelength pairs of 488/521 nm (FITC filter; 42 nm bandpass) and 561/600 nm (TRITC filter; 45 nm bandpass) were used to differentiate between the M/S-MPs and membrane surfaces, respectively. Images were obtained in resonant mode with a field of view spanning 896×896 μm and a z -step of 0.875 μm . The collected images were analyzed using *NIS-Elements AR* software (Nikon) and the *Fiji* distribution of *ImageJ*.

4.3 Results & Discussions

4.3.1 Characterization of Irregularly-Shaped Microplastic Particles

The milling and sieving process produced irregularly-shaped MPs from the spherical feedstock, as is visible in Figure 4.3. The irregular nature of M/S-MPs are representative of those found in WWTPs, such as those found in studies by Talvitie *et al.* (2017) and Lares *et al.* (2018) [1, 7]. Based on the two-dimensional brightfield image in Figure 4.3A, the average “size” of M/S-MPs particles ($N = 295$) in the dry feedstock was estimated, as was done previously [11] and described in §3.3.1. The size of *each* particle was obtained by measuring the minimum and maximum Feret diameters (*i.e.* “caliper sizes”), where a particle’s “size” is reported as the *mean of the two Feret diameters*. The average size of *all* the particles was then obtained by averaging the aforementioned mean Feret diameters: $10\ \mu\text{m} \pm 7\ \mu\text{m}$ (average \pm one standard deviation). In addition to the average particle size, the *median* particle size was computed as $8.1\ \mu\text{m}$. As before, no attempts were made to exclude particle aggregates from the particle size analysis; however, ImageJ was instructed to exclude any artefacts less than an arbitrary limit of 3×3 pixels ($4\ \mu\text{m}^2$) such that noise introduced during the manual thresholding process would not be considered as “particles”. Consequentially, it is expected that the average size of $10\ \mu\text{m}$ is an overestimation, pursuant to the inherent limitations of the image analysis procedure that was used. From this image analysis, the MPs particles are somewhat polydisperse in size, ranging from $2.6\text{--}48\ \mu\text{m}$, with d_{10} and d_{90} values of the size distribution found to be $3.3\ \mu\text{m}$ and $20.2\ \mu\text{m}$, respectively. To illustrate the irregular shape of the M/S-MPs, the aspect ratio of the measured particles was calculated as 1.78 ± 0.70 , where aspect ratios farther from unity imply more elongated/less regular particles. Furthermore, the difference in maximum/minimum Feret diameters was calculated as $4.8 \pm 4.9\ \mu\text{m}$. Both these observations indicate that while some particles are still roughly circular in shape, a significant portion of the particles are elongated in one axis.

Subsequently, the M/S-MPs were suspended in Tween 20 solutions and used in filtration experiments. The fluorescent nature of the particles—evident in Figure 4.3B—was exploited to indicate the presence and relative concentrations of the suspended MPs. From the assay shown in Figure 4.3C, it is shown that the suspended M/S-MPs are easily detectable using a fluorometric plate reader down to $\sim 0.1\ \text{mg MPs/L}$, where the fluorescent signal is correlated to the mass concentration of MPs suspended in the water. On log-log axes, the relationship between the fluorescent intensity and MP

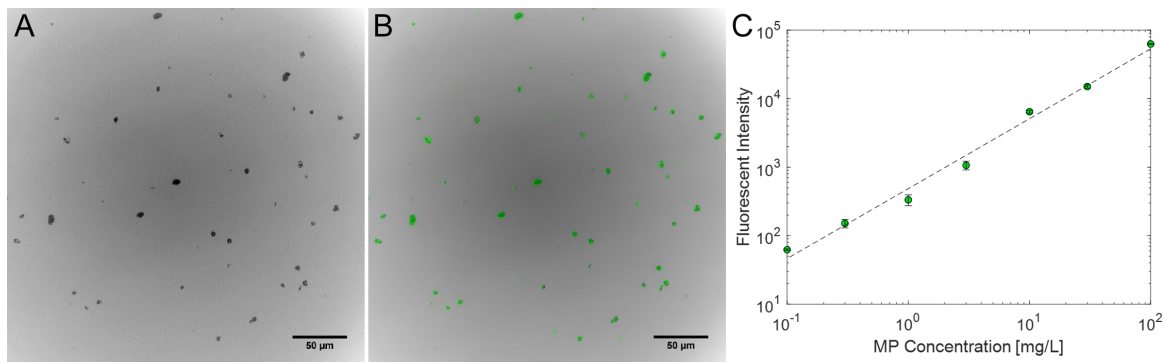


Figure 4.3: Verification of the fluorescent behaviour of the M/S-MPs used in filtration experiments. (A) Brightfield optical microscopy image of the M/S-MPs (B) artificially overlaid with the signal from the FITC fluorescent filter. Fluorescing MPs are shown in green. Microscopy images of the Sph-MPs (before milling) can be found in Figure B.4. (C) Calibration curve of sample fluorescent intensity (a.u.) versus MP mass concentration using the fluorometric plate reader. Error bars refer to one standard deviation about the average of triplicate experiments. The dotted line (- -) represents the power-law line of best fit.

concentration is close to proportional, evidenced by the best-fit model. This indicates that the plate reader is an effective tool at quantifying the presence of these fluorescent MPs in aqueous samples: a particularly useful development as identifying very small MPs (*e.g.* $< 20 \mu\text{m}$) via conventional techniques (*e.g.* visual, FTIR, etc.) is known to be challenging [14, 15].

While it is clear that there is a strong relationship between the mass concentration of suspended MPs and the fluorescent intensity of the suspension, henceforth in this work, I have opted to report the transmission of M/S-MPs in “arbitrary units of fluorescence” as oppose to “absolute concentrations”. In the measurement of fluorescent intensity, incident photons from the plate reader enter the M/S-MP particles, a fraction of which are scattered and/or absorbed. Another fraction reaches the fluorophore molecules which produce a fluorescent emission of photons, a portion of which are scattered and/or absorbed as they leave the particles. A remaining fraction of the emitted photons can then be detected via the plate reader. The deeper the penetration of the photons into/out of a particle, the more the light that is attenuated [16]. This phenomenon has previous been observed in microspheres (agarose; 70–140 μm), for example [17]. As such, it is reasonable to suggest that larger M/S-MPs would produce a somewhat weaker fluorescent signal than smaller M/S-MPs. With this in mind, the correlation between fluorescent intensity and mass concentration (Figure 4.3C) was made for stock suspensions of polydisperse M/S-MPs which were fed to membranes in subsequent filtration experiments (see §4.3.2). In these filtrations, it is reasonably expected that much smaller particles

with a narrower range of sizes would be found in the permeate samples. This creates two distinct populations of particle sizes, where only the “feed” population has a calibration curve accurately relating fluorescent intensity with mass concentration. Overall, it is posited that the fluorescent intensities of the *permeate samples* can only be roughly correlated to mass concentration via the “feed” calibration curves that were produced. Therefore, reporting *fluorescent intensities* better represents the nature of the permeate samples.

4.3.2 Effect of Membrane Pore Size on MP Particle Transmission

Figure 4.4 illustrates the fluorescent intensities of permeate samples (data points) which passed through the 0.45 μm and 5 μm Durapore® membranes over the course of filtration experiments. Different conditions are shown for the hour-long filtration experiments performed at a flux of 1,000 LMH. Firstly, control experiments are shown: unmilled ~ 60 μm Sph-MPs (10 mg/L) in Tween 20 solution (10 mg/L), just Tween 20 solution (10 mg/L), and pure milliQ water were filtered. Finally, the filtration of M/S-MPs (10 mg/L) in Tween 20 solution (10 mg/L) is also shown. For each of the experiments, horizontal lines represent the fluorescent intensities of solutions fed to the membranes. Filtrations of the Sph-MPs and M/S-MPs were performed in triplicate (Tests 1–3). It is clearly visible that these replicates are either coincident or fall reasonably adjacent to each other, which verifies the reproducibility of the data and highlights the robustness of this work.

The filtration performance of the 0.45 μm membrane is considered in the top row of Figure 4.4. When the Sph-MPs are filtered (Panel A), these “control” data points fall within fluorescent intensities of approximately 60–70 a.u. The fluorescent intensities of samples where only water or water plus surfactant are filtered fall in the same range. Note that the feed fluorescent intensities fall between 8,000–11,000 a.u., in contrast. This indicates that there is no evidence of transmission of the Sph-MPs through the membrane. This is critical for experiments to proceed as it suggests that there are no significant leaks of MPs around the membrane or through the O-ring seal. When the M/S-MPs were filtered using this membrane (Panel B), the fluorescent intensities of the permeate samples were representative of the intensities of the “control” samples. The M/S-MPs data points largely fall within the blue “Control Experiments Region”, meaning that the fluorescent intensities of these samples are akin to the fluorescent intensities of the control samples. This is also illustrated

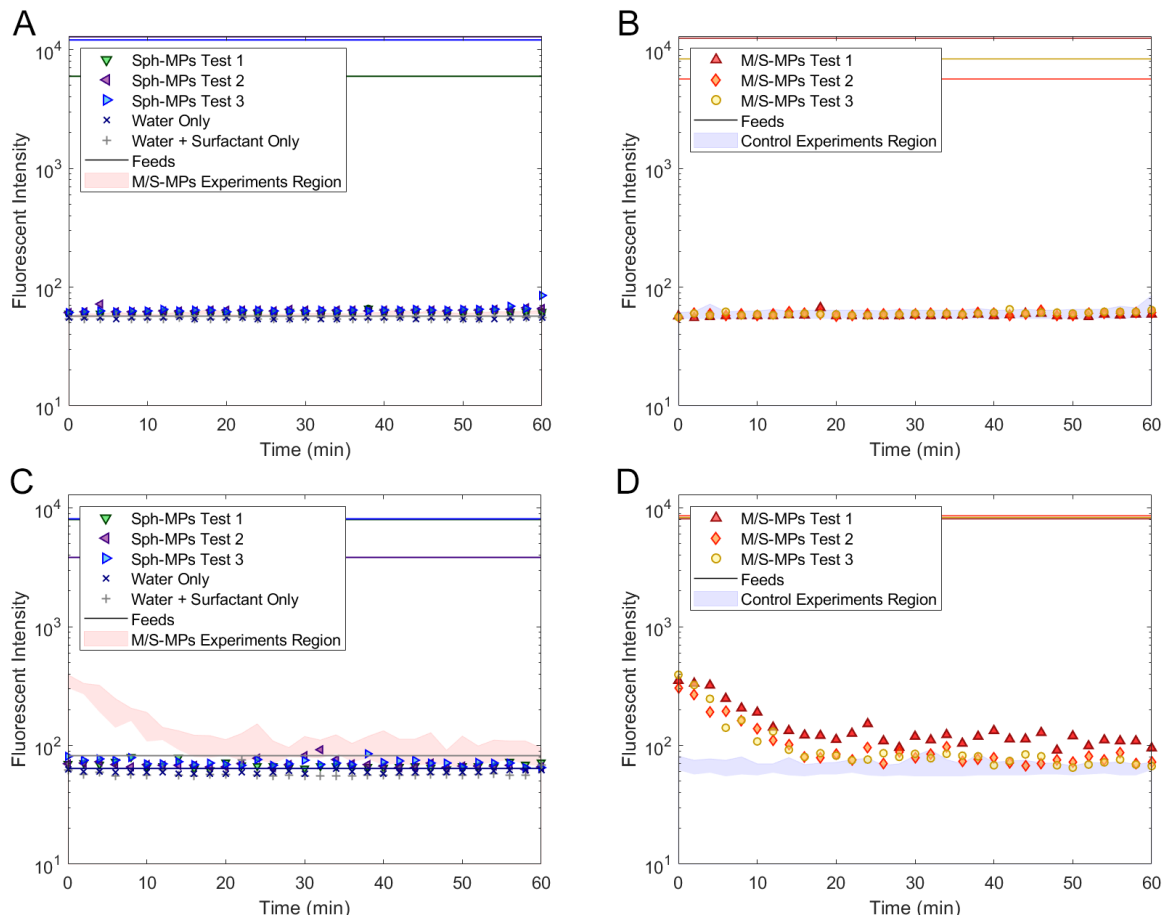


Figure 4.4: Fluorescent intensities (a.u.) of permeate and feed samples filtered through (A & B) $0.45 \mu\text{m}$ and (C & D) $5 \mu\text{m}$ Durapore® membranes at a constant flux of 1,000 LMH ($0.83 \text{ mL}/\text{min}$), with (A & C) control experiments and (B & D) the filtration of M/S-MPs shown. “Feed” lines (—) refer to the average fluorescent intensities of the feed suspensions.

by the red “M/S-MPs Experiments Region” which overlaps the control data points in Panel A. These results imply no evidence of significant transmission of M/S-MPs through the $0.45 \mu\text{m}$ membrane.

The bottom row of Figure 4.4 considers the filtration performance of the $5 \mu\text{m}$ membrane. As before, evidence suggests that the large Sph-MPs did not leak around the $5 \mu\text{m}$ membrane or the O-ring, as indicated by the results in Panel C. Note that all the fluorescent intensities of the control permeate samples, like before, are largely between 60–80 a.u., as compared to the feed intensities which are very near to 10,000 a.u. In stark contrast, there is good evidence of the transmission of M/S-MPs into the permeate of the $5 \mu\text{m}$ membrane. As shown in Panel D, the fluorescence intensities of the permeate samples when M/S-MPs were filtered deviated significantly (*i.e.* higher)

from the blue “Control Experiments Region”. Initially at a time of 0 min, the fluorescent intensities ranged from 300–400 a.u. Over the course of these experiments, the permeate sample fluorescent intensities declined until they became just slightly greater (~ 80 – 100 a.u.) than the fluorescent intensities of the control experiment samples. This can also be seen in Panel C as the red “M/S-MPs Experiments Region” falls significantly above control experiment data points. These observations can be interpreted as greater transmission of M/S-MPs at the start of the experiment with decreased transmission (*i.e.* increased rejection) over the course of the experiment.

Previous studies in the literature have also noted the transmission of micro- or nanoparticles through the pores of membranes which are similar in size to the particles that they attempt to reject. For example, Taylor *et al.* (2021a) describe the filtration of 200 and 300 nm polystyrene (PS) latex spheres using *Sartobran® P Sartoscale 25* MF membranes having a multilayer structure (pore sizes = 0.45 μm and 0.2 μm); they report significant transmission of both sizes of particles, despite the fact that the 300 nm latex spheres are larger than the nominal pore size of the 0.2 μm membrane layer [18]. In a subsequent work, Taylor *et al.* (2021b) noted that the aforementioned *Sartobran® P* membrane exhibited a much higher transmission of 400 nm particles than the *Sartopore® Platinum Sartoscale 25* membrane, though both membranes have the same nominal pore sizes. Even more surprising, the *Sartobran® P* membrane demonstrated even greater transmission than a *Supor® EKV* membrane which has a larger nominal pore size (0.65 μm) [19]. These counter-intuitive results highlight the need for additional research in this area and indicate the importance of evaluating prospective membranes experimentally using suspensions that are representative of those in the end-use application.

For M/S-MPs which were filtered through the 5 μm membrane (Figure 4.4D), recall that a decrease in fluorescent intensity in the permeate samples was seen, corresponding to a decrease in transmission of the M/S-MPs. This phenomenon is attributable to the fouling of the membranes: as the filtration proceeded in dead-end mode, MPs were retained on the feed side of the membrane and accumulated on the membrane’s surface. Over time, the cake deposit of MPs grew thicker and helped to retain MPs which may have previously passed through the membrane if the cake layer was not present. That is, the MP “cake” that formed on the surface of the membrane acted as a dynamic membrane which also helped to reject subsequent MPs. This incidence of membrane fouling

is corroborated in the former study performed by Taylor *et al.* (2021a) who saw an initial increase in transmission of the 200 and 300 nm particles; however over time, there was a sharp decline in transmission of the larger particle size, while the smaller particles reached a plateau in transmission exceeding 80%. A corresponding increase in transmembrane pressure—particularly associated with the filtration of suspensions containing the larger particle size—supported the incidence of fouling in these experiments [18].

As the filtrations were operated in a constant-flux mode, a fouling-induced increase in feed pressure over time was observed in every experiment. An example of this phenomenon is shown in Figure B.5 for filtration experiments using the 5 μm membrane at a flux of 1,000 LMH. The pressure-versus-time data for these three replicates are described by a constant flux fouling model with an assumption of a *compressible cake* [20], as fit by minimizing the sum-of-squares of the errors (SSE) between the data and the model (Equation B.1). A derivation of this model can be found in §B.3. The model’s fit to the data is good for the first two trials in particular, whereas the third trial demonstrated a brief “lag” period (potentially due to excess rinse test water left in the apparatus) which hindered the model fit. For the first two trials shown, the increasing slope of the pressure-versus-time data earlier in the experiments (*i.e.* less than ~ 40 min) reflects the compression of the cake layer formed by the MPs—not in the sense of squeezing the rigid MPs like in soft matter such as solvated polymers, but in the sense of packing/repacking the particles into a denser cake. The fit compressibility indices (n) of the three individual models ranged from 0.222–0.353, indicating a fairly incompressible cake: the specific cake resistance is only a weak function of pressure. Later into the filtration experiments (at higher pressures), the compressible cake filtration model tends to deviate from the data, reflecting maturation of the cake and transition to a different modality of filtration.

4.3.3 Characterization of Microplastics in Permeate Samples

An FBRM instrument was used to report particle chord lengths (*i.e.* as a proxy for size) and counts (*i.e.* as a proxy for concentration) in permeate versus feed samples from filtration experiments, as outlined in §4.2.4. Reporting the size distribution of irregular particles (*e.g.* MPs) is a difficult endeavour as there is “no consistent particle size distribution result from different particle measurement techniques due to the influence of shape” [21]. However, FBRM can be advantageous for analyzing

samples with irregular MPs whereby chord length distributions can be used to approximate particle size distributions. In this manner, FBRM has been widely used in other recent separation studies, such as for measuring particles in flotation processes [22], quantifying particle sizes/distributions in crystallization processes [23], and monitoring the flocculation of wastewater solids [24]; however the use of FBRM in this study represents a novel application of the technique.

Figure 4.5 shows the results of the FBRM analysis of M/S-MP feed and permeate suspensions which corroborate the results from Figure 4.4. Recall that the permeate measurements via FBRM were composite samples: they were obtained from the permeate water collected over the course of an entire one-hour filtration experiment. For the first five minutes of an FBRM measurement (Panels A–D), the probe was immersed in milliQ water. The total counts of chord lengths over the entire 1–1,000 μm range were low. Counts that were recorded can generally be attributed to measurement noise, the occasional dust particle in the water, and tiny air bubbles which were seen as particles. After five minutes, the probe was inserted into the feed or cumulative permeate suspension, and chord lengths of potential M/S-MPs were recorded. It is visible that when either membrane was used, there was a greater incidence of particles recorded (counts > 0) when the FBRM probe was immersed in the permeate solution than when it was only immersed in milliQ water. When the 5 μm membrane was used versus the 0.45 μm membrane, there was a significantly greater concentration of particles found in the permeate (*i.e.* a greater number of counts). However, the 0.45 μm membrane still saw a slight, but perceptible increase in particle concentrations in permeate samples. For this membrane, when the data produced by the plate reader is also considered, a slight increase in sample fluorescent intensities is also seen, with values ranging from 58–61 a.u. in the three experiments where M/S-MPs were filtered versus 55 a.u. for when milliQ water/milliQ water and surfactant were filtered. However, in two out of three of the filtration experiments, $p \geq 0.05$ when comparing the permeate samples to the “control” water/surfactant samples. Therefore practically speaking, there is no *significant* evidence of the transmission of the M/S-MPs through the 0.45 μm membrane when the plate reader data is considered.

Panels E and F from Figure 4.5 summarize the data found in the other four panels: the median counts of particles with chord lengths binned between 1–1,000 μm during the experiments for both feed and permeate samples. The median numbers of particles in the feeds to both membranes are

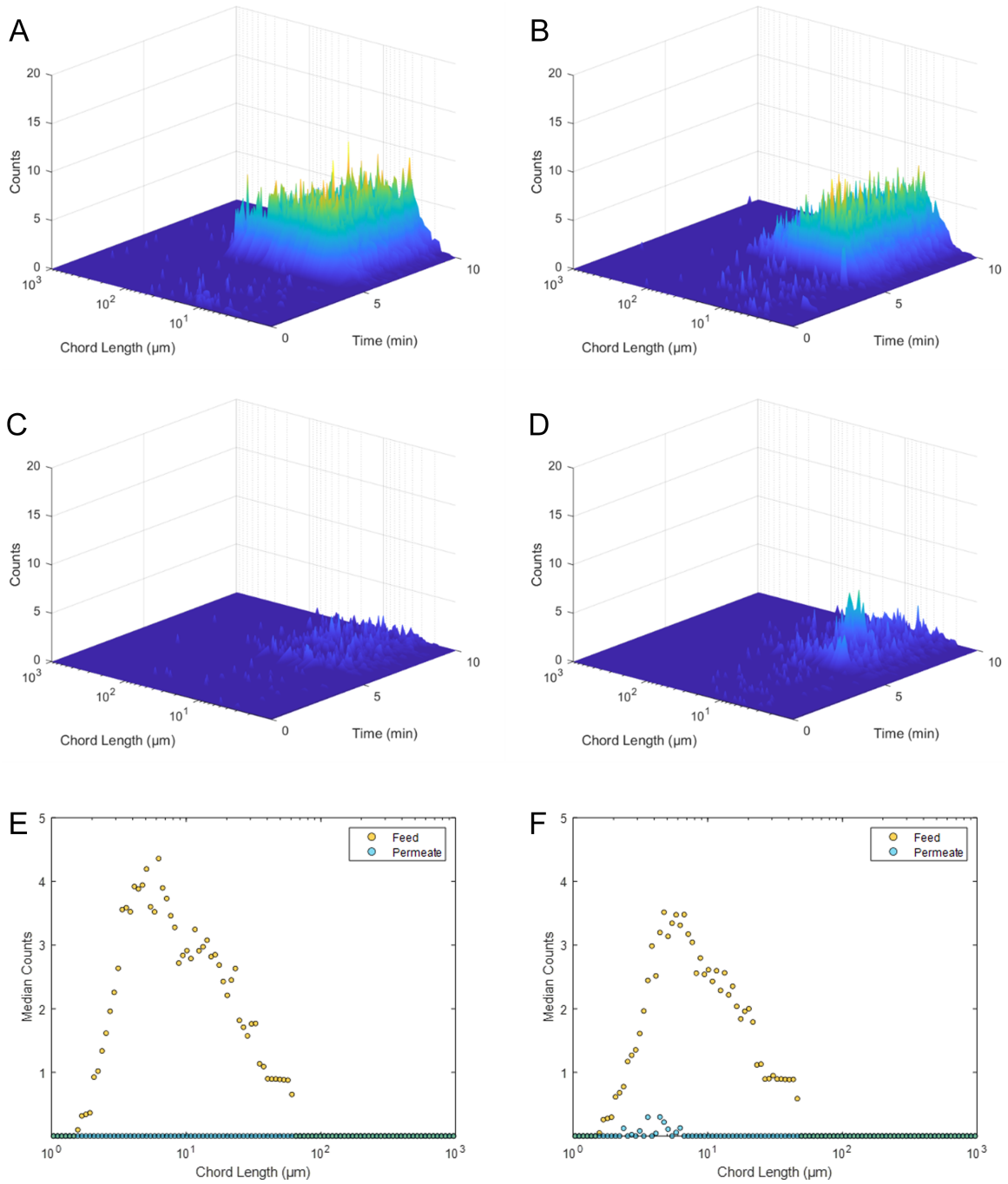


Figure 4.5: FBRM analysis of permeate and feed samples from filtration experiments with the (A, C, E) 0.45 μm and (B, D, F) 5 μm Durapore® membranes. (A, B) Feed samples. (C, D) Permeate samples collected over one-hour experiments. (E, F) Median counts of particle chord lengths in the analysis of feed (●) and permeate (●) samples.

shown; the chord length distributions span from approximately 1–60 μm , with the mode of the distributions at 6 μm and 5 μm , respectively, for the experiments with the 0.45 μm and 5 μm membranes. Both feed distributions are roughly log-normal in nature with positive skew. The median number of particles in the permeate of the 0.45 μm membrane was zero for all chord lengths, which infers that particles of non-zero chord length were detected rarely (*i.e.* < 50% of events). However, the median number of particles in the permeate of the 5 μm membrane was non-zero for small chord lengths ($\sim 2\text{--}7$ μm) which indicates that there are significant numbers of M/S-MPs in the membrane permeate. However, the total counts of these permeated M/S-MPs were much lower than the feed counts of the same bin sizes, which infers that the majority of the M/S-MPs were still rejected by the 5 μm membrane, even though there was still transmission. This skewing towards smaller particle sizes in the cumulative permeate samples can also be seen in Panels A–D.

Restating what is written in Equation 2.5b, the observed rejection coefficient (R_0) of a given analyte can be computed as follows, where C_p and C_f are the analyte concentrations in the permeate and feed streams, respectively. Here, we will assume the concentrations to be on a number basis as oppose to mass or molar bases.

$$R_0 = \left[1 - \frac{C_p}{C_f} \right] \times 100\% \quad (4.1)$$

As an approximate measure of the rejection of the M/S-MPs by the membranes, the FBRM “median counts” versus “chord length” plots can be used. Given that the stirring speed (and all other geometric factors) was the same when both the feed and permeate samples were measured, the numbers of counts seen by the FBRM probe can be assumed to be roughly proportional to the concentrations of particles in the samples. Therefore, we can rewrite Equation 4.1 as the following:

$$R_0 = \left[1 - \frac{\sum_{x=1}^{100} \tilde{n}_p(x)}{\sum_{x=1}^{100} \tilde{n}_f(x)} \right] \times 100\% \quad (4.2)$$

where $\tilde{n}_p(x)$ and $\tilde{n}_f(x)$ are the median number of MP counts recorded in the x th chord length “bins” ($x = 1, 2, 3, \dots, 100$) for the permeate and feed samples, respectively.

From Panels E and F in Figure 4.5, the approximate MP rejections over the one hour-experiment are estimated to be $\sim 100\%$ for the 0.45 μm membrane and $\sim 99\%$ for the 5 μm membrane. A substantial fraction of particles in this study were smaller than the nominal pore size of the 5 μm

Durapore® membrane, however, transmission of this “smaller” fraction remained relatively low (see Figure 4.5F). This finding is in contrast with what was observed by Taylor *et al.* (2021a) who noted > 80% transmission of particles smaller than the membrane pore size [18]. Differences in the membrane structure, fluxes used, particle concentrations, and particle morphologies may have contributed to increased particle rejection in these experiments. One possibility that cannot be disregarded is that the highly irregular shape of the M/S-MPs contributed to their increased rejection which may be driven by hindrances in traversing the porous matrix of the membrane. Therefore, it is posited that there is substantial value in using irregularly-shaped particles in MP filtration experiments.

To corroborate the fluorescence intensity data which was collected, permeate samples were observed using optical microscopy to verify the presence of M/S-MPs. Fluorescent MPs were detected against the non-fluorescing background via the FITC filter on the microscope. In all permeate samples from the 0.45 μm membrane that were analyzed, no fluorescent MPs were seen. In contrast, in the permeate samples from the 5 μm membrane, several M/S-MPs per sample were seen under the fluorescent filter. A composite of microscopy image of dried permeate samples from a filtration experiment with the 5 μm membrane (flux = 1,000 LMH) is shown, for reference, in Figure B.6. This corroborates what was seen in the fluorescent intensity plots: partial transmission of the M/S-MPs when this membrane was used.

Subsequently, ImageJ was employed to estimate the size of the particles seen under the microscope (*i.e.* in Figure B.6). For the feed sample shown, the four particles seen ranged from 2.0 μm to 12.4 μm in their largest dimension. In contrast, the permeate samples yielded particles of approximately 2 μm in their largest dimension. However, a different permeate sample from a separate experiment (shown in Figure B.7) yielded particles which ranged in size from 1.8 μm up to 4.8 μm . Two points are evident: the 5 μm membrane was generally effective at removing the largest particle sizes thus leaving only the smaller particle fractions, and particles with at least one dimension nearing the stated pore size of the membrane (*e.g.* 4.8 μm) could be transmitted under the conditions that were tested. These findings are corroborated by the FBRM results from Panel F of Figure 4.5: particles with chord lengths from approximately 2–7 μm were detected in the 5 μm membrane permeate samples. Further, 50% of particles (by count) from the *feed distribution* had chord lengths that were ~ 7.4 μm or smaller (*i.e.* the d_{50} value) when interpolating within cumulative chord length

frequency data. However, the corresponding d_{50} value for the *permeate distribution* was reduced to $\sim 4.2 \mu\text{m}$. While the particle concentration was reduced substantially (*i.e.* 99%) in the permeate, there was still a significant fraction of particles seen that had measured chord lengths which were similar to the stated membrane pore size. See Figures B.8–B.9 for the cumulative chord length frequency distributions of particles in the feed and permeate FBRM samples from both membranes and for multiple replicates.

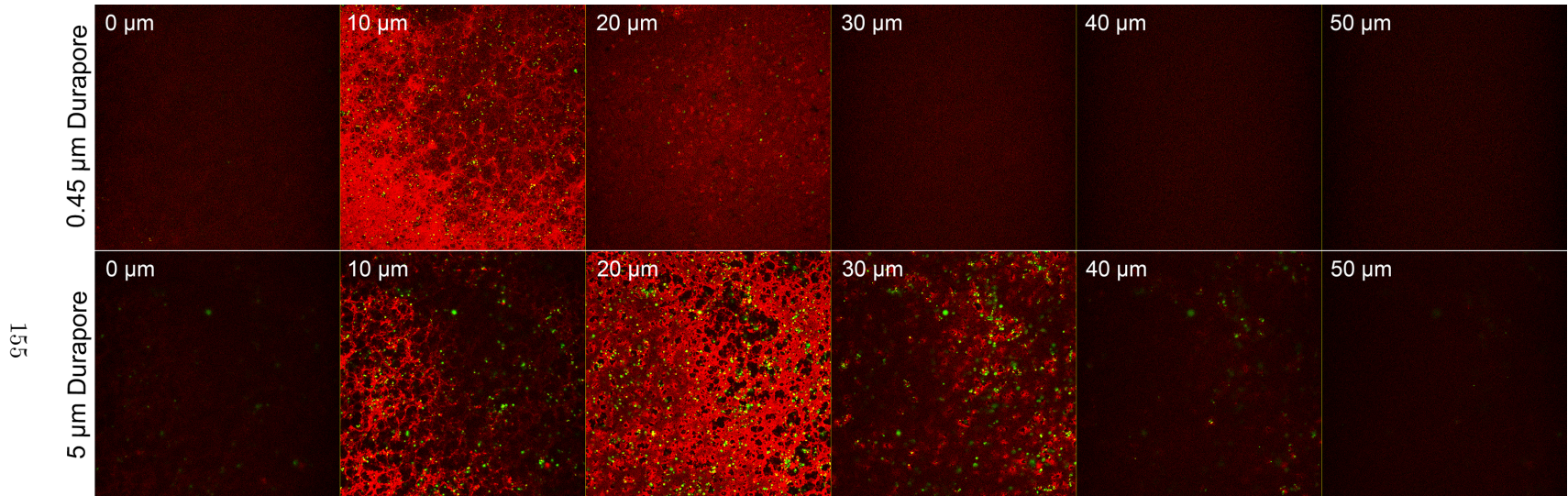
Consequentially, the importance of choosing an appropriate membrane pore size is crucial when designing and implementing membrane technologies for the removal of MPs from WWTP effluents. As seen with the $5 \mu\text{m}$ membrane, MPs with dimensions near to the stated pore size of the membrane were shown to be transmissible. In contrast, there is little indication of MPs in the permeate water filtered through the $0.45 \mu\text{m}$ membrane. The smallest bin size ($\sim 1.5 \mu\text{m}$) of particle found in the feed to this membrane was not conclusively seen in the permeate of the membrane. As such, the $0.45 \mu\text{m}$ membrane proved to be effective at removing particles which are roughly three times larger than the stated pore size. Therefore, a stated membrane pore size that is significantly less than the size of the smallest MP is needed in order to obtain full rejection of the particles.

The membranes used in this study were chosen to be reasonable for laboratory-based filtration experiments based on the sizes of irregular MPs that were easily producible. It is currently difficult to source irregular MPs—representative of those in WWTPs—around the order of the pore sizes of MF membranes. While PVDF membranes with a pore size of $0.45 \mu\text{m}$ might be a reasonable selection for the 3° filtration of wastewater, it is unlikely that a $5 \mu\text{m}$ membrane would be effective for wastewater polishing. However, findings from the experiments with this larger pore size membrane are valuable to the field, namely the observation that irregular particles up to the nominal pore size of the membrane can be readily transmitted. The obvious solution to removing MPs is by using membranes with yet smaller pore sizes: UF versus MF, and so on. Smaller pore sizes are more effective for removing both plastic particles as well as organic matter from wastewater effluents. However, the inherent tradeoff that facilities must bear is that membranes with smaller pore sizes have lower permeabilities and require higher pressures to permeate water. Higher capital costs due to greater membrane areas required and higher operational pumping costs may be incurred with the choice of smaller pore size membranes.

4.3.4 Spatial Analysis of Captured Microplastics via CLSM

Figures 4.4 and 4.5 demonstrated that the majority of the M/S-MPs were rejected by both the 5 μm and 0.45 μm Durapore® membranes, despite the fact that the 5 μm membrane did permit the transmission of significant quantities of particles. This transmission was limited over the course of the filtration experiments by the fouling of the membrane. As such, a visualization of the spatial distribution of captured M/S-MPs was sought to ascertain where in the membrane (on the surface, in the pore entrances, deep within the pores, etc.) the particles were captured. To this end, CLSM—a tool which has shown growing use in the membrane field for characterizing membrane filtration processes—was employed. Its utility exists as it combines the spatial resolution of optical microscopy, the feature identification/detectability of fluorescence microscopy, and the ability to spatially-resolve features along the depth of materials. Recent work in the contemporary literature has seen CLSM used in a variety of ways, such as for visualizing the fouling of nylon and PVDF membranes during the filtration of oil (dodecane) emulsions [25], understanding the adsorption of fluorescently-labelled PS nanoparticles onto polyethersulfone membranes in a sterile filtration process [26], studying the effects of pressure on the penetration and capture of viruses (ϕ X174 bacteriophage) using Ultipor® and Viresolve® membranes [27], and visualizing/quantifying protein fouling (bovine serum albumin, lysozyme, formate dehydrogenase) on Sartobind® ion exchange membranes [28].

Pursuant to the method described in §4.2.5, Figure 4.6 shows a series of CLSM images of the 0.45 μm and 5 μm Durapore® membranes after they were used in filtration experiments at fluxes of 1,000 LMH. Top-down profiles of the membranes (“slices”) were collected from just above the plane of the specimen’s top surface, down to below the full depth of the membranes (0.45 μm : $\sim 110 \mu\text{m}$ and 5 μm : $\sim 150 \mu\text{m}$) at a z -step of 0.875 μm . The images in the figure were extracted from the z -stacks at intervals of $\sim 10 \mu\text{m}$ in order to build the montage. It is evident that the distribution of the M/S-MPs (green regions) at various depths within the first $\sim 50 \mu\text{m}$ is different between the two membranes (red regions). However, it should be noted that comparisons between the surface density (*i.e.* quantity) of deposited MPs on the membranes cannot be made from the montages. As the membranes were removed from their filter cells, excess water on the surfaces of the membranes tended to drain away, carrying MPs from the surface. Although the possible effect was not quantified, the immersion of the membranes in the Nile Red solution may have liberated deposited MPs.



155

Figure 4.6: Top-down CLSM image montages of the 0.45 μm (top row) and 5 μm (bottom row) Durapore® membranes which were used in filtration experiments at a flux of 1,000 LMH. Red areas (TRITC filter) are indicative of the membrane surface and green areas (FITC filter) represent fluorescent M/S-MPs. Each image in the montage measures $896 \times 896 \mu\text{m}$. For both membranes, the first image (0 μm) represents the depth in the z -stack where the surface of the specimen just comes into focus. The depth markers represent the approximate z -distance down into the membrane's structure, as measured from the datum set at the $z = 0 \mu\text{m}$ image. Orthogonal views and 3D representations of the z -stacks are found in Figures B.10–B.11.

The result is that the quantities of M/S-MPs deposited at the end of the filtration experiments is not likely to be representative of the quantities of M/S-MPs seen during CLSM imaging.

For the 0.45 μm membrane, some MPs are visible in the 10 μm slice while few are visible in the 20 μm slice. No MPs are visible deeper into the membrane structure. This affirms that the MPs were captured on the surface of the membrane and intrusion into the pore structure would only be expected in cases of defects. In contrast, the MPs are visible in additional image slices with the 5 μm membrane. Many MPs are visible in the 10, 20 and 30 μm slices; there are still MPs visible in the 40 μm slice, as well. Deeper into this membrane, MPs are not clearly identified. Overall, this infers that M/S-MPs are found farther below the upper surface of the 5 μm membrane. However, it is unclear whether this is due to the significant roughness of the membrane surface, or the capture of MPs deeper into its structure. Furthermore, the bright fluorescent signal from the M/S-MPs tended to scatter and bleed across focal planes which makes it difficult to precisely localize the particles. See Figure B.10 for orthogonal views of the 20 μm -deep slice of the 5 μm membrane for a demonstration of these observances. While it is clear that the MPs are found at greater depths beyond the upper surface of the membrane, it is unclear whether this is due to significant membrane roughness/large pore entrances, or due to penetration into the membrane structure, or a combination of factors. Further work is needed to explicate this observation.

It is evident from the CLSM montages in Figure 4.6 that the brightness of the fluorophores significantly decreases beneath the surface of the membranes, even despite the usage of Nikon's in-built laser compensation feature. This effect is attributable to scattering of the laser by the polymer, with greater scattering occurring as the focal plane is dropped deeper into the membrane. Furthermore, it is hypothesized that there is a commensurate decrease in the brightness of the TRITC signal from the Nile Red dye deeper into the z -stack due to evaporation kinetics during the drying of the Nile Red solution. A "coffee ring"-like effect [29] was observed (see Figures B.10–B.11): higher concentrations of the dye were seen at the edge of the membrane sample due to convective transport of ethanol solution from its center towards its periphery to the dilute higher concentrations of Nile Red left at the edge as the ethanol quickly evaporated. It is suspected that this convection drew the Nile Red dye towards the membrane surface, causing the very bright interface and darker interior of the membrane when imaged using CLSM. A prospective method to overcome this phenomenon

could involve briefly rinsing or immersing dyed membrane samples in pure water to wash away remaining ethanol, thus mitigating significant outward transport of dye originating from the rapid ethanol evaporation kinetics. Overall, it is clear that CLSM is a powerful tool for analyzing the deposition of fluorescent MPs in the structure of membranes, but further efforts are needed to clarify the localization of the MPs within the structure of membranes such as ones evaluated in this work.

4.3.5 Flux-Dependent Transmission of Microplastics

Figure 4.7 demonstrates the effect of permeate flux on the transmission of the M/S-MPs for the 5 μm membrane. Four different fluxes were used from 250–8,000 LMH (a 32-fold range). The fluorescent intensities are plotted as *relative fluorescent intensities*: the permeate intensity divided by the feed intensity. As oppose to Figure 4.4, samples were taken after a particular *volume* of permeate water was collected for a total of 46.67 mL; this is similar to the volumes obtained (49.8 mL) during the experiments at a flux of 1,000 LMH (Figure 4.4). As such, note that Figure 4.7 is volume-dependent as oppose to time-dependent. This is important as in real filtration processes, the goal is often to treat a certain prescribed volume of water (independent of flux). When different fluxes are compared, the independent variable of volume permeated may be more relevant than the variable of time.

From Figure 4.7, it can be seen that higher fluxes resulted in a greater fluorescent intensities of the permeate samples at a given volume of water permeated. Note that the higher fluxes are commensurate with higher transmembrane pressures as the filtrations were performed in constant flux mode. Because fluorescent intensity is positively correlated to particle concentration, it proceeds that higher fluxes created increased transmission of MPs and caused higher concentrations of the MPs to be found in the permeate stream. However, in the initial permeate samples which were taken (“0 mL” permeated), the fluorescent intensities measured at the 8,000 LMH flux were not 32 times greater than in the samples obtained at the 250 LMH flux: the intensities roughly *doubled*, instead. The differences in fluorescent intensities are more pronounced early in the experiment (low volumes permeated), and become less pronounced at higher cumulative volumes permeated. For example, before 20 mL of water was permeated, there are statistical differences ($\alpha = 0.05$) in the fluorescent intensities of samples permeated at the 8,000 LMH flux versus the 250 LMH flux. At the 20 mL measurement and beyond, there are no statistical differences (*i.e.* $p > 0.12$) between the average

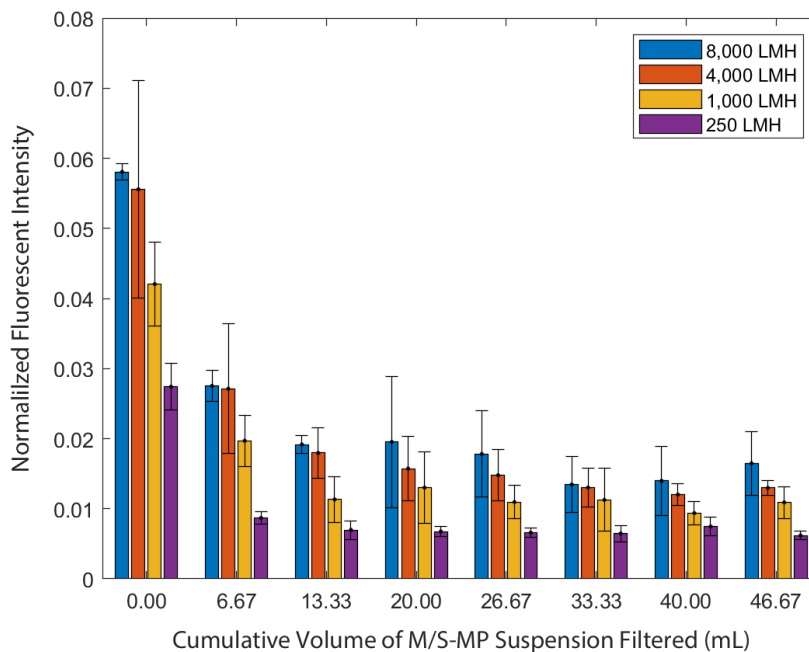


Figure 4.7: The effect of flux on the fluorescent intensity of permeate samples, measured over the course of filtration experiments using the $5\ \mu\text{m}$ membrane. Bars represent the normalized fluorescent intensity for permeate samples relative to the feeds, averaged over triplicate experiments. Error bars represent one standard deviation about the average.

fluorescent intensities at the 8,000 LMH and 250 LMH fluxes.

Increased transmission of suspended matter at higher fluxes/pressures has been shown in the literature. It has been documented in the filtration of various systems including macromolecules (*e.g.* proteins) [30], viruses [31], as well as nanoparticles [18, 32, 33]. As such, the increased transmission of the M/S-MPs at the higher fluxes could be attributable to a couple of factors. In a study on the rejection of viruses (akin to nanoparticles) via UF membranes, Arkhangelsky & Gitis (2008) note that virus transmission through the membrane increased with higher transmembrane pressures. They concluded that it is likely a result of pore deformation, evidenced by incidences of increased pore diameters at the higher transmembrane pressures [31]. Furthermore, Chen *et al.* (1997) observed that the rejection of colloidal silica by a $0.22\ \mu\text{m}$ PVDF MF membrane decreased at higher permeate fluxes. They rationalized that it was not the pore structure that was changing at higher fluxes, but instead, the polarized layer of aggregated colloids that formed on the membrane surface during filtration. They write that “the aggregated colloids would form an open secondary

membrane and lead to an unstirred boundary layer [that] achieved high concentrations which would leak into the permeate through larger pores” [33]. The investigation by Taylor *et al.* (2021a) found that the yield of latex spheres (200 and 300 nm) which passed through a MF membrane increased as the filtrate flux was increased for fluxes below 200 LMH, but reached a plateau in yield beyond that point. The authors attributed this phenomenon to enhanced particle capture, citing the adsorptive interactions between the particles and the membrane [18]. It is also feasible that the greater pressures (*i.e.* force per unit area) associated with the higher fluxes enabled the reorientation of irregularly-shaped particles and forced them through pore openings. Regardless of the mechanism, it can be seen that—at least initially—higher fluxes result in a greater concentration of M/S-MPs transmitted through the 5 μm membrane. While these higher fluxes are beneficial in that a greater volume of water can be processed in a smaller period of time or with a smaller membrane area, a balance must be achieved in order to offset higher/lower membrane productivity with lower/higher rejection of MP particles.

It is also noted that in Figure 4.7, the intensities of the permeate samples fell as the filtrations proceeded, akin to the data shown in Figure 4.4. This is irrespective of permeate flux. Again, this is a consequence of the fouling of the membranes due to the dead-end filtration of the MPs. Accumulation of the MPs on the membrane caused cake layer formation which restricted the transmission of the MPs through the membrane’s pores. With reference to the accumulation of the M/S-MPs on the membrane surface, it is estimated that rates of accumulation ranged from 2.1–66 $\mu\text{g}/\text{min}$ for the 250 LMH and 8,000 LMH fluxes, respectively. This produced final surface coverages ranging from $(0.29\text{--}9.33) \times 10^6$ μg MPs/ m^2 for the 250–8,000 LMH fluxes, corresponding to total accumulated masses of approximately 15–467 μg M/S-MPs, respectively. While this fouling of the membrane via the MPs is advantageous in the sense that it prevents MP transmission, it does increase the pressure requirements to permeate the water (greater energy usage). To reduce pressure demands, more frequent backwashing may be required to reverse fouling due to the faster accumulation of foulants at higher fluxes; else, a greater membrane area will be needed to achieve filtration targets (greater capital cost outlay). It should also be noted that membrane processes for wastewater treatment are usually not operated in dead-end filtration mode with flat-sheet membranes, as was done here. For the MF of wastewater, crossflow filtration with hollow fiber membranes can be expected, with periodic cleaning steps (*e.g.* backwashing, chemical flushes, etc.) used to prevent the

build-up of organic material and coincidentally, MPs as well. If the back-transport of foulants and the cleaning processes are effective at removing the MPs, the magnitude of the pore blockage and reduction in MP transmission may not be as great as what is seen in the results shown in this study. However, the presence of various colloidal and dissolved solids which are typically found in wastewater are expected to influence the transmission behaviour of the MPs and the dynamics of the cleaning processes needed to remove the foulants (as seen in Chapter 3). More investigations are needed in order to understand the filtration of MPs in realistic water matrices such as wastewater.

4.4 Concluding Remarks

In this study, the rejection properties of two PVDF flat-sheet MF membranes (0.45 μm and 5 μm Durapore®) were quantified with respect to irregularly-shaped MP particles in constant-flux filtration experiments. These particles, with an average size of $\sim 10 \mu\text{m}$, were produced via ball-milling and sieving from a feedstock of fluorescent microspheres (53–63 μm in diameter). The MPs were easily detectable using a standard plate reader, allowing for the quantification of the MPs in feed and permeate samples from the membranes. Filtration experiments conducted at a flux of 1,000 LMH showed no demonstrable transmission of the MPs through the 0.45 μm membrane, but significant transmission through the 5 μm membrane. With this latter membrane, the greatest amount of particle transmission was observed at the initial stages of the filtrations and declined over the processes. This phenomenon was attributed to dynamic fouling of the membranes by the MPs. The implication of this finding is that allowing the formation of a cake layer under these conditions can improve the rejection of MPs. FBRM measurements of feed and cumulative permeate samples corroborated that the 0.45 μm membrane rejected almost all of the MPs, but significant quantities of MPs were transmitted via the 5 μm membrane. These transmitted particles were found to be up to the stated membrane pore size, as measured via optical microscopy. Thus, the judicious choice of membrane pore size is important in ensuring that MPs are rejected, especially when considering the removal of very small particles. CLSM of both membranes showed localization of M/S-MPs on the surface of the 0.45 μm membrane. However, MPs were deposited significantly further past the active surface of the 5 μm membrane, though more research is needed to understand if this deposition is a result of the roughness of the membrane or greater penetration into the membrane structure. When the permeate flux was varied from 250 LMH to 8,000 LMH for filtration experiments using the 5 μm

membrane, higher fluxes resulted in greater MP transmission at the initial stages of the filtration experiments. The implication of this finding is that lower fluxes are more amenable to removing MPs from feed water, even though that the permeate throughput is lower.

While the standard fluorometric plate reader proved to be useful for very efficiently quantifying the presence of fluorescent MPs in aqueous samples, this study was limited in that rejection experiments were performed in pure water which is not representative of the solution conditions in actual WWTPs. Interactions between MPs and other suspended/dissolved solids are expected to affect the filtration performance and modify the fluorescent signal produced by the M/S-MPs. Furthermore, the technique is limited in that it is a “bulk” measurement of fluorescence in a sample: it is not quantifying the *number* of MPs that are present—as is typical in the field—but instead, the quantity of fluorophore that is present. To be discussed in §5.4 in the next chapter, this could refer to a small number of large particles, or a large number of small particles. As previously mentioned in §1.1.2, small particles may prove to have more hazardous consequences from the perspectives of ingestion and contaminant adsorption, so a technique which can quantify individual particles versus perform bulk measurements is inherently valuable. For these reasons, the next chapter moves towards a different technique—flow cytometry—which shows promise at efficiently identifying individual fluorescent MPs in water samples and other more complex matrices.

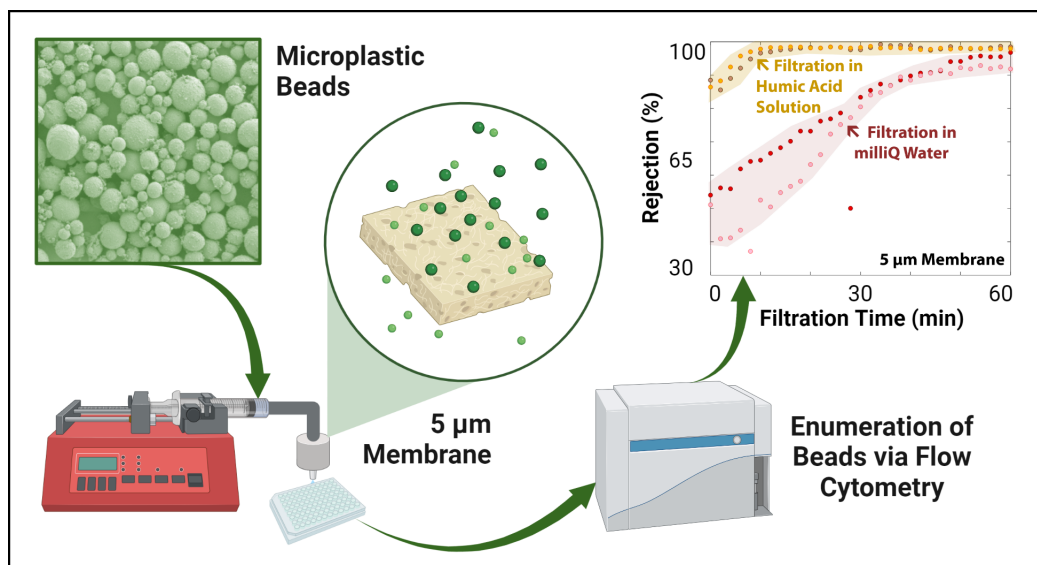
4.5 Works Cited

- [1] M. Lares, M. C. Ncibi, M. Sillanpää, and M. Sillanpää, “Occurrence, identification and removal of microplastic particles and fibers in conventional activated sludge process and advanced MBR technology,” *Water Research*, vol. 133, pp. 236–246, 2018.
- [2] A. Foglia, G. Cipolletta, N. Frison, S. Sabbatini, S. Gorbi, A. L. Eusebi, and F. Fatone, “Anaerobic membrane bioreactor for urban wastewater valorisation: Operative strategies and fertigation reuse,” *Chemical Engineering Transactions*, vol. 74, pp. 247–252, 2019.
- [3] S. Olmos, J. López-Castellanos, and J. Bayo, “Are advanced wastewater treatment technologies a solution for total removal of microplastics in wastewater effluents?” *WIT Transactions on Ecology and the Environment*, vol. 229, pp. 109–116, 2019.
- [4] M. R. Michielssen, E. R. Michielssen, J. Ni, and M. B. Duhaime, “Fate of microplastics and other small anthropogenic litter (SAL) in wastewater treatment plants depends on unit processes employed,” *Environmental Science: Water Research & Technology*, vol. 2, no. 6, pp. 1064–1073, 2016.

- [5] X. Lv, Q. Dong, Z. Zuo, Y. Liu, X. Huang, and W. M. Wu, “Microplastics in a municipal wastewater treatment plant: Fate, dynamic distribution, removal efficiencies, and control strategies,” *Journal of Cleaner Production*, vol. 225, pp. 579–586, 2019.
- [6] L. Li, D. Liu, K. Song, and Y. Zhou, “Performance evaluation of MBR in treating microplastics polyvinylchloride contaminated polluted surface water,” *Marine Pollution Bulletin*, vol. 150, p. 110724, 2020.
- [7] J. Talvitie, A. Mikola, A. Koistinen, and O. Setälä, “Solutions to microplastic pollution—Removal of microplastics from wastewater effluent with advanced wastewater treatment technologies,” *Water Research*, vol. 123, pp. 401–407, 2017.
- [8] J. Bayo, J. López-Castellanos, and S. Olmos, “Membrane bioreactor and rapid sand filtration for the removal of microplastics in an urban wastewater treatment plant,” *Marine Pollution Bulletin*, vol. 156, p. 111211, 2020.
- [9] S. Ziajahromi, P. A. Neale, L. Rintoul, and F. D. L. Leusch, “Wastewater treatment plants as a pathway for microplastics: development of a new approach to sample wastewater-based microplastics,” *Water Research*, vol. 112, pp. 93–99, 2017.
- [10] H. A. Leslie, S. H. Brandsma, M. J. M. Van Velzen, and A. Vethaak, “Microplastics en route: Field measurements in the Dutch river delta and Amsterdam canals, wastewater treatment plants, North Sea sediments and biota,” *Environment International*, vol. 101, pp. 133–142, 2017.
- [11] R. J. LaRue, B. Patterson, S. O’Brien, and D. R. Latulippe, “Evaluation of Membrane Fouling by Microplastic Particles in Tertiary Wastewater Treatment Processes,” *ACS ES&T Water*, vol. 2, 2022.
- [12] C. M. Hess, E. A. Riley, J. Palos-Chávez, and P. J. Reid, “Measuring the Spatial Distribution of Dielectric Constants in Polymers through Quasi-Single Molecule Microscopy,” *Journal of Physical Chemistry B*, vol. 117, pp. 7106–7112, 2013.
- [13] C. M. Hess, E. A. Riley, and P. J. Reid, “Dielectric Dependence of Single-Molecule Photoluminescence Intermittency: Nile Red in Poly(vinylidene fluoride),” *Journal of Physical Chemistry B*, vol. 118, pp. 8905–8913, 2014.
- [14] P. U. Iyare, S. K. Ouki, and T. Bond, “Microplastics removal in wastewater treatment plants: a critical review,” *Environmental Science: Water Research & Technology*, vol. 6, pp. 2664–2675, 2020.
- [15] J. Sun, X. Dai, Q. Wang, M. C. van Loosdrecht, and B. J. Ni, “Microplastics in wastewater treatment plants: detection, occurrence and removal,” *Water Research*, vol. 152, pp. 21–37, 2019.
- [16] G. J. Steyer, D. Roy, O. Salvado, M. E. Stone, and D. L. Wilson, “Removal of out-of-plane fluorescence for single cell visualization and quantification in cryo-imaging,” *Annals of Biomedical Engineering*, vol. 37, pp. 1613–1628, 2009.
- [17] A. Liljeborg, “Simulation of light attenuation within fluorescent microspheres used for liquid fraction separation recorded by a CSLM,” in *Three-Dimensional Microscopy: Image Acquisition and Processing III*, C. J. Cogswell, G. S. Kino, and T. Wilson, Eds., vol. 2655. International Society for Optics and Photonics, 1996, pp. 11–17.
- [18] N. Taylor, W. Ma, A. Kristopeit, S. C. Wang, and A. L. Zydney, “Evaluation of a sterile filtration process for viral vaccines using a model nanoparticle suspension,” *Biotechnology and Bioengineering*, vol. 118, pp. 106–115, 2021.

- [19] N. Taylor, W. J. Ma, A. Kristopeit, S. C. Wang, and A. L. Zydney, “Retention characteristics of sterile filters—Effect of pore size and structure,” *Journal of Membrane Science*, vol. 635, p. 119436, 2021.
- [20] D. C. Sioutopoulos and A. J. Karabelas, “Correlation of organic fouling resistances in RO and UF membrane filtration under constant flux and constant pressure,” *Journal of Membrane Science*, vol. 407–408, pp. 34–46, 2012.
- [21] M. Li, D. Wilkinson, and K. Patchigolla, “Comparison of Particle Size Distributions Measured Using Different Techniques,” *Particulate Science and Technology*, vol. 23, pp. 265–284, 2007.
- [22] X. Wang, S. Zhou, X. Bu, C. Ni, G. Xie, and Y. Peng, “Investigation on interaction behavior between coarse and fine particles in the coal flotation using focused beam reflectance measurement (FBRM) and particle video microscope (PVM),” *Separation Science and Technology*, vol. 56, pp. 1418–1430, 2020.
- [23] X. Li, D. Xu, J. Yang, Z. Yan, T. Luo, X. Li, Z. Zhang, and X. Wang, “Utilization of FBRM and PVM to analyze the effects of different additives on the crystallization of ammonium dihydrogen phosphate,” *Journal of Crystal Growth*, vol. 576, p. 126378, 2021.
- [24] J. Cobble Dick, A. Nguyen, and D. R. Latulippe, “Demonstration of FBRM as process analytical technology tool for dewatering processes via CST correlation,” *Water Research*, vol. 58, pp. 132–140, 2014.
- [25] Y.-M. Lin, C. Song, and G. C. Rutledge, “Direct Three-Dimensional Visualization of Membrane Fouling by Confocal Laser Scanning Microscopy,” *ACS Applied Materials & Interfaces*, vol. 11, pp. 17 001–17 008, 2019.
- [26] M. Pazouki, A. N. Wilton, and D. R. Latulippe, “An experimental study on sterile filtration of fluorescently labeled nanoparticles—the importance of surfactant concentration,” *Separation and Purification Technology*, vol. 218, pp. 217–226, 2019.
- [27] S. K. Dishari, A. Venkiteshwaran, and A. L. Zydney, “Probing effects of pressure release on virus capture during virus filtration using confocal microscopy,” *Biotechnology and Bioengineering*, vol. 112, pp. 2115–2122, 2015.
- [28] U. Reichert, T. Linden, G. Belfort, M. R. Kula, and J. Thömmes, “Visualising protein adsorption to ion-exchange membranes by confocal microscopy,” *Journal of Membrane Science*, vol. 199, pp. 161–166, 2002.
- [29] R. D. Deegan, O. Bakajin, T. F. Dupont, G. Huber, S. R. Nagel, and T. A. Witten, “Capillary flow as the cause of ring stains from dried liquid drops,” *Nature*, vol. 389, pp. 827–829, 1997.
- [30] W. Opong and A. Zydney, “Diffusive and convective protein transport through asymmetric membranes,” *AIChE Journal*, vol. 37, pp. 1497–1510, 1991.
- [31] E. Arkhangelsky and V. Gitis, “Effect of transmembrane pressure on rejection of viruses by ultrafiltration membranes,” *Separation and Purification Technology*, vol. 62, pp. 619–628, 2008.
- [32] H. Takaba, Y. Ito, and S. Nakao, “Rejection Properties of Silica Nanoparticles from Ultrafiltration Membranes,” *Korean Membrane Journal*, vol. 5, pp. 54–60, 2003.
- [33] V. Chen, A. G. Fane, S. Madaeni, and I. G. Wenten, “Particle deposition during membrane filtration of colloids: transition between concentration polarization and cake formation,” *Journal of Membrane Science*, vol. 125, pp. 109–122, 1997.

Flow Cytometry for Quantifying Microplastic Particle Concentrations in Membrane Filtration Processes



5.1 Motivations

As noted in §1.2.1, characterizing microplastic (MP) removal techniques heavily relies on the measurement of MP concentrations in water/wastewater samples. MP removal research via membranes is constrained by the techniques which allow researchers to quantify MPs in their samples, with number concentrations (*i.e.* MPs/L) typically used to express the quantity of MPs present. This

quantification process is non-trivial, with significant tradeoffs seen between techniques with respect to sensitivity/resolution and analysis time/efficiency. Very commonly, researchers isolate MPs from the water matrices (*e.g.* the suspended/dissolved solids in wastewater) and view the particles under a microscope, allowing for the MPs to be identified and counted [1]. While this does allow for the extraction of useful additional information such as size and shape, the whole process is extremely time-intensive and laborious. In response, investigators have turned to spectrophotometry [2] or turbidity measurements [3] to approximate MP concentrations as suspended particles absorb and scatter incident light. Enhanced MP identification can be achieved by staining or dyeing the particles (via adsorption or covalent linkages) with a fluorescent agent, and then using a fluorescent plate reader to quantify MP concentrations as the emitted fluorescence from a sample can be correlated to the amount of MPs present [4–6]. This was clearly indicated in Chapter 4. Indeed, fluorometric plate readers have been heavily used in past years to quantify the presence of (fluorescent) nanoparticles in applications such as filtration experiments containing simple water matrices (*e.g.* buffers) [7]. A similar, effective quantification method was developed by Pulido-Reyes *et al.* (2022) involving the surface labelling of nanoplastic (NP) particles with palladium and subsequent quantification by inductively coupled plasma-mass spectrometry (ICP-MS) [8]. Evidently, these types of “automated” analyses are substantially faster than quantification via microscopy, but they are still “bulk” measurements of the samples and provide no additional information on variables such as particle size.

In contrast, it was noted in §1.2.1 that various more complex techniques have also been employed which provide greater degrees of sensitivity and information (*e.g.* chemical identity). Such techniques include gas or liquid chromatography, mass spectroscopy, or combinations thereof [9–17]. These techniques are highly-advanced, not well-suited to the *efficient* quantification of MPs in simple laboratory experiments, and may experience difficulties identifying MPs in the presence of complex water matrices. However, they are advantageous as they directly quantify the presence of polymeric material, and not added components such as fluorophores or metallic coatings. For further reading, refer back to §1.2.1 and to a review by Caputo *et al.* (2021) work who present a good comparison of various parallel techniques for characterizing MP concentrations [16].

In contrast, flow cytometry (FC) is a technique which, *prima facie*, is well-positioned to be a facile, high-resolution, alternative MP quantification/characterization tool for use in laboratory

experiments. FC is typically used in the biochemical and medical sciences for cell counting and records light-scattering events by individual fluorescent particles [18] and thus, it has the potential to obtain more information than other “bulk analysis” techniques while drastically decreasing the analysis time when compared to manually counting MPs using a microscope. The technique is already employed in environmental sciences for non-MP activities such as microbial monitoring in water/wastewater analysis [19]. FC is somewhat similar to nanoparticle tracking analysis (*e.g.* NTA via a *Malvern Panalytical NanoSight NS300* [20]), but better lends itself to efficient, *high-throughput* analyses of individual particles in water/wastewater samples.

There is precedent to reason that FC would serve well for MP quantification/characterization in MP removal experiments. Prior works have detected MPs via FC, usually in the context of biological samples or MP ingestion via organisms. For example, Long *et al.* (2017) tracked the ingestion of polystyrene (PS) MPs by phytoplankton using a flow cytometer instrument [21], while Woods *et al.* (2018) measured the ingestion of polyethylene terephthalate (PET) microfibers using FC with a FlowCam visualization system [22], and Sgier *et al.* (2016) coincidentally detected the unexpected presence of fluorescent microspheres in a biofilm sample when using a flow cytometer [23]. As a further extension of the technique, Kaile *et al.* (2020) stained nine different types of polymer MPs with Nile Red dye (10 $\mu\text{g}/\text{mL}$ in 10% dimethyl sulfoxide) and found that PS, PET, polyethylene (PE), and polycarbonate (PC) particles could be detected via FC [24]. To this end, Caputo *et al.* (2021) affirm that the MPs must be fluorescent (*i.e.* containing a fluorophore, dyed with a fluorophore, etc.) for FC to be effective [16]. Recently, Wang *et al.* (2021) demonstrated the utility of FC to analyze simple water samples from MP removal experiments (3 μm fluorescent spheres) in the context of wastewater treatment [9]. Their results indicated that FC can be reliably used in coagulation, oxidation, and media filtration studies and that these processes yielded modest MP removal in most cases, with only a few conditions yielding very high ($> 95\%$) MP removal rates. In proof-of-concept tests, FC was resistant to impurities in the form of solid constituents in river water and wastewater treatment plant (WWTP) effluents; this bodes well for the prospective use of FC for MP quantification in complex water matrices. Yet as MP removal was largely incomplete in this study and the solution conditions used were largely “pristine”, there is a significant opportunity to develop and carefully validate FC in the context of removal technologies—such as membranes—which are expected to yield much higher removal efficiencies ($\gg 99\%$). While it was demonstrated that FC

can measure MP capture by these imperfect processes, the trend in MP removal is moving towards using technologies that act as *absolute barriers* (e.g. membranes), however, this requires a technique for quantifying very high removals of MPs. Thus, FC needs to be evaluated in these contexts.

In this work, FC is employed and evaluated for the quantification of minimally-disperse 1–5 μm fluorescent plastic microbeads¹ (MBs) in removal experiments using microfiltration (MF) membranes. Experiments were performed in both pure milliQ water and a solution of humic acid, a common component in the natural organic matter (NOM) found both in natural waters and in various concentrations in municipal wastewater [25–27]. Due to its ubiquity, humic acid is also a common model hydrophobic foulant in membrane filtration experiments [26]. While Vakondios *et al.* (2014) assert that the concentration of humic acid varies over the course of a WWTP and the concentration values that are measured are strongly affected by the quantification method used, they reported that a good estimate for the concentration of humic matter in WWTP 2° effluent is ~ 9 mg/L [25]. Using this value as a benchmark, filtration experiments were performed using 10 mg/L humic acid solutions to better represent the complex solution chemistries seen in WWTP effluents. In a head-to-head comparison, it is shown that the FC instrument performed as well as, or better than a fluorometric plate reader in the detection of MBs in pure water. Furthermore, the FC instrument outperformed the plate reader when the water matrix contained humic acid. Pursuant to these findings, FC was utilized to characterize permeate water samples from filtration experiments using the same Durapore® membranes with 5 μm and 0.45 μm nominal pore sizes which were investigated in Chapter 4. A correlation between the FC forward scattering light intensity and MB particle size was also developed.

5.2 Materials & Methods

5.2.1 Chemicals & Membranes

High-purity milliQ water with a resistivity of 18.2 M Ω -cm was produced by an *EMD Millipore milliQ Reference* system. Humic acid (HA; Lot = STBK1706) was obtained from Sigma-Aldrich and was used as received. Stock HA suspensions were prepared at 10 mg/L using milliQ water and diluted, as needed. Acetone and ethanol (Caledon Laboratories Ltd.) were used as received.

¹The term “microbead” is used, here, as a specific sub-category of very small *microplastic* that is spherical in shape.

Green fluorescent polymer MBs (*FMG* series; $\lambda_{ex}/\lambda_{em} \approx 414/515$ nm) were obtained from Cospheric (Santa Barbara, California) as a dry powder. The size of the particles is reported to be 1–5 μm in diameter according to the manufacturer. The exact polymer chemistry is not specified, but the manufacturer states that the MB is composed of cross-linked, inert thermoset amino formaldehyde polymer. 100 mg/L stock suspensions of MBs were subsequently produced in milliQ water or HA solution and ultrasonicated (Branson) for at least 30 minutes to disaggregate the MBs. These stock MB suspensions were further diluted for experiments, then re-sonicated to disperse the diluted suspensions. No surfactant was used as a dispersant.

EMD Millipore Durapore® polyvinylidene difluoride (PVDF) MF membranes were obtained. Pore sizes of 0.45 μm and 5 μm were chosen to be representative of membranes which should strongly reject and poorly reject (respectively) the MBs used in this study. Recall that these same membranes were utilized in Chapter 4 of this work. Prior to filtration experiments, the membranes were pre-wetted in milliQ water and cut to a diameter of 13 mm using an arch punch.

5.2.2 Scanning Electron Microscopy

The MBs were imaged using field-emission scanning electron microscopy (FESEM). Samples were prepared by pre-sonicating 100 mg/L aqueous stock suspensions of the MBs; 10 μL aliquots were then dropped onto an acetone-cleaned silicon wafer which was left to dry at 80°C. The wafers were mounted via carbon tape on an aluminum SEM stub and sputter-coated with 10 nm of platinum. The deposited MBs were then imaged at a low acceleration voltage of 750 V using a *JEOL 7000F* FESEM instrument. One micrograph of the MBs can be found in Figure 5.1A. However in total, three micrographs taken of different areas of the prepared sample were imported into the *Fiji* distribution of the *ImageJ* software. All feasible MBs in the images were measured by overlaying circles onto the particles. The major diameters (“Feret diameters”) of the circles were taken to be the particle sizes. A particle size distribution was calculated for the $N = 1,580$ particles which were measured, as depicted in Figure 5.1B.

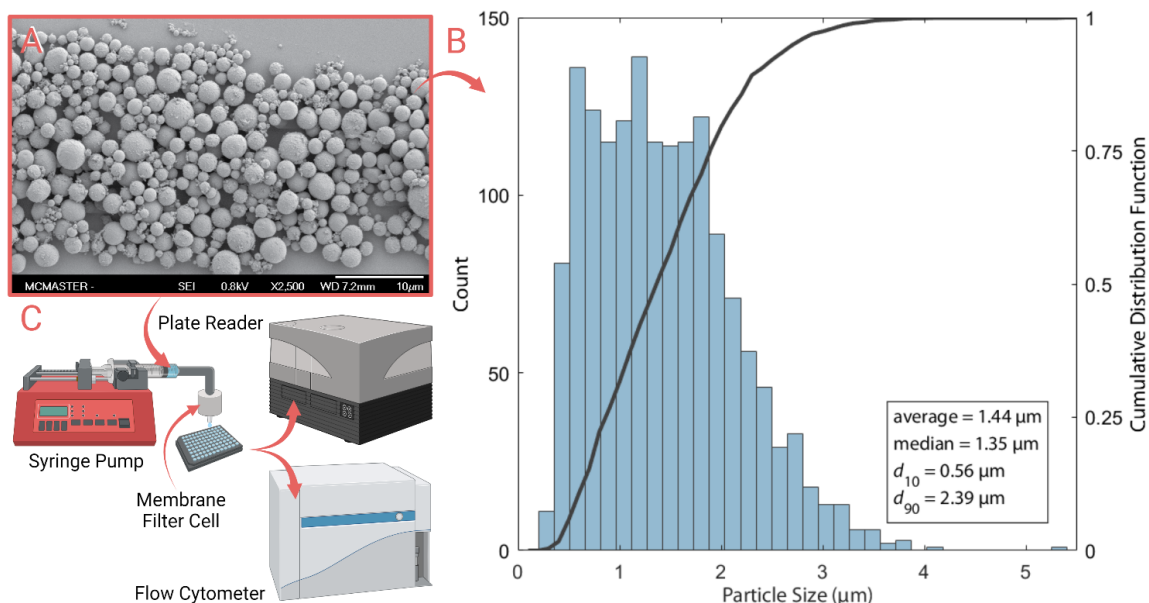


Figure 5.1: Characterization of the 1–5 μm Cospheric MBs used in experiments in this study. (A) Sample FESEM image of the MBs. (B) MB particle size distribution and cumulative distribution function ($N = 1,580$). All FESEM images from which these measurements originate are shown in Figure C.1. (C) Schematic of experimental apparatus and post-filtration analysis process.

5.2.3 Filtration Experiments

Wetted membrane discs were assembled into 13 mm-diameter filter holders (Cole-Parmer) giving an estimated active membrane area of 75 mm^2 . Filtration experiments with suspensions of MBs (1 mg/L) in either milliQ water only or a solution of 10 mg/L HA in milliQ water were conducted for 60 minutes at a constant permeate flux of $1,000 \text{ L/m}^2/\text{h}$ (LMH) using a syringe pump (*Harvard Apparatus PHD ULTRA*). Details regarding the filtration experimental protocols can be found in §4.2.3. Permeate samples ($\sim 300 \mu\text{L}$) were collected every two minutes and aliquoted into 96-well microplates for further analysis, as illustrated in Figure 5.1C.

5.2.4 Sample Analysis via Plate Reader

Water samples were analyzed for their MB content using a *Tecan Spark 10M* plate reader. The instrument gain was optimized at the highest concentration of MBs which was used (1 mg/L). This optimized gain of “55” was subsequently used in the analysis of all MB-containing samples, with $\lambda_{ex} = 485 \text{ nm}$ and $\lambda_{em} = 525 \text{ nm}$ (bandwidths = 25 nm and 20 nm, respectively).

5.2.5 Sample Analysis via Flow Cytometer

A Beckman Coulter Cytoflex LX flow cytometer was employed to measure the concentrations of MBs in samples. The instrument’s “blue” laser ($\lambda_{ex} = 488 \text{ nm}$) and “FITC” filter ($\lambda_{em} = 525 \text{ nm}$) were selected to enable MB quantification. From the analysis of MB stock suspensions, the quasi-optimal gains corresponding to forward scattering (FSC) signal intensity, side-scattering (SSC) signal intensity, and the fluorescence (FITC) signal intensity were determined empirically; these values were *fixed* and used in each subsequent experiment. The gains and other operational parameters are summarized in Table 5.1. In a given analysis, 150 μL samples were pipetted into round-bottomed 96-well microplates for analysis on the same day that they were produced. 50 μL aliquots were drawn from each well, allowing for MB counts to be recorded over a known volume. To ensure the validity and reproducibility of the results that were obtained, the instrument was calibrated daily using microbead standards, according to manufacturer specifications.

Results recorded via FC were analyzed using FlowJo software (Becton Dickinson). Empirically, gates were developed from FSC signal intensity by peak area (FSC-A; arbitrary units) versus FITC fluorescence signal intensity by peak area (FITC-A; arbitrary units) plots to isolate events corresponding to MBs from events corresponding to background noise or other contaminating particles. Samples of MBs in milliQ water versus milliQ alone, as well as MBs in HA solution versus HA alone were compared to determine the gated region which was expected to contain *just* the events corresponding to the MBs. Coordinates of the polygonal gate bounding these regions are found in Table 5.1. For the purposes of consistency, these coordinates were used in *every FC analysis* presented in this chapter.

Table 5.1: FC operational parameters and the vertices of MB polygonal gates in plots of FSC intensity versus FITC intensity by peak area (-A).

FC Parameters	Value
FSC Detector Gain (a.u.)	175
SSC Detector Gain (a.u.)	24
FITC Detector Gain (a.u.)	1
Backwashing Time per Sample	10 seconds
Mixing Time per Sample	5 seconds
Sample Flow Rate	30 $\mu\text{L}/\text{min}$
Polygon Vertices of MB Gate (FITC-A, FSC-A) in a.u.	$(7 \times 10^4, 2 \times 10^6)$ $(10^7, 2 \times 10^6)$ $(10^2, 10^4)$ $(10^7, 10^4)$

5.2.6 Excitation-Emission Matrices of Microbead Suspensions

The fluorescent intensities profiles of MB-containing suspensions (MBs in milliQ or 10 mg/L HA) were analyzed using a *Tecan Infinite M1000 Pro* plate reader over a range of excitation and emission wavelengths to produce “excitation-emission matrices” (EEMs). The instrument gain was optimized at “95” using the instrument’s built-in optimization function at the highest concentration of MBs which was used (1 mg/L). Excitation wavelengths λ_{ex} were scanned from 300–600 nm (bandwidth = 10 nm) in steps of 5 nm. Similarly, emission wavelengths λ_{em} were scanned from 400–700 nm (bandwidth = 10 nm) in steps of 5 nm.

5.3 Results & Discussions

5.3.1 Flow Cytometry for Microbead Quantification

To validate the use of a FC towards MB quantification, suspensions of MBs in both water and HA were analyzed. The analysis of samples of milliQ water only versus 1 mg/L MBs in milliQ water are shown in Figure 5.2A; the analysis of samples of 10 mg/L HA solution only and 1 mg/L MBs in 10 mg/L HA solution are shown in Figure 5.2B. Each point on the graph represents an “event” picked up by the instrument, categorized by its recorded fluorescent intensity (*i.e.* FITC-A) and its forward-scattering light intensity (*i.e.* FSC-A). The signal from the MBs occurs at “higher” fluorescent intensities (*e.g.* $\sim 10^4$ to 10^6 a.u.) regardless of the solution matrix chemistry. In contrast, when just milliQ water is sampled, there are some contamination events, but these events are found at much “lower” fluorescent intensities (*e.g.* $< 10^2$ a.u.) than the MBs. When MBs suspended in HA are sampled, there are more contamination events due to the presence of the HA (likely aggregates), however, these contamination events are again at low FITC-A values. To decisively categorize events as MBs (or non-MBs), the gate—with vertices found in Table 5.1—is applied to the FSC-A versus FITC-A graph, as seen in Figure 5.2. Events within the polygon formed to the right of the diagonal line are assumed to be MBs and quantified as such. This gate effectively excludes both contaminating events within the milliQ water as well as within the HA solution. Using the analysis of the 1 mg/L MBs in milliQ water from Figure 5.2A, of the 8,489 events which were recorded, 8,119 of these (95.6%) are assigned as MBs due to their location inside the gate. Similarly in the analysis of the milliQ water blank, 101 events were recorded, none of which (0%) were assigned as

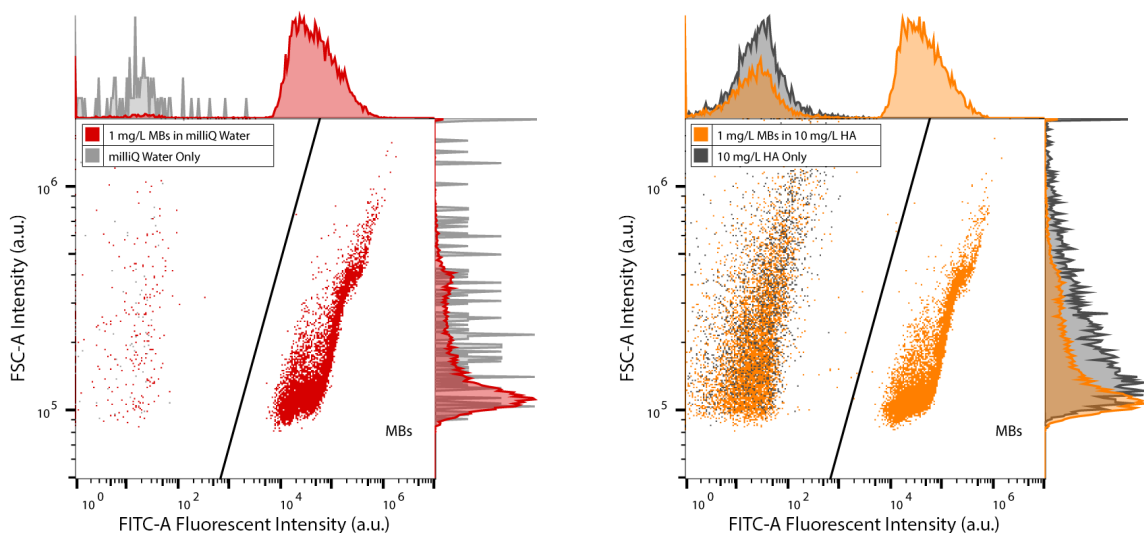


Figure 5.2: Scatterplots and corresponding adjunct histograms for FSC-A versus FITC-A data collected using the flow cytometer. (A) 1 mg/L MBs suspended in milliQ water (■) and milliQ water blank only (■). (B) 1 mg/L MBs suspended in 10 mg/L HA solution (■) and 10 mg/L HA solution blank only (■). Units for the axes are non-dimensional and a function of the instrument gains used (see Table 5.1). Counts in the polygon to the right of the diagonal line are gated as MBs. Histograms above the x -axes summarize the relative number of counts recorded at each FITC-A intensity. Histograms to the right of the y -axes summarize the relative number of counts recorded at each FSC-A intensity.

MBs. In Figure 5.2B, 14,654 events were recorded in the analysis of the 1 mg/L MBs in 10 mg/L HA, of which, 8,842 (60.3%) were assigned as MBs. Whereas in the analysis of 10 mg/L HA alone, 4,458 events were recorded and none of which (0%) were assigned as MBs. Using the differences between FITC-A/FSC-A values and the placement of the MB gate, “events” can be very effectively categorized as “MBs” versus background noise or non-MB particles. Knowing the locations of the “background” and “MB” events in FSC-A vs. FITC-A scatterplots, thresholding could easily be applied to further exclude background events from analyses.

Figure 5.2 also shows the FITC-A and FSC-A adjunct histograms for each of the four data series which are plotted. That is, the number of events (counts) at each FITC-A intensity or FSC-A intensity are shown above/to the right, respectively, of the plots. Each histogram is normalized by the total number of counts recorded in the experiment, so the relative number of counts at each intensity is displayed. These histograms display the distribution of fluorescent intensities (“brightness”) and FSC-A intensities (akin to particle “size”) in each sample. For the samples containing MBs, the FSC-A intensity peaks at a relatively low fluorescent intensity ($\sim 10^5$ a.u.) and the distribution has a

positive tail while the FITC-A distributions show a median intensity value of approximately 10^5 a.u. The FITC-A adjunct histograms, again, confirm that the MBs occur at much higher fluorescent intensities than the noise or contamination found in the samples. However, both the MBs and the contamination events contribute to a wide and overlapping distribution of FSC intensities, though by employing a second parameter (*i.e.* FITC-A), it is trivial to resolve MBs from non-MBs.

In this study, the fluorescent nature of the MBs facilitates for simple particle detection via FC. While non-fluorescing particles could be discriminated via only one parameter (*e.g.* FSC-A) [28], or particles which have been dyed with a fluorophore (*e.g.* Nile Red) could be analyzed in a typical fashion [16, 24], the use of inherently fluorescent particles with a strong signature is expected to improve particle detection/resolution and facilitate robust two-parameter discrimination of events that are recorded. The use of inherently fluorescent particles *also* negates the need for additional protocols such as particle dyeing and subsequent separation steps.

5.3.2 A Comparison of Microbead Quantification Techniques

To determine the ability of the FC instrument to quantify the concentration of MBs in samples, calibration curves were constructed using MBs suspended in milliQ water or 10 mg/L HA. MB suspensions were serially diluted from concentrations of 1 mg/L down to 10^{-5} mg/L. Aliquots were subsequently analyzed via FC and a fluorometric plate reader, for comparison. As shown in Figure 5.3, plate reader results are reported in arbitrary units of fluorescent intensity, while FC results are reported in units of MBs/mL: that is, the number of MBs counted in a sample of a given volume.

When the solution used is simply milliQ water (Figure 5.3A), it shown that the FC and plate reader obtain similar results. On the log-log plot, the relationship between the mass of MBs added to the solution matrix and the concentration via FC or plate reader fluorescent intensity is relatively linear and the relationships between the abscissa and ordinate variables are clear. At the lowest concentration depicted, individual MBs in a sample are counted (*i.e.* ~ 1 MB/50 μ L), obviating the need to extend the calibration curve to lower concentrations. At these very low concentrations, the data obtained by the plate reader deviates from the trend whereas the FC data maintains its linearity. Note that the standard deviations about the averages of triplicate measurements (*i.e.* denoted by

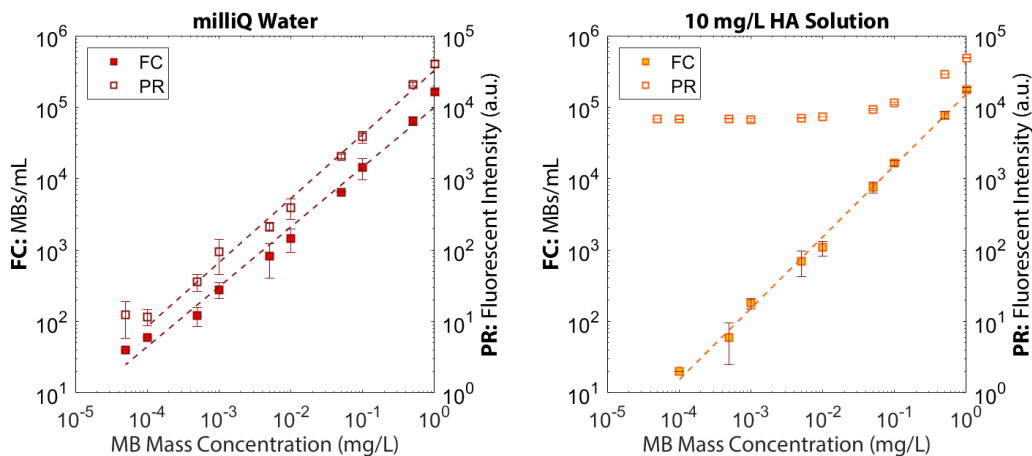


Figure 5.3: Comparison of the solution matrix effects when quantifying MB concentrations using the flow cytometer (FC; ■) and plate reader (PR; □). Solution conditions: (A) milliQ water and (B) 10 mg/L HA dissolved in milliQ water. Power-law lines of best fit are shown (---), where appropriate. Error bars refer to one standard deviation about the average of triplicate measurements, but may be obscured by the symbols where the standard deviation is low.

the error bars) also tend to increase at lower MB concentrations (*e.g.* $< 10^{-3}$ mg/L), likely reflecting inhomogeneity of the suspensions. Overall, it can be seen that the FC instrument has at least as good of a resolution as the plate reader when the MBs are suspended in pristine solutions. An additional benefit is that the FC instrument does not just provide a “bulk” correlation from fluorescent intensity to mass concentration of MBs: individual MB events are recorded, thus number concentrations and potentially MB properties can be ascertained. The utility of this observation will be explored in §5.4.

In contrast, when the water matrix is the 10 mg/L HA solution, the performance of the FC instrument versus the plate reader is markedly different. The former instrument performs as before when the milliQ water matrix was used: MB concentrations are reliably resolved at concentrations lower than $\sim 10^{-4}$ mg/L. However, the plate reader cannot resolve such concentrations under the current experimental design and the conditions that were tested (*e.g.* MB fluorophore used, concentration of HA, etc.). The trend plateaus at a fluorescent intensity of approximately 10^4 a.u., indicating that MB concentrations are not resolvable below about 10^{-1} mg/L: three orders of magnitude poorer than with the FC instrument. At these particular conditions, the FC appears to be a much more useful analytical tool for measuring MB concentrations when they are suspended in more realistic water matrices such as HA; whereas, the plate reader is seemingly unable to discern MBs from other materials.

This plateau in the plate reader fluorescent intensity versus MB mass concentration data was probed to see how the water matrix affects the detectability of the MBs in the presence of organic matter. Using *another* plate reader featuring a monochromator, “3D” EEMs were recorded for 10 mg/L HA solutions spiked with decreasing concentrations (*i.e.* dilution series) of MBs starting at 1 mg/L. The results are shown in Figure 5.4. Over the range of excitation/emission wavelengths studied, the fluorescent intensities range from 100 a.u. (blue) to $\leq 10^6$ a.u. (red). Note that where $\lambda_{ex} \approx \lambda_{em}$, very high fluorescent intensities are measured simply due to Rayleigh and Tyndall scattering [29]. To the right of these “Rayleigh scattering lines”, data is not reported as the fluorescent intensities are meaningless where $\lambda_{ex} < \lambda_{em}$. At the highest concentration of MBs (1 mg/L; right panel), there is a broad, strong fluorescent region ($O\{10^4$ a.u.}) with a maximum located at $\lambda_{ex} = 465$ nm and $\lambda_{em} = 500$ nm (3.5×10^4 a.u.) which corresponds to the emission of the MB fluorophore. The HA suspensions also show moderate fluorescence ($O\{10^2$ – 10^4 a.u.}) at excitation/emission wavelengths away from the strongly fluorescent region, over most of the spectrum that was analyzed. As the MB concentration is decreased (*i.e.* right to left in the figure), the strongly fluorescent region corresponding to the MBs decreases in intensity. Even in the absence of added MBs (far left panel), it is critical to note that the HA solution produced moderate fluorescent intensities across the majority of the spectrum of excitation/emission wavelengths that were studied, with higher fluorescent intensities seen towards the lower wavelengths.

Previous research has found that HA and humic substances exhibit fluorescent behaviour over a wide range of wavelengths, as seen here; additionally, fluorescence spectroscopy is regularly used to

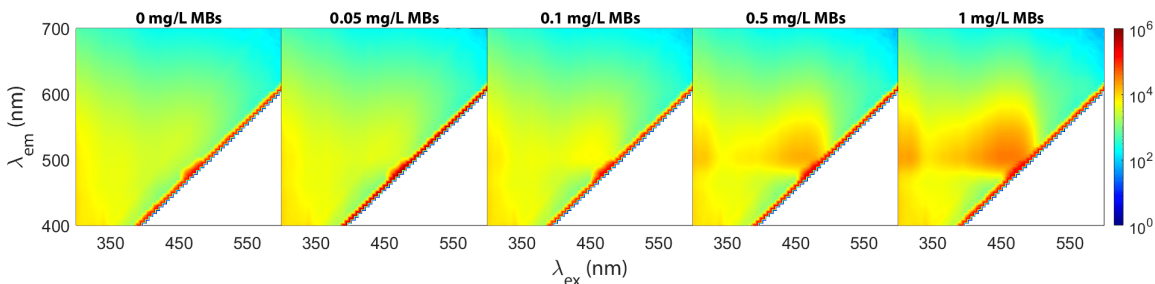


Figure 5.4: Excitation-emission matrices illustrating the obscuring effect of HA when attempting to quantify MB concentrations using the plate reader. Magnitudes of fluorescent intensities are indicated by the coloured legend, presented in arbitrary units. Suspensions of fluorescent MBs were diluted with 10 mg/L HA, with MB concentrations decreasing from right to left (1 mg/L \rightarrow 0 mg/L MBs). In all panels, the concentration of HA is 10 mg/L. White-coloured regions correspond to where $\lambda_{ex} < \lambda_{em}$. Panels showing other HA concentrations are found in Figure C.2.

characterize water and wastewater for its humic content [30–32]. The chemical makeup and structure of HA and humic substances are highly complex and differ depending on the source, thus there is variety of structures which have been proposed for HAs. As such, HAs can contain a wide variety of chemical moieties including oxygen-bearing groups (*e.g.* alcohols, phenols, acids, quinones, ethers, etc.), nitrogenous heterocyclic rings, aliphatic chains, aromatic rings, or even sugars and peptides [32, 33]. Some of these moieties have good potential for creating different regions of electron delocalization which can therefore lead to the broadly fluorescent nature of the HA seen in these experiments. However, the HA fluorescent “fingerprint” is highly dependent on the HA source [34], therefore fluorescence results from the HA used in this study may not coincide with fluorescence results from HAs originating from different sources. Furthermore, as HAs are only one common component of wastewater [31], the fluorescent fingerprint of the HAs may not be representative of wastewater as a whole, nor should it be expected that all wastewaters would have the same fluorescent properties.

Consequentially, the heterogeneous fluorescent nature of the HA, itself, proves to make quantifying the concentrations of suspended MBs more challenging using the plate reader, as previously shown in Figure 5.3; note that the MB mass concentrations just shown in Figure 5.4 match those used in the former figure! Considering Figure 5.4, the fluorescent intensities of the HA solution alone were found to exceed 10^3 a.u. in the region where the MBs fluoresce (2,182 a.u. at $\lambda_{ex} = 465$ nm and $\lambda_{em} = 500$ nm). At MB concentrations equal to, or below ~ 0.05 mg MBs/L, the EEMs were not visually distinct from the EEMs of solutions with no MBs added (10 mg/L HA only). This suggests that the fluorescent signal of the HA solution can overcome that of the suspended MBs at concentrations below ~ 0.05 mg/L. This explains the plateau in fluorescent intensity signal in Figure 5.3B when the plate reader was used. Of course, the implication of this finding is that the fluorescent plate reader—used in this particular manner—is a less effective tool for measuring fluorescent MB concentrations when other matter in the solution matrix has a significant fluorescent signal in the region where the MBs fluoresce. In theory, a MB/fluorophore combination could be chosen such that the emission wavelength corresponds to very low fluorescent intensities of the HA (*i.e.* very long wavelengths). When this is not the case, the flow cytometer proves to be a more useful MB quantification tool: it can measure lower concentrations of MBs, and discern between highly-fluorescing MBs versus weakly-fluorescing background material/contaminants.

5.3.3 Microbead Removal via Membrane Filtration

There is a strong need to validate membrane technologies for use in removing MPs from the effluents of WWTPs, with particle transmission through membranes being a concern. When quantifying transmission or rejection, particle concentrations are needed. Excellent instrumental sensitivity, and/or an efficient MP isolation/quantification procedure are required in this application, especially when very dilute permeate samples are evaluated. Previous results from the experiments indicate that FC shows promise towards these applications as individual particles can be resolved and the solution matrix does not materially interfere with the process, negating the need for intensive MB separation procedures.

To this end, the 1–5 μm MBs were filtered through two different MF membranes: one with a 0.45 μm nominal pore size and one with a 5 μm nominal pore size. The two membranes' pores are approximately an order of a magnitude different in size. Results from the (duplicate) hour-long filtration experiments are summarized in Figure 5.5. While two replicates are shown at each condition (*i.e.* pore size/solution chemistry), it should be noted that both replicates are quite consistent. Results from the quantification of MB concentrations via FC in the membrane feed and permeate samples (collected every two minutes) are reported in units of MBs/mL. Before each filtration experiment, pure milliQ water was run through the experimental setup to dislodge any remaining MBs from previous tests such that permeate sample contamination was minimized. The top row in Figure 5.5 represents filtration experiments performed in milliQ water, while the bottom row represents filtration experiments performed in 10 mg/L HA. For both solution conditions, results are reported for the 0.45 μm and 5 μm membranes.

■ **Filtration experiments in milliQ water.** When the 0.45 μm pore size membrane and milliQ water matrix is considered, it is clear that there is very little transmission of the MBs—if at all. Concentrations of MBs in permeate samples were $\leq 2 \times 10^2$ MBs/mL compared to feed concentrations of $(1.30\text{--}1.36) \times 10^5$ MBs/mL. Furthermore, the transmission is notably sporadic. Not all permeate samples collected were found to contain MBs: only 39% and 52% of samples in the two trials, respectively, contained MBs. Such little transmission of the MBs by the 0.45 μm membrane is expected as the nominal pore size is ostensibly smaller than the MB particles. In contrast, when the 5 μm pore

size membrane and milliQ water matrix is considered, there is a much greater transmission of MBs. Permeate concentrations were found to be $< 1.05 \times 10^5$ MBs/mL compared to feed concentrations of $(1.37\text{--}1.67) \times 10^5$ MBs/mL. Again, this expected as the nominal membrane pore size is on the order of magnitude of the MBs' sizes, enabling transmission—assuming that the rejection of the MBs is due to purely size-exclusion means.

■ **Filtration experiments in humic acid solution.** Filtration experiments performed in complex water matrices are better able to simulate filtration conditions in real WWTPs. The use of HA as a foulant approximates the NOM and other solid matter that is present in wastewater. Other researchers such as Wang *et al.* (2021) often default to the use of “pristine” solution conditions (*e.g.* milliQ water, buffers) to perform filtration experiments [9], however, nuances like NOM/MB fouling synergies are not elucidated in the absence of NOM or other solid matter. These types of nuances can be clearly seen in Figure 5.5.

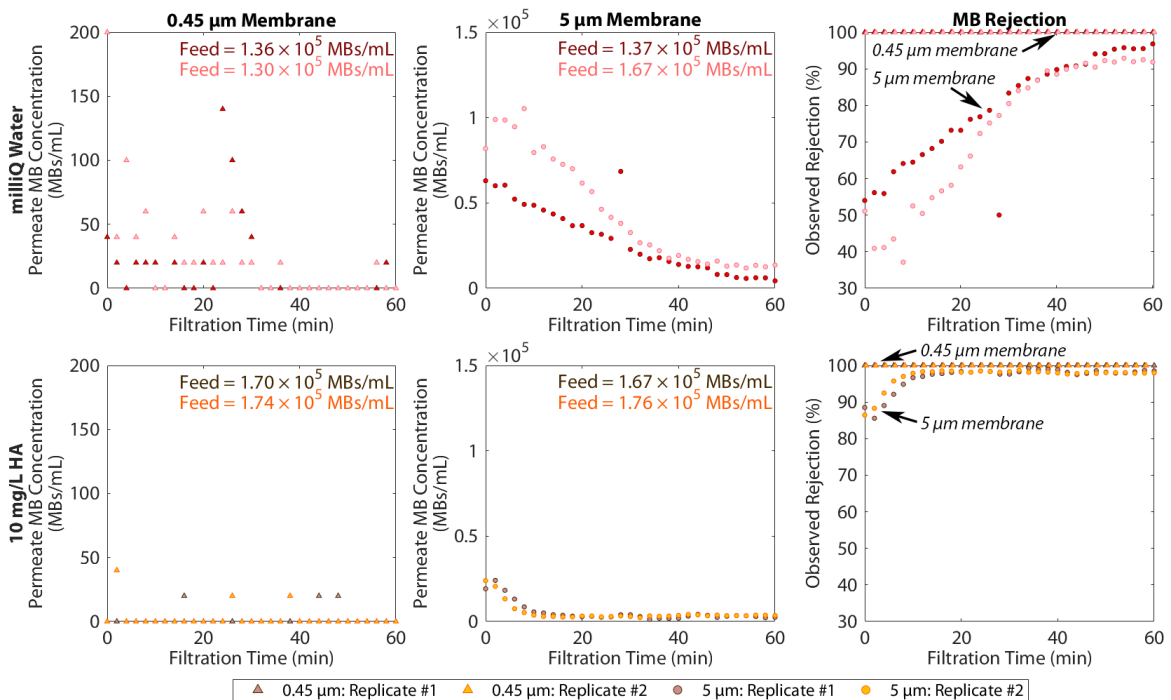


Figure 5.5: Comparison of the effect of pore size on the MB transmission and observed rejection using the Durapore® 0.45 μm (▲) and 5 μm membranes (●) operated at a constant permeate flux of 1,000 LMH. The top row represents experiments in milliQ water; the bottom row represents experiments in 10 mg/L HA solutions. MB counts, and subsequently concentrations/rejection coefficients, were obtained via FC. Experiments with each of the membranes were performed in duplicate; individual colours in the figure are indicative of the individual replicates.

When the same experiments as above were performed with the HA water matrix, MB transmission was significantly reduced when either membrane was considered. For the 0.45 μm pore size, the maximum MB concentration fell to 4×10^1 MBs/mL in the permeate samples. It should be noted that this “transmission” may even manifest as noise or sample contamination within the FC instrument. This maximum permeate concentration is equivalent to 2 MBs per 50 μL sample which is within the expected intra-sample variability at these concentrations (standard deviation = 2 MBs/sample). As such, the transmission seen is indistinguishable from instrument variability, here. Analysis of larger permeate samples would help elucidate these effects on the instrument’s MB detection limits. Furthermore, transmission was even more sporadic with only around 10% of samples collected containing measurable quantities of MBs.

With the 5 μm pore size membrane, there is also a lesser degree of transmission when the MBs were suspended in a HA matrix. In this scenario, the MBs concentrations in permeate samples did not exceed 2.5×10^4 MBs/mL which is approximately four times less than when the milliQ water matrix was used. Furthermore, strongly declining concentrations of MBs over the course of the one-hour experiments are observed in both replicates, with MB concentrations in the last sample (*i.e.* $t = 60$ min) measured at $< 3.54 \times 10^3$ MBs/mL when HA was present, versus $< 1.36 \times 10^4$ MBs/mL when the solution matrix was pure milliQ water. The strong decrease in MB concentrations in the permeate samples when HA was present can be attributable to membrane fouling caused by the HA which can adsorb to the membrane surface or inside the pores, restricting the ability of MBs to pass through the membrane. The fouling of MF membranes by HAs in this manner is well-documented in the literature [35]. Similar incidences of fouling were seen in Chapter 3 when wastewater was filtered. In addition, direct fouling of the membrane surface/pores *due to the MBs* is also an inherent possibility, corroborated by the decline in MB transmission when no HA was present. This was also seen in Chapter 4 when irregularly-shaped MPs were filtered in simple solutions. However, recent research by Pradel *et al.* (2021) suggests that heteroaggregation between the MBs and HA is unlikely as MBs with adsorbed HA can electrostatically repel other particles, while larger HA molecules can sterically hinder particle aggregation [36].

Even in the presence of membrane fouling, it is interesting to note that the MB concentrations in the 5 μm membrane permeate samples reached a *non-zero plateau*, suggesting that the fouling

layer does not completely occlude the membrane pores but constricts them enough to reduce MB transmission. When comparing the results of the filtrations in milliQ water versus HA solution, it is very clear that solution chemistry is an important factor which drives the effectiveness of the removal of the MBs, thus MP filtration experiments should be conducted in reasonable solution conditions for the results to be representative of real-world processes.

■ **A comparison of rejection coefficients.** Data from the aforementioned experiments was subsequently used to calculate the number-based MB observed rejection coefficients R_n for each of the permeate concentration values shown in Figure 5.5, where n_f and n_p are the number concentration of MBs in the membrane’s feed and permeate streams, respectively:

$$R_n = \left[1 - \frac{n_p}{n_f} \right] \times 100\% \quad (5.1)$$

Note that n_f is the initial concentration of the suspension fed to the membrane cell; no corrections were made in the rejection calculation for concentration polarization in the dead-end filtration. See §2.1.2.2 for more information on this phenomenon.

The results in the “MB Rejection” panels of Figure 5.5 are directly translated from the neighbouring “0.45 μm Membrane” and “5 μm Membrane” panels. When the milliQ water matrix is considered, as expected, R_n values for the 0.45 μm membrane are very high: in excess of 99.2%. The MBs are strongly rejected by the smaller membrane pores, however, the rejection is not complete. For the 5 μm membrane, R_n values ranged from 40 to 60% at the start of the filtration experiments, but steadily climbed in excess of 90% towards the one-hour mark (*i.e.* ≥ 48 min) as particle fouling restricted the transmission of the MBs. It is interesting to note that the MB manufacturer states that 90% of the particles fall less than 5 μm in size (*i.e.* the d_{90} value), however, transmission of 90% of the MBs is never seen by the 5 μm membrane. The inference is that the stated 5 μm pore size does not accurately reflect the true nature of the pore size/size distribution, therefore this rating does not adequately reflect the size of these MBs that can be rejected.

The effects of HA fouling further increase the rejection coefficient. R_n values produced by both membranes are significantly higher when HA was present, exceeding 99.5% for the 0.45 μm mem-

brane, versus 85–90% initially for the 5 μm membrane, but rapidly climbing to $> 95\%$ by the sample taken at the 10-minute mark. From these results, it is clear that the presence of HA mitigates the transmission of MBs through both membranes. The implication of this statement in the context of scientific research is that performing filtration experiments in pristine solution matrices (*e.g.* water, buffer, etc.) is not sufficient to elucidate all filtration phenomena. Moreover, if results are sought which should mimic filtration performance in real WWTPs, there is an inherent need to also use solution matrices that mimic those in WWTPs.

The results from the MP removal experiments in this work demonstrate just how effective membranes can be with respect to other technologies. In their study, Wang *et al.* (2021) considered the removal of commercial fluorescent PS spheres with a diameter of 3 μm suspended in water matrices (*i.e.* buffers), river water, or WWTP effluent [9]. Removal techniques which were considered included six iron or aluminum coagulants (5–50 mg/L), ferrate as an oxidant (1–100 mg Fe/L), and media filter materials (*e.g.* garnet, zeolite, activated carbon, etc.); however, the removal experiments were unfortunately performed in buffer or pure water. Among other techniques (*e.g.* turbidimetry), FC was used to measure MP removal. These results indicate that via coagulation, MP removal was clearly dose- and coagulant-dependent. Low removal rates were typically seen, widely ranging from ~ 10 –60% except when the “best” coagulants were used at the highest doses (*i.e.* $\sim 90\%$ removal possible). Media filtration also demonstrated mediocre MP removal with rates ranging from approximately 30–70%. In contrast, the authors found that MP removal via ferrate oxidation (≥ 10 mg Fe/L) could be quite effective, with removal rates roughly 96–98% [9]. Pulido-Reyes *et al.* (2022) noted similar coagulation/filtration findings in the removal of Pd-labelled PS NPs, however, up to a 3-log removal (99.9%) was found to be possible when *consecutive* rapid sand filtration, activated carbon filtration, and slow sand filtration processes were employed [8]. The use of a single 0.45 μm membrane in this study demonstrated similar MP removal performance, with almost complete MP removal ($\gg 99\%$) at either solution condition that was investigated. In the presence of 10 mg/L HA, even the 5 μm membrane saw similar MP removal rates. To maximize MP removal performance, a 0.45 μm pore size MF membrane is a reasonable choice for 3^o wastewater filtration processes and could offer good MP removal performance for MPs ~ 1 μm and larger, especially in comparison with other removal techniques including those highlighted in §1.2.2.2.

5.4 A Strategy to Estimate Microbead Size via Flow Cytometry

MPs are well-understood to vary with regards to their properties: size, shape, chemical identity, and so on. In particular, MP size is a crucial parameter when considering the environmental consequences of marine MP pollution. Consider two samples with the same absorbance or fluorescence readings: one could feasibly contain a small number of large MPs while the other could contain a large number of small MPs. In this example, the quantity of MPs could be isogravimetric or isovolumetric, however there is reason to believe that the sample with the large number of small particles would be more ecologically harmful due to the enhanced ingestion risk caused by the small particles and their higher surface area-to-volume ratios [37–41], as described in §1.1.2. Mathematically, the profound effect of MP size on particles per unit mass and specific surface area is illustrated in Figure C.3. Overall, there is substantial value in measuring MP particle size in conjunction with MP particle concentrations in MP removal experiments.

There is good reason to believe that FC can be used to provide an estimate of particle sizes [42] *in addition* to particle counts. In fact, polymer microparticle standards of various sizes are routinely used to calibrate FC instruments! To elaborate, the intensity of light scattered by particles at small angles ($\sim 0.5\text{--}2^\circ$) in a flow cytometer (*i.e.* FSC intensity) is influenced to a great degree by the particle size [18]. Akin to analysis via laser diffraction, FSC intensity is reported to increase with increasing particle size [18, 28, 43, 44], though the exact nature of this relationship is dependent on the refractive indices, the shape of the particle, its structure and composition, as well as characteristics of the instrument. As an aside, the intensity of light scattered by particles at large angles ($\sim 15\text{--}135^\circ$) in a flow cytometer (*i.e.* SSC intensity) is influenced to a great degree by the “composition” or “complexity” or “granularity” of the particle, which describes the presence of surface irregularities or cell organelles; while SSC intensity also increases with particle size, the correlation is not as strong [18]. As such, given a population of particles which are the same in shape and composition and similar in diameter (*e.g.* the MBs in this study), FSC intensity measurements should prove to increase monotonically with particle size and thus correlate well with MB size [44].

With this in mind, noting a monotonic increase in light scattering intensity as particle size increased, Julià *et al.* (2000) developed a procedure to correlate FSC intensity data to the sizes of five

different species of bacteria via FC; this correlation takes the form of a non-linear relationship between size and FSC intensity [43]. This original method was adapted in various ways by subsequent investigators for measuring bacterial biovolume in samples or estimating the size of bacteria/plankton cells [28, 45–47]. Of particular interest to this study, Foladori *et al.* (2008) correlated FSC intensity measurements of silica microspheres having known diameters to the sizes and biovolumes of bacterial cells [28]. Similarly, Tzur *et al.* (2011) utilized various FC light scattering measurements to quantify cell sizes within a subpopulation for the purpose of sorting the cells based on volume, utilizing samples of fluorescent PS MBs (3–10 μm) to calibrate the protocol [18].

To this end, I have adapted Julià *et al.*'s methodology to provide size (*i.e.* diameter) estimates for MBs in simple filtration experiments; the derivations below originate from the work of these authors [43]. For a given sample, define $F_i(i)$ to be the cumulative distribution function (CDF) of the FSC-A intensities i of MBs in a sample, as determined via FC. Define $F_d(d)$ to be the analogous CDF of the particle diameters d of MBs in a sample, determined using an *ex situ* method. Note that a CDF function $F(j)$ outputs the fraction of the particles/events in a population which have a value less than or equal to j such that $0 \leq F(j) \leq 1$. From this method, the premise of the relationship is: since F_i and F_d model distributions describing the same population of particles:

$$F_i(i^*) \approx F_d(d^*) \quad (5.2)$$

where a particle of size d^* produces a FSC-A intensity of i^* , noting that the relationship relies on i increasing as d increases, which is typically noted in the literature [28, 43].

5.4.1 Model Formulation

The particle size distribution of the MBs was obtained *ex situ* through image analysis of the electron micrographs previously discussed in §5.2.2 (*i.e.* Figure 5.1). Particle sizes $d \in [d_1, d_2, \dots, d_N]$ were recorded ($N = 1,580$) and $F_d(d)$ was subsequently calculated at each value of d . Similarly, a 1 mg/L “feed” sample of MBs in milliQ water was analyzed via FC. The FSC-A intensities $i \in [i_1, i_2, \dots, i_M]$ ($M = 9,429$) for the gated events were obtained from the FlowJo software and $F_i(i)$ was calculated at each value of i . As both F_d and F_i are derived from finite vectors of collected data points, the CDFs

are discrete functions. In MATLAB, linear interpolation between the data points was therefore used to produce piecewise continuous versions of these functions, \bar{F}_d (“size CDF”) and \bar{F}_i (“intensity CDF”), respectively. In the next step of the process, values of d could be estimated from measurements of i via $\bar{F}_i(i)$ and $\bar{F}_d(d)$ by a new monotonically-increasing function φ . That is, $d = \varphi(i)$ transforms i values into d values through the CDFs and is represented as follows [43]:

$$\bar{F}_i(i) = \bar{F}_d(d) \quad (5.3a)$$

$$\bar{F}_i(i) = \bar{F}_d(\varphi(i)) \quad (5.3b)$$

$$\varphi = (\bar{F}_d^{-1} \circ \bar{F}_i) \quad (5.3c)$$

The existence of \bar{F}_d^{-1} in Equation 5.3c requires that \bar{F}_d be invertible. This overall mathematical process by which i values could be used to estimate d values is illustrated in Figure 5.6.

In practice, an arbitrary vector of i values was generated and their corresponding values $\bar{F}_i(i)$ were read from the already-computed “intensity CDF”. Via Equation 5.3a, values of d were then read off the “size CDF” where $\bar{F}_d(d) = \bar{F}_i(i)$. This mapping of i to d generated $d = \varphi(i)$, shown in Figure C.4. As a final note, the model data was truncated just before $i = 4 \times 10^6$ a.u. to avoid creating a non-smooth $\varphi(i)$ at high i due to the very small number of particles with very high intensities (*i.e.* outliers). The model is thus valid for $i \in [7 \times 10^4, 4 \times 10^6]$.

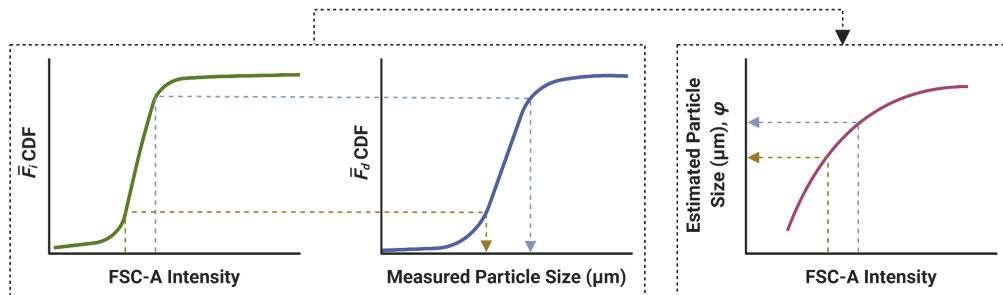


Figure 5.6: Graphical illustration of the process used to estimate MB particle sizes from FC FSC-A intensity measurements.

5.4.2 Estimates of Particle Size

To estimate particle sizes of MBs in actual samples, the FSC-A intensity values associated to events gated as MBs were output from FlowJo. Again using MATLAB, values from this vector of intensities i were passed to the previously-formulated $\varphi(i)$ function. Interpolation was employed to map the measured i values to estimated d values using $d = \varphi(i)$. To this end, Figure 5.7 illustrates the estimated particle size distributions for the feed and permeate samples of a filtration experiment using the 5 μm membrane to filter 10 mg/L HA solutions containing MBs. Here, the sizing model was used estimate particle size using the FSC-A intensity values obtained via FC at the same time as the MB concentration measurements were obtained. To verify the model's suitability, Figure C.5 shows overlays of particle size distribution histograms/CDFs for the MBs sized *ex situ* (via FESEM) which were used in "training" the model, and the MBs suspended in "feed" HA solutions which were sized using FSC-A intensity measurements (via FC) according to the formulated model. It is easily seen that the estimated MBs size distributions of the "feed" samples—both Replicates #1 and #2—are in good agreement with the size distribution of MBs measured *ex situ*, implying that the model is applicable in this particular system. However, one additional experiment should be performed to verify that the FSC-A intensity does indeed increase monotonically with MB size by testing samples containing (otherwise-identical) MBs of differing known diameters (1–5 μm).

In Figure 5.7, note that the results for *just Replicate #1* are considered as variability between replicates is low (see Figure 5.5). For the interest of the reader, the particle size results for Replicate #2 can be found in Figure C.6. In the feed sample, 8,366 particles were analyzed via FC and evidently, the particle size distribution of these MBs has a positive skew: a greater number of events are seen corresponding to smaller particle sizes. Here, the estimated median particle size (\tilde{d}) is calculated to be 1.24 μm , with estimated d_{10} and d_{90} sizes found to be 0.61 μm and 2.24 μm , respectively. In Figure 5.7, permeate samples were analyzed every twenty minutes for the duration of the experiment, and evidently, they contained significantly fewer particles (95–959). This is corroborated by the transmission analysis in Figure 5.5. Furthermore, the particle size distributions shift noticeably to the left when the permeate samples are compared to the feed sample. For example, while the feed sample had a median particle size of 1.24 μm , the equivalent value in the permeate samples decreased to 0.82 μm (averaged over the four permeate samples): a 33% decline. Similar findings can be seen

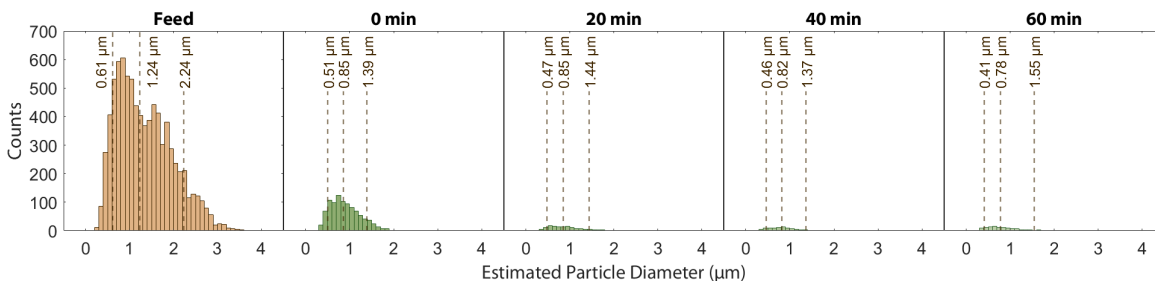


Figure 5.7: Estimation of MB particle sizes in selected permeate samples for the filtration of 1 mg/L MBs in 10 mg/L HA solution using the 5 μm membrane. Only Replicate #1 is shown. Frequency histograms of estimated particle diameters (μm) in feed samples (■) and permeate samples (■) taken at 20-minute intervals are shown. From left to right, the d_{10} , median, and d_{90} statistics of the particle size distributions are included (---).

when the d_{10} and d_{90} values of the distributions are considered. This is summarized in Table C.1 for *both* replicates. Overall, the results infer that the membrane effectively rejects the larger particles in the feed, while the passage of smaller particle sizes into the permeate can still occur. These particle sizes are expected to be particularly hazardous as they are more likely to be ingested by aquatic organisms such as fish, plankton, and filter-feeders [48, 49]. A similar preferential transmission of smaller particles was also seen in §4.3.3, as measured via FBRM. However, the tremendous benefit to using the FC is that only 150 μL per sample was necessary, as compared to the 100 mL of sample needed when using the FBRM instrument.

In Figure 5.7, estimated particle size results are shown for the filtration of MBs in 10 mg/L HA (Replicate #1). However, it can also be noted that when comparing the effects of solution conditions—10 mg/L HA versus milliQ water alone—the decline in size statistics from the feed to the permeate samples is *greater in the presence of HA*. These apparent size declines are summarized for the two solution conditions in Table C.2. This result implies HA’s role in fouling-induced MB rejection as larger fractions of MBs see a greater degree of rejection when HA is present. A composite analysis of MB sizes in the feed/permeate samples from all of the filtration experiments using the 5 μm membrane, including both solution conditions, is found in Figure C.7.

The method of particle detection described here relies on light scattering. The Rayleigh-Gans approximation to Mie Theory states that the (forward) light scattering intensity increases with the sixth power of the particle’s radius and the square of its volume; it is applicable where the particles are smaller than, or similar to, the wavelength of the incident light (valid for $\lesssim 3 \mu\text{m}$) and the

particle refractive index is close to that of the medium [28]. Scattering by larger particles is better described by the more complex and comprehensive Mie Theory [50]. However, empirical experiments have measured the aforementioned exponents to be smaller than what the theory predicts and the relationship is found to decrease as particle size increases [42, 51].

In the system that was investigated in this work, it was found that the estimated particle diameter non-linearly increased with FSC-A intensity, where the function was concave-downwards (Figure C.4). Taking the inverse of this function, it can be seen that the FSC-A intensity non-linearly increases with particle diameter, where the function is concave-upwards. This fits in accordance with the theory and with results obtained by Foladori *et al.* (2008) who developed a correlation between FSC intensity measurements and the size of silica beads [28]. In contrast, Julià *et al.* (2000) found that the FSC intensity versus particle diameter function was concave-upwards when actual bacteria were sized [43]. These bacteria differ in refractive properties, size, and geometry from the spherical polymer MBs used in this study. Any discrepancies, here, likely arise from the fact that the exact FSC-A values produced are a complex function of particle properties, the sensitivity/linearity of the FC detectors, and the calibration/alignment of the instrument optics [28, 42]. However, the noted variations in concavity are likely to be immaterial to the results presented in this work.

Additionally, authors such as Galbusera *et al.* (2020) caution that even if a (non-linear) relationship between the scattering intensity and particle size can be generated, such a relationship is not necessarily universal and is a function of system parameters [52]. This implies that new relationships would need to be generated for different instruments, different particle shapes/sizes/compositions, and different solution chemistries. For example, where the MPs have diverse refractive indices or optical properties (*e.g.* absorption of light by pigments), the solutions contain various solids, or there is a propensity for solid matter (*e.g.* NOM, biofilms) to deposit on the MPs, it would be expected that different relationships between FSC-A intensity and MB size would exist. These relationships could even change over time, such as due to the transient growth of biofilms. The technique is thus limited in that the properties of the MPs and solution matrix need to be controlled for, in advance. Overall, it is evident that analyses of MP size via FC require careful planning.

To my knowledge, this study represents the first time that FC has been used to estimate the size of filtered MPs which has broad-ranging implications in the study of MP removal processes. It is well-known that MP size is an important characteristic when considering the toxicity of the particle towards aquatic organisms. Whereas other methods such as fluorometry take bulk measurements of MPs in solution and thus can produce estimates of MP concentrations, FC provides additional value by having the ability to record estimates of MP size. Therefore, a user of FC can also quantify the size fractions of MPs that are removed by their process. Similar to how other researchers have utilized FC to measure cell biovolume, this technique could be extended to measure MP volume, then MP mass: an important parameter which quantifies the presence of MPs in samples. While the MBs used in this study have a fairly narrow dispersity (*i.e.* $d_{90} - d_{10}$), MPs within WWTPs and the environment see much larger inherent dispersities. As such, a removal process for MPs with a larger size dispersity could see a larger difference in particle sizes when comparing the particles entering and leaving the process. Thus, any size reduction would be readily apparent.

5.5 Concluding Remarks

Membrane technologies promise to be an effective tool for removing MPs from the effluents of municipal wastewater treatment facilities. However, conflicting accounts in the literature regarding MP rejection have necessitated the commissioning of studies to evaluate MP rejection under controlled and realistic conditions. To facilitate such research, there is an opportunity to develop techniques to efficiently quantify and analyze MPs, especially in extremely dilute samples such as membrane permeate water. To this end, the efficacy of FC has been demonstrated for the quantification of (nominally) 1–5 μm fluorescent MBs. It was found that FC can efficiently count these MBs in pure water samples, down to $\sim 10^{-4}$ mg/L: roughly on par with a standard fluorometric plate reader. In contrast, MBs suspended in a 10 mg/L HA solution were poorly detected by the plate reader, but showed a similar degree of detection when using the FC instrument. This was facilitated by the gating process which differentiated the MBs from background noise and autofluorescence of HA molecules in solution. In filtration experiments, MB-containing suspensions in pure water or HA solution were filtered using 0.45 μm and 5 μm Durapore® MF membranes. The FC procedure was used to compare MB concentrations in permeate and feed samples in order to obtain rejection coefficients for the MBs. In pure water, these values exceeded 99% for the 0.45 μm membrane and ranged

from 40%–90% with the 5 μm membrane. In the presence of HA—more representative of the water qualities which would be seen in WWTPs—rejection coefficients significantly increased, exceeding 99.5% for the 0.45 μm membrane and ranging from 85% to > 95% for the 5 μm membrane. It could thus be expected that fouling by organic matter in WWTPs may form a dynamic membrane which would aid in the rejection of MPs. For the first time, FC was also used to provide estimates of MP particle sizes from a correlation involving FSC-A intensity values and *ex situ* measurements of the MBs. This method was used to compare MB sizes in feed and permeate samples from the 5 μm membrane. A notable reduction in median particle size was seen—especially when HA was present—which affirms the membrane’s ability to reject larger particles while allowing a fraction of the smaller particles to pass through. This preferential passage of smaller MBs is a concern from an environmental standpoint, highlighting the value in performing these experiments.

Overall, this study demonstrates the utility of FC in well-controlled laboratory MP removal experiments, especially where the MPs are small and dilute in concentration. However, it is limited in that the solution conditions and the small-scale flat-sheet membranes (especially the 5 μm pore size) used in a dead-end configuration are not particularly representative of membrane processes seen in actual WWTPs. Furthermore, the HA solution used here simply mimics the organic matter found in wastewater. Whereas it has been shown that FC is able to perform MP quantification in this more complex solution condition, the next chapter will further extend the technique through the measurement of MP concentrations in actual wastewater. As such, a bench-scale hollow-fiber MF membrane *module* was employed which operates in a crossflow configuration to process actual 2° clarifier effluent wastewater obtained from a local WWTP. Over the course of four-hour filtration experiments, the wastewater doped with fluorescent PS MBs was filtered and periodic concentration measurements of the MBs were made using the FC instrument. To this end, the FC technique honed in this chapter is extended to a more realistic system such that the performance of an actual membrane module is quantified towards the rejection of MBs.

5.6 Works Cited

- [1] J. Sun, X. Dai, Q. Wang, M. C. van Loosdrecht, and B. J. Ni, “Microplastics in wastewater treatment plants: detection, occurrence and removal,” *Water Research*, vol. 152, pp. 21–37, 2019.
- [2] M. Enfrin, C. Hachemi, D. L. Callahan, J. Lee, and F. Dumée, “Membrane fouling by nanofibres and organic contaminants-mechanisms and mitigation via periodic cleaning strategies,” *Separation and Purification Technology*, vol. 278, pp. 1383–5866, 2022.
- [3] M. Lapointe, J. M. Farner, L. M. Hernandez, and N. Tufenkji, “Understanding and improving microplastic removal during water treatment: Impact of coagulation and flocculation,” *Environmental Science & Technology*, vol. 54, pp. 8719–8727, 2020.
- [4] T. Maes, R. Jessop, N. Wellner, K. Haupt, and A. G. Mayes, “A rapid-screening approach to detect and quantify microplastics based on fluorescent tagging with Nile Red,” *Nature Scientific Reports*, vol. 7, pp. 1–10, 2017.
- [5] H. A. Nel, A. J. Chetwynd, L. Kelleher, I. Lynch, I. Mansfield, H. Margenat, S. Onoja, P. G. Oppenheimer, G. H. S. Smith, and S. Krause, “Detection limits are central to improve reporting standards when using Nile red for microplastic quantification,” *Chemosphere*, vol. 263, p. 127953, 2021.
- [6] G. Erni-Cassola, M. I. Gibson, R. C. Thompson, and J. A. Christie-Oleza, “Lost, but Found with Nile Red: A Novel Method for Detecting and Quantifying Small Microplastics (1 mm to 20 μm) in Environmental Samples,” *Environmental Science & Technology*, vol. 51, pp. 13 641–13 648, 2017.
- [7] M. Pazouki, A. N. Wilton, and D. R. Latulippe, “An experimental study on sterile filtration of fluorescently labeled nanoparticles—the importance of surfactant concentration,” *Separation and Purification Technology*, vol. 218, pp. 217–226, 2019.
- [8] G. Pulido-Reyes, L. Magherini, C. Bianco, R. Sethi, U. von Gunten, R. Kaegi, and D. M. Mitrano, “Nanoplastics removal during drinking water treatment: Laboratory- and pilot-scale experiments and modeling,” *Journal of Hazardous Materials*, vol. 436, p. 129011, 2022.
- [9] X.-S. Wang, H. Song, Y.-L. Liu, X.-R. Pan, H.-C. Zhang, Z. Gao, D.-Z. Kong, R. Wang, L. Wang, and J. Ma, “Quantitatively analyzing the variation of micrometer-sized microplastic during water treatment with the flow cytometry-fluorescent beads method,” *ACS ES&T Engineering*, vol. 1, pp. 1668–1677, 2021.
- [10] E. Dümichen, A. K. Barthel, U. Braun, C. G. Bannick, K. Brand, M. Jekel, and R. Senz, “Analysis of polyethylene microplastics in environmental samples, using a thermal decomposition method,” *Water Research*, vol. 85, pp. 451–457, 2015.
- [11] E. Fries, J. H. Dekiff, J. Willmeyer, M. T. Nuelle, M. Ebert, and D. Remy, “Identification of polymer types and additives in marine microplastic particles using pyrolysis-GC/MS and scanning electron microscopy,” *Environmental Science: Processes & Impacts*, vol. 15, pp. 1949–1956, 2013.
- [12] A. M. Elert, R. Becker, E. Duemichen, P. Eisentraut, J. Falkenhagen, H. Sturm, and U. Braun, “Comparison of different methods for mp detection: what can we learn from them, and why asking the right question before measurements matters?” *Environmental Pollution*, vol. 231, pp. 1256–1264, 2017.

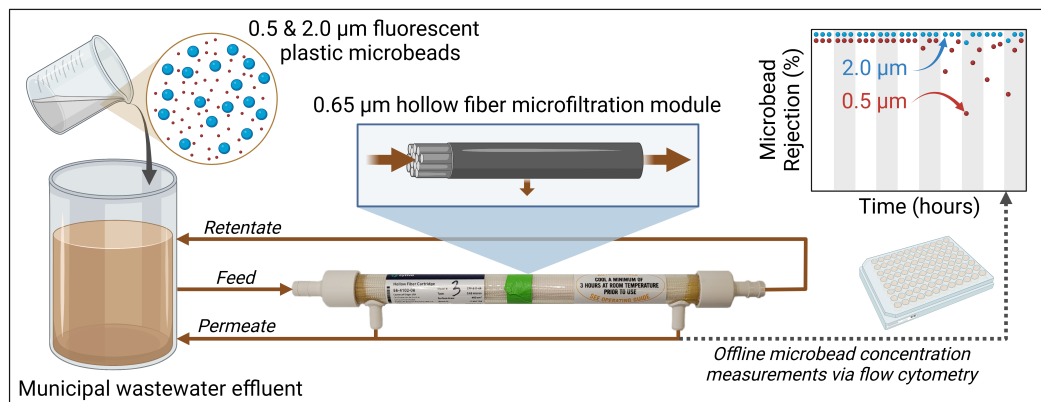
- [13] H. A. Leslie, S. H. Brandsma, M. J. M. Van Velzen, and A. Vethaak, “Microplastics en route: Field measurements in the Dutch river delta and Amsterdam canals, wastewater treatment plants, North Sea sediments and biota,” *Environment International*, vol. 101, pp. 133–142, 2017.
- [14] C. Bretas Alvim, J. A. Mendoza-Roca, and A. Bes-Piá, “Wastewater treatment plant as microplastics release source—Quantification and identification techniques,” *Journal of Environmental Management*, vol. 255, p. 109739, 2020.
- [15] Z. Zhang and Y. Chen, “Effects of microplastics on wastewater and sewage sludge treatment and their removal: A review,” *Chemical Engineering Journal*, vol. 382, p. 122955, 2020.
- [16] F. Caputo, R. Vogel, J. Savage, G. Vella, A. Law, G. D. Camera, G. Hannon, B. Peacock, D. Mehn, J. Ponti, O. Geiss, D. Aubert, A. Prina-Mello, and L. Calzolari, “Measuring particle size distribution and mass concentration of nanoplastics and microplastics: addressing some analytical challenges in the sub-micron size range,” *Journal of Colloid and Interface Science*, vol. 588, pp. 401–417, 2021.
- [17] Z. Gao, L. Chen, J. Cizdziel, and Y. Huang, “Research progress on microplastics in wastewater treatment plants: A holistic review,” *Journal of Environmental Management*, vol. 325, 2023.
- [18] A. Tzur, J. K. Moore, P. Jorgensen, H. M. Shapiro, and M. W. Kirschner, “Optimizing Optical Flow Cytometry for Cell Volume-Based Sorting and Analysis,” *PLOS ONE*, p. e16053, 2011.
- [19] Y. Wang, F. Hammes, K. D. Roy, W. Verstraete, and N. Boon, “Past, present and future applications of flow cytometry in aquatic microbiology,” *Trends in Biotechnology*, vol. 28, pp. 416–424, 2010.
- [20] B. K. Pramanik, S. K. Pramanik, and S. Monira, “Understanding the fragmentation of microplastics into nano-plastics and removal of nano/microplastics from wastewater using membrane, air flotation and nano-ferrofluid processes,” *Chemosphere*, vol. 282, p. 131053, 2021.
- [21] M. Long, I. Paul-Pont, H. Hégaret, B. Moriceau, C. Lambert, A. Huvet, and P. Soudant, “Interactions between polystyrene microplastics and marine phytoplankton lead to species-specific hetero-aggregation,” *Environmental Pollution*, vol. 228, pp. 454–463, 2017.
- [22] M. N. Woods, M. E. Stack, D. M. Fields, S. D. Shaw, and P. A. Matrai, “Microplastic fiber uptake, ingestion, and egestion rates in the blue mussel (*Mytilus edulis*),” *Marine Pollution Bulletin*, vol. 137, pp. 638–645, 2018.
- [23] L. Sgier, R. Freimann, A. Zupanic, and A. Kroll, “Flow cytometry combined with viSNE for the analysis of microbial biofilms and detection of microplastics,” *Nature Communications*, vol. 7, pp. 1–10, 2016.
- [24] N. Kaile, M. Lindivat, J. Elio, G. Thuestad, Q. G. Crowley, and I. A. Hoell, “Preliminary results from detection of microplastics in liquid samples using flow cytometry,” *Frontiers in Marine Science*, vol. 7, p. 856, 2020.
- [25] N. Vakondios, E. E. Koukouraki, and E. Diamadopoulou, “Effluent organic matter (EfOM) characterization by simultaneous measurement of proteins and humic matter,” *Water Research*, vol. 63, pp. 62–70, 2014.
- [26] M. A. Zazouli, S. Nasser, and M. Ulbricht, “Fouling effects of humic and alginic acids in nanofiltration and influence of solution composition,” *Desalination*, vol. 250, no. 2, pp. 688–692, 2010.

- [27] R. Zhuang and J. Wang, “Degradation of diclofenac in aqueous solution by ionizing radiation in the presence of humic acid,” *Separation and Purification Technology*, vol. 234, p. 116079, 2020.
- [28] P. Foladori, A. Quaranta, and G. Ziglio, “Use of silica microspheres having refractive index similar to bacteria for conversion of flow cytometric forward light scatter into biovolume,” *Water Research*, vol. 42, pp. 3757–3766, 2008.
- [29] K. R. Murphy, C. A. Stedmon, D. Graeber, and R. Bro, “Fluorescence spectroscopy and multi-way techniques. PARAFAC,” *Analytical Methods*, vol. 5, no. 23, pp. 6557–6566, 2013.
- [30] E. M. Carstea, J. Bridgeman, A. Baker, and D. M. Reynolds, “Fluorescence spectroscopy for wastewater monitoring: a review,” *Water Research*, vol. 95, pp. 205–219, 2016.
- [31] L. Yang, J. Hur, and W. Zhuang, “Occurrence and behaviors of fluorescence EEM-PARAFAC components in drinking water and wastewater treatment systems and their applications: A review,” *Environmental Science and Pollution Research*, vol. 22, pp. 6500–6510, 2015.
- [32] B. A. G. De Melo, F. L. Motta, and M. H. A. Santana, “Humic acids: structural properties and multiple functionalities for novel technological developments,” *Materials Science and Engineering: C*, vol. 62, pp. 967–974, 2016.
- [33] H. R. Schulten and M. Schnitzer, “A state of the art structural concept for humic substances,” *Naturwissenschaften*, vol. 80, pp. 29–30, 1993.
- [34] R. L. Malcolm and P. MacCarthy, “Limitations in the use of commercial humic acids in water and soil research,” *Environmental Science & Technology*, vol. 20, pp. 904–911, 1986.
- [35] W. Yuan and A. L. Zydney, “Humic acid fouling during ultrafiltration,” *Environmental Science and Technology*, vol. 34, pp. 5043–5050, 2000.
- [36] A. Pradel, S. Ferreres, C. Veclin, H. E. Hadri, M. Gautier, B. Grassl, and J. Gigault, “Stabilization of fragmental polystyrene nanoplastic by natural organic matter: insight into mechanisms,” *ACS ES&T Water*, vol. 1, pp. 1198–1208, 2021.
- [37] A. Bakir, S. J. Rowland, and R. C. Thompson, “Enhanced desorption of persistent organic pollutants from microplastics under simulated physiological conditions,” *Environmental Pollution*, vol. 185, pp. 16–23, 2014.
- [38] Y. Chae and Y. J. An, “Effects of micro- and nanoplastics on aquatic ecosystems: current research trends and perspectives,” *Marine Pollution Bulletin*, vol. 124, pp. 624–632, 2017.
- [39] J. P. da Costa, P. S. Santos, A. C. Duarte, and T. Rocha-Santos, “(Nano)plastics in the environment—sources, fates and effects,” *Science of The Total Environment*, vol. 566–567, pp. 15–26, 2016.
- [40] J. N. Hahladakis, C. A. Velis, R. Weber, E. Iacovidou, and P. Purnell, “An overview of chemical additives present in plastics: migration, release, fate and environmental impact during their use, disposal and recycling,” *Journal of Hazardous Materials*, vol. 344, pp. 179–199, 2018.
- [41] M. Enfrin, L. F. Dumée, and J. Lee, “Nano/microplastics in water and wastewater treatment processes—origin, impact and potential solutions,” *Water Research*, vol. 161, pp. 621–638, 2019.
- [42] W. L. Chandler, W. Yeung, and J. F. Tait, “A new microparticle size calibration standard for use in measuring smaller microparticles using a new flow cytometer,” *Journal of Thrombosis and Haemostasis*, vol. 9, pp. 1216–1224, 2011.

- [43] O. Julià, J. Comas, and J. Vives-Rego, “Second-order functions are the simplest correlations between flow cytometric light scatter and bacterial diameter,” *Journal of Microbiological Methods*, vol. 40, pp. 57–61, 2000.
- [44] M. Díaz, M. Herrero, L. A. García, and C. Quirós, “Application of flow cytometry to industrial microbial bioprocesses,” *Biochemical Engineering Journal*, vol. 48, pp. 385–407, 2010.
- [45] P. Foladori, L. Bruni, S. Tamburini, and G. Ziglio, “Direct quantification of bacterial biomass in influent, effluent and activated sludge of wastewater treatment plants by using flow cytometry,” *Water Research*, vol. 44, pp. 3807–3818, 2010.
- [46] M. R. García, J. A. Vázquez, I. G. Teixeira, and A. A. Alonso, “Stochastic individual-based modeling of bacterial growth and division using flow cytometry,” *Frontiers in Microbiology*, vol. 8, p. 2626, 2018.
- [47] Y. Jacobi, G. Yahel, and N. Shenkar, “Efficient filtration of micron and submicron particles by ascidians from oligotrophic waters,” *Limnology and Oceanography*, vol. 63, pp. S267–S279, 3 2018.
- [48] W. Liu, J. Zhang, H. Liu, X. Guo, X. Zhang, X. Yao, Z. Cao, and T. Zhang, “A review of the removal of microplastics in global wastewater treatment plants: Characteristics and mechanisms,” *Environment International*, vol. 146, p. 106277, 2021.
- [49] R. Qiao, Y. Deng, S. Zhang, M. B. Wolosker, Q. Zhu, H. Ren, and Y. Zhang, “Accumulation of different shapes of microplastics initiates intestinal injury and gut microbiota dysbiosis in the gut of zebrafish,” *Chemosphere*, vol. 236, p. 124334, 2019.
- [50] J. Toepel, U. Langner, and C. Wilhelm, “Combination of flow cytometry and single cell absorption spectroscopy to study the phytoplankton structure and to calculate the chl *a* specific absorption coefficients at the taxon level,” *Journal of Phycology*, vol. 41, pp. 1099–1109, 2005.
- [51] A. L. Koch, B. R. Robertson, and D. K. Button, “Deduction of the cell volume and mass from forward scatter intensity of bacteria analyzed by flow cytometry,” *Journal of Microbiological Methods*, vol. 27, pp. 49–61, 1996.
- [52] L. Galbusera, G. Bellement-Theroué, A. Urchueguia, T. Julou, and E. van Nimwegen, “Using fluorescence flow cytometry data for single-cell gene expression analysis in bacteria,” *PLOS ONE*, vol. 15, 2020.

Chapter 6

Scaling-Up Microplastic Removal Studies to a Hollow Fiber Microfiltration Membrane Module



6.1 Introduction & Motivations

In §1.3.2, an assertion is made regarding the existence of two contrasting bodies of research studies involving particles which can be construed as microplastics (MPs), where each body exists on a spectrum of “scale”. At one end of the spectrum, there exist many large-scale observational studies (*e.g.* [1–5]) of wastewater treatment plants (WWTPs) where investigators passively assess the ability of the facilities to remove MPs. These types of studies typically deal with large facilities which can potentially process hundreds of millions of liters of complex wastewater each day, where various water quality parameters can change substantially over time [6], and sampling can take place

over days/seasons/etc. To prevent disruptions in these facilities, investigators can usually only take samples without directly changing variables of interest or controlling for factors which may be transient (*e.g.* suspended solids concentration). Specific information regarding the membrane processes in these studies is often not detailed. For example, Ziajahromi *et al.* (2017) assessed the removal characteristics of a facility which uses ultrafiltration (UF) and reverse osmosis (RO) membranes [7]. While they report MP concentrations in the process streams, they do not provide any information regarding the membrane manufacturer(s), the pore size of the UF membranes, the operating fluxes, the transmembrane pressures, nor any other membrane properties or operational conditions. At the opposite end of the spectrum, there exist many laboratory-scale experimental studies (*e.g.* [8–12]) where fundamental filtration phenomena are actively probed using various polymer nano- and micro-particles. These types of studies, in contrast, typically deal with small volumes of relatively simple solutions (*e.g.* buffers), well-characterized particles (*e.g.* spherical polystyrene latexes), and short experimental durations. As these experiments are performed under controlled settings, individual parameters can be varied and investigated. As an example, Kirschner *et al.* (2019) formulated and tested a series of models to describe UF membrane fouling in a crossflow configuration [11]. In their experiments, the researchers suspended 0.22 μm polystyrene (PS) latex microbeads in a pH 6 buffer solution with a fixed ionic strength. Fairly short (*i.e.* < 3 h) crossflow filtration experiments at constant flux were performed by challenging flat sheet polyethersulfone (PES) UF membranes (*Nanostone PES-10*; area = 19.4 cm^2) to 200 mg/L suspensions of the particles in order to validate the particle fouling models that were proposed. Clearly, there are significant differences between the regions where these two studies were performed in terms of experimental scale, solution complexity, duration, the microparticles/membranes involved, and so on.

Between these regions at the two extremes of the spectrum lies a large region which involves investigations performed using *moderate* volumes of fluid, membrane areas, and experimental durations (*e.g.* “pilot scale”). Unfortunately, this region contains relatively few studies. However, the opportunity is presented for the commission of novel filtration research involving MPs and membranes. An illustration of this opportunity can be seen in Figure 6.1. As an example of a study performed within this central region on the spectrum, Li *et al.* (2020) performed a month-long experiment which assessed the performance of two parallel membrane bioreactors (MBRs; unspecific membrane; pore size = 0.1 μm ; area = 0.1 m^2): one system where polyvinyl chloride MP particles

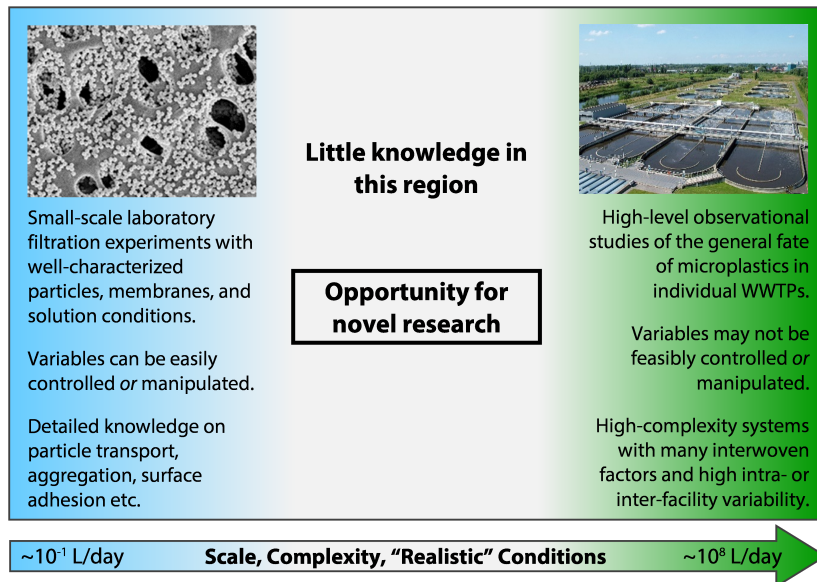


Figure 6.1: Spectrum illustrating the two main “scales” of investigations involving MPs and membranes and the opportunity for novel research that is created as a result.

(PVC; $< 5 \mu\text{m}$) were added, versus one control system where no MPs were added [13]. They noted that the removal performance of organics and nutrients immediately declined following the addition of the MPs to the first bioreactor, versus no change in performance in the second bioreactor where no MPs were added. They also found that membrane fouling was exacerbated when the MPs were added to the feed wastewater, evidenced by higher transmembrane pressures (TMPs) in the constant-flux experiments. Furthermore, the authors noted that MPs were not detected in the permeate water of the MBR, however, they were not diligent in their assessment of transmitted MPs: the stated pore size of the filter ($0.45 \mu\text{m}$) used to isolate MPs in permeate samples was *larger* than that of the MBR membrane. However, scaling this process upwards allowed for new insights to be gained, not just regarding the membrane in isolation, but how it interacted with the biological process as well.

New insights in the field of membrane science share a complementary outlook regarding the opportunities for novel research. In their 2022 perspective piece entitled “Membrane research beyond materials science”, U. Beuscher, E.J. Kappert and J.G. Wijmans assert that the field of membrane science largely focuses on the development of new membrane materials rather than the deployment of these materials into modules, modules into processes, and processes into overall applications [14]. In order to successfully implement new innovations in the field, they advocate for a holistic approach

to the development of membrane technologies which not only considers the membrane material, but the module and the membrane process, in addition to their mutual interconnections. However, the authors note that “research on modules and processes is indeed crucial for the success of membrane technology, but also that for various reasons this research is rarely carried out” [14]. In the context of 3^o wastewater treatment, the membrane materials that are used are fairly mature, thus the “real” opportunity for improvement lies above the level of the membrane material, in the module or the process. We can see at a fundamental level (*e.g.* Chapter 4) that a particular membrane should be very effective towards the removal of MPs, however, only once that membrane coupon is scaled up and sealed into a module can we start to encounter additional considerations. Properties at the module level including the flow configuration (crossflow versus dead-end), packing density, spacer thickness, the impact of concentration polarization and fouling governed by the module hydrodynamics, and the structural stability have an impact on the feasibility and performance of the process [14].

Given the opportunity for novel research highlighted on the spectrum in Figure 6.1 and the approach advocated by Beuscher and colleagues, the direction which needs to be taken is clear in order to evaluate membranes as candidate technologies in 3^o treatment applications. The scale of studies should shift from left side of the spectrum to regions of greater scale, complexity, and integration within the overall process—while still maintaining the ability to change variables of interest and keeping others constant. To this end, the study presented herein builds upon the work completed in previous chapters and characterizes the performance of bench-scale hollow fiber microfiltration (MF) membrane *modules* operated in a crossflow configuration with alternating filtration/backwashing cycles to simulate treatment in a real facility. Data from the filtration of actual 2^o effluent wastewater doped with *two* different sizes of monodisperse fluorescent plastic microbeads¹ (MBs; 0.5 μm and 2 μm) is presented. The goal, here, is to characterize membrane fouling and MB rejection within this module over many filtration/backwashing cycles, simulating longer-term operations in a real WWTP. Furthermore, the effects of the feed crossflow velocity in the module are considered along with the fate of the MBs during backwashing processes.

The careful selection of a membrane module was necessary in order to sufficiently mimic the types of 3^o membrane filtration processes seen in actual WWTPs and to achieve the objectives of this study.

¹Recall: the term “*microbead*” is used as a specific sub-category of small *microplastic* that is spherical in shape.

Ultimately, bench-scale *Cytiva Xampler CFP-6-D-4A* hollow fiber crossflow MF membrane modules were purchased for use in this study; they are described subsequently in §6.2.3.1. In particular, the following characteristics of the chosen modules should be noted:

- ▶ A hollow-fiber membrane module was chosen as hollow fiber UF/MF is commonly used in wastewater applications. The hollow fibers are amenable to backwashing, and the crossflow filtration mode is preferable as it can lower the potential for fouling. In some instances, *dead-end* crossflow filtration is used (*e.g. no retentate flow*) as the water recovery can be higher. However, significant efforts are needed (*e.g. additional backwashing*) to account for the greater rate of fouling that is incurred [15]. Hollow fiber filtration can operate with an inside-out or outside-in flow path [15], depending on the membrane and the process, though outside-in flow paths are quite commonly seen in commercial modules (*e.g. Pall's Microza™* line of 0.1 μm MF membranes). Conversely, Cytiva emphasizes that their product *must* be used with an inside-out flow path. In this configuration, the simple hydrodynamics are actually quite amenable to preventing membrane fouling due to the high shear rates attainable inside the hollow fiber lumens [16], though it must be acknowledged that the hydrodynamics are expected to differ in comparison to the more complex outside-in flow paths seen in some other modules [17].
- ▶ MF membranes are commonly used in 3rd wastewater treatment for removing leftover suspended solids and organic matter to produce a high-quality final effluent [18]. MF is also useful as a pre-treatment step before subsequent nanofiltration or RO processes [19]. MF nominal pore sizes between 0.1 μm and 0.45 μm are commonly seen in WWTP membrane modules. A slightly larger nominal pore size of 0.65 μm , however, was selected so that larger, more easily detectable MBs could be sourced and used in this work. Furthermore, one size of MB (2 μm) was chosen to be larger than the nominal pore size (high expected rejection) and one size of MB (0.5 μm) was chosen to be smaller than the nominal pore size (low expected rejection).
- ▶ A “bench-scale” MF module was desired in this study—that is, a series of membranes pre-assembled into a module with a total area between those used in small-scale filtration experiments (*i.e.* a few cm^2) and those used in commercial applications (*i.e.* tens of m^2). Unfortunately at the time, few companies stocked full hollow fiber MF modules that possessed the desired properties and were still at a manageable size scale. Potential options included *Repligen's Spectrum®* line of MF modules, Sartorius' line of hollow-fiber tangential flow membrane

modules, or Cytiva’s *Xampler* line of MF modules. Toray also manufactures an interesting offering, the *Torayfil*TM *HFU* module, but it is only produced with a 150 kDa ultrafiltration membrane. Tradeoffs associated with cost, lead time,² and membrane module properties led to the selection of the Cytiva module.

While the chosen module possesses many of the desired attributes for this experiment at a manageable size scale (*e.g.* 460 cm²), the membrane choice does present a few limitations in this application. Firstly, it has a polysulfone (PSf) chemistry which is not typically used in wastewater treatment applications; in contrast, polyvinylidene fluoride (PVDF) is much more commonly seen [15]. As such, membrane-MB or membrane-solids interactions may not be representative of the interactions seen in an actual WWTP. Furthermore, the Cytiva modules are geared towards bioprocessing applications, so their performance may not be perfectly representative of a MF module specifically designed for use in WWTPs.³ Regardless, scaling up the MF process to this degree presents the opportunity to provide new and valuable insights with respect to membrane module filtration performance in the presence of MPs.

6.2 Materials & Methods

6.2.1 Chemicals & Wastewater

High-purity milliQ water with a resistivity of 18.2 M Ω ·cm was produced by an *EMD Millipore milliQ Reference* system. 1 M citric acid, 3 M HCl, and 1 M NaOH solutions were obtained from VWR Chemicals BDH. All chemicals mentioned herein were used as-received.

Wastewater was collected in 5-gallon buckets from the surface of a 2° clarifier at the Dundas Wastewater Treatment Plant (Hamilton, Ontario). This wastewater was subsequently stored at 4°C until it was needed for filtration experiments. Aliquots of the wastewater were taken and characterized in triplicate to ascertain the quality parameters associated with each bucket. The test methodologies are previously described in §2.2.3. A summary of the quality parameters for wastewater samples used in experiments in this study can be found in Table 6.1.

²At this time, supply chain issues were rampant in manufacturing due to the COVID-19 pandemic.

³See Beuscher *et al.*’s discussion regarding developing membrane technologies for their end use application [14].

Table 6.1: Properties of wastewater (WW) samples used in this study. The average of three measurements is presented \pm one standard deviation. TS = total solids; TOC = total organic carbon; COD = chemical oxygen demand.

Wastewater Sample	TS (mg/L)	TOC (mg/L)	COD (mg/L)	pH	Conductivity (μ S/cm)
WW1	777 \pm 13	38.3 \pm 0.4	6 \pm 5	7.14 \pm 0.02	1,193 \pm 38
WW2	758 \pm 19	11 \pm 1	20 \pm 4	7.12 \pm 0.03	1,558 \pm 22
WW3	640 \pm 10	8.91 \pm 0.04	19 \pm 2	6.73 \pm 0.06	1,012 \pm 15
WW4	640 \pm 10	9.78 \pm 1	21 \pm 6	6.73 \pm 0.04	1,005 \pm 21
WW5	665 \pm 35	8.50 \pm 0.4	19 \pm 2	6.73 \pm 0.09	1,009 \pm 8

Prior to use in filtration experiments, the wastewater was passed through a polypropylene commercial bag filter (Pentek) to remove aggregates, prolonging the lifespan of the membrane module. This step was necessitated from prior experimentation (data not shown).

6.2.2 Preparation & Characterization of Microbeads

Carboxylated polystyrene (PS) MBs with nominal sizes of 0.5 μ m and 2.0 μ m were purchased from ThermoFisher Scientific (*Invitrogen FluoSpheres*; Lots 2339877, 2521052, & 2342759) as 2% aqueous latex suspensions. Using a proprietary swelling process, the manufacturer labelled each size of MB with a particular fluorophore: the 0.5 μ m MBs contained a “red” fluorophore ($\lambda_{ex}/\lambda_{em} = 580/605$ nm) while the 2 μ m MBs contained a “blue” fluorophore ($\lambda_{ex}/\lambda_{em} = 365/415$ nm). From these as-purchased suspensions, 100 mg/L stock suspensions of MBs were prepared in milliQ water to be diluted and used in subsequent experiments. All as-purchased, stock, and diluted suspensions were sonicated in a bath (Branson) for a minimum of 30 minutes prior to dilution or further use in order to disaggregate the microparticles. For filtration experiments, suspensions of both sizes of MBs were sonicated, then added to wastewater to final concentrations of 1 mg/L 0.5 μ m MBs and 1 mg/L 2 μ m MBs. As noted in §3.2.4, no attempts were made to characterize the “natural” concentrations of MPs as it was deemed that the MPs doped into the wastewater would significantly outnumber any that were already present.

The MBs were subsequently imaged using field-emission scanning electron microscopy (FESEM). Samples were prepared by cleaning silicon wafers with Piranha solution—3:1 98% sulfuric acid (Caledon Laboratories Ltd.) to 30% hydrogen peroxide (FisherSci)—for one hour. 100 mg/L suspensions

of 0.5 μm or 2 μm MBs in milliQ water were sonicated for one hour, then individually aliquoted onto separate silicon wafers. The droplets were left to dry, then the wafers were mounted on aluminum stubs and sputter-coated with 5 nm of platinum. The samples were finally imaged at 2.0 kV using a JEOL 7000F FESEM instrument, as seen in Figure 6.2A–B.

The MBs were also characterized via dynamic light scattering (DLS) measurements. 10 mM citric acid was prepared using milliQ water and then titrated via NaOH/HCl to produce buffered solutions with pH values between 3.5 and 7.5. 100 mg/L suspensions of 0.5 μm or 2 μm MBs were then prepared in the pH-adjusted citrate buffers. The suspensions were analyzed in triplicate in disposable plastic cuvettes using a Malvern Zetasizer Nano ZS instrument (173° backscatter angle). Each measurement consisted of 12 runs and was performed at a constant temperature of 25°C. The accompanying Zetasizer software was used to obtain “size” results, assuming a refractive index of the PS latex of 1.59. The results are summarized in Figure 6.2C–D and indicate that the particles

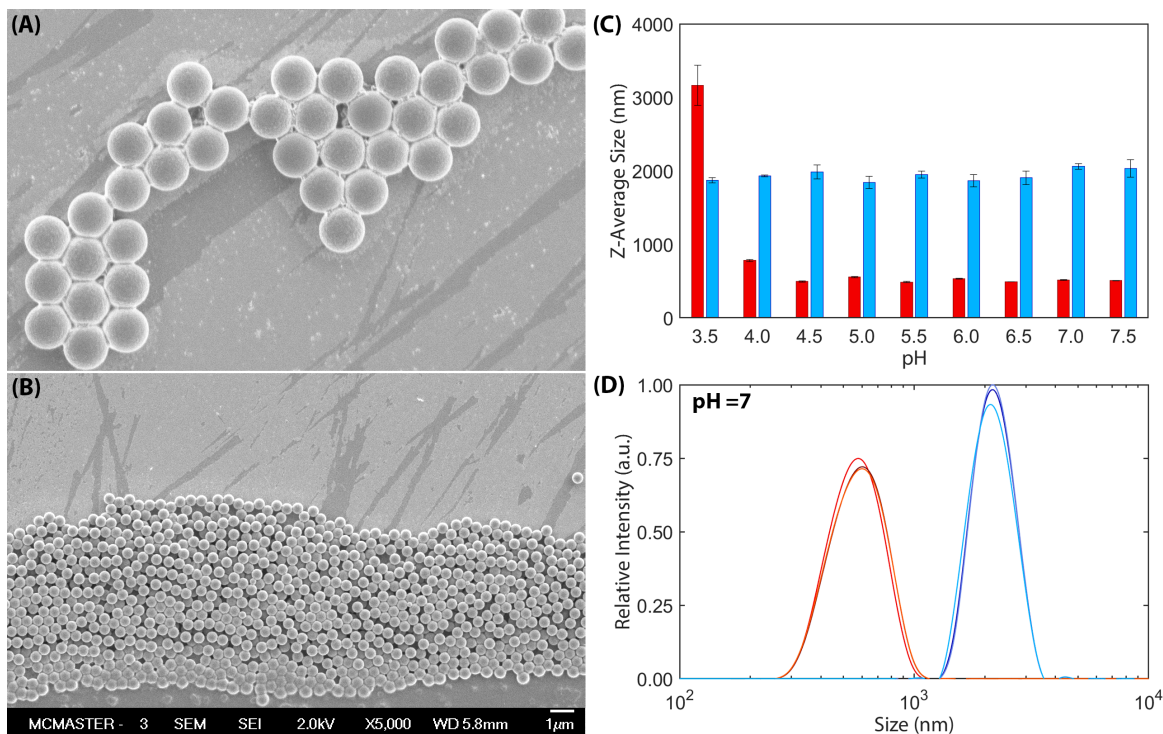


Figure 6.2: Characterization of the Invitrogen FluoSphere MBs used in this study. FESEM images of the (A) 2 μm and (B) 0.5 μm MBs. (C) DLS results corroborate the average sizes of the 2 μm (■) and 0.5 μm (■) MBs in suspension. (D) Via DLS, a demonstration of the dispersity of the particles at an environmentally-relevant pH of 7 is shown. The error bars in Panel (C) refer to one standard deviation about the average size of the particles from triplicate measurements.

are stably suspended at pH levels 4.0 and greater, and are quite narrowly-disperse.

6.2.3 Filtration Experiments

6.2.3.1 Membrane Module Properties

For use in filtration experiments, three membrane modules containing parallelized hollow fiber membranes having a nominal 0.65 μm pore size were purchased from Cytiva Life Sciences: one module was used to calibrate the system (data not reported) and two modules were used in filtration experiments (data reported). The modules were equipped with barbed feed and retentate ports and dual permeate ports (merged together) enabling crossflow filtration. Table 6.2 highlights the properties of the modules and the membranes within. Refer to Figure 6.3 for an image of a module and FESEM images which reveal the internal structure of the hollow fiber membranes.

6.2.3.2 Apparatus

A filtration apparatus was customized to service the Cytiva membrane modules. A piping and instrumentation diagram (P&ID) depicting the construction of the system set up for normal operation can be found in Figure 6.4. An extended version of this P&ID as well as a summary of the valve/instrumentation codes can be located in Appendix D.1.

Table 6.2: Properties of the Cytiva membrane and module used in this study, as reported by the manufacturer.

Property	Value
Name	Xampler Microfiltration Cartridge
Model	CFP-6-D-4A
Nominal Membrane Pore Size	0.65 μm
Membrane Geometry	Unsupported hollow fiber
Membrane Chemistry	Polysulfone
Normal Filtration Flow path	Inside-out
Normal Filtration Mode	Crossflow
Nominal Membrane Area	460 cm^2
Fibers per Module	75
Nominal Fiber Inner Diameter	0.75 mm
Module Length	36.2 cm
Hold-Up Volume (Lumen Side)	10 mL
Hold-Up Volume (Shell Side)	40 mL

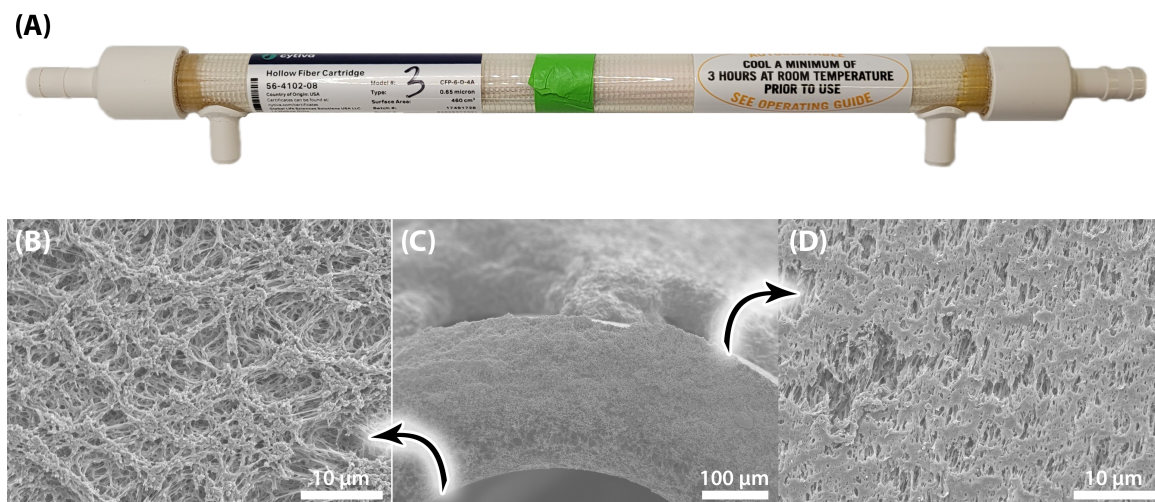


Figure 6.3: Depiction of the Cytiva Xampler 0.65 μm MF membrane module used in this study. (A) Image of the entire module containing 75 individual hollow fiber membranes arranged in parallel. For reference, the module is 36.2 cm in length. (B–D) FESEM images showing the microstructure of the hollow fiber membranes. (B) Top-down image of the inner surface of a hollow fiber (lumen). (C) Cross-sectional image of a single hollow fiber, showing the internal structure of the membrane. (D) Top-down image of the outer surface of a hollow fiber.

Briefly, a polyethylene (PE) feed tank (nominally 37.8 L) supplied a diaphragm pump (Wanner Engineering Hydra-Cell M03) equipped with a variable frequency drive (VFD) to allow for the pump speed and volumetric output to be controlled. During typical filtration experiments, pressurized water from the pump was fed to the membrane module whereby water which permeated through the membrane (inside-out flow path) was directed back into the feed tank via the permeate return line. The water that did not pass through the membrane exited the module via its retentate port and was also directed back into the tank via its dedicated return line. As such, the system was operated in full-recycle mode.

Periodic backwashing (BW) was achieved using a second variable-speed gear pump (Cole-Parmer 75211-50) which drew BW solution from a second tank and fed it to the module's permeate port, through the membrane, and out of the module via the retentate port where it was evacuated from the apparatus. The BW water was not recycled.

The transmembrane pressure (TMP) and water flow rates were monitored and logged via pressure and flow transducers (Omega Engineering). Three USB pressure transducers (Omega PX409) were

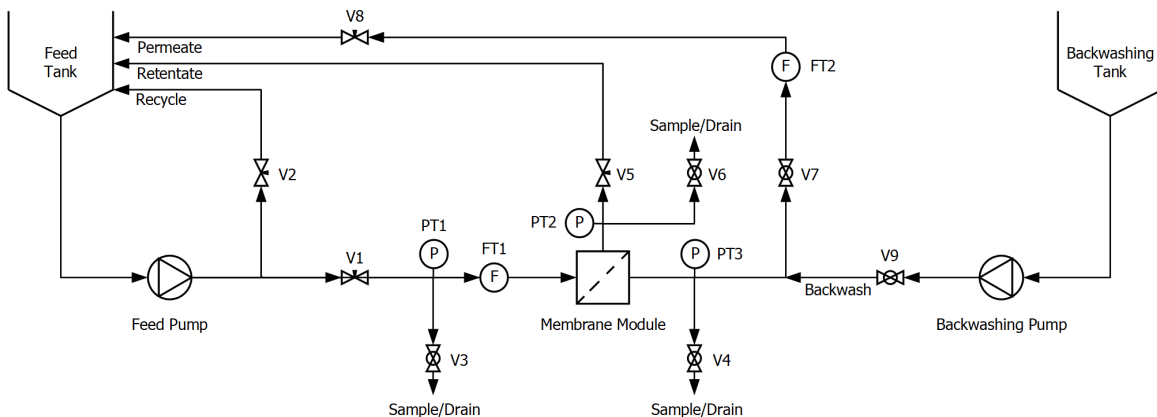


Figure 6.4: Simple P&ID of the membrane module evaluation setup. A more detailed version of this diagram can be found in Figure D.1.

located near the feed, retentate, and permeate ports of the membrane module; pressure data was acquired directly via USB with Omega’s Digital Transducer Application. Using the pressure data, the TMP at a given timepoint t was calculated as follows:

$$TMP(t) = \frac{P_{feed}(t) + P_{ret}(t)}{2} - P_{perm}(t) \quad (6.1)$$

where P_{feed} , P_{ret} , and P_{perm} are the measured feed (via $PT1$), retentate (via $PT2$), and permeate (via $PT3$) pressures in matching units (*e.g.* psi).

Water flow rates were measured via paddlewheel (*Omega FPR302*; K -value = 618) and turbine (*Omega FLR1008ST*) flow meters plumbed into the feed and permeate lines, respectively. Flow rate data acquisition (DAQ) was achieved using a *National Instruments USB-6000 Multifunction I/O Device* DAQ board and *LabView 2015* software. Thus, the permeate water volumetric flux $J_v(t)$ (LMH) was calculated from the measured volumetric flow rate of permeate water $Q_{perm}(t)$ (via $FT2$) at each timepoint t , as seen previously in Equation 2.2, where $A = 0.046 \text{ m}^2$ (see Table 6.2).

6.2.3.3 Operational Protocol

In this work, the membrane modules were evaluated according to a set of strictly-controlled protocols in order to maximize the comparability of the tests that were performed on one module versus the other. Operational parameters in this section were informed by membrane manufacturer recommen-

dations, data in the literature (*e.g.* [16, 20]), and personal experience. Initial experiments consuming one of the three membrane modules were heavily used to inform the selection of these parameters (*e.g.* operation below the so-called “critical flux” [14, 21]). In each experiment that was performed, the following (simplified) procedure was used, except where explicitly identified otherwise:

1. **Washing.** The module was flushed with copious amounts of deionized (DI) water to remove any membrane preservative.
2. **Hydration.** Prior to any experimentation, the module was acclimated with DI water, with the pump held at a constant VFD setting (“15 Hz”, producing $\sim 2.3 \pm 0.4$ L/min). The TMP was manually maintained at 5 psi predominately through the use of the feed and recycle valves (*V1*, *V2*) which diverted the water towards/away from the recycle stream to maintain the TMP. DI water was recycled from both the retentate and permeate streams back to the tank. This process served to hydrate the membrane, remove any soluble residues which might affect filtration performance, and pre-compact the membrane module.
3. **Filtration experiment.** Filtration experiments commenced by charging the feed tank with ~ 15 L of 2° clarifer effluent wastewater—with or without MBs, depending on the experiment that was performed. Each experiment was divided in 24 filtration/BW cycles:

3.1 **Filtration.** In each cycle, wastewater was filtered in a crossflow mode at *constant pressure* and fixed pump output (VFD = 15 Hz). As usual, the TMP was manually held at 0.5 psi. The system operated in a full recycle loop such that the permeate and retentate water was recycled back to the feed tank. During this phase, the TMP, permeate flux, and feed flow rate measurements were constantly recorded to data files on an accompanying laptop computer. Feed samples of ~ 10 mL were taken from the feed sample valve (*V3*) at the start of every filtration cycle (*i.e.* $t \approx 0$ min). Samples of permeate water were taken from the permeate sample valve (*V4*) at 1, 5, and 9 minutes after the start of each filtration cycle. Samples were collected in glass scintillation vials and stored at 4°C until needed.

3.2 **Backwashing.** Following ten minutes of filtration, the membrane module was isolated from the wastewater feed, and the BW valve (*V9*) and retentate drain valve were opened (*V6*). A chemically-enhanced backwashing (CEB) process proceeded at a high flow rate (~ 2.5 L/min) for one minute, whereby the BW water was discarded through the open retentate drain valve. As recommended by the membrane manufacturer, 0.2% Tergazyme®

enzymatic cleaning powder was dissolved in DI water and used as a CEB solution. Subsequently, the applicable drain valves ($V4$, $V6$) were allowed to open to allow the majority of the BW solution to leave the module and apparatus; a small amount of feed wastewater was also introduced to purge the remaining solution before the drain valves were closed.

The repetition of filtration/BW cycles proceeded for a total of four hours at which point, the wastewater was drained from the system.

4. **Cleaning.** Following each filtration experiment, the apparatus and membrane module were thoroughly cleaned, using parameters derived from the membrane module’s manufacturer’s usage instructions.

4.1 **Initial tank rinse.** The tank was filled with DI water which was pumped through the apparatus at a fixed output ($VFD = 15$ Hz) with the feed pressure to the membrane module held constant at 5 psi, as before. The water was *not* recycled back in the tank through the permeate/retentate lines, but sent to the drain instead. This fill/drain process was performed a total of three times.

4.2 **Warm chemical cleaning.** Subsequently, the tank was charged with 0.2% Tergazyme® solution heated to 40–50°C using a removable immersion heating coil. The membrane manufacturer recommended the higher temperature for better cleaning performance. This solution was recirculated (full recycle mode) through the membrane module ($VFD = 15$ Hz; feed pressure = 5 psi) for a total of one hour.

4.3 **Final tank rinse.** The “initial tank rinse” protocol was performed again in triplicate to rid the apparatus of leftover Tergazyme® and solids.

5. **Storage.** The cleaned membrane module was removed from the apparatus and impregnated with a 0.1 w/v% solution of sodium azide (Sigma-Aldrich) in milliQ water as a preservative, as recommended by the membrane manufacturer. The fittings were plugged, and the module was stored at 4°C until its next use.

Deviations from this procedure are explicitly indicated in the text.

6.2.3.4 Experiments Performed

In this work, a series of filtration experiments were designed to investigate the performance of the membrane modules. Experiments were performed first with no MBs (“Condition A”) to elucidate the baseline performance of the membranes, with subsequent tests (“Conditions B & C”) performed using 1 mg/L of each of the 0.5 μm and 2 μm MBs. A summary of the experiments and experimental conditions that were used can be found in Table 6.3. It should be noted that the conditions were tested in the same order (A \rightarrow C) for both modules so that the comparability could be maximized.

6.2.4 Analysis via Flow Cytometry

Similar to what was described in §5.2.5, the concentrations of MBs in permeate and feed samples were measured using a *Beckman Coulter Cytoflex LX* flow cytometry (FC) instrument. Separate excitation lasers and emission filters were used *in parallel*, corresponding to the different fluorophores incorporated into the 0.5 μm and 2 μm MBs. The quasi-optimal gains corresponding to the side scattering (SSC) signal intensity, the forward scattering (FSC) signal intensity, and the emission filter fluorescent intensities were determined empirically from stock MB suspensions; these values were *fixed* and used in each subsequent experiment. A SSC signal intensity *threshold* was used to discard events where $|SSC| < 10^4$ a.u. in order to remove the significant background noise (at low SSC intensities) which overwhelmed the detector when attempting to resolve the signals from the very small 0.5 μm MBs. A full list of FC parameters used can be found in Table 6.4. In a given analysis, 150 μL samples were pipetted into 96-well round-bottomed microplates and analyzed via FC on the same day that they were produced. 50 μL aliquots were drawn from each well, allowing

Table 6.3: List of experimental conditions and wastewater (WW) samples used in each experiment performed in this study.

	Module A	Module B
Condition A: Wastewater Only High Crossflow Velocity	Experiment #1 WW1	Experiment #2 WW2
Condition B: Wastewater + 1 mg/L MBs (Each) High Crossflow Velocity	Experiment #3 WW3	Experiment #4 WW4
Condition C: Wastewater + 1 mg/L MBs (Each) Low Crossflow Velocity	Experiment #5 WW5	Not Performed

for MB counts to be recorded over a known volume. Note that the instrument was calibrated daily using microbead standards, pursuant to manufacturer specifications, to ensure the validity and reproducibility of the results that were obtained.

As before, results were analyzed using FlowJo software. Measurements of FSC intensity by peak height (FSC-H) and emission filter fluorescent intensities by peak height (“Y610-H” for 0.5 μm MBs; “NUV450-H” for 2 μm MBs) were used in the analysis: plots of FSC-H versus Y610-H and FSC-H versus NUV450-H were created, and empirical gates were developed to categorize applicable events to one of the two MB sizes. Here, FSC/Y610/NU450 signal peak *heights* were used as oppose to the *areas* used in Chapter 5 as the smaller MBs employed in this study empirically were more discernible when viewing signals by peak height rather than peak area. Again for the purposes of consistency, the gates shown in Table 6.4 were used in *every FC analysis* presented herein. For reference, plots of FSC-H versus Y610-H *and* NUV450-H (with gates) for a 1 mg/L “standard” sample of *both* MBs in milliQ water can be seen in Figure D.2. Finally, an analysis of the consistency of the FC technique can be seen in Table D.2 which shows that MBs are reliably quantified by the instrument.

Table 6.4: Detailed list of flow cytometer operational parameters and polygonal gates used in quantifying MB concentrations.

General Parameters	
FSC Detector Gain (a.u.)	100
SSC Detector Gain (a.u.)	400
SSC Lower Threshold (a.u.)	10^4
Backwashing Time Per Sample	10 seconds
Mixing Time Per Sample	5 seconds
Sample Flow Rate	50 $\mu\text{L}/\text{min}$
0.5 μm MBs	
Excitation Laser	Yellow-Green ($\lambda_{ex} = 561 \text{ nm}$)
Emission Filter	Y610 ($\lambda_{em} = 610 \text{ nm}$)
Y610 Detector Gain (a.u.)	50
Polygon Vertices of MB Gate (Y610-H, FSC-H) in a.u.	$(6 \times 10^4, 10^6)$ ($10^7, 10^6$) $(2.5 \times 10^3, 5 \times 10^2)$ ($7 \times 10^4, 10^2$)
2 μm MBs	
Excitation Laser	Near-UV ($\lambda_{ex} = 375 \text{ nm}$)
Emission Filter	NUV450 ($\lambda_{em} = 450 \text{ nm}$)
NUV450 Detector Gain (a.u.)	1
Polygon Vertices of MB Gate (NUV450-H, FSC-H) in a.u.	$(2 \times 10^3, 10^6)$ ($2 \times 10^5, 10^6$) $(2 \times 10^3, 7.5 \times 10^4)$ ($2 \times 10^5, 7.5 \times 10^4$)

6.2.5 Analysis via Confocal Laser Scanning Microscopy (CLSM)

In preparation for confocal laser scanning microscopy (CLSM) analysis, membrane modules were dissected following the completion of all filtration experiments. The module casing was removed and the individual hollow fibers were separated from the module right at the potting resin. Individual hollow fibers were selected at random from the modules and ~ 1 cm sections were cut to be imaged. The fiber sections were sliced in half length-wise (“half-sections”) to exposure the surfaces of their lumens.

Fluorescein isothiocyanate isomer I (FITC; 90% purity) dye was obtained from Sigma-Aldrich and dissolved to a concentration of 1 mg/mL in methanol (Sigma-Aldrich). Sufficient dye solution was dropped onto the PSf hollow fiber half-sections in order to cover them. The methanol was left to evaporate, leaving a coating of fluorescent FITC on the surfaces of the membranes. This was performed so that the membrane, itself, could be seen via CLSM.

Imaging of lumen surfaces of the hollow fiber half-sections was performed using a *Nikon AIR* confocal laser scanning microscope mounted on a *Nikon Ni-E Eclipse* upright base using a 10 \times objective lens. Three lasers were used to excite the fluorescent FITC dye which stained the membranes as well as the deposited fluorescent MBs. Excitation/emission wavelength pairs of 405/447 nm (*i.e.* DAPI filter; 57 nm bandpass), 561/652 nm (*i.e.* TRITC filter; 45 nm bandpass), 488/521 nm (*i.e.* FITC filter; 42 nm bandpass), were used to visualize the 2 μm MBs, 0.5 μm MBs, and membrane surfaces, respectively. Images were obtained in resonant mode with a field of view spanning 1,270 by 1,270 μm . The depth that was imaged (~ 500 μm ; z -step ≈ 2 μm) was dependent on the actual thickness of the sample. Efforts were made to keep the laser power levels/detector gains constant when analyzing half-sections from a given hollow fiber. The collected CLSM images were processed and analyzed using Nikon’s *NIS-Elements AR* software.

6.3 Results & Discussions

6.3.1 Module Performance in the Filtration of Wastewater Only

In the first two experiments that were performed (Condition A; Experiments #1–2), only 2 $^\circ$ clarifier effluent wastewater was filtered—no MBs were added. This serves as a “baseline case” for the

performance of the modules in the absence of added MBs. Results for both of the modules under this condition are shown in Figure 6.5. Note that this figure is divided into 24 “sections”, each of which represents an independent 10-minute filtration cycle followed by a membrane backwash (no data shown). The top row summarizes the TMP over the course of the experiments, as calculated via Equation 6.1. Since a constant-pressure filtration mode was used ($\text{TMP} = 0.5 \text{ psi}$), it is unsurprising that the TMPs over the course of both experiments with Module A and B were relatively steady at $0.52 \pm 0.03 \text{ psi}$ and $0.54 \pm 0.02 \text{ psi}$, respectively (average \pm one standard deviation). In contrast, the measured permeate wastewater fluxes shown in the bottom row—calculated as outlined in §2.1.2.1—were not constant. It should be noted that over the course of most filtration cycles, the permeate fluxes decline noticeably. To quantify a “typical” example, in the third filtration cycle (20–30 min), the permeate flux in Module A (Experiment #1) declines over time from its maximum of 281 LMH to 221 LMH (21%). During the same filtration cycle, the permeate flux in Module B (Experiment #2) declines over time from its maximum of 176 LMH to 125 LMH (29%). As an additional remark, during this same filtration cycle, it can be seen that the permeate flux in Module B reaches its maximum value roughly one minute into the filtration cycle, while in parallel, the TMP climbs to its steady value of $\sim 0.5 \text{ psi}$ over that first minute of the filtration. This is as opposed to what is seen with Module A where the highest flux in the cycle is seen immediately at the beginning of the filtration cycle. Module B’s “lag” in TMP/flux is a consequence of the manual control of the TMP throughout the experiment which is not as consistent as it could be if an automated process control system was implemented (*e.g.* a feedback loop and control valve instead of *V1*).

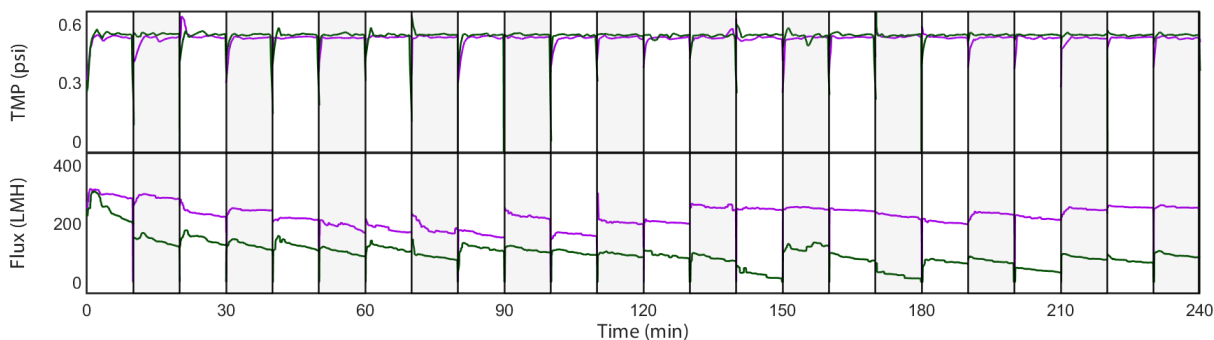


Figure 6.5: *TMP and permeate flux of filtered wastewater (only) plotted over the course of 4-hour filtration experiments. The results for both Modules A (—) and B (—) are shown. Each vertical “section” of the plot represents a 10-minute filtration cycle, each of which were interspersed by BW processes.*

The flux declines seen here are the consequence of fouling of the membranes due to the presence of the organic matter in the wastewater. Over time, this matter partitions onto the surfaces of the membranes, occluding the pore openings and possibly the internal porous structure, restricting the ability of the water to pass through the membrane. At constant TMP, this results in a lower permeate flux over time. This phenomenon was also seen in Chapter 3 in the absence or presence of added MP particles. However, due to the longer duration of filtration (24 hours) and higher TMPs used (10 psi) in the previous study, the magnitude of the flux decline was significantly more severe. Refer to Figure 3.3 in §3.3.2 for detailed analyses of the flux declines seen in the previous study. A discussion of the effect of BW on flux decline can also be found in §6.3.5.

It should also be noted that there is a significant difference in the filtration performances when comparing Modules A and B. Despite the fact that the membrane modules are ostensibly identical and the TMPs are very similar in Experiments #1 and #2, the permeate flux in Module A is significantly higher than in Module B. Having never been exposed to wastewater prior to Experiments #1–2, both modules *initially* produce similar permeate fluxes of approximately 310 LMH, however, the flux profiles of these two membrane modules diverge soon thereafter—within the first cycle. Over the course of the two filtration experiments, Module A produces a flux $1.5\times$ greater than Module B. This is despite the fact that the measured *new-module* pure water permeabilities (*e.g.* before wastewater or MBs were ever filtered) were found to be similar: 18,172 LMH/bar and 19,353 LMH/bar for Modules A and B, respectively. See §2.1.2.1 for a description of the measurement process. Initially, Module B appears to have a slightly (6%) greater permeability than Module A! These observations serve to highlight two key considerations. Firstly, quantitative performance findings must be compared within the same module; the magnitudes of these findings are not directly comparable between modules, however, the use of the two modules can be considered as replicates. Secondly, it should be reinforced that two nominally-identical modules can have significant differences with respect to the productivity of the permeate water, which is a further demonstration of the variability in product performance of membrane offerings.

6.3.2 Module Performance in the Filtration of Wastewater Containing Added Microbeads

Following the quantification of the baseline performance of the two modules—and the stark differences which are seen—Experiments #3 and #4 were completed at Condition B, which included the addition of 1 mg/L (each) of 0.5 μm and 2 μm MBs to the 2^o clarifier effluent wastewater. Expanding upon the format used in Figure 6.5, Figure 6.6 summarizes the results of these two filtration experiments. As before, the upper two rows show the TMPs and permeate fluxes in Modules A and B. Now, two additional rows at the bottom of the figure are included which demonstrate how effectively the membranes withhold the MBs in the wastewater feed.

As before, each experiment was performed at a constant TMP, with these recorded values for Modules A and B (Experiments #3 and #4) averaging 0.52 ± 0.05 psi and 0.50 ± 0.02 psi, respectively. Note that the anomalously-low TMP during the first cycle of the filtration using Module A was due to an error which was corrected in subsequent cycles. The corresponding permeate flux profiles are also shown and share the same characteristics (*e.g.* flux declines within cycles/the whole experiment, flux recoveries, etc.) as the profiles seen at Condition A in §6.3.1. For reference, a

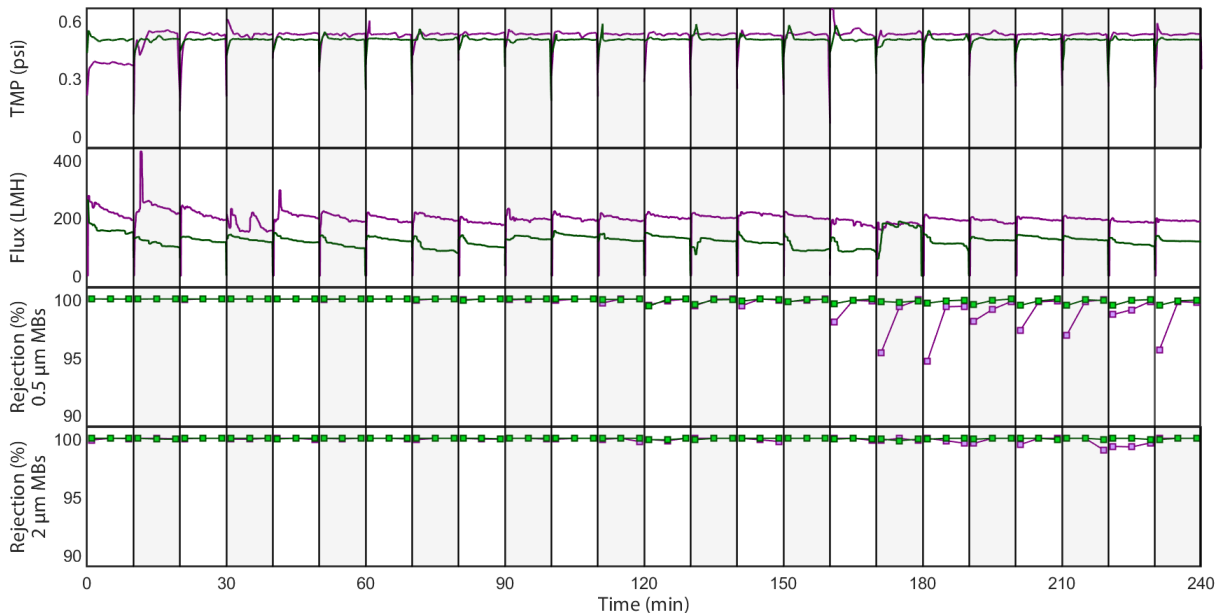


Figure 6.6: TMP, permeate flux, and MB rejection during the filtration of wastewater containing 1 mg/L (each) of the 0.5 μm /2 μm MBs in four-hour experiments using both Modules A (—; ■) and B (—; ■). Each vertical “section” of the plot represents a 10-minute filtration cycle interspersed by BW processes.

remarkable similarity between the permeate flux decline profiles can be seen in Figure D.3 where the profiles corresponding to the *same module at the two conditions* are superimposed. This observation is notwithstanding the solution conditions (*i.e.* wastewater, MB content) were different depending on the experiment. Whereas the MP content of the wastewater was a significant driver in the magnitude of the flux decline and fouling seen in Chapter 3, in this study, it does not appear to be the case. One mitigating factor here may be the use of the crossflow filtration mode which is often used in full-scale applications for mitigating fouling [15]. The tangential forces exerted by the steady-state crossflow of wastewater increases the back-transport of accumulated solids at the membrane surface and in the boundary layer, while disrupting the concentration polarization layer at the solid-liquid interface which normally promotes fouling in the first place [21, 22]. Work by Belfort *et al.* (1994) suggests that the back-transport mechanisms which most strongly affect the MB sizes used in this study include Brownian diffusion ($< 1 \mu\text{m}$) and shear-induced hydrodynamic diffusion ($\sim 1 \mu\text{m}$ to roughly $30\text{--}40 \mu\text{m}$) whereby the MBs experience “random displacements from the streamlines in a shear flow as they interact with and tumble over other particles” [23]. Thus, higher shear rates at the membrane’s surface—proportional to the crossflow velocity—are expected to contribute to a greater permeate flux and a lesser incidence of permeate fouling. This is in contrast to the dead-end filtration mode used in Chapter 3 where no tangential forces were present, likely contributing to the aforementioned fouling and flux decline observations.

In addition to these productivity metrics, the performance of the modules towards the removal of the $0.5 \mu\text{m}$ and $2 \mu\text{m}$ MBs was quantified, using the technique of FC to obtain MB concentration measurements in the samples that were taken. This instrument proved to be an ideal tool for MB enumeration as its multiple (excitation) lasers and emission filters allowed for the *parallel detection of the two different sizes of MBs* containing fluorophores which were chosen to be distant in terms of their excitation and emission wavelength profiles. The gating process summarized in Table 6.4 enabled the instrument to effectively discern the two MB sizes from each other (see Figure D.2). Analogous to the findings presented in Chapter 5, the MBs were also discernible from the wastewater solids which are also a source of background fluorescence, especially at low wavelengths. A “3D” excitation-emission matrix (EEM) illustrating this wastewater fluorescence can be found in Figure D.4 which demonstrates this effect. *The value of these finding should not be overlooked:* it has been demonstrated that FC can—in an efficient and automated process—quantify the concentrations of

two different sizes of fluorescent MBs simultaneously, even in the presence of autofluorescent natural organic matter.

Moving forward, at the nominal mass concentration of MBs fed to the membrane ($m = 1$ mg/L for each size of MB), the expected number concentration of MBs (n ; MBs/mL) can be calculated simply, assuming a PS MB density of $\rho_{MB} = 1,050$ kg/m³:

$$n(d) = \frac{m}{\rho_{MB} \left[\frac{4}{3} \pi \left(\frac{d}{2} \right)^3 \right]} \times 10^{-9} = \frac{6m}{\rho_{MB} \pi d^3} \times 10^{-9} \quad (6.2)$$

where d is the MB diameter (m), and 10^{-9} is a unit conversion factor. As such, n for the 0.5 μm MBs is expected to be 1.5×10^7 MBs/mL, and for the 2 μm MBs, it is expected to be 2.3×10^5 MBs/mL. These estimated number concentrations align well with the measurements of feed samples performed via FC, as detailed subsequently in Figures D.5–D.9.

Instead of considering particle concentrations which could vary by orders of magnitude, the performance of the modules to remove the MBs was quantified via the number-based observed rejection coefficient, R_n —a *ratio* of concentrations. The rejection results from these experiments are shown in Figure 6.6. The formula for R_n is written as Equation 5.1 in Chapter 5, and is a function of the number concentrations of the MBs in the permeate (n_p) and feed streams (n_f), as measured offline via FC. The permeate MB concentration measurements were taken at discrete points—1, 5, and 9 minutes into each filtration cycle—therefore the MB rejection coefficients were also calculated at these timepoints. Since the feed concentrations were only measured at the start of each filtration cycle, values of n_f at the 1-, 5-, and 9-minute marks were estimated reasonably via linear interpolation between the feed concentration at the start of that cycle and the start of the subsequent cycle. Whereas rejection coefficients are plotted in Figure 6.6, a comprehensive summary of all the collected data (including the MB concentration measurements from which R_n was calculated) is shown in Figures D.5–D.9.

When considering the rejection of the MBs doped into the feed wastewater, there is clear variation in performance when comparing the two modules, as was also seen previously with the flux data. It is clear that Module B demonstrates significantly higher rejection coefficients than Module

A. This is particularly evident when the 0.5 μm MBs are considered and towards the second half of the filtration experiments. For example, the permeate samples taken at 171 min into the filtration experiment (Cycle 18) indicate that $R_n = 95.3\%$ for Module A versus $R_n = 99.8\%$ for Module B. While this effect is not as pronounced with the 2 μm MBs, it is still visible (*e.g.* Cycle 23). In addition to its poorer MB rejection, it can be seen in the second row of Figure 6.6 that Module A still produces a higher overall flux than Module B when wastewater is filtered at essentially the same TMP. Where two nominally-identical membranes give different performances, invisible variations in the manufacturing processes which produced the membranes may have result in membranes with different porous structures: the inclusion of small defects (*e.g.* pinholes), variations in the pore structure, or a broader pore size distribution all could result in a membrane which is inherently more permeable and less capable of rejecting the MBs [24, 25]. Unseen damage to Module A during Experiment #1 or handling may be feasible a contributing factor. Only after the modules are exposed to the wastewater in Experiments #1 and #2 does Module A begin to display a higher permeate flux/permeability. The wastewater source used in the first two experiments may be a contributing factor in these observations; for example, the “WW2” used in Experiment #2 may have irreversibly fouled Module B, constricting its pores. However, there is nothing inherently obvious in the water quality analysis that was performed on the two different wastewaters—as summarized in Table 6.1—although the composition of wastewater is complex enough such that a bulk-property water quality analysis may be insufficient for identifying a root cause of this phenomenon. Overall, the reason for this difference in membrane performance remains unknown and therefore further investigation would be required. Regardless, the significance of these observations is that a lower throughput of permeate water is produced using Module B, however, the water also contains a lower concentration of MBs. The two nominally-identical membrane modules perform differently in terms of flux *and* rejection.

When the 0.5 μm MBs are specifically considered, it is clear that the rejection of these particles is generally quite high ($> 94\%$). Until approximately the twelfth filtration cycle (110–120 min), MB rejection is nearly complete ($\sim 100\%$). Beyond this twelfth cycle however, some 0.5 μm MB rejection coefficients significantly decrease in magnitude, ranging from 94.7–100% for Module A and 99.4–100% for Module B. This decrease indicates the presence of higher concentrations of the MBs in the permeate samples. In particular, the permeate sample taken at a filtration time of 181 min

(Module A, Cycle 19) indicated a rejection coefficient of only 94.7%, the lowest value of R_n that was observed up until this point. However, this poorer rejection performance is transient in that the magnitude of the decline in R_n varies cycle-by-cycle and *no apparent relationship between the permeate flux at R_n* can be seen. As the 0.5 μm MBs are smaller in diameter than the stated pore size of the membrane (nominally 0.65 μm), it is not surprising that significant quantities of the particles are found in the membrane's permeate water. Typically, the nominal pore size of a membrane is an imprecise or poor descriptor of the minimum size of analytes as it is a function of process conditions (*e.g.* flux), the nature of the analyte used (*e.g.* chemical composition, shape), and is not easily reduced to a single number because of the *distribution* of pore sizes found in most membranes. Nevertheless, the work performed in Chapter 4 which characterized the transmission of milled and sieved MPs through Durapore® MF membranes also showed significant transmission of MPs through the membrane with particles sizes approaching the membrane's nominal pore size.

Furthermore, in many of the cycles where there is significant observable breakthrough of the 0.5 μm MBs, a pattern in the rejection coefficients can be seen: R_n improves over the course of the cycle. Using Module A and Cycle 19 as an example again, R_n increases from 94.7% (181 min) to 99.3% (185 min) to 99.4% (189 min). Module B typically shows the same patterns, but in a much less pronounced fashion. This increase in rejection over the course of the filtration cycles is indicative of the mediating role of fouling on the rejection of the MBs as the increase in particle rejection is met with a commensurate decline in permeate flux. As wastewater is filtered through the membrane, wastewater solids plus the MBs accumulate at the feed-membrane interface. The foulant layer grows over the course of the filtration cycle, constricting the membrane pores, reducing the permeate flux, and contributing to the steric exclusion of the MBs which further limits their ability to traverse the membrane. This finding mirrors the observations in §5.3.3 where the presence of humic acid significantly increased the rejection of MBs over time when filtered using the 5 μm Durapore® membrane. This implies a tradeoff between permeate water productivity and MB rejection.

In contrast, the 2 μm MBs are rejected to a greater degree than the 0.5 μm MBs. The mode rejection coefficient for both Module A and B is 100% (*i.e.* complete rejection), with R_n not falling below 98.9% for Module A and 99.8% for Module B. Again, it is evident that 2 μm MB breakthrough varies cycle-by-cycle and a simple relationship between the permeate flux at R_n is not easily derived.

It is clear that these MBs are well-rejected by the membranes as the particles are larger than the majority of the pores found in the membrane modules. Interestingly, the minimum number-based rejection of 0.5 μm MBs from Module B *exceeds* the minimum rejection of 2 μm MBs for Module A! Permeate samples which contain the 2 μm MBs may result from the inherent pore size distribution of MF membranes. A manifestation of this polydispersity in pore size can be seen in Figure 6.3B–C where there is a clear variability in the size of the pore openings due to the structure of the polymeric membrane. The consequence of this is that there may be a minuscule fraction of pores in the membranes which are large enough for the MBs to traverse, leading to a small quantity of 2 μm MBs found in some permeate samples. That is not to say that *all* membranes with the same nominal pore size will perform the same when subjected to the same microparticles under the same conditions (*e.g.* wastewater composition, flux, etc.). A substantial body of work indicates that membranes with similar characteristics will not necessarily exhibit similar quantity- or quality-based performance metrics. In one notable case, Taylor *et al.* (2021) documented a wide range of rejection coefficients for particles filtered through various MF membranes with similar properties. For example, 0.2 μm Meissner STyLUX® and SteriLUX® sterile filters were challenged to suspensions of 300 nm fluorescent PS MBs. Whereas the MB transmission approached nearly 80% for the former membrane, the maximum MB transmission only just exceeded 10% with the latter membrane. Clearly, even similar membranes by the same manufacturer can exhibit vastly diverging performances, attributable to differences in the membrane polymer, structure, surface charge, and so on [12]. These factors can therefore affect the mechanism(s) by which the particles are rejected. This emphasizes the need to properly evaluate membranes and membrane modules towards the end goal of maximizing MP retention to prevent the efflux of these particles into the environment.

6.3.3 Effect of Crossflow Velocity

One final experiment (#5) was performed with Module A to elucidate the effect of varying the crossflow velocity of the wastewater which was fed to the membrane module. The crossflow velocity inside the hollow fibers is a driver of the fouling propensity of the membranes, where it would be expected that higher crossflow velocities mitigate the fouling propensity [26]. Guo *et al.* (2012) write that normal concentration polarization at the feed-membrane interface increases the particle and solute concentrations there at the interface which contributes to their deposition and possible

breakthrough into the permeate stream. Greater polarization at the interface contributes to more severe fouling as higher concentrations of particles and solutes can, to a greater degree, interact with and adsorb to the surface of the membrane [27–29]. As such, increasing the crossflow velocity and the rate of mass transfer of the particles/solutes back from the interface can mitigate the effects of concentration polarization. According to Belfort *et al.* (1994), this is because the nominal shear rate at the feed-membrane interface γ_0 is proportional to the radially-averaged crossflow velocity v_{avg} in the hollow fiber’s lumen, where higher shear rates can effectively resuspend polarized or adsorbed solids and mitigate the effects of fouling from particulates or colloidal solids [23]. As such, varying the crossflow velocity is expected to affect the fouling dynamics and may correspondingly influence the rejection performance of the membrane towards the MBs. The nominal shear rate is described according to Equation 6.3 as follows [23]:

$$\gamma_0 = \frac{4v_{avg}}{R} \quad (6.3)$$

where R is the inner radius of the hollow fiber (see Table 6.2) and the velocity profile within is parabolic (Poiseuille velocity profile) for fully-developed laminar flow of a Newtonian fluid [23]:

$$v(r) = 2v_{avg} \left(1 - \frac{r^2}{R^2}\right) \quad (6.4)$$

Here, r is the radial distance from the centerline of the hollow fiber’s lumen ($0 \leq r \leq R$). The assumption of “laminar flow” implies that the unitless Reynolds Number Re is less than 2×10^3 in the case of a circular conduit such that [23]:

$$Re = \frac{2\rho v_{avg}R}{\mu} \quad (6.5)$$

where ρ and μ are the density (998 kg/m³ at 20°C) and dynamic viscosity of water (10⁻³ Pa·s at 20°C). In an “ideal” analysis, the average crossflow velocity (m/s) can be calculated simply from the volumetric flow rate of wastewater passing through the lumen of one single hollow fiber (Q_{HF} ; m³/s) and the known circular cross-sectional area of the fiber’s lumen, πR^2 (m²), such that:

$$v_{avg} = \frac{Q_{HF}}{\pi R^2} \quad (6.6)$$

The value of Q_{HF} can be determined by equally apportioning the total volumetric flow rate of wastewater feed entering the module (Q_{feed}) to each of the individual hollow fibers therein ($N = 75$). As such, the average crossflow velocity inside each of the hollow fiber lumens can be estimated as:

$$v_{avg} = \frac{Q_{feed}}{\pi N R^2} \quad (6.7)$$

Equation 6.7 assumes that each hollow fiber receives the same fraction of Q_{feed} and thus v_{avg} is the same for each fiber. Additionally in this analysis, no correction to Q_{HF} was made to account for the loss of wastewater to the permeate stream over the length of the membrane. This implies that Q_{HF} and v_{avg} are only (strictly) valid at the feed-side entrance to each of the hollow fibers. A more rigorous analysis of the crossflow velocity would take into account the flow rate of water leaving in the permeate stream (Q_{perm}) to obtain a crossflow velocity \bar{v}_{avg} which is not only a *radial* average, but also an axial average over the length of each fiber:

$$\bar{v}_{avg} = \frac{Q_{feed} + (Q_{feed} - Q_{perm})}{2} \cdot \frac{1}{\pi N R^2} = \frac{Q_{feed} - 0.5Q_{perm}}{\pi N R^2} \quad (6.8)$$

Here, $(Q_{feed} - Q_{perm})$ is just the retentate volumetric flow rate. Where Q_{perm} is small, Equation 6.8 reduces to Equation 6.7. The data collected shows that the ratio Q_{perm}/Q_{feed} at a given timepoint is generally under 25%; to simplify the calculation and subsequent analysis, Equation 6.7 will be used henceforth. As such, v_{avg} is to be interpreted as the crossflow velocity at the entrance to the hollow fibers or equivalently, the “maximum” average crossflow velocity in each fiber.

To lower the crossflow velocity within Module A in Experiment #5 (Condition C), the retentate and permeate valves ($V05$ & $V08$, respectively) were throttled while still maintaining the standard TMP of 0.5 psi across the module. At this condition, the value of v_{avg} averaged over the four-hour experiment was calculated to be 0.26 ± 0.09 m/s. Experiment #5 is in direct comparison with Experiment #3, where the latter experiment just differs in that a higher average crossflow velocity was seen (0.65 ± 0.04 m/s)— $2.5\times$ the average value in Experiment #5. These values are potentially lower than those seen in some *external* crossflow membrane systems for the treatment of wastewater (*e.g.* anaerobic membrane bioreactors) where crossflow velocities of 1–5 m/s might be seen, but for submerged membrane bioreactors, crossflow velocities less than 0.6 m/s are to be expected [30]. Within the lumens of inside-out hollow fiber membranes, velocities of up to 1 m/s can be expected

in UF [26] or even up to 2.5 m/s in MF [16]. Therefore the ranges of crossflow velocities seen in these experiments are likely low, but not unreasonably so. Given the average crossflow velocities computed above, the corresponding average Reynolds Numbers could be calculated, as outlined in Equation 6.5. For Experiments #3 and #5, $Re = 484 \pm 30$ and $Re = 192 \pm 69$, respectively. These values predict that the flow within the hollow fiber lumens is indeed laminar, therefore the analysis in Equations 6.3–6.8 are assumed to be valid with respect to the flow regime. In typical systems, crossflow MF is also performed in the laminar regime (but preferentially at higher crossflow velocities) as the pressure drop along the hollow fiber is proportional to the crossflow velocity in the laminar regime, whereas pressure drop is undesirably proportional to the square of crossflow velocity in turbulent flow [21].

A comparison of the crossflow velocities for these two experiments are plotted in Figure 6.7 along with the standard TMP, flux, and MB rejection data. Similar to Experiment #3, the average TMP of Experiment #5 was quite constant at 0.49 ± 0.07 psi. The resulting flux for the first ~ 130 minutes of Experiment #5 was noticeably lower than the previous experiment, which aligns with the initial hypothesis that a lower crossflow velocity would induce a greater severity of fouling. Beyond ~ 130 minutes of filtration time, the fluxes both reached a similar pseudo-steady state. In terms of MB rejection, the same pattern which was described on page 216 applies to most filtration cycles at the lower average crossflow velocity: rejection generally improves over the course of the cycle. Considering the magnitude of the $0.5 \mu\text{m}$ MB rejection coefficients, values of R_n ranged from 91.7–100% which aligns well with R_n values from the previous experiment. While most of the computed $0.5 \mu\text{m}$ MB rejection coefficients exceeded 96%, the value measured at 221 minutes (Cycle 23) was found to be particularly poor at 91.7%, lower than values of R_n measured in other experiments. Now considering the magnitude of the $2 \mu\text{m}$ MB rejection coefficients at the lower crossflow velocity, similar observations are made: values of R_n ranged from 99.2% to 100% which are slightly higher at Condition C than at Condition B, but still align well with R_n values from Experiment #3. One particularly unusual set of data points was recorded at a time of 145 min (Experiment #5) where values of R_n fell significantly below the typical trends. The concentrations that were measured were re-verified via FC and were found to be correct. This anomalous measurement may be a result of sample contamination—as oppose to breakthrough—which is a common nuisance in MP research [31]. While some small differences may be present between the datasets from Experiments #3 and #5,

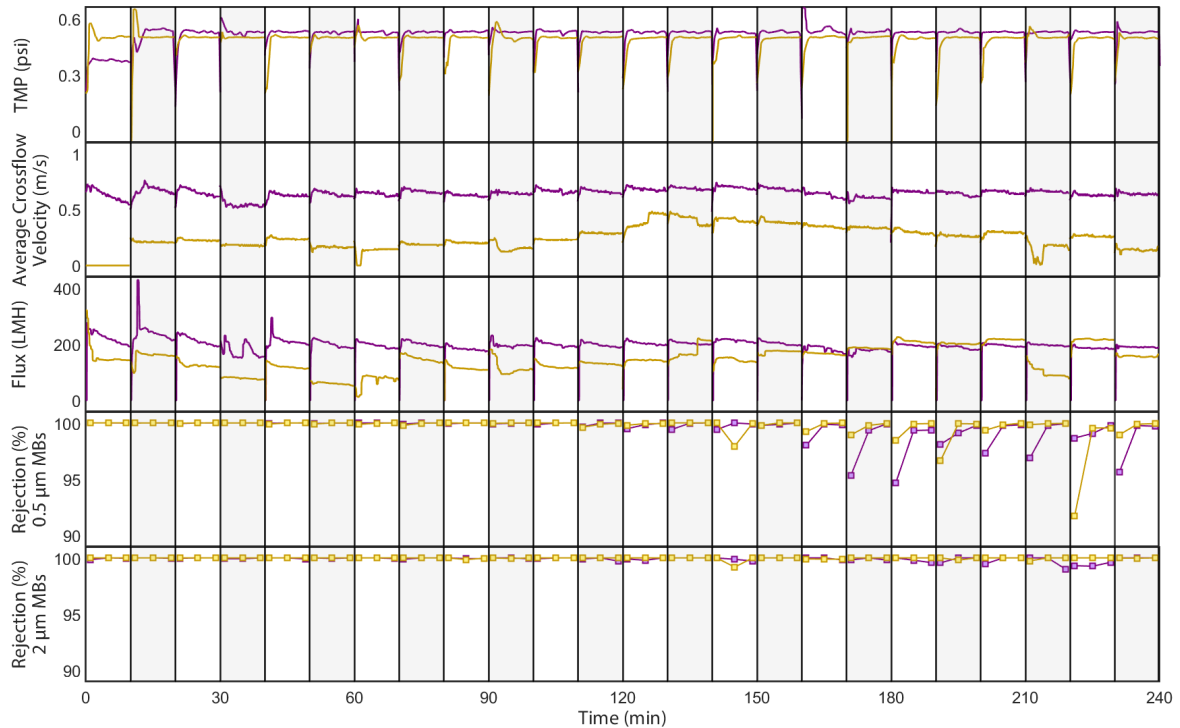


Figure 6.7: Comparison of filtration performance results in Experiment #3 versus #5, where Module A is operated at “high” (—; ■) and “low” (—; ■) levels of crossflow velocity. In both experiments, wastewater with 1 mg/L (each) of 0.5 μm /2 μm MBs is filtered. TMP, average crossflow velocity, permeate flux, and MB rejection are shown. Due to a sensor malfunction, no crossflow velocity data was recorded in the first cycle of Experiment #5. The data for Experiment #3 is transcribed from Figure 6.6.

the rejection data is very similar and no clear conclusions can be made, here, regarding the effect of the crossflow velocity on the rejection of MBs, perhaps as a consequence of the particularly low crossflow velocities that were used. A subsequent experiment may attempt to use a much higher crossflow velocity, instead.

It was initially hypothesized that lowering the crossflow velocity from Experiment #3 to Experiment #5 would increase the rejection of MBs, particularly the 0.5 μm size as the commensurate reduction in crossflow velocity and shear rate would encourage a greater severity of membrane fouling. It is possible that decrease in the crossflow velocity was not significant enough in magnitude to affect the magnitude of fouling in a manner which is perceivable given the natural variability in the filtration performance. Judd & Till (2000) performed a crossflow filtration study using 2° WWTP effluent and polypropylene MF membranes (pore sizes = 0.2–1.3 μm) [32]. In this study, they observed

a $2\times$ increase in specific flux (*i.e.* permeability) through a membrane with a $0.67\ \mu\text{m}$ pore size when the crossflow velocity was roughly quadrupled from $0.9\ \text{m/s}$ to $3.8\ \text{m/s}$. This was rationalized by an increase in turbulence which decreased the size of the fouling layer. Interestingly, when the rejection of fecal coliform bacteria (which can be considered as “microparticles”) was measured under these conditions, no clear trend was visible over the range of crossflow velocities that were studied. A likely contributing factor alluded to in the aforementioned study is the role of internal pore fouling. In retrospect, if a significant portion of the membrane fouling occurs deep within the pores—or at least in deep “wells” formed at the pore mouths—the turbulence and shear of the moving fluid may not be able to interact with the foulant layer. Then, the effect of the crossflow velocity would be negligible. Anecdotally, the fact that the wastewater in this chapter was pretreated using a bag filter—removing larger suspended solids—lends favour to the idea that remaining wastewater solids could internally foul the pores. Future work should characterize the relative incidences of internal versus surface fouling and their effects on MP rejection in crossflow wastewater MF.

6.3.4 Interpretation of a Curious Breakthrough Effect

Another interesting finding with respect to the rejection of the MBs in Experiments #3–#5 involves the time at which MB “breakthrough” begins to occur and thus significant quantities of MBs are observed in the permeate samples. It can be seen in Figures 6.6–6.7 that the MBs are mostly rejected in an “induction period” prior to ~ 120 min of filtration time. Past this point, elevated concentrations of $0.5\ \mu\text{m}$ MBs can be consistently measured in permeate samples and in turn, lower rejection coefficients are produced. It appears that roughly twelve filtration/BW cycles are required before the MBs break through in significant quantities. That is, there are multiple repetitions of forward applied pressure for 10 minutes, a release of that pressure, another minute of applied pressure (but in the reverse direction) during BW, and then another release of pressure before the cycle repeats. Previous studies in the contemporary literature have documented a similar phenomenon, where after forward filtration and a pressure release, the rejection or transmission of particles or viruses is modified in the subsequent filtration cycle.

In their 2013 study, Woods *et al.* employed a pressure release between filtration cycles where a Pall Ultipor® DV20 membrane was challenged to solution containing fluorescent ΦX174 bacterio-

phages. The analysis of “banding” in CLSM images indicated that a pressure release caused the membrane to also liberate some of the phages which may have been captured by pore constrictions; at which point, diffusion of the phages away from the constriction could then proceed as the convective forces holding them there were temporarily withdrawn. The phages were then able to migrate further into the membrane when the pressure was reapplied. Following the pressure release, a spike in the phage concentration was noted in the permeate solution which rapidly decreased in magnitude over the cycle [41].

Similarly, Dishari *et al.* (2015a) applied this methodology and noted a similar effect when they challenged *Ultipor® DV20* and *EMD Millipore Viresolve® NFP* membranes to the same bacteriophages: the phages could diffuse or migrate from the pores after the pressure was released, resulting in re-capture deeper into the membrane and transmission to the permeate stream upon the re-application of pressure [42]. In contrast, they noted that the filtration of the phages using a highly-asymmetric *EMD Millipore Viresolve® Pro* membrane proceeded via a different phenomenon, whereby phages were captured in pore constrictions (“retentive sites”) during the first filtration cycle, but no migration occurred during the pressure release. Subsequent phages were captured vacant retentive sites deeper into the membrane in the subsequent filtration cycle. The authors suggest that differences in the transmission and capture behaviours are a function of the membrane pore structure, which varies substantially over the three membranes that were used [42]. In a parallel investigation, Dishari *et al.* (2015b) affirm that the solution conditions (*e.g.* ionic strength, pH, etc.) play a key role in governing interactions between the phages and the membranes which, in turn, affects the capture/transmission of the particles during filtrations with pressure release events [43]. Fallahian-bijan *et al.* (2017) replicated Dishari *et al.*’s original results, except with the use of fluorescent PS nanoparticles in sizes ranging from 20–100 nm in diameter. The results using these particles were similar and the phage capture mechanisms seen with the “DV20” and “Pro” membranes were largely replicated, emphasizing the role of different membrane structures on particle capture/transmission. Furthermore, longer intervals of pressure release when the DV20 membrane was used allowed for a longer diffusion time (1–30 min), and consequently, a noticeably greater intrusion of the particles into the membrane’s structure when pressure was re-applied [9].

The observations in this study regarding the delayed breakthrough of the MBs—in particular, the 0.5 μm MBs—show a similar behaviour as the DV20 membrane from the aforementioned studies. Here, it is hypothesized that when the pressure is applied in each filtration cycle, 0.5 μm MBs are forced into the membrane’s pores via the forward-directed convective flow of the wastewater through the membrane. The MBs are caught in regions where the pore structure constricts or where aggregates become lodged. The MBs accumulate there until the filtration cycle is finished after 10 minutes. At that point, the pressure is removed and a brief amount of time elapses (~ 1 min) before BW is performed. The aforementioned studies noted the back-diffusion of particles during this relaxation. But compared to the phages used in the work by Dishari *et al.* (2015a) which were approximately 0.026 μm in size, the MBs used in this work are quite large. The implication is that during the brief period without convection, the diffusion of the MBs would be relatively slow due to their size.⁴ Therefore, it is expected that back-diffusion plays a less significant role in transporting the particles away from constrictions in the membrane. In contrast, the high-flux BW processes are expected to play a much more significant role in transporting the particles away from these constrictions by way of backward-directed convective forces. This convection feasibly transports the MBs or MB aggregates to *new* constrictions in the membrane structure nearer to the membrane’s feed-side interface, possibly delaying the onset of breakthrough. Now after one more respite from convective forces, the pressure is re-applied and the MBs can then migrate deeper into the membrane structure via forward-directed convection. Only after multiple filtration-relaxation-backwashing-relaxation cycles are the MBs forced all the way through to the permeate stream, as seen in Figures 6.6–6.7. Once breakthrough occurs, the lowest rejection measurements are seen at the start of the filtration cycles—an observation mirrored by Woods *et al.* (2014) [41].

To confirm the mechanisms behind these observations, additional investigations are still needed. Building off the works performed by Woods, Dishari, and Fallahianbijan, CLSM could be employed to track the location of MBs (*i.e.* containing different fluorophores) within the membrane’s structure over a given number of filtration-relaxation-backwashing-relaxation cycles. To elucidate the relative importance of MB diffusion versus convection, a series of two parallel tests could be performed. In the one test, the filtration cycles would be interspersed with BW cycles, but in the second test, no BW would be used. The times at which MB breakthrough occurs could then be compared.

⁴The MBs are *also* quite large with respect to the 0.65 μm nominal pore size of the membrane, further hindering diffusive transport through the tortuous porous network.

Overall, the observation that significant quantities of MBs can be found in the membrane permeate streams after several filtration and BW cycles implies that the choice of membrane for use in 3^o wastewater treatment applications is critical. As Dishari, Fallahianbijan, and their colleagues noted, the nature of the membrane that is used can affect the particle capture and transmission phenomena that are found to occur [9, 42, 43]. A greater understanding of how membrane structure facilitates or inhibits the transmission of MPs—especially those that are irregular in shape—is needed so that membrane modules can be better selected for use in WWTPs. Furthermore, engineers and WWTP operators may be able to exploit induction periods where few MPs are transmitted. Perhaps filtration of wastewater can be performed up until the end of the induction period at which point, a membrane cleaning step can be used to remove all labile MPs. Finally, researchers studying MP filtration phenomena must be aware that differences in rejection performances can be seen at different experimental times scales, and therefore, they should design their experiments accordingly to observe results which are representative of the “real” filtration processes used in WWTPs.

6.3.5 Examination of Module Backwashing

6.3.5.1 Effect of Backwashing on Flux

As is detailed in §6.2.3.3, the modules were backwashed after every cycle. Interspersing filtration cycles with BW processes can mitigate the severity of the flux declines that are seen as the BW can disrupt the foulant layer on the surface of a membrane and reverse some of its build-up. This can help recover the flux to higher levels; the magnitude of this flux recovery is a complex function of the filtration and BW conditions that are employed, as well as the composition of the water that is filtered [33]. As expected, it can be seen that the permeate fluxes in Experiments #1–#5 experience recoveries after many of the backwashing cycles that were performed. A flux recovery is seen when the flux at the start of a cycle (or slightly thereafter) is greater than the flux at the end of the previous cycle.

Over the course of the whole four-hour filtrations in Experiments #1 and #2 at Condition A, the flux recoveries are insufficient to return to the initial flux levels seen at the outset of the experiments: irreversible fouling occurs which limits the magnitude of the flux recovery that is accomplished via BW alone [33]. While the permeate flux appears to decline, overall, from $t = 0$ min to $t = 240$

min, no precipitous drop is seen, unlike in Chapter 3. Using Module A from Experiment #1 as a particularly evident example (Figure 6.5), a pseudo-steady state appears to be reached after roughly 130 min of filtration, where no clear long-term trend in flux appears over time, implying that the deposition of solid material due to fouling is—more or less—balanced by the removal of solid material during the BW cycles. For the filtrations in Experiments #3 and #4 with added MBs, the flux stabilizes much earlier at roughly 200 LMH for Module A and 140 LMH for Module B. In fact, there is little long-term change in permeate flux seen by either module over four hours, implying that the solids deposition/removal balance is reached and insignificant irreversible fouling is occurring. This pseudo-steady state behaviour may be an indicator of longer-term performance of these membranes in the absence of changes to the feed wastewater quality or process conditions.

6.3.5.2 Quantification of Microbeads in Backwashing Water

While the process of BW evidently improves the long-term performance of the membrane modules by disrupting the boundary layer at the interface between the feed wastewater and the membrane and/or stripping away solids caked onto the membrane surface, the question remains to what extent the MBs are resuspended into the BW water. There is precedent to believe that significant quantities of MBs would be found there. As an example, Pramanik *et al.* (2019) performed an analysis on the BW water from forward osmosis membranes to identify the organic molecules which desorbed during BW [34]. Furthermore, the findings in Chapter 3 imply that MPs removed via BW must leave in the BW water, by virtue of a simple mass balance.

As such, “used” BW water was collected (~ 2.5 L) from the BW process at the end of every sixth filtration cycle in Experiments #3 and #4 (Condition B). Samples from this BW water were analyzed for MB concentrations via FC; the results are reported in Figure 6.8. Substantial number concentrations of MBs were detected (n_{BW}), ranging from 7.91×10^4 to 8.23×10^5 MBs/mL when considering the $0.5 \mu\text{m}$ MBs, and 8.00×10^2 to 1.09×10^4 MBs/mL when considering the $2 \mu\text{m}$ MBs. Evidently, higher concentrations of the $0.5 \mu\text{m}$ MBs versus the $2 \mu\text{m}$ MBs are liberated relative to the concentration of MBs fed to the modules. To contextualize these observations, this represents 8–53% ($0.5 \mu\text{m}$) and 4–28% ($2 \mu\text{m}$) of the average MB number concentrations *fed* to the modules (n_f) during the cycles where the BW water was collected (*i.e.* n_{BW}/n_f). To ensure that these MBs

in the BW water were not just originating from feed wastewater that was purged during BW, the modules were first drained of feed and permeate water as a physical measure. Furthermore, the volume of feed wastewater required (V_f) to produce the concentration of MBs in the volume of BW water that was collected ($V_{BW} \approx 2.5$ L) was computed in a simple dilution calculation:

$$n_f V_f = n_{BW} V_{BW} \quad (6.9)$$

These computed volumes ranged from 0.102 L to over 1.32 L, far exceeding the total void volume of the entire membrane module (see Table 6.2) including both feed and permeate sides (0.05 L). A summary of n_{BW}/n_f and V_f values can be found in Table D.3 for each of the BW analyses at Condition B. The implication, here, is that the MBs could not have all originated from the leftover feed wastewater in the modules and therefore at least some were removed from the surfaces of the hollow fiber membranes or the module, itself. With significant quantities of MBs removed and resuspended, the fate of these MBs should be considered.

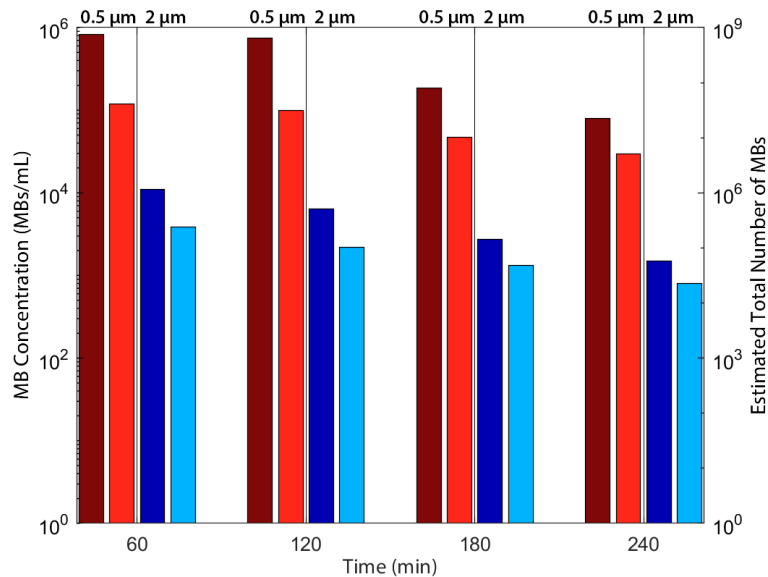


Figure 6.8: Concentration of MBs in the BW water that was collected after every sixth cycle (*i.e.* 60 min) for the two experiments run at Condition B (wastewater with MBs). The quantity is reported as a measured concentration and as a calculated estimate of the total number of MBs collected in the BW water. Bars in red refer to the 0.5 μm MB concentrations for Modules A (■) and B (■), while bars in blue refer to the 2 μm MB concentrations for Modules A (■) and B (■).

In a typical municipal WWTP that utilizes membrane technologies in a 3° treatment step—as oppose to a 2° membrane bioreactor—the rejected water (*e.g.* retentate or concentrate) is enriched in non-dischargeable components (*i.e.* residuals) which require further treatment prior to discharge. Perhaps the simplest method of doing so is to recycle it back to an earlier stage in the treatment process, such as the plant headworks [31, 35]. In a similar fashion, membrane BW water also contains residuals and therefore requires further treatment. It is often returned to earlier stages in the wastewater treatment process [36] such as the headworks (*e.g.* in facilities discussed by Michielssen *et al.* (2016) and Bergman *et al.* (2006) [37, 38]) or 2° treatment (*e.g.* in facilities discussed by Bergman *et al.* (2006) and Mitch & Sedlak (2004) [38, 39]). Doing so is the equivalent of adding a recycle loop within a chemical process: either the concentration of MPs will accumulate within the process, or there is a feasible route by which the MPs can leave. Unfortunately, there is little actual clarity to this end, as elegantly presented by Koutnik *et al.* (2021), who report that 94% of MPs which enter WWTPs are unaccounted for in outlet streams. The authors suggest that this finding is attributable to a lack of standardization in MP quantification techniques and reporting practices, the difficulties associated with separating the MPs from water and especially sludge/biosolids, the fragmentation and biodegradation of the particles within WWTPs, the adsorption of particles, and inconsistent/poor limits of detection [40]. The effective “recycling” of the MPs within WWTPs via the retentate or BW streams adds an additional level of complexity to the mass balance on the facility and the unit operations contained therein. It is generally expected that MPs in wastewater treatment should exit the process in the biosolids mainly produced in 1° or 2° treatment steps, but additional research is needed to understand the fate of the considerable quantities of MPs which leave 3° membrane processes in reject streams.

6.3.5.3 Visualization of Microbead Deposition via CLSM

To further explore the effects of the BW and cleaning processes on MB deposition on the membranes, Module B was backwashed and cleaned at the end of its final experiment (#4), as usual, according to the procedure set out in §6.2.3.3. However, Module A was neither backwashed nor cleaned following its final experiment; it was gently rinsed with DI water. Subsequently, both of the used modules were autopsied and imaged using CLSM, a technique sometimes used in the analysis of hollow fiber membrane fouling [44].

Figure 6.9 exhibits the results of the CLSM analysis for *a single hollow fiber* taken from Module A, and *another single hollow fiber* taken from Module B. Each panel depicts a hollow fiber half-section: the semi-circular “troughs” are the surfaces of the hollow fiber lumens. The two edges at the top of each “trough” are where the hollow fiber was sliced in half axially. Half-sections were excised from fibers at three specific axial locations along the hollow fibers, shown in the *columns* of the figure. Panels in the left column of the figure correspond to half-sections excised from the ends of hollow fibers closest to where the feed wastewater enters the modules. Conversely, panels in the right column of the figure correspond to half-sections excised from the ends of hollow fibers *opposite* to where the feed enters; that is, at the retentate ends of the modules. In between these two extremes, the panels in the central column correspond to half-sections excised at the center (axially) of the hollow fibers, halfway between the “feed” and “retentate” sample locations. To improve the visibility of deposited MBs on the surfaces of the hollow fiber lumens, two different versions of the image taken at each location are shown. The (upper) rows marked “All Image Channels Active” include “green” colorations corresponding to the FITC-dyed membrane polymer (FITC emission filter), red colorations corresponding to the 0.5 μm MBs (TRITC emission filter), and purple colorations corresponding to the 2 μm MBs (DAPI emission filter). For additional clarity in resolving the deposition of the MBs, the (lower) rows marked “Only MB Channels Active” depict the *exact same half-sections*, but with the FITC channel disabled such that only signal from the MBs is shown. For the purposes of brevity, one replicate (*i.e.* a single fiber) for each module is depicted in Figure 6.9 as the data is largely reproducible between fibers/replicates. Analyses were performed in triplicate and the additional replicates can be found in Figure D.10. Note that autofluorescence of the molecules in the wastewater would be expected to present itself in the DAPI channel associated with the 2 μm MBs (see Figure D.4). However, the intensity of this autofluorescence was found to be low and did not significantly impact the visualization of the MBs.

On inspection of Figure 6.9, two key findings can be noted. Firstly, the effect of the BW and post-experimental module cleaning⁵ processes can be seen when comparing the surface density of the MBs present on the backwashed/cleaned samples (Module B) versus the non-backwashed/cleaned samples (Module A). The more saturated red and purple (*i.e.* magenta) colorations seen in the “MBs Only” row of the Module A subfigure are indicative of a higher concentration of particles in compar-

⁵Post-experimental module cleaning is akin to periodic chemical cleaning-in-place (CIP) processes which are common in commercial membrane applications.

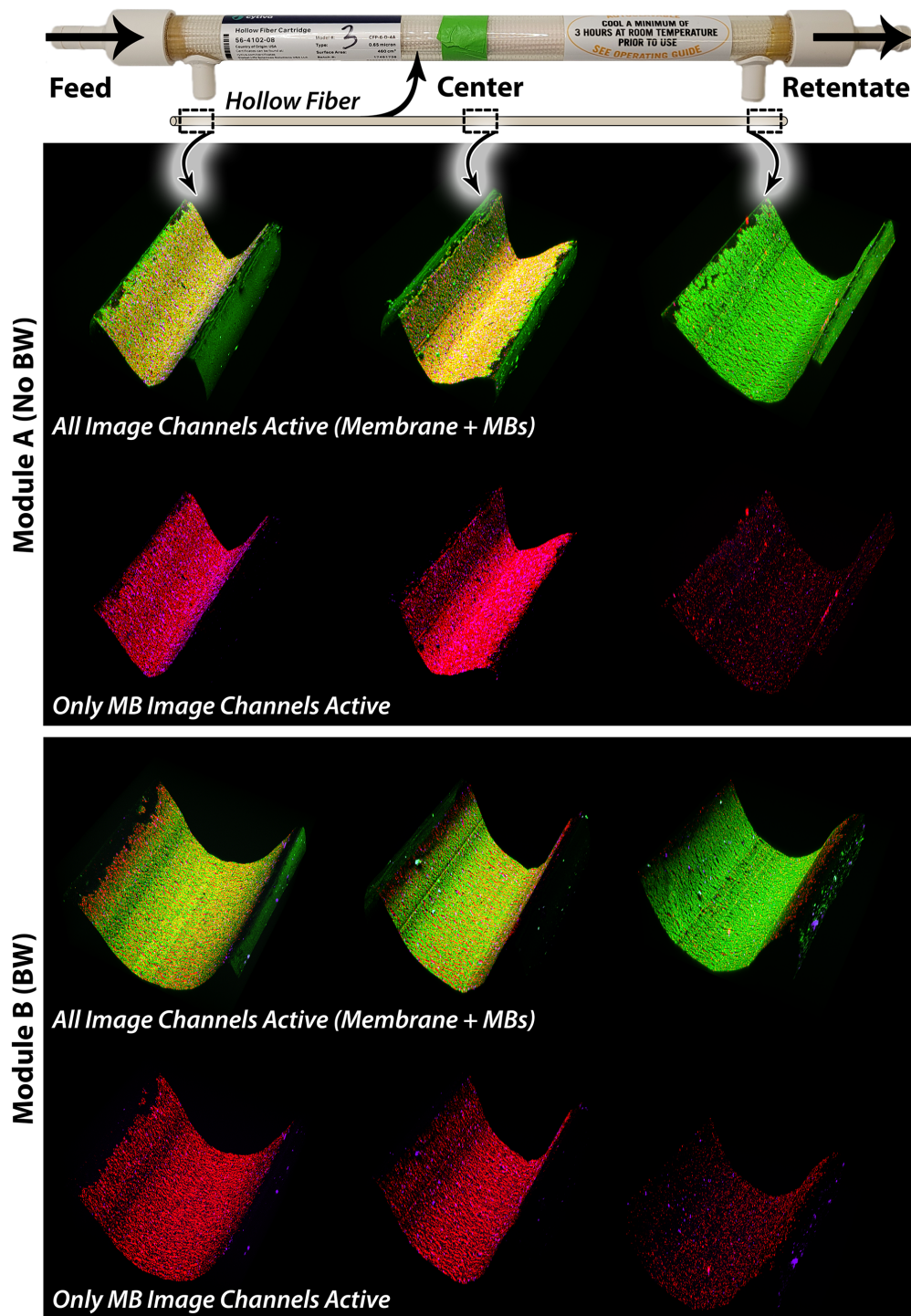


Figure 6.9: Composite of CLSM images of half-sections excised from a single hollow fiber extracted from either Module A (top; *BW not used*) or Module B (bottom; *BW used*) following the culmination of all filtration experiments. The membrane polymer (dyed with FITC), 0.5 μm MBs, and 2 μm MBs appear green (■), red (■), and purple (■), respectively, in the images.

ison to the same row in the Module B subfigure. The difference in coloration is especially apparent for the half-sections taken from the feed side and center of the hollow fibers. In conjunction with the flux decline and recovery results from Figures 6.5–6.7, this finding indicates that the BW process was at least somewhat effective at removing adsorbed MBs from the surface of the membranes. This further helps to validate the findings presented in Figure 6.8 regarding the concentration of MBs in the BW water. It should be noted, however, that Module A underwent one more filtration of wastewater and MBs (Experiment #5) than Module B, therefore, some of MBs partitioned onto the membranes in Module A could be attributable to this additional experiment. In spite of this, there is no evidence of a significant flux decline over the entire Experiment #5 which indicates that additional MB deposition over the experiment was managed by the periodic BW up until the start of the last filtration cycle. While this observation lends credibility to the CLSM findings, a future experiment could be performed to strengthen this assertion whereby two identical modules undergo the same filtration experiment, but one module is backwashed at the end while the other is not.

The second key finding from Figure 6.9 is the disparity in the surface concentrations of MBs at the feed side and center versus at the retentate side of the hollow fibers, regardless of the module. Taking into account the colour saturation, there is clearly a greater concentration of MBs deposited at the the feed and the center of the fibers in comparison to the retentate. This indicates a spatial variation in MB fouling over the length of the hollow fibers. A likely cause for the lesser degree of fouling at the retentate ends of the fibers stems from the pressure gradient along the lumen of each individual hollow fiber. According to the Hagen-Poiseuille Equation for laminar flow of a fluid through a straight conduit with a circular cross-section of radius R (m), the pressure drop $\Delta P = P_{feed} - P_{ret}$ (Pa) over its entire length L (m) is computed as follows [45]:

$$\Delta P = \frac{8\mu\bar{v}_{avg}L}{R^2} \quad (6.10)$$

where μ is the fluid's dynamic viscosity (Pa·s) and \bar{v}_{avg} is the *constant* average velocity of the fluid within the conduit. From this model, the pressure drop increases linearly along the fiber from P_{feed} to P_{ret} , meaning that the local pressure P within the lumen decreases accordingly. This analysis is simplistic given that a portion of the feed permeates through the membrane, thus v_{avg} varies along the length of the fiber (see §6.3.3). Yoon *et al.* (2008) take this into account in their study of flow

inside hollow fibers and apply a differential form of Equation 6.10, instead:

$$\frac{dP}{dx} = -\frac{8\mu v_{avg}(x)}{R^2} \quad (6.11)$$

where dP/dx is the change in pressure inside the lumen along the fiber's length ($0 \leq x \leq L$) and the radially-averaged velocity $v_{avg}(x)$ changes with x . Using this model instead, the pressure decreases non-linearly across the length of the fiber [46].

As the permeate fluid can leave the Cytiva modules via two large exit ports—one on each end of the module—it is reasonable to approximate the pressure of the permeate stream P_{perm} as essentially constant outside of the fiber. All factors considered, the *pressure driving force* $P - P_{perm}$ decreases across the length of each hollow fiber.⁶ The decline in pressure driving force along each fiber implies a lower localized permeate flux passing through the membrane at the retentate end of the fiber versus the feed end of the fiber. This is expected to reduce the convective transport of solids and MBs to the membrane surface [47] at the retentate end, and concurrently, reduce the incidence of MB fouling.

Unfortunately, the spatial distribution of fouling along the length of inside-out hollow fiber membranes is not a well-studied area. However Li *et al.* (2017) do remark that some relevant investigations are documented in the literature [44]. Carroll & Booker (2000) corroborate the above observation, stating that the internal fouling of hollow fiber membranes occurs non-uniformly and transiently along the length of the fiber, depending on the flux profile, membrane permeability, and fiber dimensions [48]. As an example, Sun *et al.* (2011) operated a *Zenon ZW10* pilot module containing submerged hollow fiber UF membranes (stated pore size = 0.04 μm) operating in outside-in configuration. Via CLSM analysis, the authors noticed a spatial variation in the localization of biofouling on the hollow fibers whereby significantly thicker biofilms were found towards the bottom of the fibers. However, they did not provide a rationale for this finding [49]. A similar result was seen by Lee *et al.* (2009) who investigated biofouling on the surface of *Zenon ZeeWeed 500c* hollow fibers (stated pore size = 0.04 μm) arranged in a submerged bioreactor operating in an outside-in configuration. As measured via CLSM, biofouling categorized into cellular matter and polysaccharides was found to vary along the length of the fibers depending on local TMP conditions [50]. In another example,

⁶This reiterates that the value of *TMP* from Equation 6.1 is a metric that is averaged over the *length* of all of the hollow fiber membranes!

Li *et al.* (2014) used an *in situ* ultrasonic spectrum analysis technique to monitor fouling via a yeast suspension filtered by a submerged hollow fiber membrane (stated pore size = 0.1 μm) [51]. They found that initially, the deposition of foulant material coincided with areas of higher flux along the hollow fiber, however, the deposition became more uniform over time. The lengthier experimental duration in Li *et al.*'s study (360 minutes, versus the 10 minute cycle length from this study) likely explains why that observation was not noted, here. Overall, a key implication of this finding is that the retentate ends of the membranes appear to be significantly underutilized in terms of their capacity to filter wastewater. The intelligent design of future membranes and module (*e.g.* module hydrodynamics [44]) may be able to resolve shortcomings and improve system performance in terms of total flux and analyte rejection.

6.4 Concluding Remarks

In this study, two PSf Cytiva hollow fiber membrane modules with nominal 0.65 μm pore sizes were evaluated for their ability to withhold fluorescently-labelled MBs (0.5 and 2 μm) suspended in real 2° effluent wastewater under constant TMP filtration conditions (0.5 psi for 4 hours). Key findings from the investigation include:

- ▶ Despite the fact that the two membrane modules that were tested were ostensibly identical, they demonstrated substantially different filtration performances. For both Conditions A and B, Module A produced a significantly greater permeate flux over the course of the experiments. However, this was at the expense of its ability to reject MBs: Module A also showed a significantly lower rejection of the 0.5 μm MBs, in particular.
- ▶ The effects of membrane fouling were clearly seen in all filtration experiments. The permeate fluxes tended to reach pseudo-steady state values, indicating a balance between the deposition of solids onto the surfaces of the membranes and the removal of these solids via BW between each of the filtration cycles. Short-term declines in permeate fluxes were measured during most of the individual filtration cycles. In the experiments where the MBs were added, concurrent increases in the rejection coefficients of the MBs were observed which indicate the mediating effect of the foulant layers on the ability of the MBs to traverse the membranes. Paradoxically, while membrane fouling is undesirable from the perspective of permeate water throughput,

it is advantageous in that it increases the rejection of MPs, preventing them from entering the permeate water streams. The design and operation of membrane systems in 3° polishing applications must consider this tradeoff between MP removal and permeate water productivity.

- ▶ FC was used to quantify the concentration of MBs in feed and permeate samples. Due to the different fluorophores in the 0.5 μm and 2 μm MBs, the technique was able to differentiate between the different MBs, even in the presence of autofluorescent organic matter in the wastewater.
- ▶ Via MB concentration measurements, it was found that the rejection of MBs was initially almost complete in the first half (~ 120 minutes) of the filtration experiments. However, rejection coefficients decreased significantly in the second half of these experiments, which was especially evident with the 0.5 μm MBs. This phenomenon is previously described, where multiple cycles of filtration and relaxation encourage particles to traverse the membrane. MP filtration researchers and engineers who design or operate WWTPs should be aware of this “breakthrough” phenomenon so that they can properly design their experiments or membrane filtration systems.
- ▶ An experiment was performed to elucidate the effect of the feed crossflow velocity on the performance of Module A. Despite clear differences in the average crossflow velocities in the two experiments that were compared, no clear differences in the rejection of the MBs were seen. Though theory suggests that the lower crossflow velocity could increase the severity of membrane fouling and this additional fouling layer can contribute to a dynamic increase in particle rejection, this was not observed. The relative magnitudes of membrane surface fouling versus fouling within the pores is a likely driver of this phenomenon.
- ▶ An analysis of BW water samples collected periodically found considerable MBs concentrations which could not have originated from the feed wastewater alone, implying that they were dislodged from the membranes/modules during the BW processes. The implication of this finding is that proper management of the BW water must be ensured to prevent these MBs from entering the environment via haphazard disposal practices. A better understanding of the fate of these rejected MBs is needed in the typical case where they are returned to an earlier stage in the wastewater treatment process.

- CLSM analysis of used hollow fibers from both modules provided a qualitative assessment of the effectiveness of the BW and cleaning processes used in this study. The backwashed and cleaned fibers saw substantially lower surface concentrations of the MBs than fibers which did not undergo BW/cleaning. Furthermore, there was substantially less deposition of MBs at the retentate ends of the hollow fibers, likely due to the lower pressure driving force at those ends of the modules. This implies that retentate ends may be underutilized in terms of local flux under the specific filtration conditions that were employed.

Overall, this study provides unique and novel insights to the operation of an *entire membrane module* used for the filtration of 2° effluent wastewater containing MPs. Additional bench- and pilot-scale research is needed to validate the use of membranes in these types of applications.

6.5 Works Cited

- [1] S. A. Carr, J. Liu, and A. G. Tesoro, “Transport and fate of microplastic particles in wastewater treatment plants,” *Water Research*, vol. 91, pp. 174–182, 2016.
- [2] S. M. Mintenig, I. Int-Veen, M. G. J. Löder, S. Pimpke, and G. Gerdt, “Identification of microplastic in effluents of waste water treatment plants using focal plane array-based micro-Fourier-transform infrared imaging,” *Water Research*, vol. 108, pp. 365–372, 2017.
- [3] M. Lares, M. C. Ncibi, M. Sillanpää, and M. Sillanpää, “Occurrence, identification and removal of microplastic particles and fibers in conventional activated sludge process and advanced MBR technology,” *Water Research*, vol. 133, pp. 236–246, 2018.
- [4] L. Yang, K. Li, S. Cui, Y. Kang, L. An, and K. Lei, “Removal of microplastics in municipal sewage from China’s largest water reclamation plant,” *Water Research*, vol. 155, pp. 175–181, 2019.
- [5] E. A. Ben-David, M. Habibi, E. Haddad, M. Hasanin, D. L. Angel, A. M. Booth, and I. Sabbah, “Microplastic distributions in a domestic wastewater treatment plant: Removal efficiency, seasonal variation and influence of sampling technique,” *Science of The Total Environment*, vol. 752, p. 141880, 2021.
- [6] M. Barchiesi, A. Chiavola, C. D. Marcantonio, and M. R. Boni, “Presence and fate of microplastics in the water sources: focus on the role of wastewater and drinking water treatment plants,” *Journal of Water Process Engineering*, vol. 40, p. 101787, 2021.
- [7] S. Ziajahromi, P. A. Neale, L. Rintoul, and F. D. L. Leusch, “Wastewater treatment plants as a pathway for microplastics: development of a new approach to sample wastewater-based microplastics,” *Water Research*, vol. 112, pp. 93–99, 2017.
- [8] K. Trzaskus, M. Elshof, A. Kemperman, and K. Nijmeijer, “Understanding the role of nanoparticle size and polydispersity in fouling development during dead-end microfiltration,” *Journal of Membrane Science*, vol. 516, pp. 152–161, 2016.

- [9] F. Fallahianbijan, S. Giglia, C. Carbrello, and A. L. Zydney, “Use of fluorescently-labeled nanoparticles to study pore morphology and virus capture in virus filtration membranes,” *Journal of Membrane Science*, vol. 536, pp. 52–58, 2017.
- [10] M. Pazouki, A. N. Wilton, and D. R. Latulippe, “An experimental study on sterile filtration of fluorescently labeled nanoparticles—the importance of surfactant concentration,” *Separation and Purification Technology*, vol. 218, pp. 217–226, 2019.
- [11] A. Y. Kirschner, Y. H. Cheng, D. R. Paul, R. W. Field, and B. D. Freeman, “Fouling mechanisms in constant flux crossflow ultrafiltration,” *Journal of Membrane Science*, vol. 574, pp. 65–75, 2019.
- [12] N. Taylor, W. J. Ma, A. Kristopeit, S. C. Wang, and A. L. Zydney, “Retention characteristics of sterile filters—Effect of pore size and structure,” *Journal of Membrane Science*, vol. 635, p. 119436, 2021.
- [13] L. Li, D. Liu, K. Song, and Y. Zhou, “Performance evaluation of MBR in treating microplastics polyvinylchloride contaminated polluted surface water,” *Marine Pollution Bulletin*, vol. 150, p. 110724, 2020.
- [14] U. Beuscher, E. J. Kappert, and J. G. Wijmans, “Membrane research beyond materials science,” *Journal of Membrane Science*, vol. 643, 2022.
- [15] D. M. Warsinger, S. Chakraborty, E. W. Tow, M. H. Plumlee, C. Bellona, S. Loutatidou, L. Karimi, A. M. Mikelonis, A. Achilli, A. Ghassemi, L. P. Padhye, S. A. Snyder, S. Curcio, C. D. Vecitis, H. A. Arafat, and J. H. Lienhard, “A review of polymeric membranes and processes for potable water reuse,” *Progress in Polymer Science*, vol. 81, p. 209, 2016.
- [16] J. G. Jacangelo and C. A. Buckley, “Microfiltration,” in *Water Treatment Membrane Processes*, J. Mallevialle, P. R. Odendall, and M. R. Wiesner, Eds. McGraw-Hill, 1996.
- [17] J. Günther, P. Schmitz, C. Albasi, and C. Lafforgue, “A numerical approach to study the impact of packing density on fluid flow distribution in hollow fiber module,” *Journal of Membrane Science*, vol. 348, pp. 277–286, 2010.
- [18] K. Gupta and S. Chellam, “Contributions of surface and pore deposition to (ir)reversible fouling during constant flux microfiltration of secondary municipal wastewater effluent,” *Journal of Membrane Science*, vol. 610, p. 118231, 2020.
- [19] T. Wintgens, T. Melin, A. Schäfer, S. Khan, and M. Muston, “The role of membrane processes in municipal wastewater reclamation and reuse,” *Desalination*, vol. 178, pp. 1–11, 2005.
- [20] M. Raffin, E. Germain, and S. Judd, “Wastewater polishing using membrane technology: a review of existing installations,” *Environmental Technology*, vol. 34, no. 5, pp. 617–627, 2013.
- [21] J. W. Chew, J. Kilduff, and G. Belfort, “The behavior of suspensions and macromolecular solutions in crossflow microfiltration: An update,” *Journal of Membrane Science*, vol. 601, p. 117865, 2020.
- [22] G. Belfort and N. Nagata, “Fluid mechanics and cross-flow filtration: some thoughts,” *Desalination*, vol. 53, pp. 57–79, 1985.
- [23] G. Belfort, R. H. Davis, and A. L. Zydney, “The behavior of suspensions and macromolecular solutions in crossflow microfiltration,” *Journal of Membrane Science*, vol. 96, pp. 1–58, 1994.
- [24] T. Urase, K. Yamamoto, and S. Ohgaki, “Effect of pore structure of membranes and module configuration on virus retention,” *Journal of Membrane Science*, vol. 115, pp. 21–29, 1996.

- [25] ———, “Effect of pore size distribution of ultrafiltration membranes on virus rejection in crossflow conditions,” *Water Science & Technology*, vol. 30, pp. 199–208, 1994.
- [26] C. Anselme and E. P. Jacobs, “Ultrafiltration,” in *Water Treatment Membrane Processes*, J. Mallevalle, P. R. Odendall, and M. R. Wiesner, Eds. McGraw-Hill, 1996.
- [27] W. Guo, H.-H. Ngo, and J. Li, “A mini-review on membrane fouling,” *Bioresource Technology*, vol. 122, pp. 27–34, 2012.
- [28] W. C. Lay, Y. Liu, and A. G. Fane, “Impacts of salinity on the performance of high retention membrane bioreactors for water reclamation: A review,” *Water Research*, vol. 44, pp. 21–40, 2010.
- [29] S. Shirazi, C. J. Lin, and D. Chen, “Inorganic fouling of pressure-driven membrane processes—A critical review,” *Desalination*, vol. 250, pp. 236–248, 2010.
- [30] P. R. Bérubé, E. R. Hall, and P. M. Sutton, “Parameters Governing Permeate Flux in an Anaerobic Membrane Bioreactor Treating Low-Strength Municipal Wastewaters: A Literature Review,” *Water Environment Research*, vol. 78, pp. 887–896, 2006.
- [31] J. Sun, X. Dai, Q. Wang, M. C. van Loosdrecht, and B. J. Ni, “Microplastics in wastewater treatment plants: detection, occurrence and removal,” *Water Research*, vol. 152, pp. 21–37, 2019.
- [32] S. J. Judd and S. W. Till, “Bacterial rejection in crossflow microfiltration of sewage,” *Desalination*, vol. 127, pp. 251–260, 2000.
- [33] M. Raffin, E. Germain, and S. Judd, “Influence of backwashing, flux and temperature on microfiltration for wastewater reuse,” *Separation and Purification Technology*, vol. 96, pp. 147–153, 2012.
- [34] B. K. Pramanik, L. Shu, V. Jegatheesan, and M. A. Bhuiyan, “Effect of the coagulation/persulfate pre-treatment to mitigate organic fouling in the forward osmosis of municipal wastewater treatment,” *Journal of Environmental Management*, vol. 249, p. 109394, 2019.
- [35] S. de Boer, J. González-Rodríguez, J. J. Conde, and M. T. Moreira, “Benchmarking tertiary water treatments for the removal of micropollutants and pathogens based on operational and sustainability criteria,” *Journal of Water Process Engineering*, vol. 46, p. 102587, 2022.
- [36] Metcalf & Eddy Inc., G. Tchobanoglous, F. Burton, and H. Stensel, *Wastewater Engineering: Treatment and Reuse*, 4th ed. McGraw-Hill, 2003.
- [37] M. R. Michielssen, E. R. Michielssen, J. Ni, and M. B. Duhaine, “Fate of microplastics and other small anthropogenic litter (SAL) in wastewater treatment plants depends on unit processes employed,” *Environmental Science: Water Research & Technology*, vol. 2, no. 6, pp. 1064–1073, 2016.
- [38] R. A. Bergman, R. Porter, D. Joffe, and E. Minchew, “Commissioning and Operation of a 50 MGD Ultrafiltration Advanced Reclamation Facility for Gwinnett County, Georgia,” in *Proceedings of the Water Environment Federation*, vol. 2006, no. 10, 2006, pp. 2698–2715.
- [39] W. A. Mitch and D. L. Sedlak, “Characterization and Fate of *N*-Nitrosodimethylamine Precursors in Municipal Wastewater Treatment Plants,” *Environmental Science and Technology*, vol. 38, pp. 1445–1454, 2004.

- [40] V. S. Koutnik, S. Alkidim, J. Leonard, F. DePrima, S. Cao, E. M. V. Hoek, and S. K. Mohanty, “Unaccounted Microplastics in Wastewater Sludge: Where Do They Go?” *ACS ES&T Water*, vol. 1, pp. 1086–1097, 2021.
- [41] M. A. Woods and A. L. Zydney, “Effects of a pressure release on virus retention with the Ultipor DV20 membrane,” *Biotechnology and Bioengineering*, vol. 111, pp. 545–551, 2014.
- [42] S. K. Dishari, A. Venkiteswaran, and A. L. Zydney, “Probing effects of pressure release on virus capture during virus filtration using confocal microscopy,” *Biotechnology and Bioengineering*, vol. 112, pp. 2115–2122, 2015.
- [43] S. K. Dishari, M. R. Micklin, K. J. Sung, A. L. Zydney, A. Venkiteswaran, and J. N. Earley, “Effects of solution conditions on virus retention by the Viresolve® NFP filter,” *Biotechnology Progress*, vol. 31, pp. 1280–1286, 2015.
- [44] X. Li, Y. Mo, J. Li, W. Guo, and H. H. Ngo, “In-situ monitoring techniques for membrane fouling and local filtration characteristics in hollow fiber membrane processes: A critical review,” *Journal of Membrane Science*, vol. 528, pp. 187–200, 2017.
- [45] C. Geankoplis, A. Hersel, and D. Lepek, *Transport Processes and Separation Process Principles*. Prentice Hall, 2018.
- [46] S. H. Yoon, S. Lee, and I. T. Yeom, “Experimental verification of pressure drop models in hollow fiber membrane,” *Journal of Membrane Science*, vol. 310, pp. 7–12, 2008.
- [47] J. Kim and F. A. DiGiano, “Critical review fouling models for low-pressure membrane systems,” *Separation and Purification Technology*, vol. 68, pp. 293–304, 2009.
- [48] T. Carroll and N. A. Booker, “Axial features in the fouling of hollow-fibre membranes,” *Journal of Membrane Science*, vol. 168, pp. 203–212, 2000.
- [49] C. Sun, L. Fiksdal, A. Hanssen-Bauer, M. B. Rye, and T. Leiknes, “Characterization of membrane biofouling at different operating conditions (flux) in drinking water treatment using confocal laser scanning microscopy (CLSM) and image analysis,” *Journal of Membrane Science*, vol. 382, no. 1–2, pp. 194–201, 2011.
- [50] W. N. Lee, W. S. Cheong, K. M. Yeon, B. K. Hwang, and C. H. Lee, “Correlation between local TMP distribution and bio-cake porosity on the membrane in a submerged MBR,” *Journal of Membrane Science*, vol. 332, pp. 50–55, 2009.
- [51] X. Li, J. Li, J. Wang, H. Wang, B. He, H. Zhang, W. Guo, and H. H. Ngo, “Experimental investigation of local flux distribution and fouling behavior in double-end and dead-end submerged hollow fiber membrane modules,” *Journal of Membrane Science*, vol. 453, pp. 18–26, 2014.

Conclusions & Recommendations for Future Work

In Chapter 1, it was asserted that membrane technologies are positioned to be an “ideal” solution to mitigate the discharge of microplastics (MPs) into the aquatic environment from the effluents of municipal wastewater treatment plants (WWTPs). However, this assertion is somewhat undercut by the observation that the contemporary literature is limited in its understanding of how membranes perform in the presence of MPs, and how the rejection of these particles is affected by membrane/MP properties, solution conditions, and system operating parameters. The implementation of such technologies can be risky if we do not properly understand the how they perform, given the interactions between the MPs and the process. This is especially true given the fact that membranes are not currently designed for the express purpose of the removal of MPs from wastewater. To seize upon these opportunities, I described “six thematic elements” for guiding novel research at the intersection of MPs and membranes. These elements informed research in this work towards the characterization of membrane fouling effects by irregular-shaped MPs suspended in 2° effluent wastewater, the assessment of the transmission of these MPs through microfiltration membranes over a range of operating conditions, the development of a better protocol which employs flow cytometry (FC) to quantify the presence of fluorescent MPs in complex samples, and the scaling-up of filtration experiments to assess MP fouling and rejection effects under more realistic filtration conditions. Accordingly, the findings outlined in this work are summarized, below.

7.1 Summary of Research

Chapter 3 sought to quantify how the presence of varying concentrations of irregular and polydisperse MP particles affects the fouling of microfiltration and ultrafiltration (MF/UF) membranes when 2° effluent wastewater is filtered. To this end, it was found that sourcing MPs which are representative of those found in WWTPs for filtration experiments is a challenging endeavour. This study employed a novel milling and sieving process to create irregularly-shaped polyethylene (PE) MPs approximately 10 μm in size which were then suspended in actual 2° effluent wastewater such that the solution conditions used in the experiments reflected those in WWTPs. Membrane fouling due to the presence of the MPs interactions was investigated via constant pressure filtration experiments using commercial MF/UF membranes. It was found that even low concentrations of MPs in the wastewater increased the extent of membrane fouling under dead-end filtration. Subsequently, the underlying fouling mechanisms—dominated by cake filtration—were elucidated. These findings lay the groundwork for the optimization of membranes and membranes processes which are resistant to irreversible MP fouling. To this end, a backwashing (BW) process was found to significantly—but not completely—restore the permeate flux through the membranes by removing deposited MPs and wastewater solids. This study is particularly valuable in that various authors have considered the effects of MPs on membrane fouling [1, 2], however, experiments were conducted merely in “pristine” solutions. “Real” 3° wastewater polishing processes contain suspended/dissolved solids, thus, this study provides important insights into the factors governing membrane fouling by MPs in water chemistries representative of WWTP effluents.

Chapter 4 sought to quantify how the pore size of MF membranes affects the transmission of irregularly-shaped, polydisperse MP particles over a range of permeate fluxes. The rejection of these irregularly-shaped MPs—like those found in WWTPs—is poorly documented, even in small, controlled laboratory filtration experiments. Utilizing the ball-milling/sieving technique developed in the previous chapter, irregular MPs $\sim 10 \mu\text{m}$ in size were produced from a fluorescent PE feedstock. The inherent value of using such a fluorescent feedstock lies in the fact that the MPs that were created are simple to detect (versus MPs created using a non-fluorescent feedstock) as samples could be analyzed via a standard fluorometric plate reader to ascertain the *bulk concentrations* of particles in aqueous samples. Very small MPs (*e.g.* $< 20 \mu\text{m}$) are known to be particularly challenging to

identify, thus automating measurements in this way greatly simplifies the MP quantification process as oppose to the other conventional “visual” enumeration techniques. To address the gap in the contemporary literature, a series of experiments characterized the filtration of irregular MP particles through Durapore® MF membranes (nominal pore sizes = 0.45 and 5 μm). Permeate samples originating from the 0.45 μm membrane exhibited low fluorescent intensities relative to feed samples, inferring little to no MP transmission. Conversely, samples from the 5 μm membrane exhibited fluorescent intensities up to ~ 6 times greater, indicating significant MP transmission. With this particular membrane, the transmission was exacerbated at higher permeate fluxes which indicates the effect of operating conditions on the retention of MPs. Evidence suggests that the dimension of the *irregular* particles which transmitted through the 5 μm membrane could approach the membrane’s nominal pore size. Post-filtration analyses demonstrated that the capture of these MPs occurred largely at the membrane’s feed-side interface, where greater MP intrusion into the porous structure was seen with the 5 μm membrane. This study’s results reaffirm the importance of choosing an appropriate membrane/membrane pore size and operating conditions to maximize MP retention.

Chapter 5 sought to develop and characterize an analysis technique to individually quantify the presence of fluorescent MPs that are suspended in membrane feed/permeate samples. To this end, it was hypothesized that flow cytometry (FC) could constitute an efficient and effective tool for identifying and quantifying the presence of fluorescent plastic microbeads (MBs) in aqueous suspensions. Indeed, this technique was shown to be a powerful method for automating MP concentration measurements. Even in the presence of humic acid (HA), a common constituent in wastewater and a model organic foulant, FC discerned and quantified the concentrations of MBs that were three orders of magnitude more dilute than a fluorometric plate reader could resolve. The implication of this finding is that given the fluorophore that was used, FC proved to be a more sensitive tool for measuring MB concentrations even in the presence of autofluorescent natural organic matter like HA. Furthermore, the “events” recorded by the FC instrument correspond to the detection of individual MBs in samples and are not “bulk” measurements of fluorescent matter in the sample, as is the case with the plate reader. For researchers who are evaluating MP removal technologies at a laboratory scale, FC provides substantial value as it enables efficient MP quantification in samples with (potentially) large numbers of dilute, very small particles, as well as other confounding organic substances. To this end, FC was applied to quantify 1–5 μm MB rejection in HA solutions filtered via

MF membranes. Over the course of these experiments, FC easily identified/quantified wide ranges of MB concentrations in permeate samples, resulting in the computation of widely-varying MB rejection coefficients. Very high retention of the MBs was seen with a 0.45 μm membrane, whereas MB rejection proved to be transient for a 5 μm membrane, depending on the solution conditions and filtration time. Finally, a simple model was formulated to estimate MB particle sizes in the membrane feed and permeate samples. During filtrations using the 5 μm membrane, significant reductions in median particle size (25–36%) were seen, affirming the preferential rejection of larger MBs while permitting the passage of smaller ones. The preferential transmission of smaller MBs is particularly concerning as it is expected that smaller particles pose a greater ecological hazard than larger particles (see §1.1.2). While the value of this technique for providing MB removal data was demonstrated using 3° MF as an example, FC could easily be applied to evaluate many other MB removal processes such as media filtration or adsorption. Or, it could be applied to investigations of entire WWTPs, as to be discussed in §7.2.

Chapter 6 sought to use the knowledge produced in the previous three chapters to assess membrane performance (*e.g.* fouling behaviour, MB rejection, etc.) when 2° effluent wastewater containing MPs is processed via a “scaled-up” membrane module. This study was positioned to fill a gap in the literature between small-scale, controlled laboratory filtration experiments with simple solutions/operating conditions, and large-scale, observational studies of MP removal in WWTPs with highly complex solutions/operating conditions. The actual 2° effluent wastewater, the four-hour experimental duration involving 24 filtration/backwashing cycles, and the hollow fiber crossflow MF module (nominal pore size = 0.65 μm) used in the experiments position this study to provide valuable insights into filtration performance under more realistic conditions at a scale which is still controllable. The results show that the permeate flux reached a favourable pseudo-steady state, indicative of a balance between undesirable membrane fouling and the periodic removal of the solids via BW. The rejection of 0.5 μm and 2 μm fluorescent MBs doped into the wastewater were simultaneously obtained via FC. Notably, the instrument was able to discern between the two sizes of MBs even in the presence of the organic matter in the wastewater. MB rejection proved to be almost complete for the 2 μm MBs; for the 0.5 μm MBs, it was very high for roughly 120 minutes, at which point, a “breakthrough effect” was noted whereby significant quantities of MBs were found in permeate samples. The finding has significant implications with respect to the *minimum length* that a fil-

tration experiment needs to be in order to elucidate important phenomena. It also highlights the need for realistic module operation, such as the use of BW. Considering the BW process in detail, significant quantities of MBs were measured in the backwashed water which underscores the need for the effective treatment of this waste stream. Finally, an autopsy of the used membrane modules uncovered a greater extent of MB fouling at the feed terminuses of the hollow fibers versus the retentate terminuses. This implies that regions closer to the retentate ends of the modules are underutilized in terms of local flux along the fibers. Overall, this study is—to my knowledge—the first to consider the performance of hollow fiber MF membrane modules for the 3^o treatment of wastewater effluents containing MPs and thus provides substantial novel insights to the field.

In summary, this work has improved our understanding of the interactions between MP particles and membrane technologies in the context of municipal wastewater treatment effluent polishing.

7.2 Opportunities for Future Study

As the study of MPs is still quite new and our understanding of the field still developing, there are plenty of opportunities for future study. This includes the limitations inherent to this particular work. To this end, a discussion of some interesting knowledge gaps can be found, below.

■ **Improved leak detection in filtration studies.** Various researchers have noted the presence of MPs in the permeate streams of membrane processes when it would not normally be expected for them to be there, as noted in §1.3.1. For example, Ziajahromi *et al.* (2017) observed an average MP concentration of 0.21 MP/L in the permeate water of a WWTP which utilizes reverse osmosis technologies [3]. The presence of these MPs may have resulted from sample contamination (*e.g.* fibers from clothing worn by the investigators), defects in the membranes, or leaks in seals which permitted the transport of the MPs to the permeate stream. Lares *et al.* (2018) studied a pilot-scale MBR (stated pore size = 0.4 μm) and determined that the overall removal rate of MPs was 99.4%. Surprisingly, $\sim 40\%$ of the MPs in the permeate stream exceeded 1,000 μm in size, whereas another $\sim 40\%$ were 250–1,000 μm in size, whereas the remaining $\sim 20\%$ were below 250 μm . These size measurements suggest possible sample contamination, the presence of membrane defects, or leaks in the seals in the modules that were studied. As one final example, Leslie *et al.* (2017) studied

another pilot-scale MBR with an even smaller stated pore size (0.08 μm), yet still found an average of 51 MPs/L in the permeate samples [4]. Again, similar explanations are possible: membrane defects/gaps/leaks in the seals, sample contamination, and so on. As is evident, the explanation of “leaks” or “defects” is commonly used, however, these explanations have largely gone untested.

In Chapter 4, the integrity of the sealing of the membrane coupons was evaluated through the use of large, fluorescent spherical MPs (Sph-MPs; 53–63 μm) which should, under no circumstances, be expected to pass through membranes nominally rated with 5 μm and 0.45 μm pore sizes. The analysis of permeate samples using the plate reader and presented in Figure 4.4 showed no evidence of the fluorescent Sph-MPs in permeate samples, validating the quality of the sealing in the tests. However, these tests were performed parallel to the regular filtration experiments with the smaller milled-and-sieved (M/S) MPs. As such, *new membrane coupons* were sealed into the cells to collect data for the filtration of the M/S-MPs, therefore, the sealing integrity of the cells was not necessarily guaranteed in all experiments. An improved version of this suite of experiments would spike a low concentration of the large Sph-MPs into suspension *with* the small M/S-MPs such that the sealing integrity of the membrane cell could be evaluated *in situ* in each experiment. One complication in this methodology is that the Sph-MPs and M/S-MPs utilized the same “green” fluorophore. However at the time of writing, the same PE chemistry and MP particle size can be bought from the same supplier (*Cospheric*), but with different fluorophores. For example, 53–63 μm Sph-MPs could be purchased with a “red” fluorophore ($\lambda_{ex} = 575 \text{ nm}$; $\lambda_{em} = 607 \text{ nm}$) such that the presence of leaks could be evaluated at a different excitation/emission wavelength pair than that used to evaluate the transmission of M/S-MPs.

An exciting variation of this leak evaluation technique could be extended to probing the integrity of membrane processes in actual WWTPs. A large, fluorescent MP would be first selected, informed by a sampling campaign which confirms that similar MPs are not present naturally in the feed to the membrane process or in the permeate samples. Then, the feed wastewater could be doped with the selected MPs. Subsequent sampling of the permeate water would be performed, with the samples analyzed via FC to identify the potential presence of the MPs. Finding these large MPs in the permeate samples would be a strong indicator that there are defects in the membranes or leaks in the seals.

■ **Fluorophore choice when using a plate reader to quantify MP concentrations.** In Chapter 5, the utility of a flow cytometer versus a fluorometric plate reader was discussed when fluorescent MBs were suspended in HA solutions. In Figure 5.3, it was demonstrated that a “plateau” in fluorescent intensity was seen when the plate reader was used, caused by the autofluorescence of the HA. This was further elucidated in the excitation-emission matrices (EEMs) shown in Figure 5.4. It was asserted that this autofluorescence obscured the signal associated with the fluorescence of the MBs. As such, it was suggested that the flow cytometer—which does not suffer from this apparent limitation—would be a more appropriate tool in this scenario. However, it should be noted that FC is a more complex, expensive, and time-consuming technique, as compared to analysis via fluorometric plate reader. A few simple modifications to the experimental process could have made analysis via plate reader more practical. For example, the manufacturer’s estimate of the “peak” excitation/emission wavelengths of the “green” fluorophore incorporated into the MBs used in these experiments is $\lambda_{ex}/\lambda_{em} = 414/515$ nm. However, this wavelength pair corresponds to a region of high fluorescent intensity caused by the HA. Instead, a MB containing a different fluorophore could be utilized, such as *Cospheric*’s analogous *FMCE* series of MBs containing a “cerise” fluorophore, where $\lambda_{ex}/\lambda_{em} = 576/609$ nm.¹ This peak wavelength pair would experience far less interference from the HA as it falls outside of the aforementioned region of high fluorescence. Via Figure 5.4, the HA fluorescence at the peak wavelength pair for the cerise fluorophore is two orders of magnitude less than that at the peak wavelength pair for the green fluorophore. In HA solution, the plate reader should be able to discern lower concentrations of MBs with cerise fluorophores than MBs with green fluorophores, however, it should be noted that any additional background fluorescence at λ_{em} of the MP fluorophore would be expected to reduce the detectability of the MPs. An improved version of this study would utilize a more judicious choice of MB and fluorophore—such as the one above—to facilitate for better MB detection by a plate reader.

As a second option, the technique of fluorescence *excitation-emission matrices-parallel factor analysis* (EEM-PARAFAC) is a powerful mathematical tool used to characterize the presence and quantity of different organic matter species in water and wastewater samples [5]. This technique can deconvolute the overlapping fluorescence spectra in EEMs associated with different organic molecules. EEM-PARAFAC analysis could easily be applied to EEMs of samples containing fluorescent MBs,

¹Other options exist from other manufacturers (*e.g.* *ThermoFisher Scientific*), such as MBs with near-infrared/infrared fluorophores.

HA, or other fluorescent matter, enabling the quantification of the signal associated with the MBs versus other species. While this option is more mathematically complex than the previous option, it also should facilitate the use of a plate reader to characterize the concentrations of fluorescent MBs in samples containing other fluorescent matter.

■ **Validation of the FC technique for analyzing samples with irregularly-shaped MPs.**

Recall that the work presented in Chapters 5–6 was *inherently limited* in that the MPs used were spherical in shape, despite the fact that MPs in WWTPs tend to be irregular in shape and poly-disperse in size (see §1.1.1). A natural extension of these experiments would be to validate the quantification of irregularly-shaped MPs using the FC instrument. To do so, the ball-milling/sieving protocol used in Chapters 3–4 could be optimized to produce very small MPs (*e.g.* $O\{1\ \mu\text{m}\}$) from fluorescent feedstocks. To obtain such small, irregular particles, modifications to this procedure may be necessary, such as through the use of *wet* or *cryogenic* ball-milling which is further discussed on page 253. Sieves with very small apertures would likely be needed to isolate the particle sizes of interest. Subsequently, suspensions of these very small MPs could be analyzed via FC to verify that the instrument is effective towards quantifying the particles. As a foreseen challenge, significant variations in irregular MP size and shape would reasonably be expected to affect the scattering of light by these particles, as noted in §5.4. FSC intensity measurements may not easily correlate to MP size when analyzing MPs with various oblique or irregular surfaces. However, it is noted that *side scattering* (SSC) intensity measurements can be correlated to the “granularity” or “complexity” of particles [6]—relating to the presence of oblique surfaces. It may be possible to employ SSC intensity measurements as a descriptor of particle irregularity or perhaps roughness. More research is required to investigate these possibilities. As one final note, the analysis of MP fibers may be particularly challenging via FC due to the minuscule dimensions of various flow channels which could be occluded via long fibers. Care must be taken if attempts are made to quantify the presence of MP fibers via FC. Similar challenges may be encountered in the analysis of irregular particles, as well.

■ **Extensions to the performance study of the hollow fiber MF module.** In Chapter 6, scaled-up experiments were performed using a hollow fiber MF module. The intersection of parameters chosen (*e.g.* scale, duration, solution and operating conditions, membrane module, etc.) make

it unique within the field of study. There are many realistic and valuable directions in which this research can be extended by changing the membrane pore size (MF versus UF), geometry (hollow fiber versus spiral wound), chemistry (polymer versus ceramic), flow path (inside-out versus outside-in), flow configuration (crossflow versus direct feed), MP properties (beads versus fibers), experimental scale (benchtop versus pilot), and so on.

As one example, a crossflow configuration (*open* retentate port) was used in this study. This is a common method to mitigate the effects of membrane fouling, however, not all membrane modules operate in this fashion. Some processes employ a “direct feed” configuration: akin to a dead-end filtration, the retentate port is *closed* and feed water must exit the module through the permeate [7]. A lesser degree of tangential flow is achieved across the fibers, as a result. This configuration is suitable where the fouling propensity of the feed water is low, if very high water recoveries are desired, or if a reduction pumping costs associated with recirculating retentate water is desired. A future series of experiments could investigate membrane module performance in this new configuration. Due to the dead-ended flow path, it would be expected that the extent of membrane fouling would be significantly worse [8] due to the presence of suspended/dissolved solids and MPs. Elucidating possible spatial variations in MP fouling would be of special interest, given that it was shown in §6.3.5.3 that the MPs preferentially deposited towards the feed ends of the hollow fibers, indicating that the retentate ends were underutilized in terms of the local flux under the filtration conditions that were employed. The extent to which this effect occurs under a direct feed configuration is yet to be elucidated for MPs, though spatial variations in fouling during dead-end hollow fiber filtration have been documented in other applications [9].

As a second extension, we return to the idea of filtration experiments with *irregularly-shaped* MPs. Again, recall that spherical microparticles were used in the filtration studies shown in Chapter 6. Previous work has indicated that MPs of different shapes (*e.g.* irregular particles versus long fibers) interact with membranes in different fashions [10, 11]. For example, the fouling experiments highlighted in Chapter 3 were performed using irregular MP particles. However, one additional experiment was performed where MP fibers—synthesized in-house—were filtered instead. A comparison of the results for the filtration of MP fibers versus particles can be seen in Figure A.9. It is evident that different shapes of MPs display different fouling behaviours or mechanisms, depending on the

membrane that is used. In parallel, it would be expected that the transmission behaviour of a suspension of MP fibers would be different than a suspension of MP particles, all else equal. So, there is inherent value in performing the types of experiments seen in Chapter 6 using fibers. However, the discussion regarding the re-validation of the FC instrument (see page 246) should be considered in the context of this proposed extended module filtration study.

Extending the work performed in Chapter 6, confocal laser scanning microscopy (CLSM) could be employed to probe the capture of fluorescent MPs at *different depths* in the membrane's structure, as demonstrated in Chapter 4. This is of particular interest in the operation of the Cytiva membrane module due to the “breakthrough effect” that was observed (§6.3.4) whereby particle transmission was only seen after a number of filtration/BW cycles were performed. To visualize the intrusion of the MPs into the pore structure as a function of filtration time, a specialized experimental apparatus to immobilize individual hollow fibers should be used, such as the high-throughput hollow fiber evaluation device developed by Kazemi *et al.* (2019) [12]. After each filtration/BW cycle, individual hollow fibers could be extracted from the setup and analyzed via CLSM to observe the eventual breakthrough of the MPs, akin to what was seen by Dishari *et al.* (2015) who noted a step-wise migration of bacteriophages through a membrane's cross-section resulting from cyclical periods of applied pressure and pressure release [13].

As one last extension, a benchtop-scale membrane module (area = 460 cm²) was employed to model a 3° treatment process in a WWTP. Similar benchtop-scale experimentation has been performed with respect to MPs and MBRs [14], and even assessments of pilot-scale MBR performance in the presence of MPs have been made [15, 16]. However, analogous pilot-scale studies for 3° treatment membrane processes are lacking. As an example at the intersection of many of the “new” potential parameters mentioned previously, an entire module from Toray's *HFU-2020AN* series of hollow fiber outside-in UF membranes designed for dead-end operation in water/wastewater treatment [17] could be employed in a long-term MP filtration experiment at a pilot scale. The assessment of a full skid containing a membrane module and co-requisite equipment moves the experimental scale further right on the spectrum implied in Figure 6.1. Whereas the Cytiva module in Chapter 6 has a membrane area of 0.046 m², the Toray module has a membrane area of 72 m²: three orders of magnitude larger in scale. Performing such an experiment at a pilot scale would be better able to

predict the behaviour of a membrane installation in a WWTP, but under more controlled conditions.

■ **The effect of MP and membrane surface properties on fouling and rejection.** Over time, MPs can undergo various transformations in the natural or man-made environment [18]. Alimi *et al.* (2018) assert that weathering of MPs is known to change their surface properties; oxidation, such as through the process of photodegradation, can add charged carbonyl groups to the surface of MPs can lead to an increase in negative surface potential. Additionally, the particles can adsorb proteins, natural organic matter (*e.g.* humic acid [19]), and a variety of macromolecules that are present [18]. As was noted in §1.2.2.2, the growth of biofilms on the surfaces of “larger” MPs—especially due to the presence of microorganisms in 2° treatment—is expected to modify the size and overall density of the particles as well as alter their surface characteristics [20]. Depending on the initial surface properties of the MPs, molecular adsorption or the formation of biofilms may increase or decrease the MP hydrophilicity/hydrophobicity, surface charge, and the surface roughness [20–22]. The result is that MP properties are expected to change over time within a WWTP due to interactions with the solution matrix. Changes in hydrophilicity/hydrophobicity, surface charge (*e.g.* formation of hydroxyl/carboxyl groups), and roughness of MPs would be expected to influence the propensity of the particles to homo- or heteroaggregate [18] and influence their interactions with treatment processes, such as via adsorption to polymeric membranes.

The work presented herein is inherently limited in that “pristine” MPs were spiked into wastewater samples. However, future experiments should take into consideration the various surface properties of MPs in WWTPs. One valuable experiment would involve dosing a bioreactor with a quantity of pristine MPs and allowing them to recirculate within the vessel for a reasonable period of time. This “retention time” should be varied between a set of natural limits: either assuming that the MPs remain in the bioreactor for merely its hydraulic retention time (HRT; $O\{\text{hours}\}$), or, the MPs can resuspend from within the sludge and remain in the bioreactor for up to its solids retention time (SRT; $O\{\text{days}\}$). Revisit §2.2.1.2 for a summary of bioreactor operations. Subsequently, overflow wastewater from the bioreactor could then be fed to a 3° membrane process and the effects of (potential) organic matter adsorption and biofilm growth could be probed. Potential measurable effects include the degree of MP aggregation, the incidence and severity of membrane (bio-)fouling, as well as the overall effects on MP rejection. A second potential experiment could involve varying

the overall surface charge on the MPs via oxidative processes, chemical surface modifications, the adsorption of ionic surfactants, or through the use of different MP polymers. The effects of MP surface charge on MP rejection or the fouling of a charged membrane could then be probed.

Investigations that consider the surface characteristics of MPs should also characterize the membranes that are used, such as via contact angle and/or surface (zeta) potential measurements. For example, the Durapore® membranes used in Chapters 4–5 are negatively charged above a pH of ~ 3 , as ascertained using *Anton Parr's SurPASS* instrument. Recall that membrane surface potential is discussed in §B.2. The measurements performed to create the plot of surface zeta potential versus pH for the 5 μm Durapore® membrane in Figure B.2 were performed using a 1 mM KCl electrolyte in milliQ water (*i.e.* to control solution conductivity). For reference, a 1 mM KCl standard can be purchased from companies such as Hach (Product #2974249) with a conductivity of 147 $\mu\text{S}/\text{cm}$. In contrast, the average wastewater conductivity used in Chapter 3 was $1,102 \pm 140 \mu\text{S}/\text{cm}$: almost $10\times$ higher than the standard solution. The wastewater used in Chapter 6 shows a similar composition. Furthermore, real wastewater contains a variety of suspended and dissolved solids. Thus, the significance is that the membranes were evaluated under solution conditions that are not representative of those in WWTPs, and as such, the measured surface properties may be different in actuality. To this end, an extension of these experiments could be performed where membranes are evaluated at conductivities representative of those in WWTPs, depending on the composition of the wastewater that is sampled. Or, the experiments could be performed using actual wastewater. Over time, it is hypothesized the deposition of solids—or even MPs—in the wastewater would alter the surface potential of the membranes, which has implications in the design and operation of the process (*e.g.* fouling). Overall, great care must be taken such that the sensitive instrument is not compromised by species in the wastewater.

■ **Selected criticisms and opportunities regarding studies of MPs in WWTPs.** As evidenced by the contemporary literature, substantial efforts over the last decade have been expended on understanding the fate of MPs in WWTPs. This is notably a difficult task. These studies are largely observational in nature as parameters are not (typically) manipulated in a fully-functioning WWTP. As documented in §1.2.2, there is still much that we do not know regarding how MPs with different properties are removed at different stages of different facilities. Definitive, all-encompassing

conclusions are hard to make. For example, on page 36, it is generally posited that larger MPs are more likely to be removed from wastewater than smaller MPs [22–24]. However, potential counterexamples do exist to this trend [25]. In these types of studies, the quantification of MPs in wastewater samples is notoriously challenging, as highlighted in §1.2.1, exacerbated by the lack of a standardized methodology for collecting, isolating, and quantifying the MPs. As a particularly notable example, the comprehensive protocol developed and used by Mintenig *et al.* (2017) requires over 18 days to isolate MPs ($< 500 \mu\text{m}$) from wastewater samples [24]. Towards the standardization of MP quantification and reporting procedures, Koelmans *et al.* (2019) have issued several key recommendations [26] to which the reader is referred. Furthermore, MP concentrations in these samples are typically reported in terms of number concentrations—quantities which are not necessarily conserved over the course of a WWTP due to possible fragmentation or aggregation. Both of these processes are known or expected to occur in WWTPs, however the phenomena are not yet well-understood [18, 20, 27, 28]. In particular, researchers studying membranes in WWTPs have cited fragmentation as a cause of unusual/low MP rejection results [29, 30].

As an additional criticism, it was noted in §1.2.2.2 and §1.3.1 that several investigations are documented in the literature involving WWTPs that incorporate membrane processes. While this is a good starting point for assessing the performance of these technologies for the purpose of MP removal, unfortunately, the depth of information provided is wholly insufficient to make reliable inferences or comparisons. For example, various studies (*e.g.* [3, 31]) do not provide *any* information with respect to the membrane manufacturer or the membrane’s properties (*e.g.* pore size, material, geometry, active area, etc.). Most studies also do not list *any* information regarding the process conditions used (*e.g.* flux, transmembrane pressure, etc.). In spite of these criticisms, it must be acknowledged that the minutiae of these membrane systems is out-of-scope for most investigations, and while it is too late to amend these already-published works, future studies should be conducted which fully describe the membrane systems which are being studied. The possession of a full suite of data will facilitate meaningful comparisons and conclusions.

Despite the limitations associated with studies of WWTPs in the current literature—both those that use membrane technologies and those that do not—there exist many opportunities for novel research to improve the state of knowledge in the field. For example, whereas the aforementioned

studies of these facilities consider the fate of the MPs naturally received, a “contrived” approach to assessing MP removal would be to dope a facility’s influent with a known concentration of MPs having a known set of properties. As researchers performing this experiment would have the ultimate control over these properties, MPs—such as those containing a fluorophore—could be used. Better yet, MPs with ranges of sizes/chemistries/surface charges/etc. could be doped in the facility’s influent, where each type of MP has a different fluorophore. Via this method, the effect of a variety of parameters on removal efficiency could be ascertained in a more controlled manner. Following the introduction of the target MPs to the wastewater influent, samples from different stages in the facility (*e.g.* influent, 1°/2°/3° effluents) would then be taken over time, using methods recommended by other researchers such as Koelmans *et al.* (2019) [26]. When quantifying the potential presence of fluorescent MPs in samples, it is expected that the rigorous procedures (*e.g.* digestion) typically used in WWTP studies to isolate nondescript MPs [24] could be eschewed for simpler isolation methods. Subsequently, FC would be employed to simultaneously measure the concentrations of the different populations of fluorescent MPs in the aqueous samples, in a similar fashion to how the instrument was used in Chapter 6. In this manner, the FC technique could be applied to measure fluorescent MPs in not only laboratory experimental studies, but large-scale studies of WWTPs or other systems.

As an added potential benefit, FC could be used to monitor samples for MP fragmentation or aggregation/biofouling. It was shown in §5.4 that forward scattering (FSC) intensity measurements could be used to produce estimates of particle sizes. Given measurements of FSC intensity originating from the population of MPs doped into the influent, positive or negative deviation from these original measurements may indicate the presence of MP aggregation or fragmentation, respectively. Furthermore, a flow cytometer coupled to a cell sorter [6] could be used to isolate particles which give anomalous FSC intensity readings. Subsequent *ex situ* analysis could then be used to probe the actual identity (*e.g.* aggregated or fragmented MPs, etc.) of the particles. The use of FC in this manner would serve to automate the MP quantification process and greatly expedite sample analysis in the study of WWTPs. However, pursuant to the technical limitations discussed previously in §5.4.2 and recently on page 246, it must be cautioned that MP sizing via FC under “realistic” conditions may be challenging as the relationship between FSC intensity and particle size is a complex function of particle size, shape, composition (*e.g.* presence of pigments, adsorbed matter, etc.), refractive indices, solution properties, characteristics of the FC instrument, and so on. This is especially true in

the analysis of irregularly-shaped particles. Careful methodological validation is required to ensure that the results obtained are truly representative of the system. Furthermore, care must be taken to ensure that irregular or aggregated MPs do not interfere with the operation of the FC instrument.

■ **Investigations of the removal of nanoplastics in WWTPs.** This work has largely focused studying the interactions between membranes and plastic particles that most researchers would consider to be “microplastics”. However, it is largely accepted that plastic pieces smaller than the ones used in this work exist: so-called “nanoplastics” (NPs), as noted in §1.1. While the exact upper size limit for NPs is not universally defined, common approaches involve calling particles less than 1 μm [20, 26, 32] or 0.1 μm as NPs [18, 33].² Regardless, the presence of NPs is generally established in WWTPs and the environment. Considering sources of these particles, primary NPs are manufactured for use in electronics, paints, and adhesives [34], while the weathering and fragmentation of MPs or larger plastic debris [20] can create secondary NPs. Overall, NPs are expected to be particularly hazardous to aquatic life (see §1.1.2–1.1.3), although specifics regarding their prevalence, distribution, and eventual effects are not yet well-understood [18, 20]. In a very recent work, Xu *et al.* (2023) quantified the specific presence and removal rate of NPs (0.01–1 μm) in two Chinese WWTPs [35]. The authors developed and employed a complex isolation procedure involving 0.01 μm /100 kDa MF/UF membranes and subsequent quantification via pyrolysis-gas chromatography-mass spectrometry (Py-GC-MS). In the influents of the facilities, the total MP/NP concentrations ranged from 11.29–26.23 $\mu\text{g/L}$ while in the effluents, these values ranged from 0.71–1.75 $\mu\text{g/L}$, resulting in overall removal rates ranging from 93.3–93.7%. The authors also found that NPs (0.01–1 μm) constituted 5.6–19.6% of all micro- and nanoparticles < 1,000 μm in size. While this study is certainly a step in the right direction, much more research is needed to quantify the presence of NPs in WWTPs and the environment, as well as to document their effects on organisms and ecosystems.

One barrier potentially limiting the pace of NP research involves the acquisition of NPs, themselves—in particular, *irregularly-shaped* NPs. The experience noted when producing very small (*e.g.* 1–10 μm) MPs for Chapters 3–4 leads to the inference that the production of even smaller, irregular NPs would be quite challenging. Whereas the MPs in these studies were produced via planetary ball-milling

²By the former definition, the 0.5 μm MBs used in Chapter 6 would be considered NPs.

at roughly room temperature, another potential route involves the use of ball-milling at cryogenic temperatures which would help to embrittle the polymers and mitigate the softening/aggregation of the particles in the milling jars. For example, Eitzen *et al.* (2019) used a cryogenic ball mill to produce 1–200 μm polystyrene (PS) MPs [36], while Pizzichetti *et al.* (2023) used a similar instrument to produce polyamide (PA) and PS MPs, some of which were $< 20 \mu\text{m}$ in size [2]. It is possible that the optimization of these cryogenic milling processes may serve as one route by which irregular NPs could be produced. As perhaps another route, Enfrin *et al.* directly isolated irregular PE NPs from facial scrubs for use in their filtration experiments [1, 37, 38]. Via nanoparticle tracking analysis (NTA), they observed that their NPs ranged from 12.5–689.6 nm in size with an average of $92.5 \pm 1.2 \text{ nm}$. While this methodology was deemed to be suitable for the needs of these researchers, it does not easily permit the acquisition of NPs having different sizes, shapes, compositions, and so on. Furthermore, Pramanik *et al.* (2021) obtained large NPs/small MPs from 75–300 μm polymer feedstocks by a fragmenting primary particles using the high shear forces associated with mixing. Particles having mean sizes between 0.74–1.88 μm were obtained by this method [39]. As a final note, it is possible that the significant forces experienced by MPs during ultrasonication may cause fragmentation, similar to what was noted by Pramanik *et al.* For example, the ultrasonication processes used to disperse the MPs in Chapters 3–6 may have resulted in their fragmentation to some degree. However, this possibility was not explored and therefore represents a limitation of this work. Future investigations should evaluate MP size and shape before/after ultrasonication to ascertain whether the process can contribute to fragmentation. If so, an opportunity may actually be presented to optimize ultrasonication towards the generation of NP suspensions. Other routes for the synthesis of irregular NPs almost certainly exist, yet more research is needed to this end.

A second barrier which hinders NP-related research involves challenges surrounding the detection and characterization of NPs in aqueous samples. For example, Enfrin *et al.* (2019) note that NP detection is limited by the inadequacy of the analytical techniques that are current available, which inhibits the research to comprehensively study the fate of NPs in water [20]. Even in the studies presented in Chapters 3–4 of this work, the ball-milling process used *may* have produced NPs (*i.e.* $< 1 \mu\text{m}$). However, the characterization techniques that were used were unsuitable for quantifying NPs. For example, the FBRM used for characterizing suspensions of MPs only resolves chord lengths down to a minimum of 1 μm . In the image analysis procedure that was used, structures

less than an arbitrarily-defined minimum of $4 \mu\text{m}^2$ (< 9 pixels) were excluded from the particle size analysis to avoid categorizing noise generated in the manual thresholding process as MP particles. Therefore, the analysis techniques that were developed and used were inherently limited in their ability to characterize *all* of the MPs/NPs that could have been produced. To this end, better identification techniques should be developed and employed to characterize NPs in samples. Current options may include: laser diffraction analysis and NTA, dynamic light scattering (DLS), (nano-) FC, and various techniques coupled with mass spectrometry such as Py-GC-MS [20, 32, 33, 39–41]. Evidently, each of these tools has its advantages and drawbacks. For example, it should be noted that certain techniques such as laser diffraction analysis and DLS assume that the particles are spherical in shape. If *irregular* particles are used, this assumption is positioned to be a significant drawback. To this end, refer to the work written by Caputo *et al.* (2021) for a good comparison of some possible MP/NP quantification techniques [41]. As one final note, the FC technique developed in Chapters 5–6 may prove to be a valuable resource for determining NP concentrations in laboratory removal experiments which may hasten the evaluation and/or development of processes to remove these particles from water and wastewater.

■ **A consideration of waste streams.** This work has focused on preventing the discharge of MPs into the environment from the liquid effluents of WWTPs. It is clear from prior investigations in the literature and the results presented herein that membrane technologies are an effective solution to accomplish this objective. However, membrane technologies are limited in that they do not *capture* the MPs, but merely withhold them. Consider the retentate wastewater from a crossflow filtration process such as the one described in Chapter 6: this stream contains the rejected suspended/dissolved solids and MPs, and must be dealt with either by recycling it to a previous stage in the facility, or by sending it to a separate process to reclaim the rejected water. The same is true for any waste streams produced by the membrane process, including the BW water. If these streams are recycled back to the WWTP such as via the plant headworks, the “removed” MPs are reintroduced to the facility from which they were just removed!³ This completely relies on the assumption that during a subsequent pass, the MPs are removed by another means, such as through sedimentation into the waste sludge.

³A common heuristic in separation science advises against remixing feed and products streams: exactly the opposite of what is done with the retentate stream.

It is largely expected that “removed” MPs are mostly relocated to the solid sludge phase through the various treatment processes, however, Koutnik *et al.* (2021) note that more than half of sludge produced is applied in the form of biosolids to agricultural lands [27]. More specifically, Liu *et al.* (2021) report estimates of the fate of wastewater sludge (*e.g.* agriculture, incineration, landfill, soil compost, etc.) in different countries: large fractions of the sludge are applied for “agricultural use” in Norway (82%), Ireland (63%), the USA (55%), China (45%) and Sweden (36%) and as “soil compost” in Finland (89%) and Scotland (40%) [42]. One estimate by Nizzetto *et al.* (2016) found that 30,000–44,000 tons of MPs are applied to agricultural soils each year in North America, compared to 43,000–63,000 tons per year in Europe [43]. In Koutnik *et al.*’s analysis, the authors estimate that in the USA alone, 785–1,080 *trillion* MPs may be released annually via the application of WWTP biosolids to land, up to 96% of which may go undetected in sampling campaigns due to aforementioned limitations (*e.g.* §1.2.1) in MP quantification methodologies [27]. The potential harm caused by these MPs is exacerbated as some of the particles may take on the order of 1,000 years to decompose [42]. In addition, these persistent terrestrial MPs can be subsequently transported to various other environmental compartments—including the aquatic environment—via precipitation and agricultural runoff, the wind, or by other mechanisms [18, 27]. This was illustrated in the very first figure in this work: Figure 1.1. Feasibly, a WWTP could even receive MPs from agricultural lands [44] via runoff which it had previously removed! Worse yet, MPs liberated in runoff or entrained into the atmosphere could be deposited into bodies of water [42, 45].

We must remember that membrane technologies do not necessarily *capture* MPs and therefore, we must simultaneously employ other processes that can fully remove, sequester and/or destroy the MPs to prevent them from unintentionally entering the environment. *The use of membrane technologies merely shifts the burden of MP capture to other technologies within WWTPs or elsewhere.* When implementing a membrane process for the removal of MPs from a WWTP effluent, efforts should be taken to ensure that complimentary processes exist to eliminate the MPs. It is suggested that MPs rejected via membranes may be eliminated via emerging technologies such as advanced oxidation processes [46], by promising novel biodegradation/bioremediation techniques [22], or through the incineration/deep well injection of biosolids [27]. Future works—especially MP removal studies—should emphasize a holistic view of the wastewater treatment process and consider the fate of MPs leaving WWTPs in all possible routes.

7.3 Concluding Remarks

MPs are ubiquitous in the aquatic environment. A substantial fraction of these particles originate from the effluents of WWTPs. A significant and still-growing body of research suggests that these particles pose a risk to ecosystems, however, the extent of this risk is yet to be uncovered. Similarly, investigators have suggested that MPs may present health consequences for humans, although research into these consequences has just begun. A cautious approach for dealing with MPs is thus recommended. By limiting their discharge into the environment and by limiting our own exposure to these particles, we can attempt to mitigate possible negative outcomes. The novel research presented in this work at the intersection of MPs and membrane technologies is aimed towards preventing these MPs from entering the aquatic environment via WWTP effluents. In particular, evidence indicates that these membrane technologies can be largely effective at withholding MPs: in many cases, removal efficiencies well surpassing 99% can be obtained when the selection and operation of these technologies is well-informed. Interactions between MPs and membranes in the form of fouling have shown to appreciably occur, however, the severity of which can be reasonably managed. In closing, implementing membrane technologies in 3^o treatment applications is recommended as one facet of a management plan for MPs. However, consideration also must be given to the fate of the MPs in rejected water streams and the biosolids such that the responsibility of managing the fate of these particles is not just shifted forward to another process or another individual.

7.4 Works Cited

- [1] M. Enfrin, J. Lee, P. Le-Clech, and L. F. Dumée, “Kinetic and mechanistic aspects of ultrafiltration membrane fouling by nano- and microplastics,” *Journal of Membrane Science*, vol. 601, p. 117890, 2020.
- [2] A. R. P. Pizzichetti, C. Pablos, C. Álvarez-Fernández, K. Reynolds, S. Stanley, and J. Marugán, “Kinetic and mechanistic analysis of membrane fouling in microplastics removal from water by dead-end microfiltration,” *Journal of Environmental Chemical Engineering*, vol. 11, p. 109338, 2023.
- [3] S. Ziajahromi, P. A. Neale, L. Rintoul, and F. D. L. Leusch, “Wastewater treatment plants as a pathway for microplastics: development of a new approach to sample wastewater-based microplastics,” *Water Research*, vol. 112, pp. 93–99, 2017.
- [4] H. A. Leslie, S. H. Brandsma, M. J. M. Van Velzen, and A. Vethaak, “Microplastics en route: Field measurements in the Dutch river delta and Amsterdam canals, wastewater treatment

- plants, North Sea sediments and biota,” *Environment International*, vol. 101, pp. 133–142, 2017.
- [5] L. Yang, J. Hur, and W. Zhuang, “Occurrence and behaviors of fluorescence EEM-PARAFAC components in drinking water and wastewater treatment systems and their applications: A review,” *Environmental Science and Pollution Research*, vol. 22, pp. 6500–6510, 2015.
- [6] A. Tzur, J. K. Moore, P. Jorgensen, H. M. Shapiro, and M. W. Kirschner, “Optimizing Optical Flow Cytometry for Cell Volume-Based Sorting and Analysis,” *PLOS ONE*, p. e16053, 2011.
- [7] J. G. Jacangelo and C. A. Buckley, “Microfiltration,” in *Water Treatment Membrane Processes*, J. Mallevalle, P. R. Odendall, and M. R. Wiesner, Eds. McGraw-Hill, 1996.
- [8] G. Belfort, R. H. Davis, and A. L. Zydney, “The behavior of suspensions and macromolecular solutions in crossflow microfiltration,” *Journal of Membrane Science*, vol. 96, pp. 1–58, 1994.
- [9] X. Li, Y. Mo, J. Li, W. Guo, and H. H. Ngo, “In-situ monitoring techniques for membrane fouling and local filtration characteristics in hollow fiber membrane processes: A critical review,” *Journal of Membrane Science*, vol. 528, pp. 187–200, 2017.
- [10] B. Patterson, “Membrane Filtration of Microplastic Fibers: Assessment of Membrane, Microplastic, and Solution Properties,” Master’s thesis, McMaster University, Hamilton ON, 2021. [Online]. Available: <http://hdl.handle.net/11375/26932>
- [11] M. Enfrin, C. Hachemi, D. L. Callahan, J. Lee, and F. Dumée, “Membrane fouling by nanofibres and organic contaminants-mechanisms and mitigation via periodic cleaning strategies,” *Separation and Purification Technology*, vol. 278, pp. 1383–5866, 2022.
- [12] A. S. Kazemi, B. Patterson, R. J. LaRue, P. Papangelakis, S. M. Yoo, R. Ghosh, and D. R. Latulippe, “Microscale parallel-structured, cross-flow filtration system for evaluation and optimization of the filtration performance of hollow-fiber membranes,” *Separation and Purification Technology*, vol. 215, pp. 299–307, 2019.
- [13] S. K. Dishari, A. Venkiteshwaran, and A. L. Zydney, “Probing effects of pressure release on virus capture during virus filtration using confocal microscopy,” *Biotechnology and Bioengineering*, vol. 112, pp. 2115–2122, 2015.
- [14] L. Li, D. Liu, K. Song, and Y. Zhou, “Performance evaluation of MBR in treating microplastics polyvinylchloride contaminated polluted surface water,” *Marine Pollution Bulletin*, vol. 150, p. 110724, 2020.
- [15] M. R. Michielssen, E. R. Michielssen, J. Ni, and M. B. Duhaime, “Fate of microplastics and other small anthropogenic litter (SAL) in wastewater treatment plants depends on unit processes employed,” *Environmental Science: Water Research & Technology*, vol. 2, no. 6, pp. 1064–1073, 2016.
- [16] M. Lares, M. C. Ncibi, M. Sillanpää, and M. Sillanpää, “Occurrence, identification and removal of microplastic particles and fibers in conventional activated sludge process and advanced MBR technology,” *Water Research*, vol. 133, pp. 236–246, 2018.
- [17] “HFU-2020AN Series,” Toray Industries Inc., 2021. [Online]. Available: https://www.water.toray/products/uf/pdf/HFU-2020ANseries_202104.pdf
- [18] O. S. Alimi, J. F. Budarz, L. M. Hernandez, and N. Tufenkji, “Microplastics and Nanoplastics in Aquatic Environments: Aggregation, Deposition, and Enhanced Contaminant Transport,” *Environmental Science & Technology*, vol. 52, pp. 1704–1724, 2018.

- [19] A. Pradel, S. Ferreres, C. Veclin, H. E. Hadri, M. Gautier, B. Grassl, and J. Gigault, “Stabilization of fragmental polystyrene nanoplastic by natural organic matter: insight into mechanisms,” *ACS ES&T Water*, vol. 1, pp. 1198–1208, 2021.
- [20] M. Enfrin, L. F. Dumée, and J. Lee, “Nano/microplastics in water and wastewater treatment processes—origin, impact and potential solutions,” *Water Research*, vol. 161, pp. 621–638, 2019.
- [21] M. Barchiesi, A. Chiavola, C. D. Marcantonio, and M. R. Boni, “Presence and fate of microplastics in the water sources: focus on the role of wastewater and drinking water treatment plants,” *Journal of Water Process Engineering*, vol. 40, p. 101787, 2021.
- [22] R. Y. Krishnan, S. Manikandan, R. Subbaiya, N. Karmegam, W. Kim, and M. Govarathanan, “Recent approaches and advanced wastewater treatment technologies for mitigating emerging microplastics contamination—A critical review,” *Science of The Total Environment*, vol. 858, p. 159681, 2023.
- [23] J. Sun, X. Dai, Q. Wang, M. C. van Loosdrecht, and B. J. Ni, “Microplastics in wastewater treatment plants: detection, occurrence and removal,” *Water Research*, vol. 152, pp. 21–37, 2019.
- [24] S. M. Mintenig, I. Int-Veen, M. G. J. Löder, S. Primpke, and G. Gerds, “Identification of microplastic in effluents of waste water treatment plants using focal plane array-based micro-Fourier-transform infrared imaging,” *Water Research*, vol. 108, pp. 365–372, 2017.
- [25] Z. Long, Z. Pan, W. Wang, J. Ren, X. Yu, L. Lin, H. Lin, H. Chen, and X. Jin, “Microplastic abundance, characteristics, and removal in wastewater treatment plants in a coastal city of China,” *Water Research*, vol. 155, pp. 255–265, 2019.
- [26] A. A. Koelmans, N. H. M. Nor, E. Hermsen, M. Kooi, S. M. Mintenig, and J. D. France, “Microplastics in freshwaters and drinking water: Critical review and assessment of data quality,” *Water Research*, vol. 155, pp. 410–422, 2019.
- [27] V. S. Koutnik, S. Alkidim, J. Leonard, F. DePrima, S. Cao, E. M. V. Hoek, and S. K. Mohanty, “Unaccounted Microplastics in Wastewater Sludge: Where Do They Go?” *ACS ES&T Water*, vol. 1, pp. 1086–1097, 2021.
- [28] X. Wu, X. Zhao, R. Chen, P. Liu, W. Liang, J. Wang, M. Teng, X. Wang, and S. Gao, “Wastewater treatment plants act as essential sources of microplastic formation in aquatic environments: A critical review,” *Water Research*, vol. 221, 2022.
- [29] Y. Ruan, K. Zhang, C. Wu, R. Wu, and P. K. S. Lam, “A preliminary screening of HBCD enantiomers transported by microplastics in wastewater treatment plants,” *Science of The Total Environment*, vol. 674, pp. 171–178, 2019.
- [30] X. Lv, Q. Dong, Z. Zuo, Y. Liu, X. Huang, and W. M. Wu, “Microplastics in a municipal wastewater treatment plant: Fate, dynamic distribution, removal efficiencies, and control strategies,” *Journal of Cleaner Production*, vol. 225, pp. 579–586, 2019.
- [31] S. Olmos, J. López-Castellanos, and J. Bayo, “Are advanced wastewater treatment technologies a solution for total removal of microplastics in wastewater effluents?” *WIT Transactions on Ecology and the Environment*, vol. 229, pp. 109–116, 2019.
- [32] Z. Gao, L. Chen, J. Cizdziel, and Y. Huang, “Research progress on microplastics in wastewater treatment plants: A holistic review,” *Journal of Environmental Management*, vol. 325, 2023.

- [33] C. Bretas Alvim, J. A. Mendoza-Roca, and A. Bes-Piá, “Wastewater treatment plant as microplastics release source—Quantification and identification techniques,” *Journal of Environmental Management*, vol. 255, p. 109739, 2020.
- [34] S. L. Wright and F. J. Kelly, “Plastic and Human Health: A Micro Issue?” *Environmental Science & Technology*, vol. 51, pp. 6634–6647, 2017.
- [35] Y. Xu, Q. Ou, X. Wang, F. Hou, P. Li, J. P. V. D. Hoek, and G. Liu, “Assessing the mass concentration of microplastics and nanoplastics in wastewater treatment plants by pyrolysis gas chromatography-mass spectrometry,” *Environmental Science & Technology*, vol. 57, no. 8, p. 3114–3123, 2023.
- [36] L. Eitzen, S. Paul, U. Braun, K. Altmann, M. Jekel, and A. S. Ruhl, “The challenge in preparing particle suspensions for aquatic microplastic research,” *Environmental Research*, 2019.
- [37] M. Enfrin, J. Lee, A. G. Fane, and L. F. Dumée, “Mitigation of membrane particulate fouling by nano/microplastics via physical cleaning strategies,” *Science of The Total Environment*, vol. 788, p. 147689, 2021.
- [38] M. Enfrin, J. Wang, A. Merenda, L. F. Dumée, and J. Lee, “Mitigation of membrane fouling by nano/microplastics via surface chemistry control,” *Journal of Membrane Science*, vol. 633, p. 119379, 2021.
- [39] B. K. Pramanik, S. K. Pramanik, and S. Monira, “Understanding the fragmentation of microplastics into nano-plastics and removal of nano/microplastics from wastewater using membrane, air flotation and nano-ferrofluid processes,” *Chemosphere*, vol. 282, p. 131053, 2021.
- [40] Z. Zhang and Y. Chen, “Effects of microplastics on wastewater and sewage sludge treatment and their removal: A review,” *Chemical Engineering Journal*, vol. 382, p. 122955, 2020.
- [41] F. Caputo, R. Vogel, J. Savage, G. Vella, A. Law, G. D. Camera, G. Hannon, B. Peacock, D. Mehn, J. Ponti, O. Geiss, D. Aubert, A. Prina-Mello, and L. Calzolari, “Measuring particle size distribution and mass concentration of nanoplastics and microplastics: addressing some analytical challenges in the sub-micron size range,” *Journal of Colloid and Interface Science*, vol. 588, pp. 401–417, 2021.
- [42] W. Liu, J. Zhang, H. Liu, X. Guo, X. Zhang, X. Yao, Z. Cao, and T. Zhang, “A review of the removal of microplastics in global wastewater treatment plants: Characteristics and mechanisms,” *Environment International*, vol. 146, p. 106277, 2021.
- [43] L. Nizzetto, M. Futter, and S. Langaas, “Are Agricultural Soils Dumps for Microplastics of Urban Origin?” *Environmental Science & Technology*, vol. 50, pp. 10777–10779, 2016.
- [44] C. Akarsu, H. Kumbur, K. Gökdağ, A. E. Kideys, and A. Sanchez-Vidal, “Microplastics composition and load from three wastewater treatment plants discharging into Mersin Bay, north eastern Mediterranean Sea,” *Marine Pollution Bulletin*, vol. 150, p. 110776, 2020.
- [45] S. Ziajahromi, P. A. Neale, and F. D. Leusch, “Wastewater treatment plant effluent as a source of microplastics: review of the fate, chemical interactions and potential risks to aquatic organisms,” *Water Science & Technology*, vol. 74, pp. 2253–2269, 2016.
- [46] I. A. Ricardo, E. A. Alberto, A. H. S. Júnior, D. L. P. Macuvele, N. Padoin, C. Soares, H. G. Riella, M. C. V. Starling, and A. G. Trovó, “A critical review on microplastics, interaction with organic and inorganic pollutants, impacts and effectiveness of advanced oxidation processes applied for their removal from aqueous matrices,” *Chemical Engineering Journal*, vol. 424, p. 130282, 2021.

Appendices

Supplementary Information for Chapter 3

A.1 Sample Calculations

■ **Sample calculations for MP concentration scale-up.** It is desired that a laboratory experiment be run in a total of $t_2 = 24$ hours which simulates a longer time period. From Simon *et al.*'s (2018) paper, a “worst-case scenario” MP concentration in the effluent would be $11 \mu\text{g/L}$ [1], or roughly $C_2 = 10 \mu\text{g/L}$. If this concentration is scaled up to $C_1 = 1,000 \mu\text{g/L}$ of MPs, then:

$$\begin{aligned}C_1 t_1 &= C_2 t_2 \\(10 \mu\text{g/L})t_1 &= (10 \mu\text{g/L})(24 \text{ h}) \\t_1 &= 2,182 \text{ h} \\t_1 &\approx 90 \text{ d} \approx 3 \text{ months}\end{aligned}$$

The implication, here, is that the 24-hour experiment at an elevated MP concentration (C_1) would scale to roughly three months of operation in a WWTP.

A.2 Supplementary Tables

Table A.1: Detailed summary of wastewater properties used in membrane fouling filtration experiments. Uncertainty values represent the standard deviation about the average of three measurements (except COD readings: two measurements). Wastewater samples A–I were used in the standard filtration experiments (*i.e.* Figure 3.3); the averages of these water quality parameters are summarized in Table 3.1. Wastewater samples J and K were only used in the BW experiments.

Wastewater	TS (mg/L)	TOC (mg/L)	TC (mg/L)	COD (mg/L)	Conductivity ($\mu\text{S}/\text{cm}$)
A	711 \pm 55	8.2 \pm 0.1	48.3 \pm 0.5	42 \pm 3	1,184 \pm 19
B	618 \pm 49	8.0 \pm 3.9	24.0 \pm 2.2	49 \pm 1	1,200 \pm 11
C	751 \pm 8	7.9 \pm 1.9	33.4 \pm 0.4	47 \pm 5	891 \pm 18
D	617 \pm 32	4.4 \pm 0.4	28.5 \pm 0.5	34 \pm 4	1,041 \pm 14
E	779 \pm 23	6.6 \pm 0.7	29.8 \pm 0.0	37 \pm 4	1,110 \pm 4
F	771 \pm 13	6.0 \pm 0.7	27.8 \pm 0.1	35 \pm 2	845 \pm 47
G	785 \pm 30	4.5 \pm 0.4	40.8 \pm 0.4	37 \pm 4	1,274 \pm 10
H	879 \pm 6	3.7 \pm 1.0	39.4 \pm 1.0	45 \pm 4	1,272 \pm 35
I	693 \pm 25	9.7 \pm 1.4	31.0 \pm 0.2	45 \pm 6	993 \pm 3
J	945 \pm 35	5.5 \pm 0.1	31.0 \pm 0.7	50 \pm 11	1,249 \pm 5
K	953 \pm 31	5.0 \pm 0.2	29.0 \pm 0.6	57 \pm 1	937 \pm 14

Table A.2: Summary of the best-fit fouling model parameters for the mechanisms which most closely describe the flux decline data in Figure 3.3. CF = cake filtration and IB = intermediate blocking. Tween was included in each wastewater suspension.

mg/L PE	UB70				V0.2			
	0	0.1	1	10	0	0.1	1	10
Best Model	CF	IB	CF	IB	CF	CF	CF	CF
J_0 (LMH)	348	276	378	282	939	834	694	449
$K \times 10^5$ (h^{-1})	2.92	253	10.6	579	1.37	2.66	3.81	12.5

A.3 Supplementary Figures

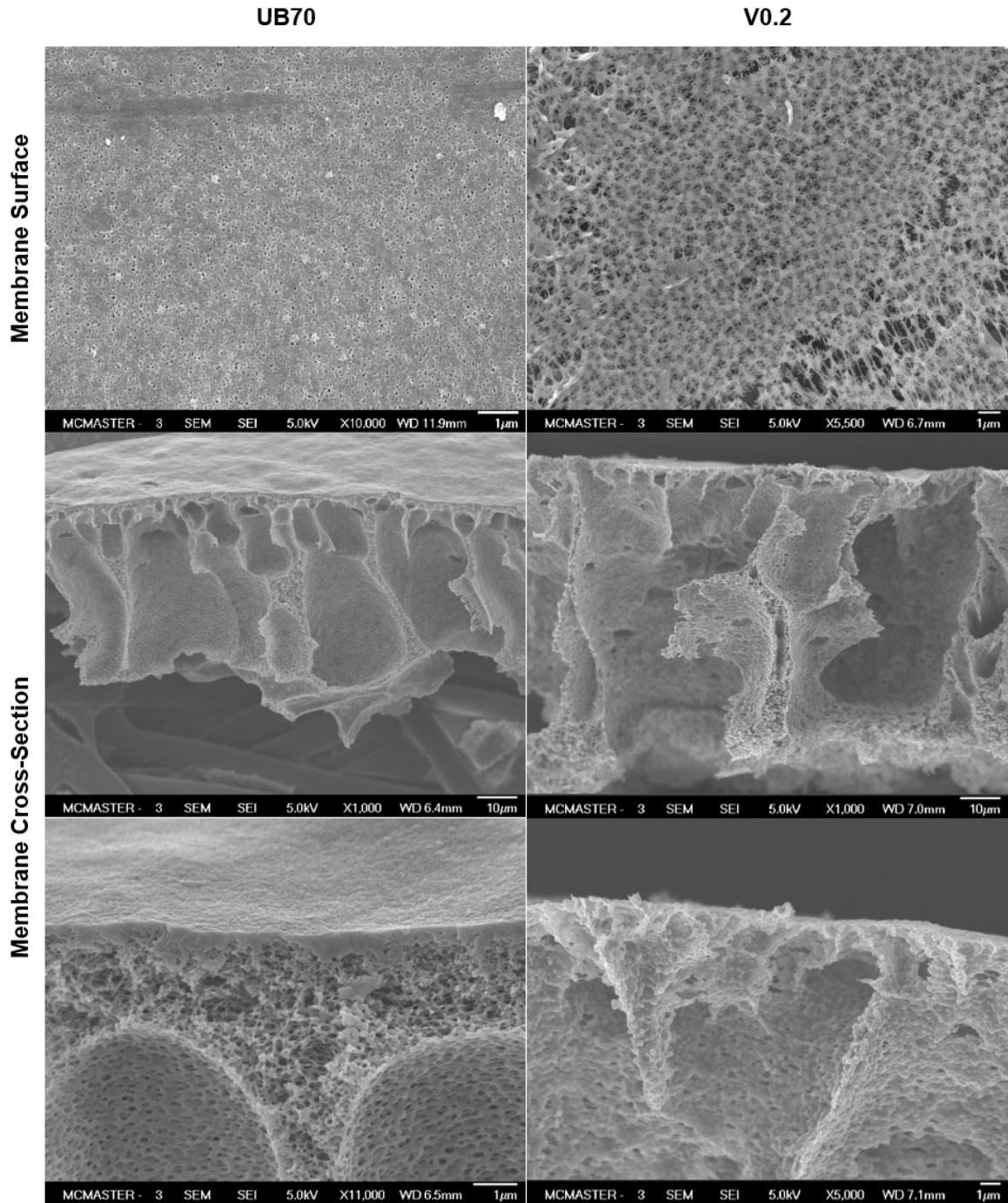


Figure A.1: FESEM images of the native membranes in top-down and cross-sectional profiles. The active surfaces of the membranes in the cross-sectional images are near the tops of the micrographs.

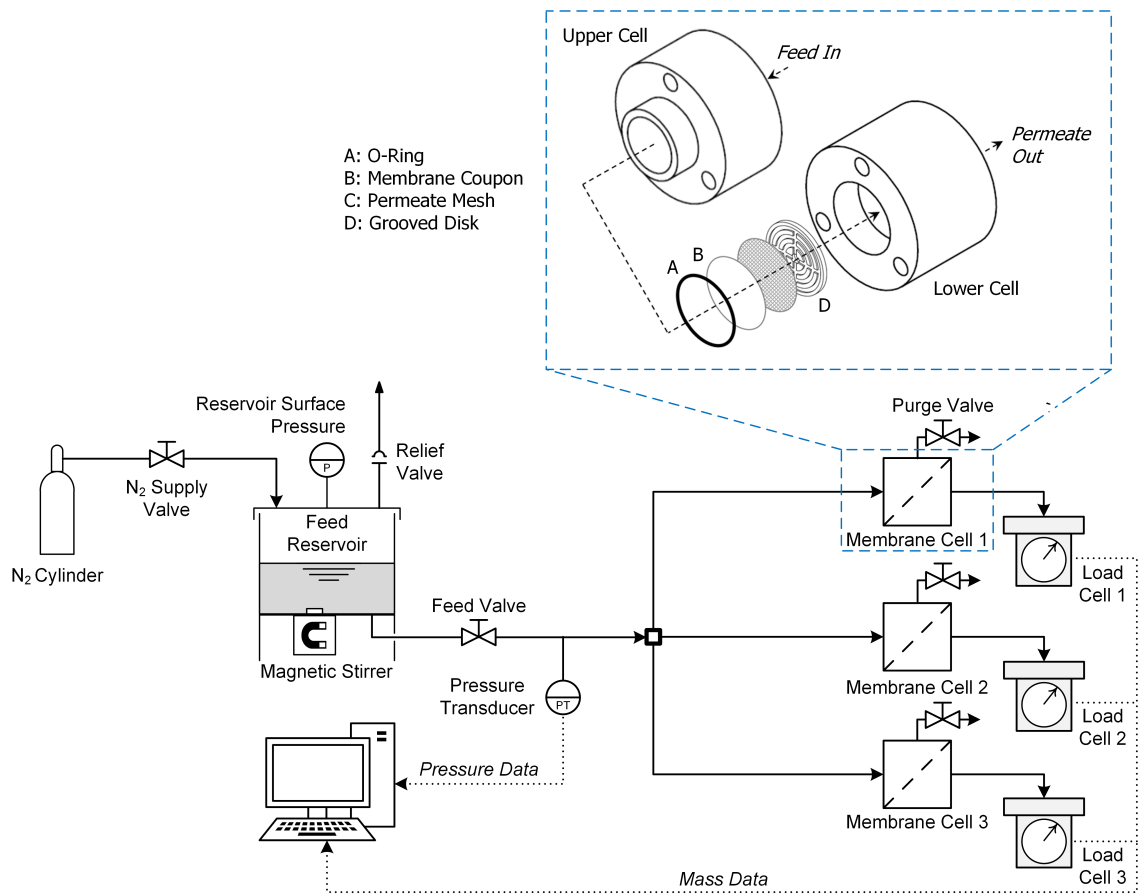


Figure A.2: Diagram of the constant-pressure filtration setup, showing the construction of the membrane cells. The cells are modelled after commercial reusable filter disc holders.

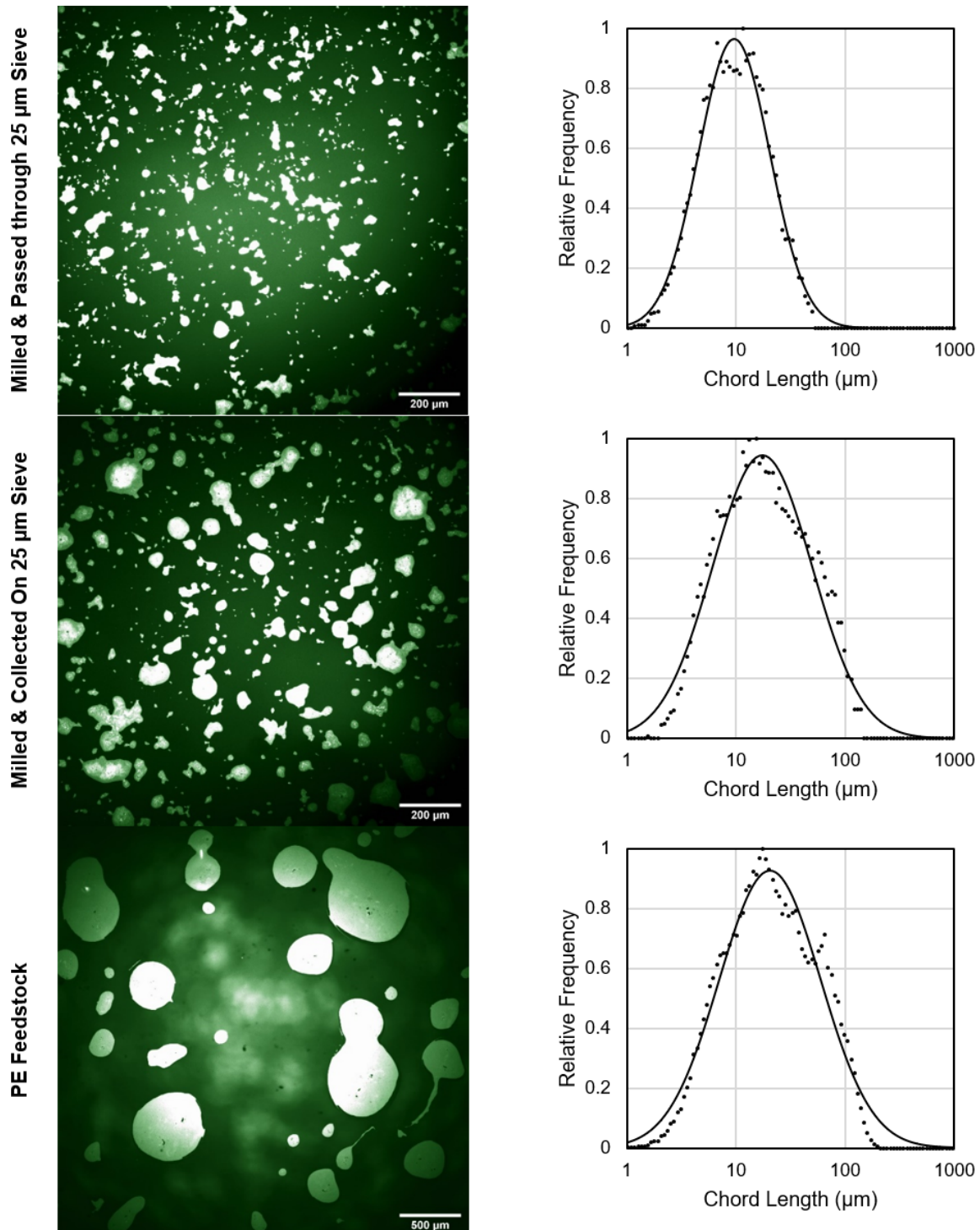


Figure A.3: Comparison of particle sizes in the raw polyethylene feedstock and the milled/sieved MP particles. False-coloured images of the particles are shown alongside chord length distribution data collected via FBRM (\bullet data; — log-normal model).

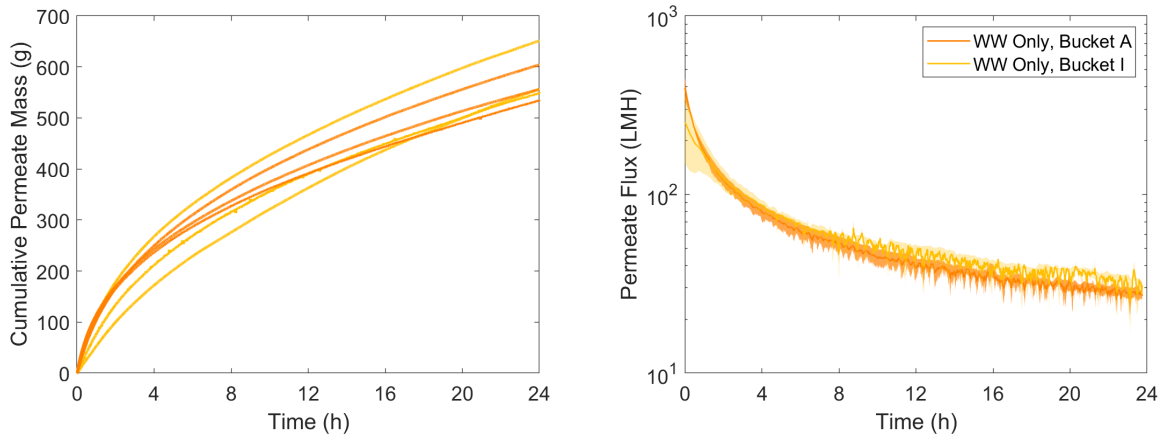


Figure A.4: Comparison of filtration behaviour when two wastewater feeds collected on separate days were filtered using the UB70 membrane. The wastewater feeds vary slightly in composition (see Table A.1) but were both accepted according to the pre-screening process. There are no significant differences in the measured cumulative permeate masses (left) or permeate fluxes (right) over time.

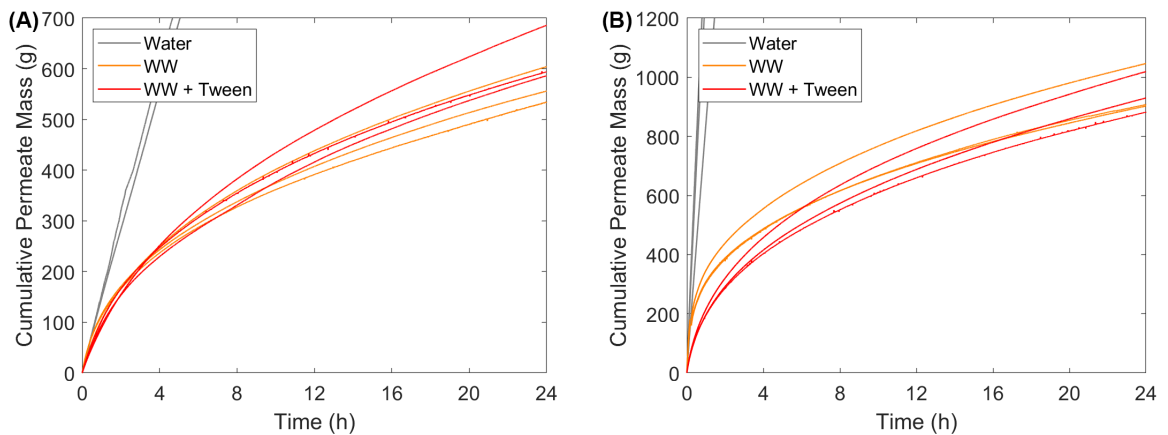


Figure A.5: Comparison of the filtration of pure deionized water versus wastewater alone versus wastewater with 0.1 mg/L Tween 20 for the (A) UB70 and (B) V0.2 membranes. There are no strong differences in the filtration behaviour between the cases where Tween 20 is/is not present in the wastewater.

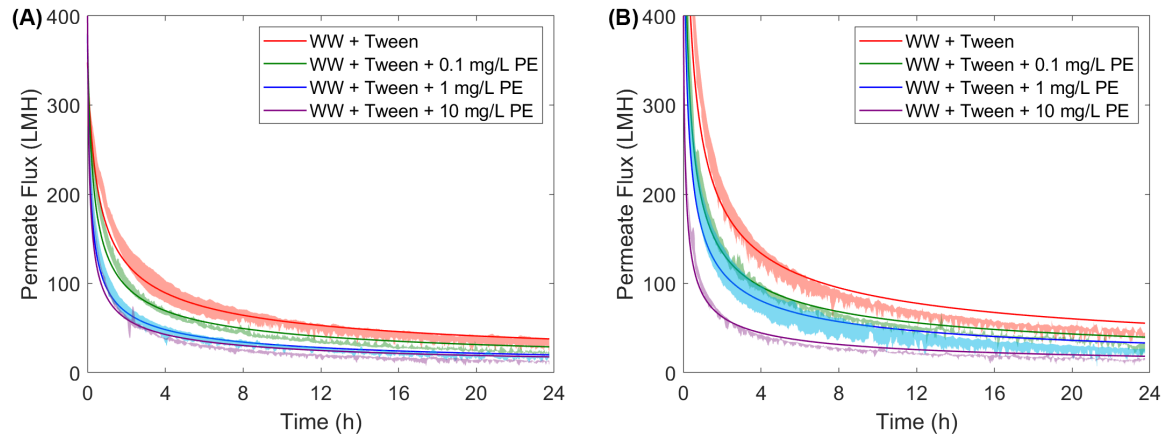


Figure A.6: Plots of permeate flux versus time for the (A) UB70 and (B) V0.2 membranes, where the solid line (—) refers best-fit “cake filtration” fouling model which was applied to the data. The colour band around each data series refers to the range of values experienced in that experimental condition (triplicate measurements).

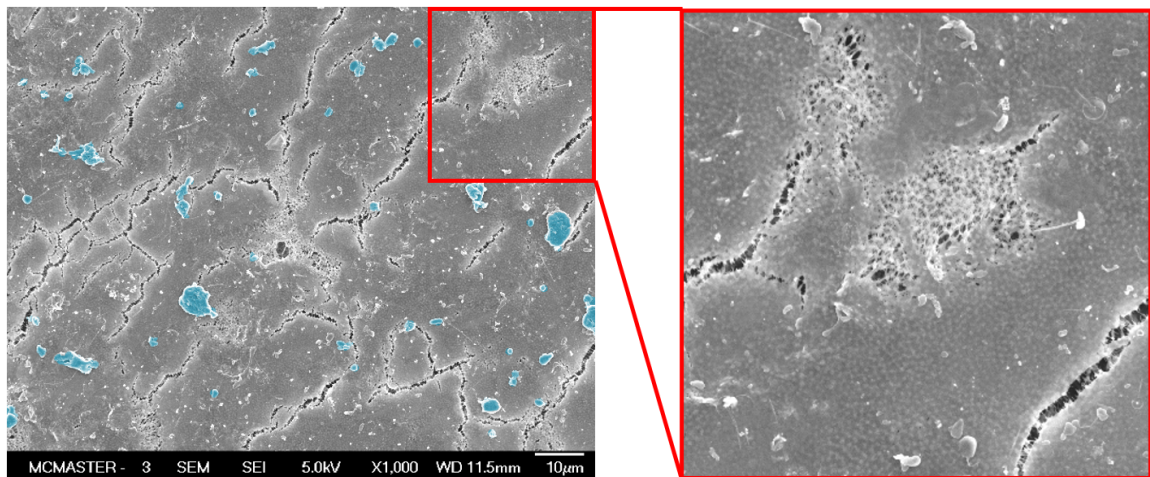


Figure A.7: Image of the backwashed V0.2 membrane which filtered wastewater containing 1 mg/L MPs. The top corner of the image is magnified to show the re-emergence of the underlying MF membrane structure.

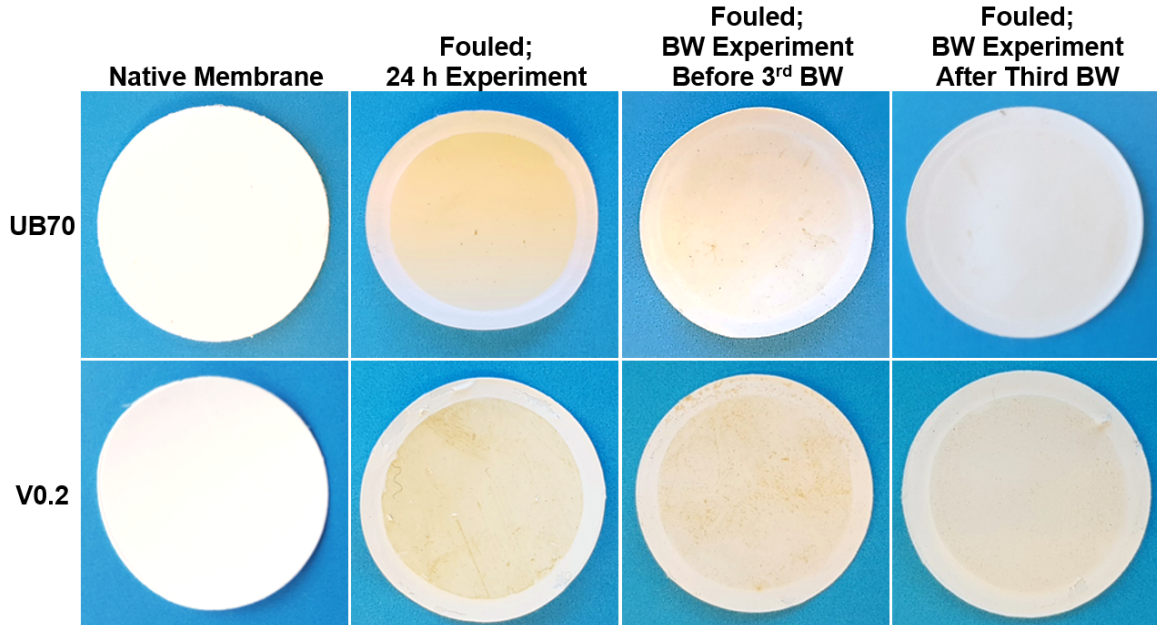


Figure A.8: Camera images of native membranes and membranes fouled under various conditions. Note that there is no visual difference between membranes that have just filtered wastewater and those that have filtered wastewater with added MPs.

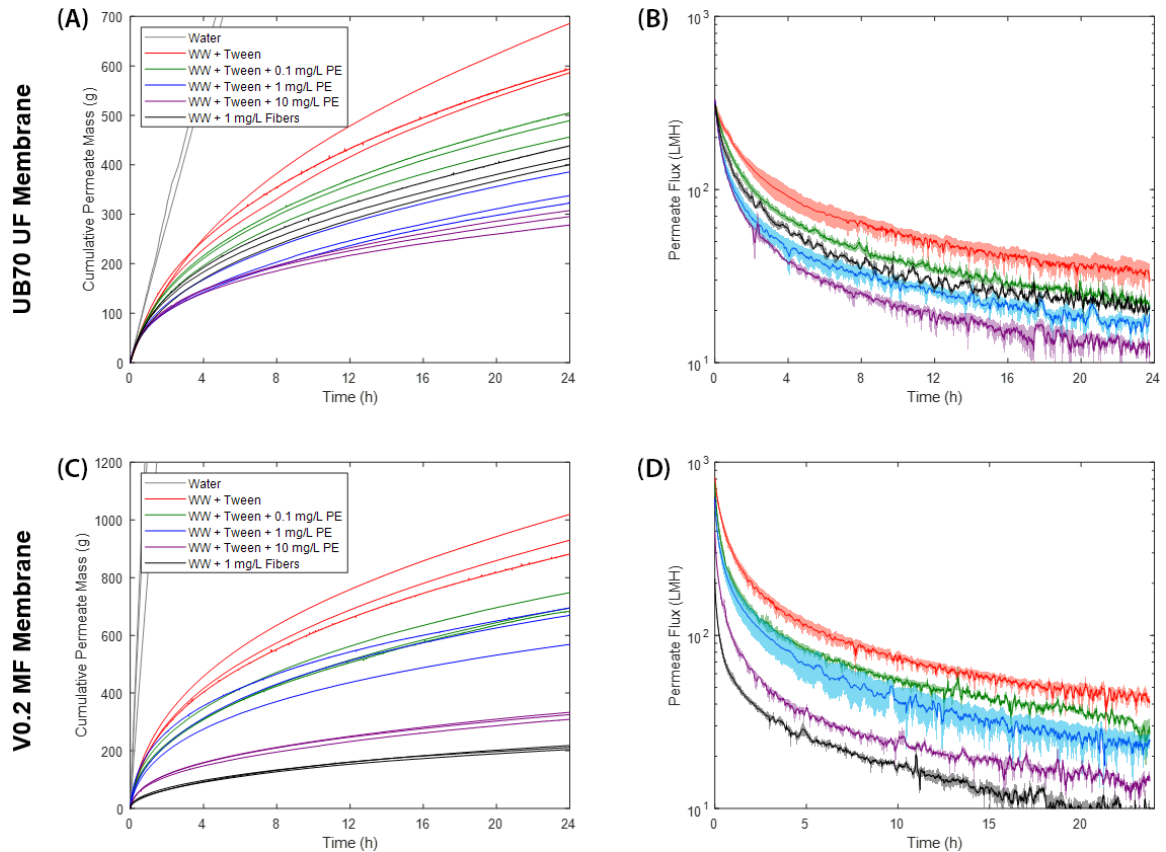


Figure A.9: Filtration of wastewater and PE MP particles along with PS MP fibers through the UB70 UF (Panels A and B) and V0.2 MF (Panels C and D) membranes. Details regarding the synthesis of the fibers can be found elsewhere [2]. Panels A and C display the cumulative permeate water mass collected the 24-hour filtration tests; the three lines in each data series reflect the triplicate measurements. Panels B and D display a transformation of the results in Panels A and C into permeate fluxes. The colour band around each data series indicates the range of values experienced in that experimental condition, while the solid line in its center is the average of the three measurements.

■ Works Cited:

- [1] M. Simon, N. van Alst, and J. Vollertsen, “Quantification of microplastic mass and removal rates at wastewater treatment plants applying Focal Plane Array (FPA)-based Fourier Transform Infrared (FT-IR) imaging,” *Water Research*, vol. 142, pp. 1–9, 2018.
- [2] B. Patterson, “Membrane Filtration of Microplastic Fibers: Assessment of Membrane, Microplastic, and Solution Properties,” Master’s thesis, McMaster University, Hamilton ON, 2021. [Online]. Available: <http://hdl.handle.net/11375/26932>

Supplementary Information for Chapter 4

B.1 Scanning Electron Microscopy

Membrane samples were left to air-dry, then were affixed to aluminum stubs with double-sided carbon tape. Cross-sections were obtained by fracturing the membranes in liquid nitrogen and affixing the samples vertically on the stubs. Nickel paste was used around the edges of the samples to enhance electrical conductivity. Sph-MPs were imaged in the “as-purchased” state. Samples were prepared by aspirating the particles onto carbon tape which was then mounted on stubs. All stubs were subsequently sputter-coated with 5 nm of platinum and imaged using field-emission scanning electron microscopy (FESEM; *JEOL 7000F*) at acceleration voltages ranging from 2.0–4.0 kV.

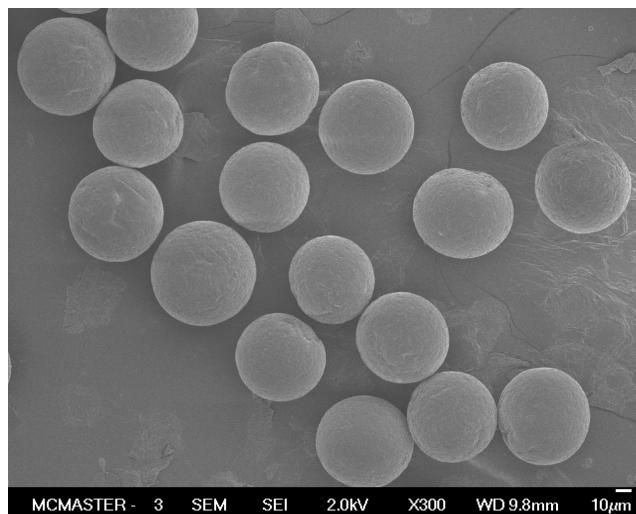


Figure B.1: FESEM image of the as-purchased Sph-MPs from Cospheric.

B.2 Membrane Surface Charge Measurements

An Anton Parr SurPASS 3 electrokinetic analyzer, equipped with the adjustable gap cell, was used to measure the surface zeta potential of membrane samples using the “streaming potential” method at room temperature. Two rectangular coupons (2×1 cm) of flat-sheet Durapore® membrane were cut for each trial and secured into the adjustable gap cell which maintained a distance of 100 ± 10 μm between the coupons. During each replicate, a 1 mM KCl (Sigma-Aldrich) electrolyte solution in milliQ water was adjusted from pH 2 to pH 10 and then back to pH 2 via 1-unit pH increments (*i.e.* to account for the effects of hysteresis). pH adjustments were made using 0.05 M HCl (Sigma-Aldrich) and 0.05 M NaOH (Sigma-Aldrich). At each new pH value, three rinses were performed using the pH-adjusted electrolyte solution before two zeta potential measurements were taken. Therefore in each replicate, four measurements of zeta potential were made at each pH. Finally, this procedure was performed for a total of two replicates, each using a different set of membrane coupons. In the end, eight zeta potential measurements were made at each pH. Figure B.2 illustrates these results.

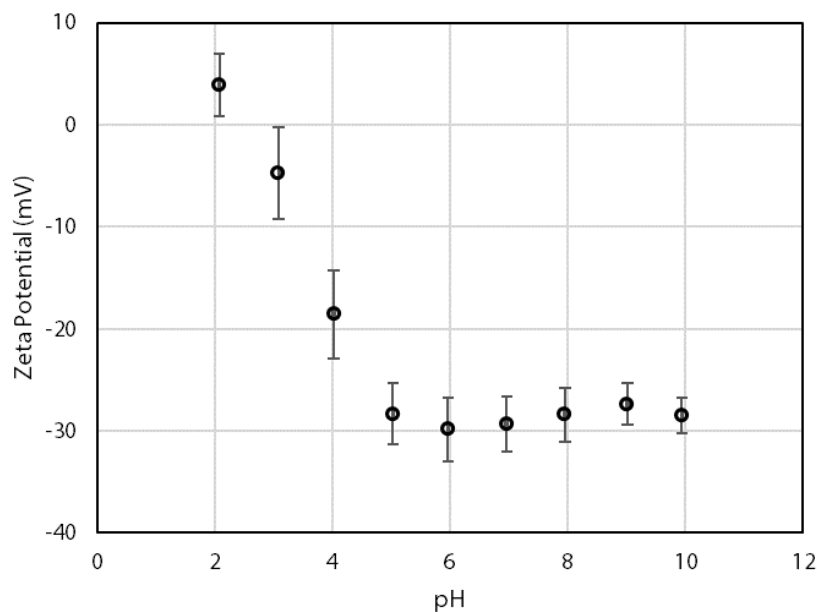


Figure B.2: Surface zeta potential of a Durapore® 5 μm membrane. Error bars represent one standard deviation about the average of eight zeta potential measurements acquired over two experimental replicates.

B.3 Supplementary Results

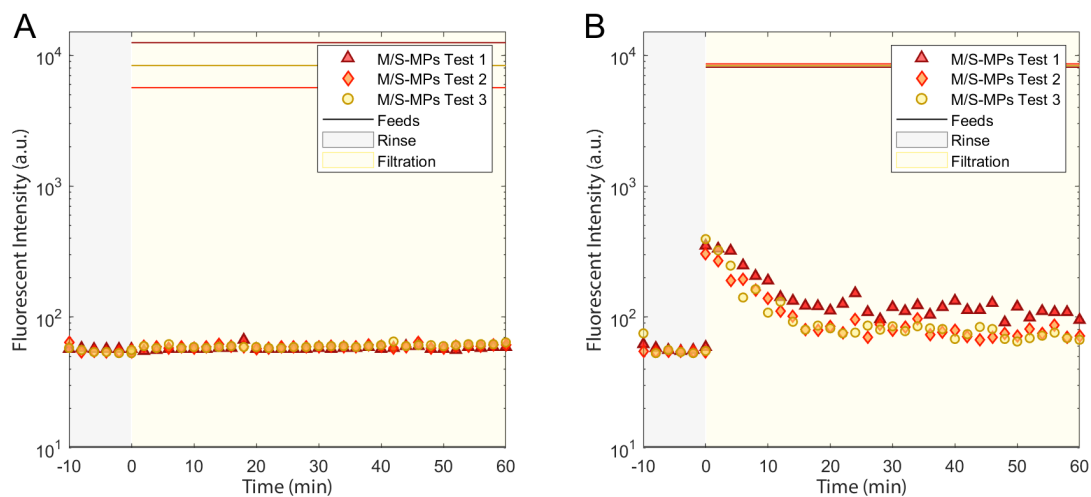


Figure B.3: Example fluorescent intensity (a.u.) profiles obtained from filtration experiments with the M/S-MPs: (A) 0.45 μm Durapore® membrane and (B) 5 μm Durapore® membrane. The gray-shaded region representing the first 10 minutes refers to the rinse step with milliQ water that was performed before each experiment. The yellow-shaded region corresponds to the 60-minute filtration test: these results duplicate the findings from Figure 4.4. The absence of fluorescent signal during the rinse step was used to verify that the fluorescent MPs from previous experiments did not contaminate the system.

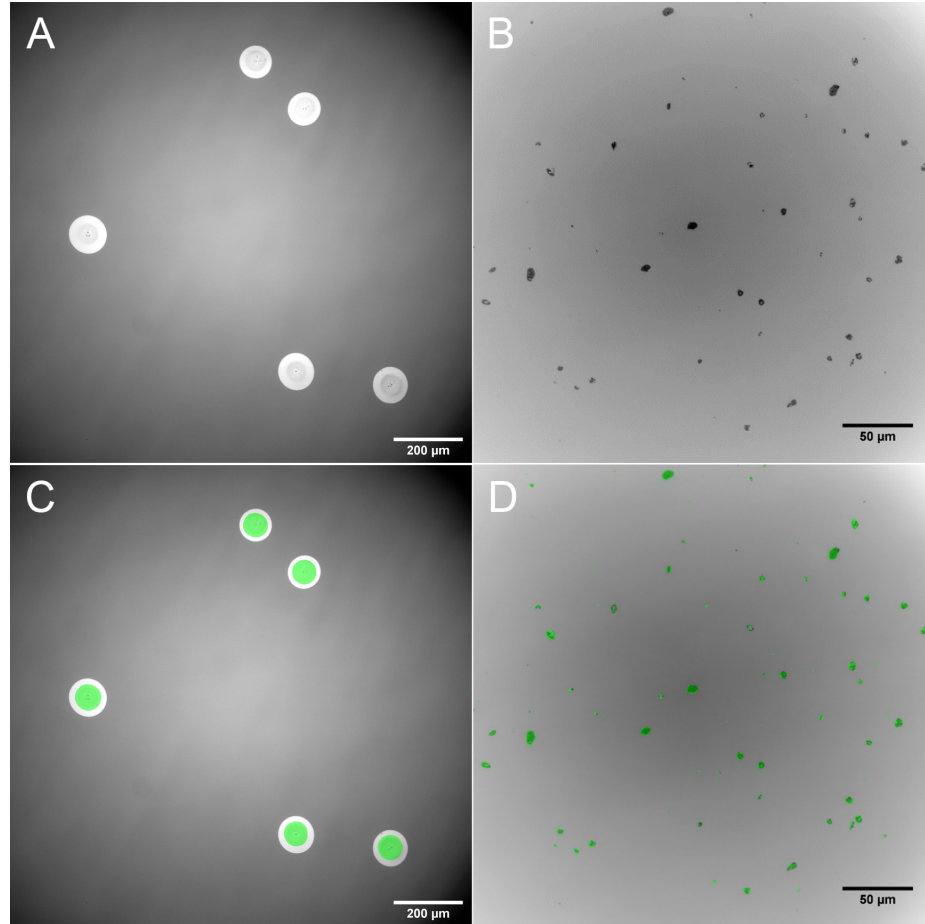


Figure B.4: Brightfield microscopy images of the (A & C) as-received Sph-MPs and (B & D) M/S-MPs used in this study. On the bottom row, the fluorescent signal from the MPs has been artificially overlaid in green on the brightfield images. The bright “halos” around the Sph-MPs result from the scattering and/or refraction of light by the symmetrical translucent spheres.

■ **Compressible cake filtration fouling model.** Following the approach used by Sioutopoulos & Karabelas (2012), the relation between the pressure drop across the cake (ΔP_c) and cumulative permeate volume V during constant flux filtration was modelled using [1]:

$$\Delta P_c = \frac{\alpha C_f \Delta P_0}{R_m} \cdot \frac{V}{A}$$

where α is the specific cake resistance parameter, C_f is the bulk concentration of particles in the feed,

ΔP_0 is the initial transmembrane pressure, R_m is the membrane resistance, and A is the membrane area. Note that ΔP_c is related to the transmembrane pressure (ΔP) as such:

$$\Delta P_c = \Delta P - \Delta P_0$$

For a compressible cake:

$$\alpha = \alpha_c \Delta P_c^n$$

where α_c is the specific cake resistance at a reference pressure and n is the compressibility index parameter. Substituting the equation for α into the original equation for ΔP_c , we obtain:

$$\Delta P_c = \frac{\alpha_c \Delta P_c^n C_b \Delta P_0}{R_m} \cdot \frac{V}{A}$$

$$\frac{\Delta P_c}{\Delta P_c^n} = \frac{\alpha_c C_b \Delta P_0}{R_m} \cdot \frac{V}{A}$$

$$\Delta P_c^{1-n} = \frac{\alpha_c C_b \Delta P_0}{R_m A} \cdot V$$

$$\Delta P_c = \left[\frac{\alpha_c C_b \Delta P_0}{R_m A} \cdot V \right]^{1/1-n}$$

$$\Delta P = \left[\frac{\alpha_c C_b \Delta P_0}{R_m A} \cdot V \right]^{1/1-n} + \Delta P_0$$

Combining and renaming constant terms, we obtain:

$$\Delta P = [\beta_1 \beta_0 \cdot V]^{1/1-n} + \beta_0 \tag{B.1}$$

$$\begin{cases} \beta_0 = \Delta P_0 \\ \beta_1 = \frac{\alpha_c C_b}{R_m A} \end{cases} \tag{B.2}$$

Model parameters were obtained by optimizing β_0 , β_1 and n in **Microsoft Excel** to minimize the sum-of-squares of error between the $\Delta P = \dots$ model and the collected pressure versus time data. Note that V is easily obtained, given that the permeate flux was constant over the experiments (*i.e.* $J = 1,000$ LMH). Additional discussions regarding “cake filtration” can be found in §2.1.3.1.

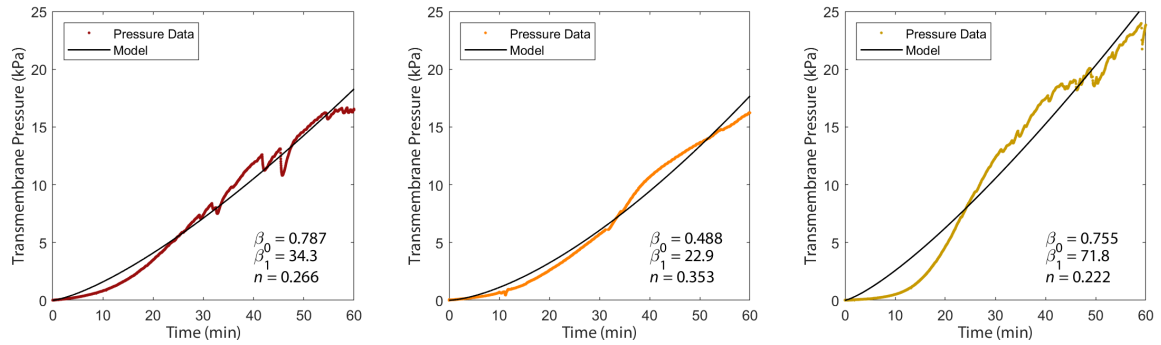


Figure B.5: Pressure profiles for three filtration experiments using the 5 μm membrane at a flux of 1,000 LMH. Pressure data points (\cdot) and the “best-fit” model line ($—$) for compressible cake filtration are shown alongside the optimized model parameters. Differences in the the magnitudes of the pressure profiles can be attributed to variations in inherent membrane permeability between the coupons that were used. The model fit is good for the first two pressure profiles but declines in quality for the third profile.

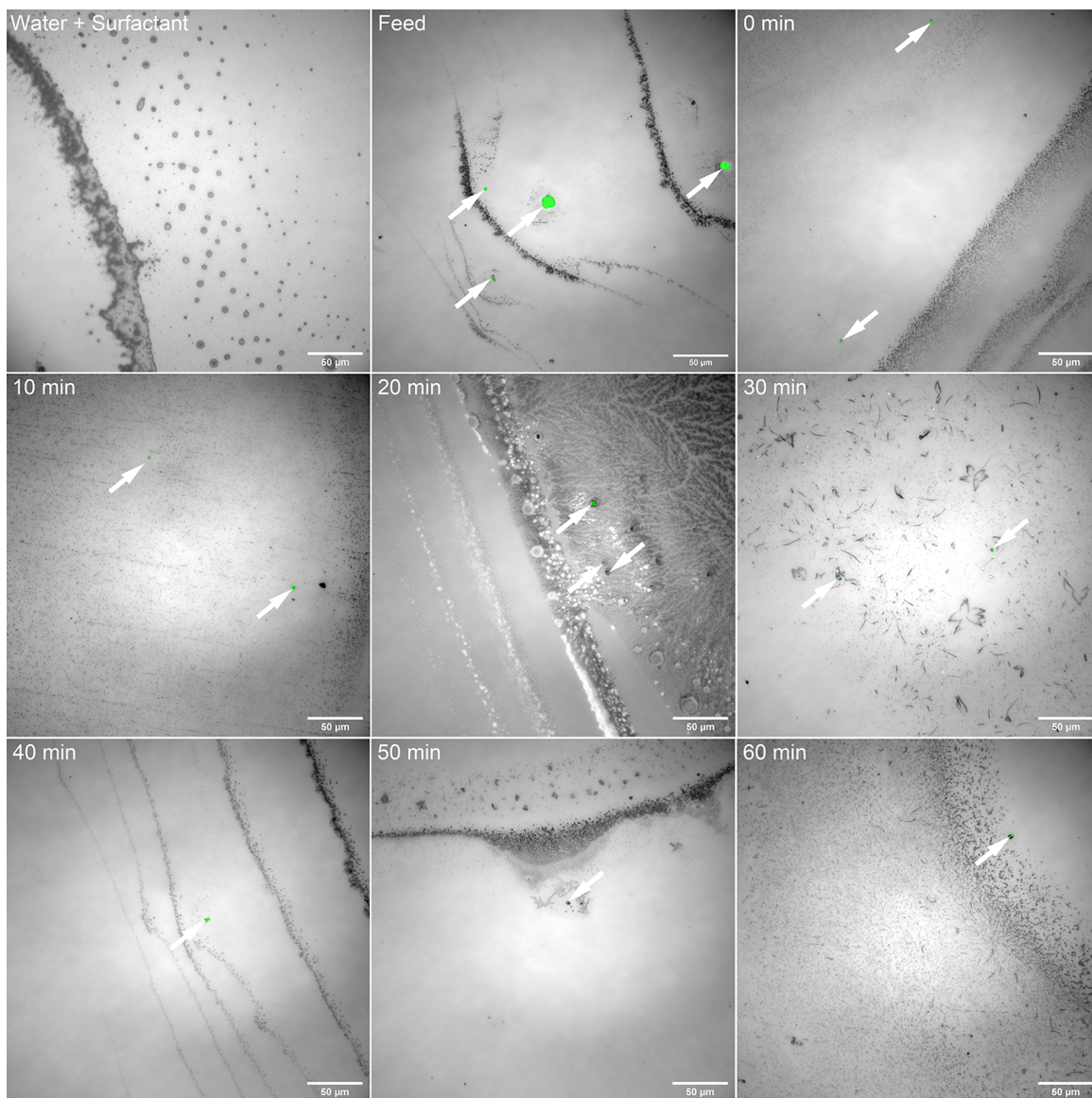


Figure B.6: Optical microscopy images of various permeate samples from filtration experiments where the 5 µm membrane was used (flux = 1,000 LMH). The permeate samples shown were taken every 10 minutes over the 60-minute experiment. MPs detected via the FITC fluorescence filter are overlaid in green and indicated by arrows (\nearrow). Every dried permeate sample where the M/S-MPs were filtered shows evidence of particles which had passed through the membrane. The image of the sample containing only Tween 20 and milliQ water shows no fluorescent artefacts, as expected. The solid debris that is visible in all four panels is attributable to residual Tween 20 (which does not evaporate like the milliQ water) and atmospheric dust which contaminated the sample/slide. Scale bars are 50 µm in length.

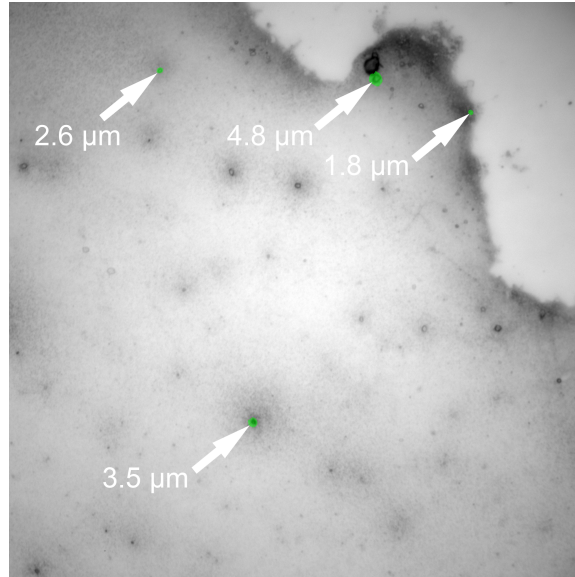


Figure B.7: Optical microscopy image of a single permeate sample (collected at 0 min) from a filtration experiment with M/S-MPs where the 5 μm membrane was used (flux = 1,000 LMH). MPs detected via the FITC fluorescence filter are overlaid in green and indicated by arrows (\nearrow). The four particle sizes were measured manually using *ImageJ* and overlaid on the figure. Note: this image was collected during a different experiment than the one shown in Figure B.6.

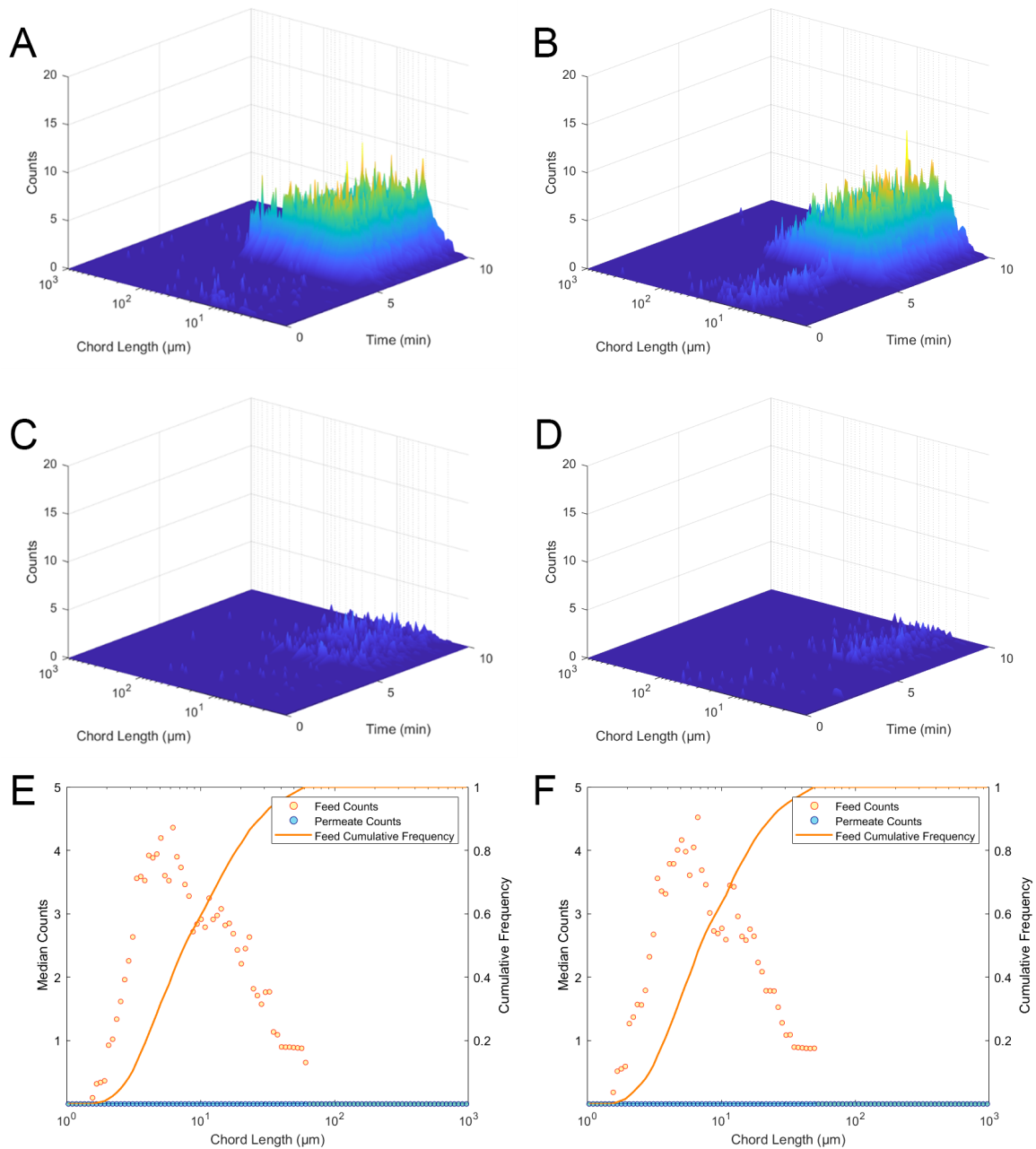


Figure B.8: Duplicate results from the FBRM analysis of permeate and feed samples from filtration experiments with the $0.45 \mu\text{m}$ membrane. (A, C, E) Results from the first replicate of this experiment. (B, D, F) Results from the second replicate of this experiment. (A, B) Feed samples. (C, D) Permeate samples collected over one-hour experiments. (E, F) Median counts of particle chord lengths in the analysis of feed (\bullet) and permeate (\bullet) samples. The cumulative chord length frequency distribution functions for the feed samples ($-$) are also shown.

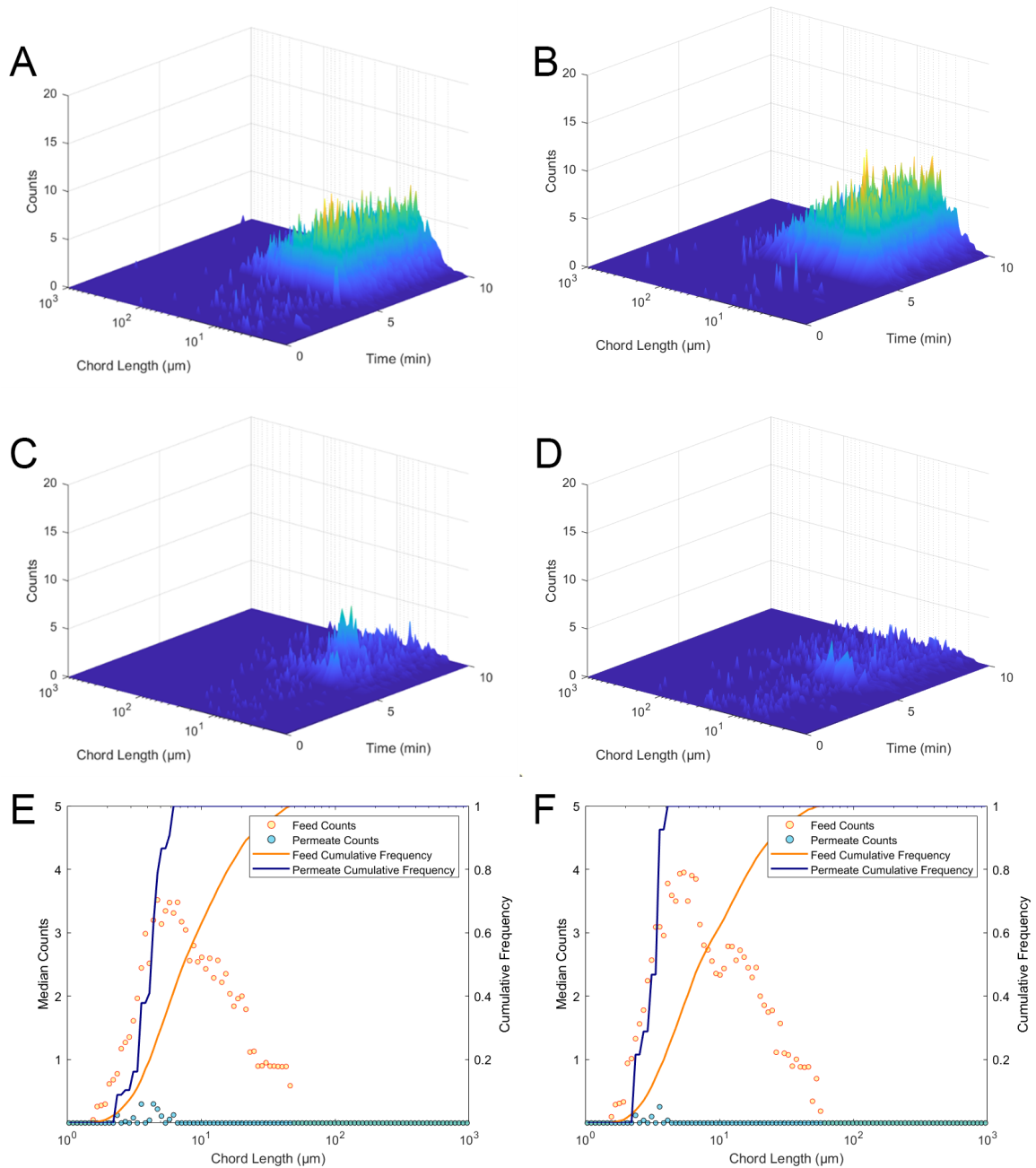


Figure B.9: Duplicate results from FBRM analysis of permeate and feed samples from filtration experiments with the 5 μm membrane. (A, C, E) Results from the first replicate of this experiment. (B, D, F) Results from the second replicate of this experiment. (A, B) Feed samples. (C, D) Permeate samples collected over one-hour experiments. (E, F) Median counts of particle chord lengths in the analysis of feed (\bullet) and permeate (\bullet) samples. The cumulative chord length frequency distribution functions for the feed ($-$) and permeate ($-$) samples are also shown.

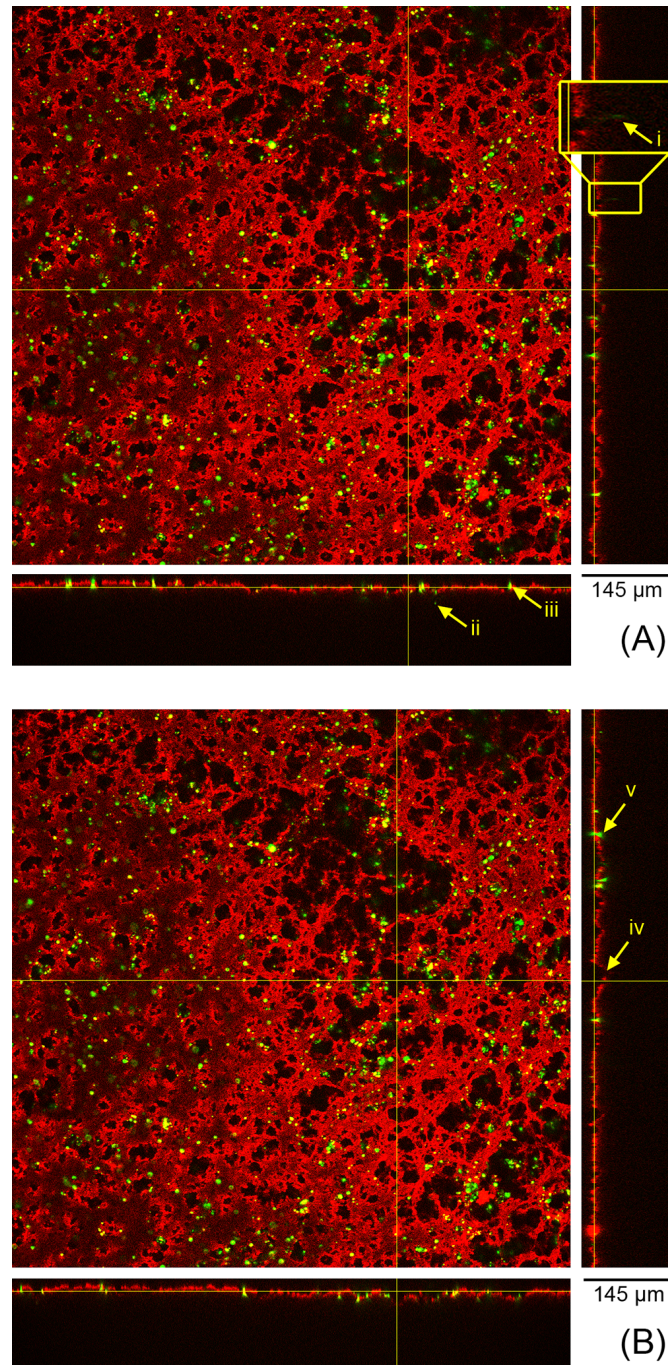


Figure B.10: CLSM orthogonal views (top-down and cross-sections) of the 5 μm membrane taken at a depth of 20 μm from the upper surface, as defined in Figure 4.6. Panel (A) highlights two individual M/S-MPs (“i” and “ii”) that appear to penetrate into the membrane structure, in contrast to other M/S-MPs which appear to accumulate at the membrane surface (e.g. “iii”). Panel (B) demonstrates the roughness of the surface of the membrane. In particular, note the depth of the indentation indicated at “iv”. A good example of the M/S-MP signal bleeding through slices is seen at “v”.

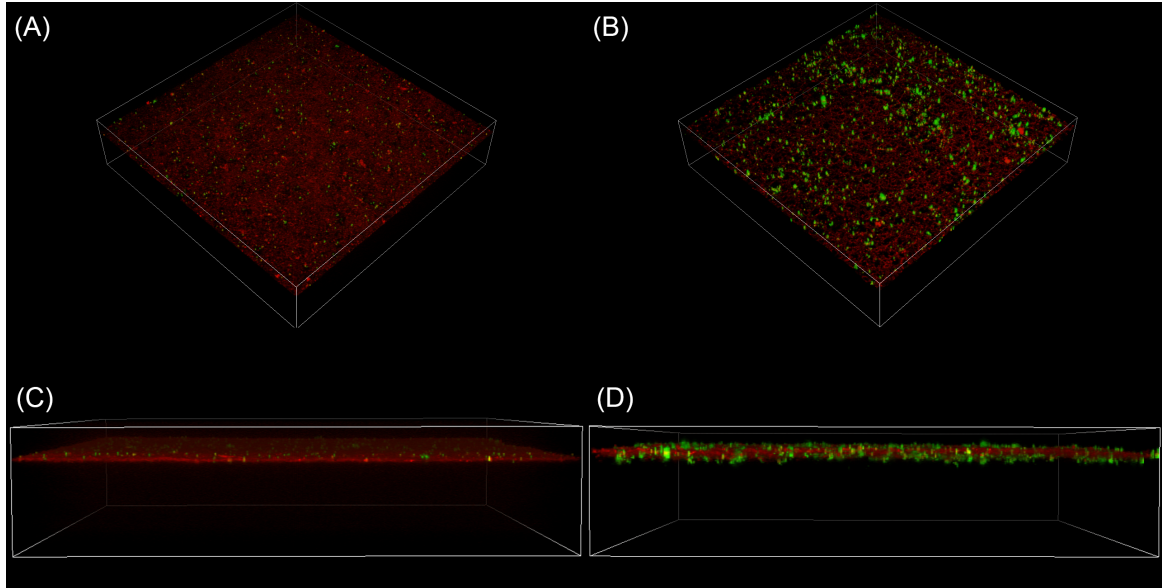


Figure B.11: 3D views of the full CLSM *z*-stacks for the (A, C) 0.45 μm and (B, D) 5 μm Durapore® membranes. The wire-frame mesh boxes measure $896 \times 896 \times 116 \mu\text{m}$ and $896 \times 896 \times 145 \mu\text{m}$ for the former and latter membranes, respectively.

■ **Work Cited:**

- [1] D. C. Sioutopoulos and A. J. Karabelas, “Correlation of organic fouling resistances in RO and UF membrane filtration under constant flux and constant pressure,” *Journal of Membrane Science*, vol. 407–408, pp. 34–46, 2012.

Appendix **C**

Supplementary Information for Chapter 5

This page has been intentionally left blank to accommodate the full-page figure, below.

C.1 Supplementary Figures

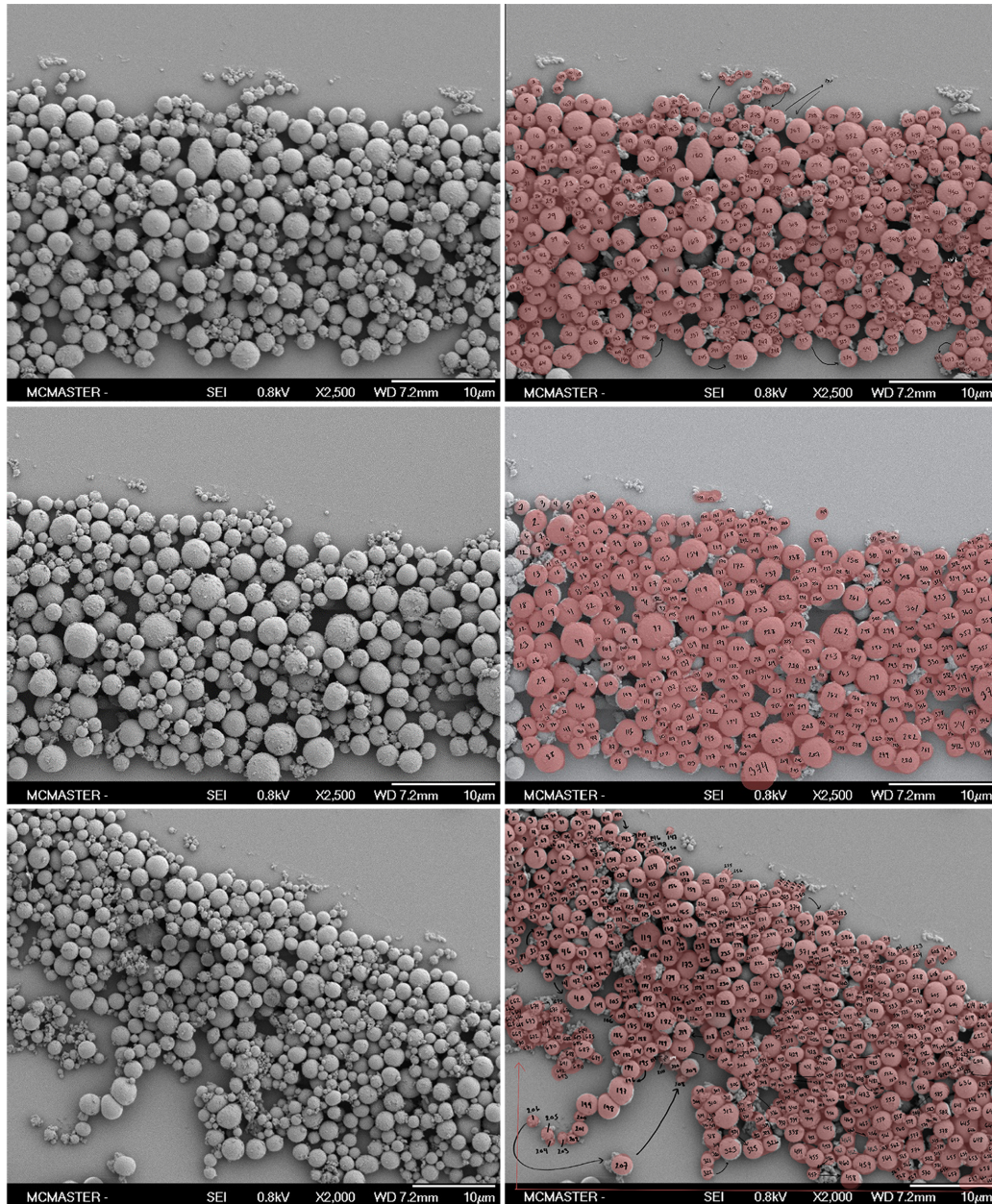


Figure C.1: FESEM micrographs of the Cospheric MBs used in this study. **(Left)** Original micrographs. **(Right)** Micrographs overlaid with annotations during the particle sizing process via image analysis. MBs that were measured are highlighted and numbered ($N = 1,580$). Scale bars at the bottom-right of the images are 10 μm .

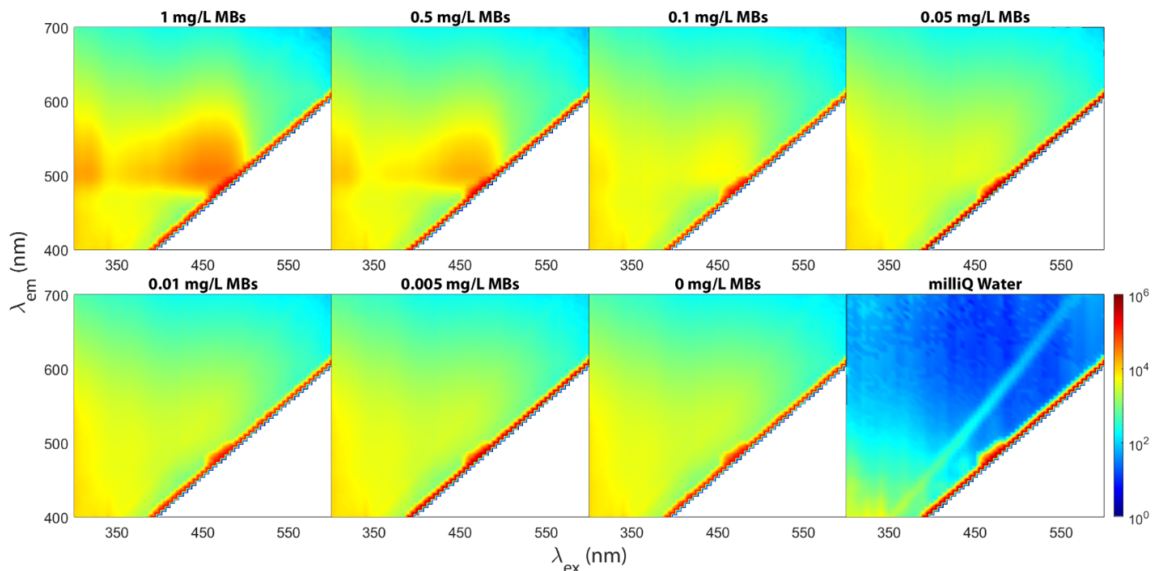


Figure C.2: Excitation-emission matrices illustrating the obscuring effect of HA when attempting to quantify MB concentrations using a fluorometric plate reader. Suspensions of fluorescent MBs were diluted with 10 mg/L HA from 1 mg/L down to 0.005 mg/L MBs. In all panels, the concentration of HA is 10 mg/L, with exception to the one experiment performed with pure milliQ water. The instrument gain was constant in all experiments. White-coloured regions to the right of the Rayleigh scattering line correspond to where $\lambda_{ex} < \lambda_{em}$. In the “milliQ water” panel, another line attributable to Raman scattering is seen at slightly higher emission wavelengths [1].

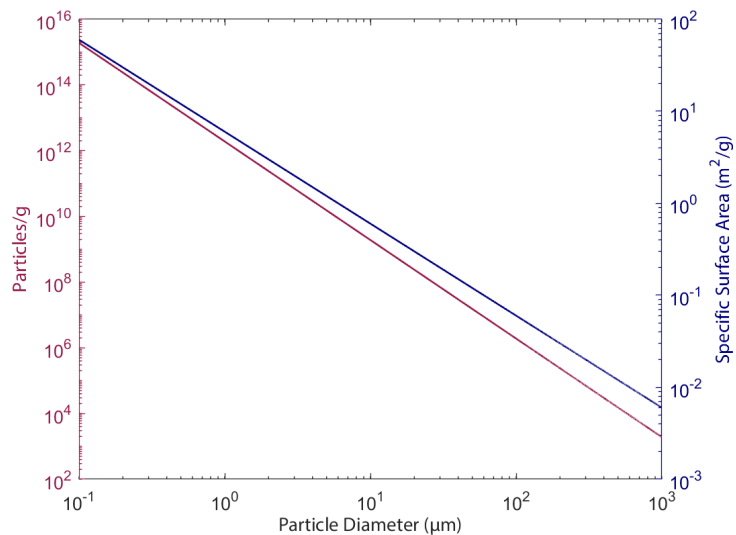


Figure C.3: The effect of the diameter of ideal spherical microparticles on the number of particles per gram and the specific surface area. A density of 1 g/cm^3 is assumed for the particles. A one-order-of-magnitude change in particle diameter results in a three-orders-of-magnitude change in the number of particles per gram.

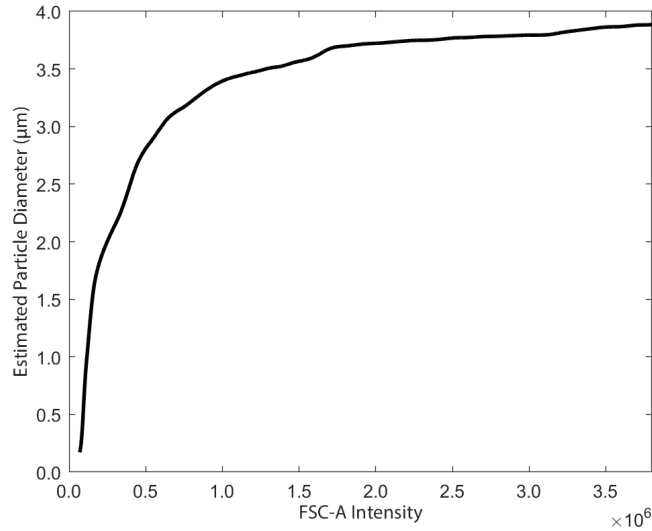


Figure C.4: The $\varphi(i)$ model relating FSC-A intensities (arbitrary units) to estimated MB particle diameters. The model is truncated before a FSC-A intensity of 4×10^6 a.u.

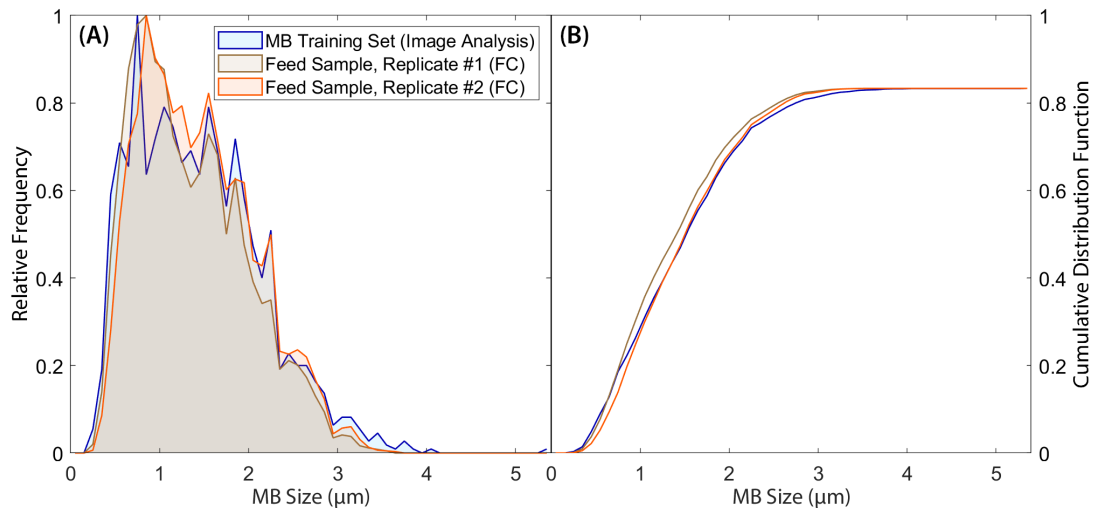


Figure C.5: Verification of the model relating FC FSC-A intensity measurements to MB size. Particle size distributions are shown for MBs measured *ex situ* via FESEM in order to formulate the sizing model (“training set”; —), and those estimated via FC in Replicates #1 (—) and #2 (—) of the MB filtration experiments using 10 mg/L HA solutions and the 5 μm membrane. **(A)** Relative frequency histograms and their corresponding **(B)** cumulative distribution function plots are shown.

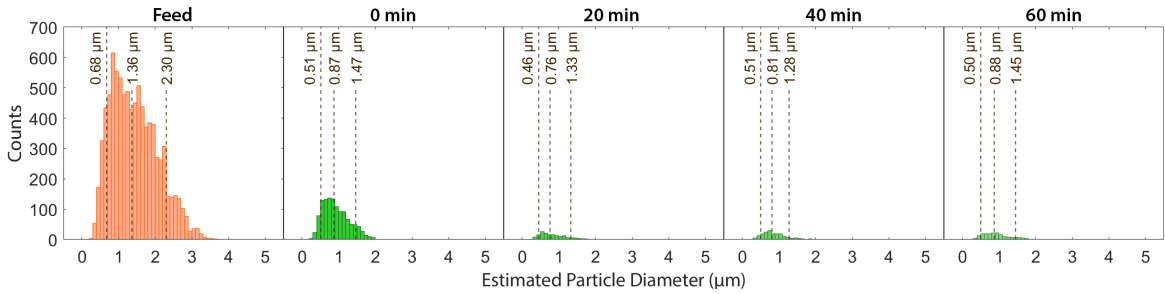


Figure C.6: Estimation of MB particle sizes in selected permeate samples for the filtration of 1 mg/L MBs in 10 mg/L HA solution using the 5 μm membrane. Only Replicate #2 is shown. Frequency histograms of estimated particle diameters (μm) in feed samples (■) and permeate samples (■) taken at 20-minute intervals are shown. From left to right, the d_{10} , median (\bar{d}), and d_{90} statistics of the particle size distributions are included (---).

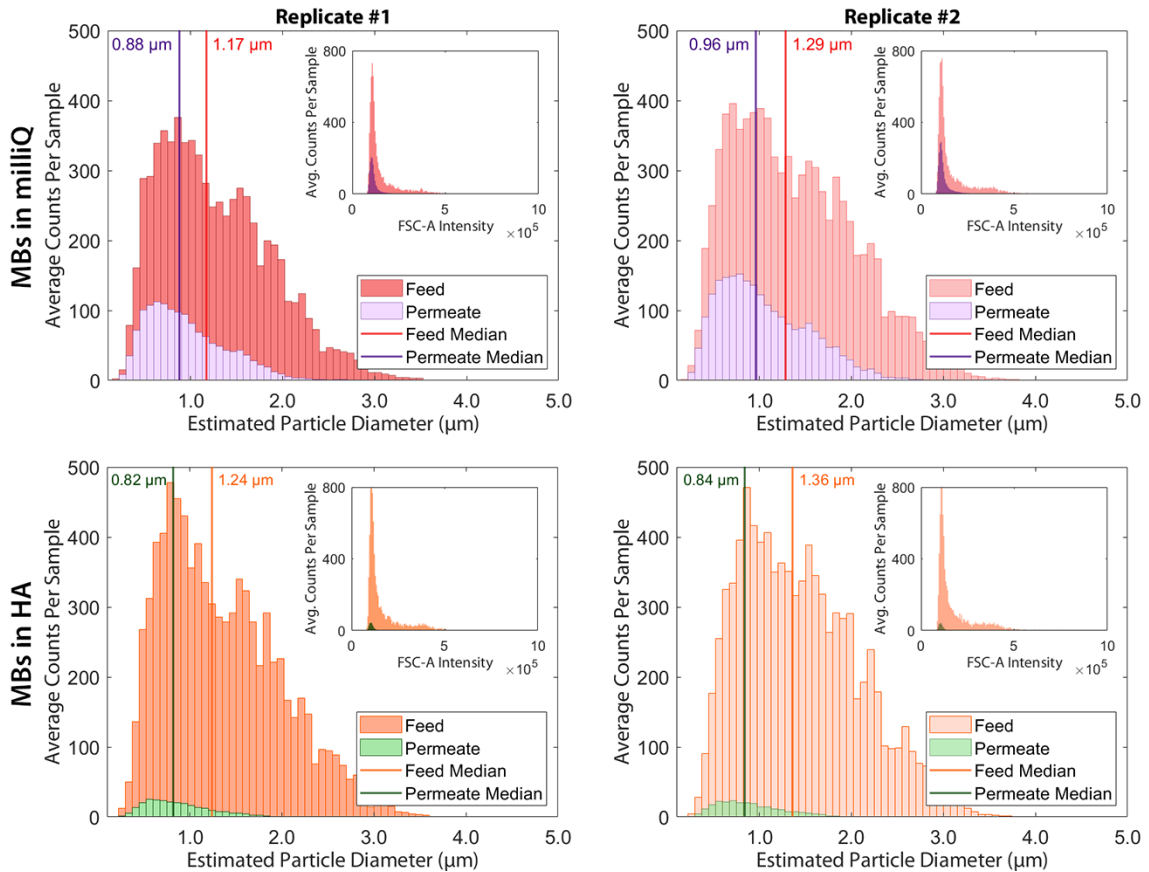


Figure C.7: Estimation of MB particle sizes from FSC-A intensity measurements in all of the filtration experiments involving the 5 μm membrane. Frequency histograms of estimated particle diameters (μm) in the feed and permeate samples are shown, as calculated from FSC-A intensity data. The permeate particle size distributions are composites, averaged over every one of the $N = 31$ permeate samples taken in the experiments. Figure insets illustrate the distribution of FSC-A intensities which were used to calculate the estimated particle sizes via $d = \varphi(i)$.

C.2 Data Tables for Microbead Size Estimation Experiments

Table C.1: Summary of estimated median (\tilde{d}) and d_{10}/d_{90} size statistics of particles in the feed/permeate samples during the filtration of 1 mg/L MBs in 10 mg/L HA by the 5 μm membrane. The reported “average” permeate value for a given replicate is the mean of all the samples taken at 10-minute intervals.

		Feed	Permeate				Average
			0 min	20 min	40 min	60 min	
Replicate #1	MBs/50 μL	8,366	959	141	95	123	-
	\tilde{d} (μm)	1.24	0.85	0.85	0.82	0.78	0.82
	d_{10} (μm)	0.61	0.51	0.47	0.46	0.41	0.46
	d_{90} (μm)	2.24	1.39	1.44	1.37	1.55	1.44
Replicate #2	MBs/50 μL	8,811	1,195	160	180	177	-
	\tilde{d} (μm)	1.36	0.87	0.76	0.81	0.88	0.84
	d_{10} (μm)	0.68	0.51	0.46	0.51	0.50	0.50
	d_{90} (μm)	2.30	1.47	1.33	1.28	1.45	1.38

Table C.2: Comparison of the estimated median (\tilde{d}) and d_{10}/d_{90} sizes of particles in the feed/permeate samples of experiments using either milliQ water or 10 mg/L HA. Results are for the 5 μm membrane only. The reported “permeate average” value for a given replicate is the mean of all the samples taken at 10-minute intervals.

		milliQ Water Only		10 mg/L HA Solution	
		Feed	Permeate Average	Feed	Permeate Average
Replicate #1	\tilde{d} (μm)	1.17	0.88	1.24	0.82
	d_{10} (μm)	0.56	0.47	0.61	0.46
	d_{90} (μm)	2.12	1.59	2.24	1.44
Replicate #2	\tilde{d} (μm)	1.29	0.96	1.36	0.84
	d_{10} (μm)	0.59	0.50	0.68	0.50
	d_{90} (μm)	2.27	1.75	2.30	1.38

■ Work Cited:

- [1] K. R. Murphy, C. A. Stedmon, D. Graeber, and R. Bro, “Fluorescence spectroscopy and multi-way techniques. PARAFAC,” *Analytical Methods*, vol. 5, no. 23, pp. 6557–6566, 2013.

Supplementary Information for Chapter 6

D.1 Filtration Apparatus

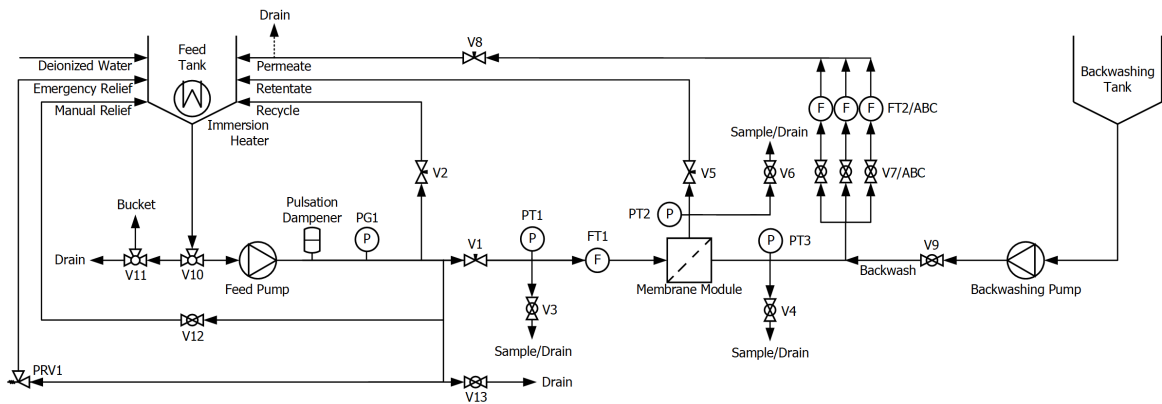


Figure D.1: Comprehensive P&ID which outlines the entire membrane module evaluation setup. A summary of the valve and instrumentation codes can be found in Table D.1.

Table D.1: Summary of valves and instrumentation, as notated on the P&ID in Figure D.1.

Valves			
Code	⟨Name⟩ Valve	Type	Function
V01	Feed	Needle	Controls pressure/flow to membrane
V02	Recycle	Needle	Diverts a fraction of pump output to tank
V03	Feed Sample	Ball	Samples feed water to membrane module
V04	Permeate Sample	Ball	Samples/drains permeate water
V05	Retentate	Needle	Applies backpressure to/isolates membrane
V06	Retentate Drain	Ball	Drains module/backwashing water
V07	Permeate Isolation	Ball	Enables/disables permeate flow
V08	Permeate	Needle	Applies backpressure to permeate stream
V09	Backwashing	Ball	Enables/disables backwash water flow
V10	Tank Diversion	Ball	Diverts water from tank to pump or drain
V11	Drain Diversion	Ball	Diverts waste directly to drain or bucket
V12	Manual Relief	Ball	Recycles pump output to tank
V13	Apparatus Purge	Ball	Low point drain in apparatus
PRV1	Pressure Relief	Relief	Automatic over-pressure actuated valve
Instrumentation			
Code	Name	Type	Function
PG1	Pump Pressure	Gauge	Pump outlet pressure
PT1	Feed Pressure	Transducer [†]	Water pressure in feed to membrane
PT2	Retentate Pressure	Transducer [†]	Retentate water pressure leaving membrane
PT3	Permeate Pressure	Transducer [†]	Permeate water pressure leaving membrane
FT1	Feed Flow	Transducer ^{††}	Flow rate of water fed to membrane
FT2	Permeate Flow	Transducer ^{†††}	Flow rate of water in permeate stream
	[†] Omega PX409	^{††} Omega FPR302	^{†††} Omega FLR1008ST

D.2 Supplementary Results

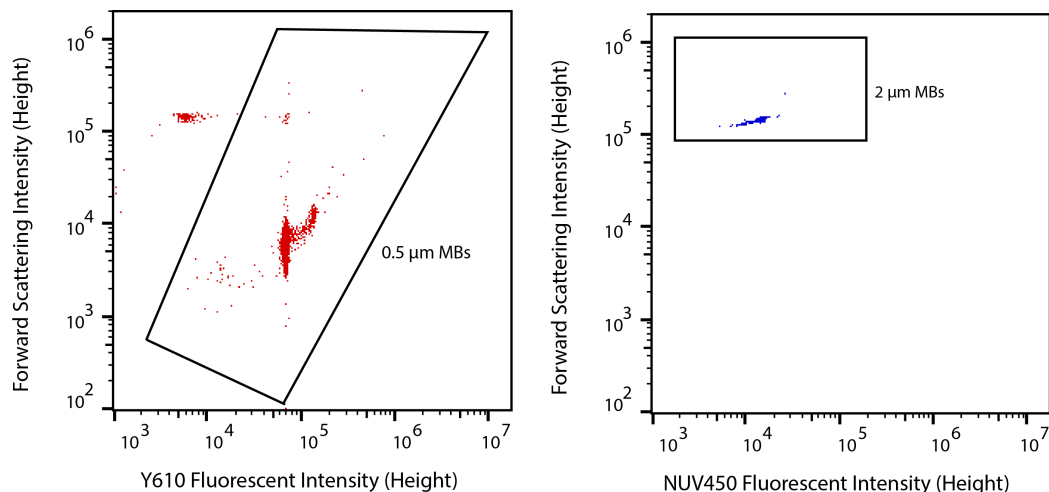


Figure D.2: Example FC data for 1 mg/L of both 0.5 μm (left) and 2 μm (right) MBs in milliQ water. FSC-H versus Y610-H or NUV450-H plots (in a.u.) with gates are shown. Events corresponding to each of the MBs are clearly discernible, even with the two sizes of MBs suspended in a single mixture.

Table D.2: Analysis of the variability of concentration measurements made via FC. Four measurements were made of MB concentrations originating from the same sample suspension (milliQ water only). The average of these measurements \pm one standard deviation is reported. The relative variability is the standard deviation divided by the average.

Prepared Suspension Concentration (mg/L)	0.5 μm MBs		2 μm MBs	
	Concentration via FC (MBs/mL)	Relative Variability	Concentration via FC (MBs/mL)	Relative Variability
10^0	$8,783,265 \pm 103,681$	1%	$150,385 \pm 4,469$	3%
10^{-2}	$106,415 \pm 1,599$	2%	695 ± 114	16%
10^{-4}	940 ± 30	8%	30 ± 26	86%
0	5 ± 10	200%	25 ± 20	80%

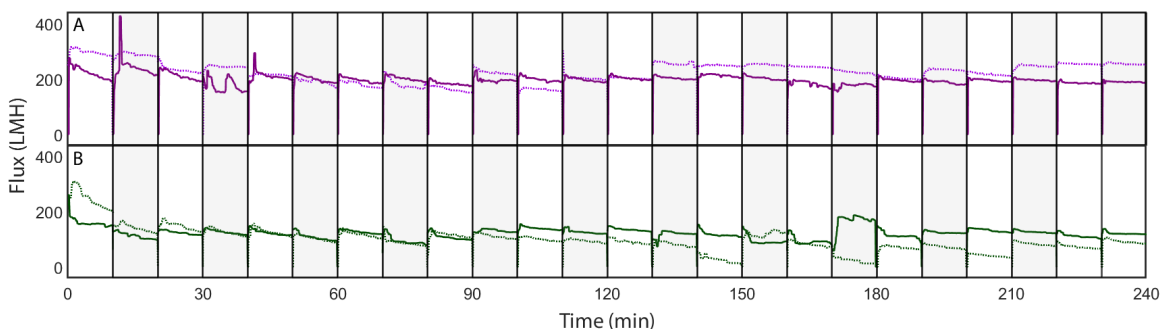


Figure D.3: Comparison of permeate flux profiles for Modules A (top) and B (bottom) in the absence of added MBs (\cdots) and in the presence of added $0.5\ \mu\text{m}/2\ \mu\text{m}$ MBs ($—$), plotted over the course of 4-hour experiments. That is, the permeate flux profiles for Experiments #1 and #3 (top), and #2 and #4 (bottom) are shown. The TMP is constant at ~ 0.5 psi.

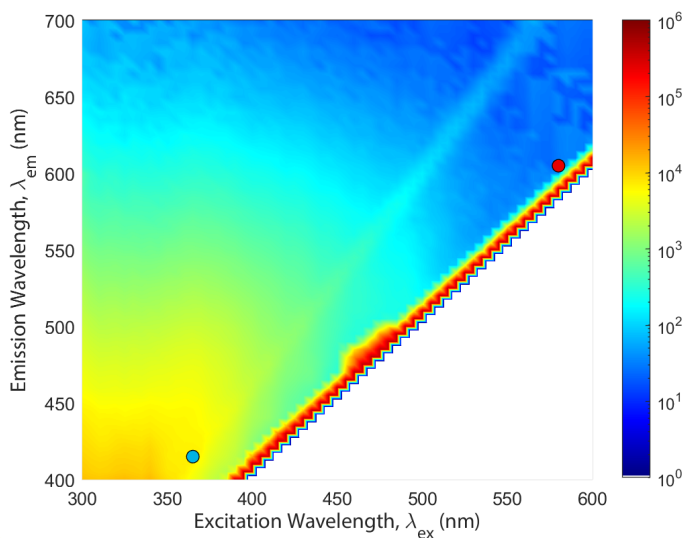


Figure D.4: Excitation-emission matrix illustrating the “background” autofluorescence of the solids in the wastewater that was used (WW1). Magnitudes of fluorescent intensities (gain = “95”) are indicated by the coloured legend (a.u.). The peak $\lambda_{ex}/\lambda_{em}$ wavelength pairs for the $0.5\ \mu\text{m}$ (\bullet) and $2\ \mu\text{m}$ MBs (\bullet) are also indicated. As opposed to the $2\ \mu\text{m}$ MBs, the $0.5\ \mu\text{m}$ MBs see little interference from the wastewater autofluorescence. White-coloured regions to the right of the Rayleigh scattering line correspond to where $\lambda_{ex} < \lambda_{em}$. Also noted in Figure C.2, another line attributable to Raman scattering is seen at slightly higher emission wavelengths. Details regarding the method for acquiring this fluorescence data can be found in §5.2.6.

Table D.3: Summary of the calculated volumes of feed wastewater required (V_f) to produce the observed concentrations of MBs in the collected BW water from Experiments #3 and #4. Note that the hold-up volume of the entire module is 0.05 L. The ratio of the concentrations of MBs in the BW water samples (n_{BW}) to the feed samples (n_f) is also reported.

Module A	Cycle 6	Cycle 12	Cycle 18	Cycle 24
0.5 μm MBs	$V_f = 0.628 \text{ L}$ $n_{BW}/n_f = 25\%$	$V_f = 1.32 \text{ L}$ $n_{BW}/n_f = 53\%$	$V_f = 0.830 \text{ L}$ $n_{BW}/n_f = 33\%$	$V_f = 1.01 \text{ L}$ $n_{BW}/n_f = 40\%$
2 μm MBs	$V_f = 0.651 \text{ L}$ $n_{BW}/n_f = 26\%$	$V_f = 0.707 \text{ L}$ $n_{BW}/n_f = 28\%$	$V_f = 0.625 \text{ L}$ $n_{BW}/n_f = 25\%$	$V_f = 0.767 \text{ L}$ $n_{BW}/n_f = 31\%$
Module B				
0.5 μm MBs	$V_f = 0.207 \text{ L}$ $n_{BW}/n_f = 8\%$	$V_f = 0.388 \text{ L}$ $n_{BW}/n_f = 16\%$	$V_f = 0.298 \text{ L}$ $n_{BW}/n_f = 12\%$	$V_f = 0.424 \text{ L}$ $n_{BW}/n_f = 17\%$
2 μm MBs	$V_f = 0.201 \text{ L}$ $n_{BW}/n_f = 8\%$	$V_f = 0.171 \text{ L}$ $n_{BW}/n_f = 7\%$	$V_f = 0.111 \text{ L}$ $n_{BW}/n_f = 4\%$	$V_f = 0.102 \text{ L}$ $n_{BW}/n_f = 4\%$

D.3 Comprehensive Summary of Data from Filtration Experiments

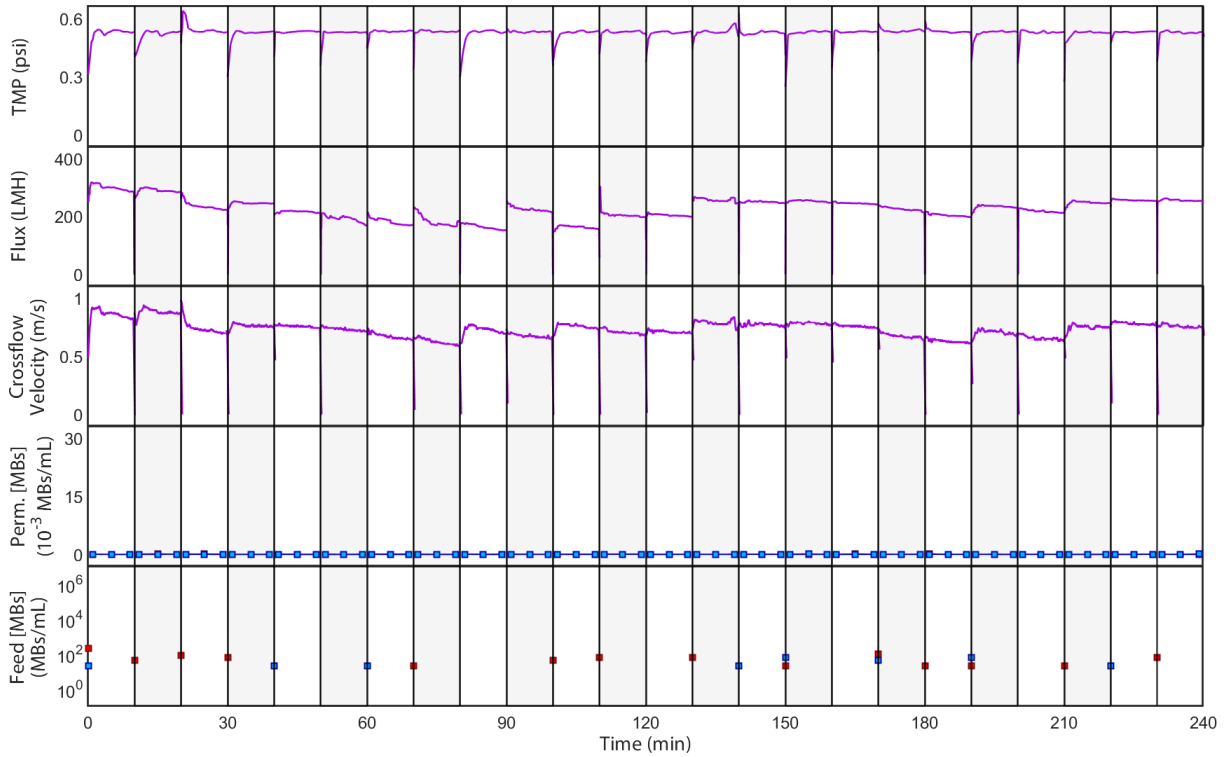


Figure D.5: Summary of data collected during Experiment #1: Module A at Condition A. The TMP, permeate flux, and crossflow velocity profiles are shown along with the concentrations of 0.5 μm MBs (■) and 2 μm MBs (■) in the permeate and feed samples. For samples where no data point is shown, no MBs were detected—as would be expected at Condition A.

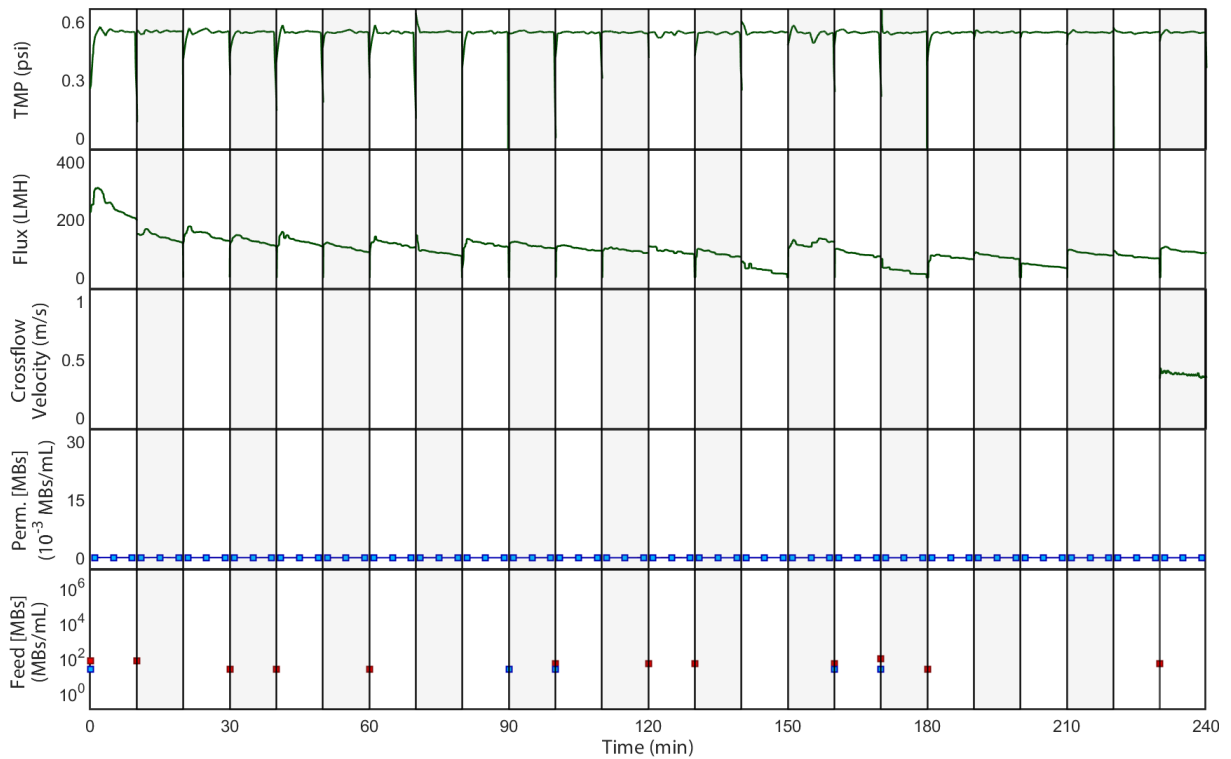


Figure D.6: Summary of data collected during Experiment #2: Module B at Condition A. The TMP, permeate flux, and crossflow velocity profiles are shown along with the concentrations of 0.5 μm MBs (■) and 2 μm MBs (■) in the permeate and feed samples. For samples where no data point is shown, no MBs were detected—as would be expected at Condition A. Note: due to a sensor malfunction, no crossflow velocity data was recorded in all but the last cycle for this experiment.

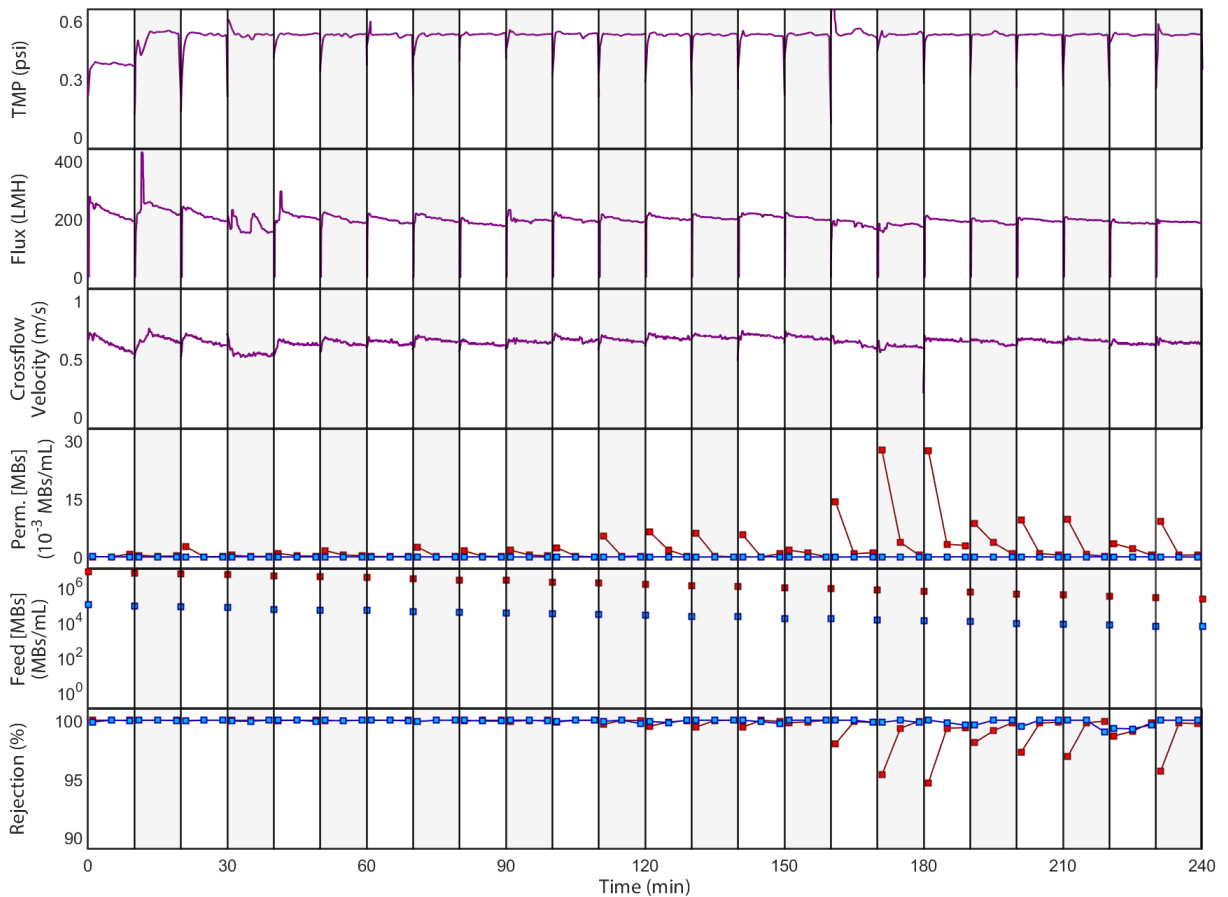


Figure D.7: Summary of data collected during Experiment #3: Module A at Condition B. The TMP, permeate flux, and average crossflow velocity profiles are shown along with the concentrations of $0.5\ \mu\text{m}$ MBs (■) and $2\ \mu\text{m}$ MBs (■) in the permeate and feed samples and the commensurate rejection coefficients.

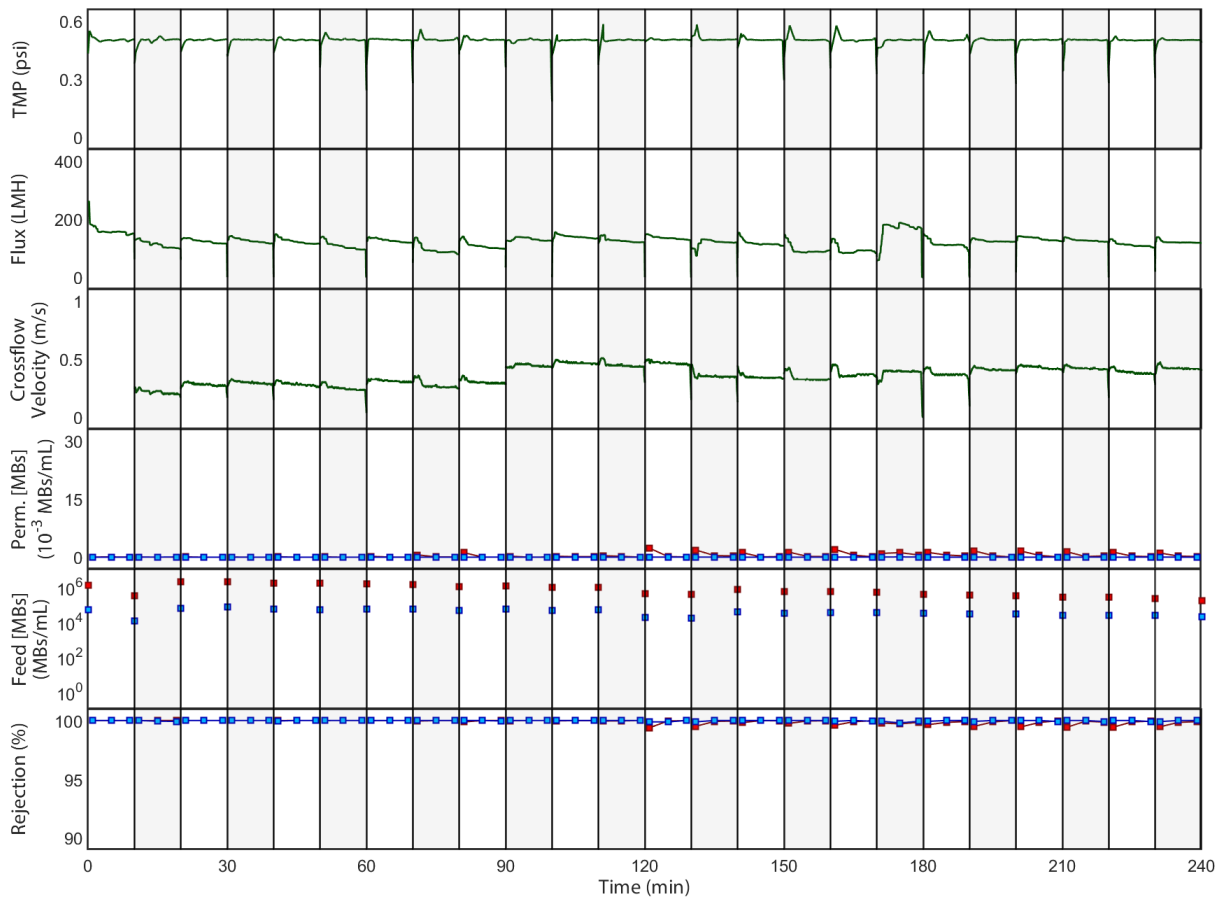


Figure D.8: Summary of data collected during Experiment #4: Module B at Condition B. The TMP, permeate flux, and average crossflow velocity profiles are shown along with the concentrations of $0.5\ \mu\text{m}$ MBs (■) and $2\ \mu\text{m}$ MBs (■) in the permeate and feed samples. Note: due to a sensor malfunction, no crossflow velocity data was recorded in the first cycle of this experiment.

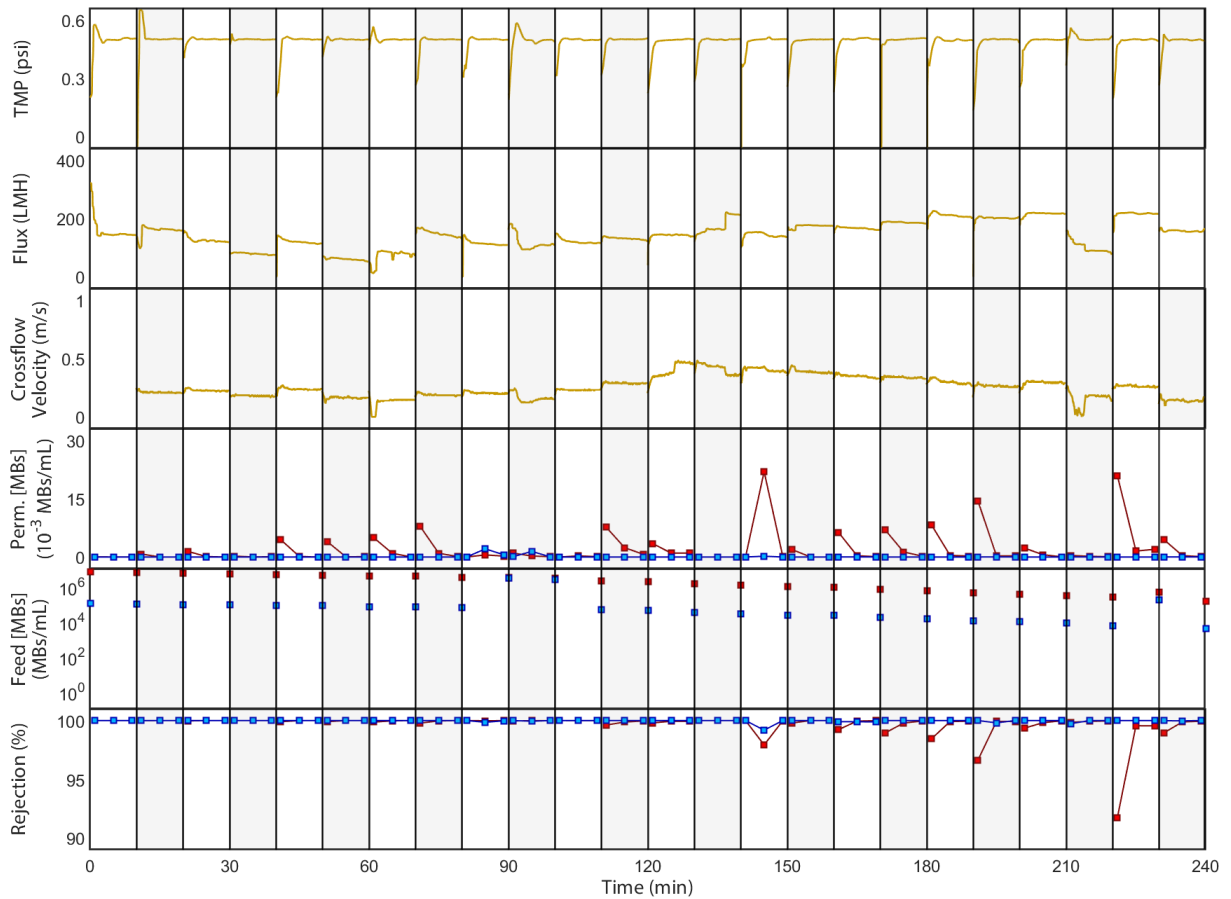


Figure D.9: Summary of data collected during Experiment #5: Module A at Condition C. The TMP, permeate flux, and average crossflow velocity profiles are shown along with the concentrations of $0.5\ \mu\text{m}$ MBs (■) and $2\ \mu\text{m}$ MBs (■) in the permeate and feed samples. Note: due to a sensor malfunction, no crossflow velocity data was recorded in the first cycle of this experiment.

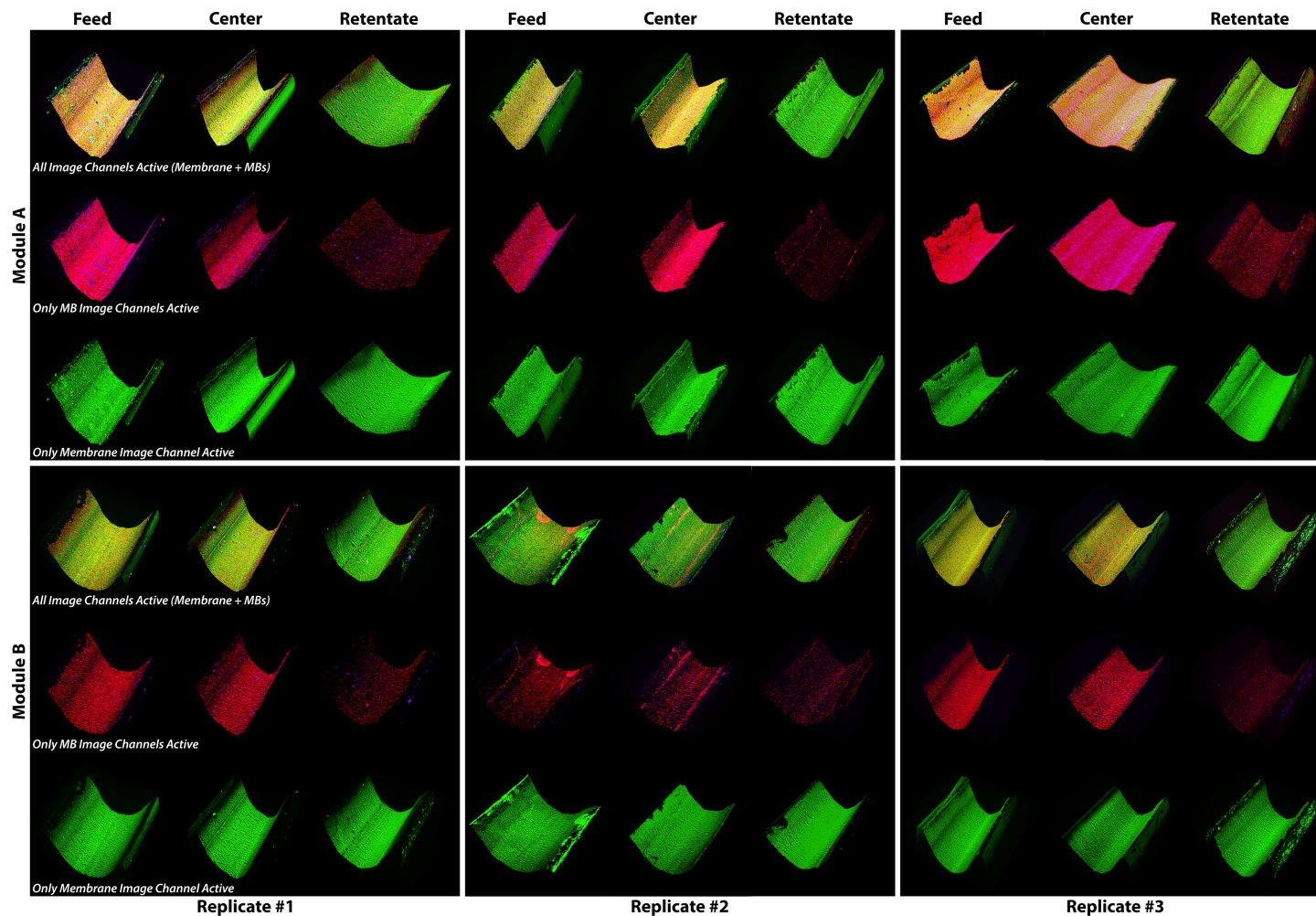


Figure D.10: Composite of all CLSM images taken of hollow fiber half-sections excised from Module A (top; *BW not used*) or Module B (bottom; *BW used*). Hollow fiber samples were taken from the feed/retentate ends as well as the centers of the fibers, as noted in §6.3.5.3. Three replicates (*i.e.* individual hollow fibers) are shown for each module. The membrane polymer (dye with FITC), 0.5 μm MBs, and 2 μm MBs appear green (■), red (■), and purple (■), respectively.